VOLUME 86 NO. ST7
JULY 1960

JOURNAL of the

Structural Division

PROCEEDINGS OF THE

AMERICAN SOCIETY OF CIVIL ENGINEERS

BASIC REQUIREMENTS FOR MANUSCRIPTS

Original papers and discussions of current papers should be submitted to the Manager of Technical Publications, ASCE. Authors should indicate the technical division to which the paper should be referred. The final date on which a discussion should reach the Society is given as a footnote with each paper. Those who are planning to submit material will expedite the review and publication procedures by complying with the following basic requirements:

1. Titles must have a length not exceeding 50 characters and spaces.

2. A 50-word summary must accompany the paper.

3. The manuscript (a ribbon copy and two copies) should be double-spaced on one side of 8½-in. by 11-in. paper.

4. The author's full name, Society membership grade, and footnote reference stating present employment must appear on the first page of the paper.

5. Mathematics are recomposed from the copy that is submitted. Because of this, it is necessary that letters be drawn carefully, and that special symbols be properly identified.

6. Tables should be typed (ribbon copies) on one side of 8½-in. by 11-in. paper. Specific reference and explanation must be made in the text for each table.

7. Illustrations must be drawn in black ink on one side of 8½-in. by 11-in. paper. Because illustrations will be reproduced with a width of between 3-in. and 4½-in., the lettering must be large enough to be legible at this width. Photographs should be submitted as glossy prints. Explanations and descriptions must be made within the text for each illustration.

8. Papers should average about 12,000 words in length and must be no longer than 18,000 words. As an approximation, each full page of typed text, table, or illustration is the equivalent of 300 words.

9. Papers must be written in the third person.

Reprints from this Journal may be made on condition that the full title of the paper, name of author, page reference, and date of publication by the Society are given. The Society is not responsible for any statement made or opinion expressed in its publications.

This Journal is published monthly by the American Society of Civil Engineers. Publication office is at 2500 South State Street, Ann Arbor, Michigan. Editorial and General Offices are at 33 West 39 Street, New York 18, New York. $4.00 of a member's dues are applied as a subscription to this Journal. Second-class postage paid at Ann Arbor, Michigan.

The index for 1959 was published as ASCE Publication 1960-10 (list price $2.00); indexes for previous years are also available.

Journal of the

STRUCTURAL DIVISION

Proceedings of the American Society of Civil Engineers

STRUCTURAL DIVISION
EXECUTIVE COMMITTEE
Robert D. Dewell, Chairman; Emerson J. Ruble, Vice Chairman;
George S. Vincent; Nathan D. Whitman, Jr.; Charles T. G. Looney, Secretary

COMMITTEE ON PUBLICATIONS
Henry G. Schlitt, Chairman; Mace H. Bell; Gerald F. Borrmann;
Edwin S. Elcock; Kurt H. Gerstle; John E. Goldberg; Wayne C. Lewis;
Alfred L. Parme; Philip A. Upp; Halsted N. Wilcox

CONTENTS

July, 1960

Papers

Page

Limit Design of Reinforced Concrete Beams
by D. T. Wright and C. Berwanger 1

Secondary Stresses in Parallel Wire Suspension Cables
by Thomas Alan Wyatt 37

Various Instability Modes of the Fixed Base Column
by D. A. Sawyer 61

Dynamic Response of Elasto-Plastic Frames
by Joseph Penzien 81

Matrix Analysis of Plane Rigid Frames
by Fernando Venancio Filho 95

(over)

Copyright 1960 by the American Society of Civil Engineers.

Page

Method for Analysis of Multibeam Bridges
by John E. Duberg, Narbey Khachaturian
and Raul E. Fradinger 109

Basic Column Strength
by Lynn S. Beedle and Lambert Tall 139

Lateral Buckling of Beams
by J. W. Clark and H. N. Hill 175

DISCUSSION

Wind Forces on Structures: Nature of the Wind, by Robert H. Sherlock. (July, 1958. Prior discussion: December, 1958, January, 1959, March, 1959. Discussion closed.)
by Robert H. Sherlock (closure) 197

Continuous Girder Bridge with Variable Moment of Inertia, by Sabri Sami. (January, 1960. Prior discussion: May, 1960. Discussion closed.)
by A. A. Eremin 215

Stability Considerations in the Design of Steel Plate Girders, by Charles E. L. Massonnet. (January, 1960. Prior discussion: April, 1960. Discussion closed.)
by A. A. Eremin 217

Properties of Steel and Concrete and the Behavior of Structures, by George Winter. (February, 1960. Prior discussion: June, 1960. Discussion closed.)
by Lester H. Gabriel 219

Digest of the Guide to Design Criteria for Metal Compression Members, by Bruce G. Johnston. (April, 1960. Prior discussion: None. Discussion closes September 1, 1960.)
by Richard H. J. Pian 221

Journal of the
STRUCTURAL DIVISION
Proceedings of the American Society of Civil Engineers

LIMIT DESIGN OF REINFORCED CONCRETE BEAMS

By D. T. Wright,[1] M. ASCE, and C. Berwanger[2]

SYNOPSIS

The paper presents complete analyses of the inelastic behavior of a two-span continuous reinforced concrete beam, for both simple plastic and strain-hardening, moment-rotation relationships. The analyses predict rotation requirements that may be compared with limiting rotation capacities in design.

INTRODUCTION

Inelastic concepts are becoming increasingly important in structural engineering. It has been evident to research workers for some time that inelastic theories are essential to an adequate understanding of the actual behavior of structures. More recently, designers have discovered that plastic and ultimate strength design methods happily combine the advantages of rationality and economy.

The plastic theory of structures is, of course, generally applicable to any structural material with suitable elastic-ductile, load-deformation characteristics. Both structural steel and reinforced concrete can be shown, with certain limitations, to possess the requisite characteristics. These limitations—essentially the tendency to instability in steel, and a limited ductility in reinforced concrete—have stimulated a flood of research that is opening the way to a general use of plastic concepts in structural design.

Note.—Discussion open until December 1, 1960. To extend the closing date one month, a written request must be filed with the Executive Secretary, ASCE. This paper is part of the copyrighted Journal of the Structural Division, Proceedings, of the American Society of Civil Engineers, Vol. 86, No. ST 7, July, 1960.

[1] Prof. and Chmn. of Dept. of Civ. Engrg., Univ. of Waterloo, Waterloo, Ontario, Canada.

[2] Lecturer, Dept. of Civ. Engrg., Univ. of Manitoba, Winnipeg, Canada.

This paper presents a complete analysis of the elastic and inelastic behavior of a simple, continuous, reinforced concrete beam. Plastic deformations required for the realization of ultimate load capacity are determined for both simple-plastic and strain-hardening behavior, and capacities for inelastic deformation in reinforced concrete beams are established. Comparison of deformation requirements and capacity in a given case permits a prediction of the amount of plastic moment redistribution possible. The results of a number of experiments intended to test the theory are also given. Although the case studied, a propped cantilever beam, has only limited direct usefulness, the results may be given much wider application in the design of continuous reinforced concrete beams.

Notation.—The letter symbols adopted for use in this paper are defined where they first appear and are arranged alphabetically, for convenience of reference, in the Appendix.

ANALYSIS OF BEHAVIOR UP TO FIRST YIELD

Consider a propped cantilever of span L, as shown in Fig. 1. A single concentrated load, P, is applied at a point KL distant from the fixed end. The moment diagram is shown in Fig. 1, and is completely described by M_1 and M_2, the moments at sections 1 and 2.
For elastic behavior, $0 < M \leq M_y$;

$$M_1 = \frac{P\,L\,K^2\,(1 - K)\,(3 - K)}{2} \quad \ldots\ldots\ldots\ldots\ldots\ldots (1)$$

$$M_2 = \frac{P\,L\,K\,(1 - K)\,(2 - K)}{2} \quad \ldots\ldots\ldots\ldots\ldots\ldots (2)$$

and:

$$\frac{M_1}{M_2} = \frac{K\,(3 - K)}{(2 - K)} \quad \ldots\ldots\ldots\ldots\ldots\ldots (3)$$

Let

$$m = \frac{M_{y_1}}{M_{y_2}} \quad \ldots\ldots\ldots\ldots\ldots\ldots (4)$$

the ratio of the yield capacities of the two critical sections, and consider only $m \leq 1.0$
Then for

$$m < \frac{M_{y_1}}{M_{y_2}} = \frac{K\,(3 - K)}{(2 - K)}$$

CASE I

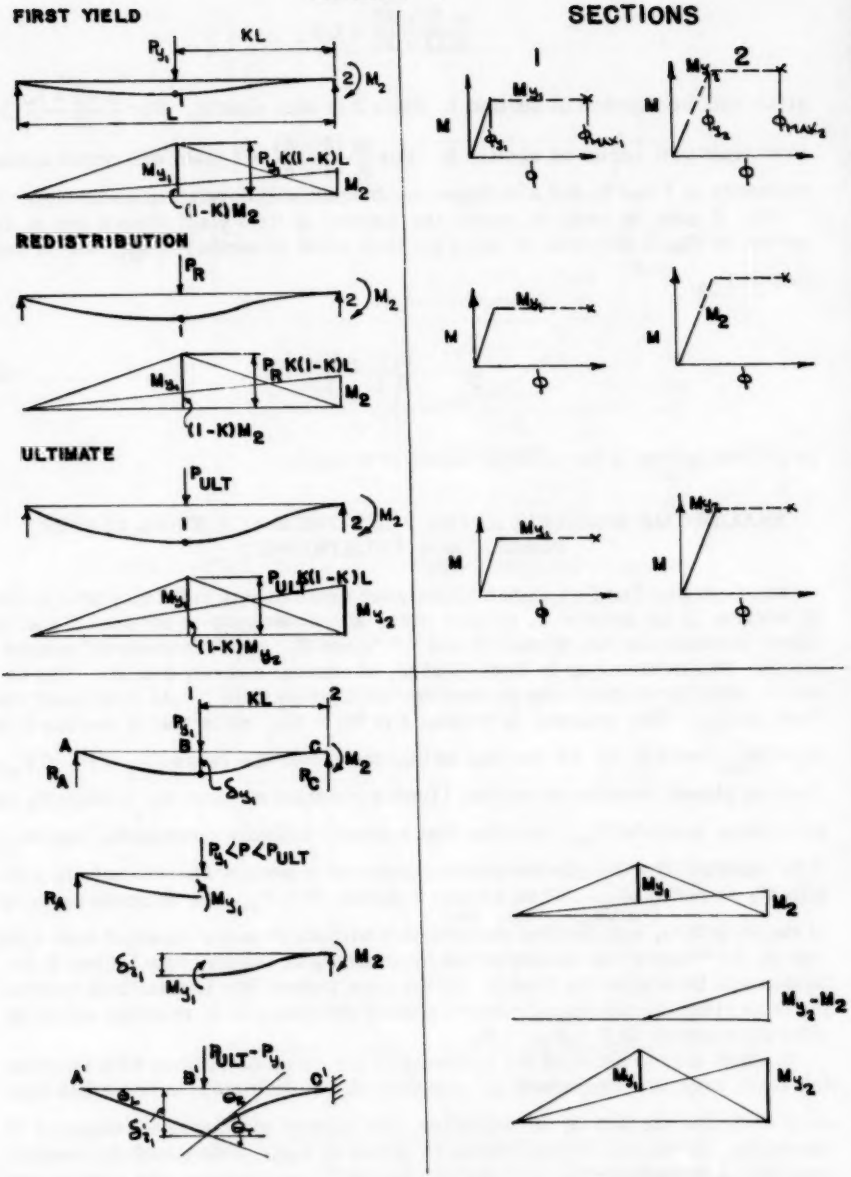

FIG. 1.—LOAD-MOMENT RELATIONSHIP (IDEAL)

or

$$\frac{m\,(2 - K)}{K\,(3 - K)} < 1.0$$

yield will be reached at section 1, while 2 is still elastic. For $\frac{m\,(2 - K)}{K\,(3 - K)} > 1$ first yield will occur at section 2. For $\frac{m\,(2 - K)}{K\,(3 - K)} = 1$ yield will occur simultaneously at 1 and 2, and a collapse mechanism will develop immediately.

Fig. 2 may be used to locate the section of first yield when K and m are known. In Fig. 3, the ratio of loads for first yield at section 1, P_{y_1}, and at section 2, P_{y_2},

$$\frac{P_{y1}}{P_{y_2}} = \frac{m\,(2 - K)}{K\,(3 - K)} \quad \ldots\ldots\ldots\ldots\ldots\ldots\ldots (5)$$

is plotted against K for various values of K and m.

ANALYSIS OF BEHAVIOR AFTER FIRST YIELD FOR IDEAL ELASTIC-PLASTIC M-ϕ RELATIONSHIP

Moments and Loads.—As has already been pointed out, yield may first occur at section 1, or section 2, or may occur simultaneously at sections 1 and 2. These alternatives are termed "Case I," "Case II," and "Mechanism" respectively. The behavior up to first yield is, of course, entirely elastic. The behavior after first yield may be seen by considering Case I. At first yield the load is P_{y1}. The moment at section 1 is $M_1 = M_{y_1}$ while that at section 2 is $M_2 < M_{y_2}$ (See Fig. 1). As the load is increased into the range $P_{y_1} < P_R < P_{ult}$ there is plastic rotation at section 1 (under constant moment M_{y_1}), while M_2 is increasing towards M_{y_2}. In order that a plastic collapse mechanism can form it is essential that the plastic rotation capacity of section 1 be adequate to permit M_2 to reach M_{y_2}. When section 2 yields, $P = P_{ult}$, the ultimate capacity of the structure, and further deformation will occur under constant load until one of the "hinges" is destroyed, as by crushing of the concrete. Case II behavior will be similar to Case I. In the case termed Mechanism both critical sections yield simultaneously and no plastic deformation is required since the ultimate capacity is $P = P_{ult} = P_y$.

To show the variation of the moments at the critical sections with increasing load, they are expressed as ratios of M_{y_2}. This yield moment has been used to define m, and is, by definition, the largest yield moment capacity of the beam. Loads will be expressed as ratios of P_{ult}. Using such dimensionless ratios facilitates the analyses and leaves the expressions as functions of two parameters, K and m.

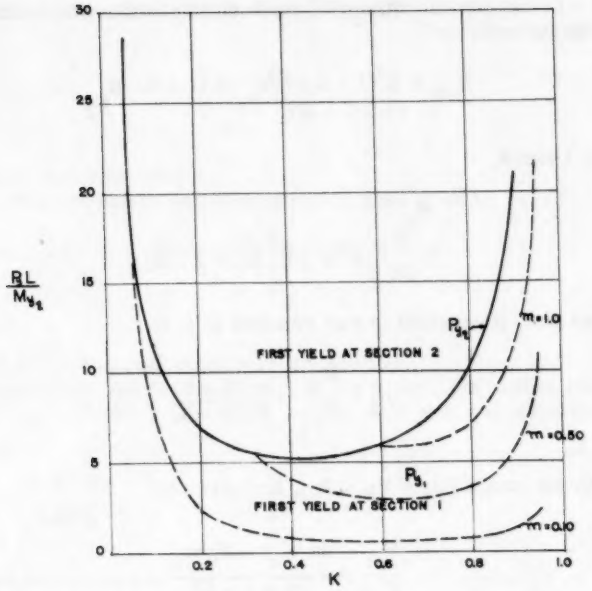

FIG. 2.—FIRST YIELD LOAD VERSUS POSITION OF LOAD

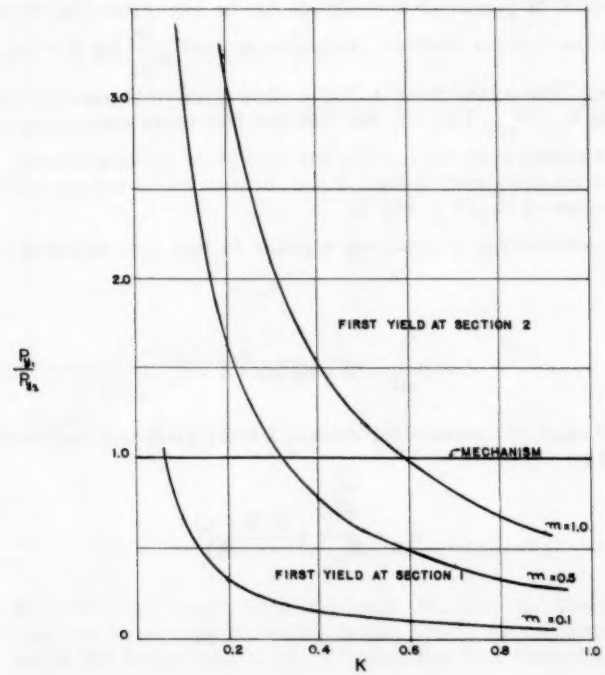

FIG. 3.—FIRST YIELD LOAD RATIO VERSUS LOAD POSITION

Case I.—From considerations of statical equilibrium the ultimate load for ideal plastic behavior is

$$P_{ult} K L (1 - K) = M_{y_1} + (1 - K) M_{y_2} \quad \ldots\ldots\ldots\ldots (6)$$

From Eqs. 1 and 4

$$\frac{P_{y_1}}{P_{ult}} = \frac{2 m}{K (3 - K) (m + 1 - K)} \quad \ldots\ldots\ldots\ldots\ldots\ldots (7)$$

The moment at 2, when yield is just reached at 1, is

$$m_2 = \frac{M_2}{M_{y_2}} = \frac{m (2 - K)}{K (3 - K)} \quad \ldots\ldots\ldots\ldots\ldots\ldots (8)$$

The loads in the range $P_{y_1} < P_R < P_{ult}$ are given by

$$\frac{P_R}{P_{ult}} = \frac{m + (1 - K) m_2}{(m + 1 - K)} \quad \ldots\ldots\ldots\ldots\ldots\ldots (9)$$

The nature of plastic redistribution can be seen from Fig. 4 where values of $\frac{M}{M_{y2}}$ for the critical sections are shown against $\frac{P}{P_{ult}}$ for K = 0.4 and various values of m. The dotted lines in Fig. 4 show first yield moment ratios, m and m_2, versus P_{y_1}/P_{ult}, (Eq. 7), and indicate how these ratios vary as P_{y_1}/P_{ult} approaches unity—when the critical sections yield simultaneously. More general variations are shown if Figs. 5 and 6 in which m and m_2 are given for a range of values of P_{y_1}/P_{ult} and K.

Case II.—Following an analysis similar to that just described, it may be shown that

$$\frac{P_{y_2}}{P_{ult}} = \frac{2}{(2 - K) (m + 1 - K)} \quad \ldots\ldots\ldots\ldots\ldots (10)$$

and m_3, the ratio of moments for section 1 when yield has just been reached at section 2 is

$$m_3 = \frac{M_1}{M_{y_2}} = \frac{K (3 - K)}{(2 - K)} \quad \ldots\ldots\ldots\ldots\ldots (11)$$

The load ratio in the redistribution range $P_{y_2} < P_R < P_{ult}$ is:

$$\frac{P_R}{P_{ult}} = \frac{(m_3 + 1 - K)}{(M + 1 - K)} \quad \ldots\ldots\ldots\ldots\ldots\ldots (12)$$

Curvatures and Rotations.—
Case I.—The curvature due to moment at first yield is

$$\phi_{y_1} = \frac{M_{y_1}}{E\,I} \quad \ldots\ldots\ldots\ldots\ldots\ldots (13)$$

in which EI is the flexural rigidity of the section.

After first yield the left hand part of the beam, AB, undergoes rigid body movement with constant moment M_{y_1}, at its right end, and additional load must

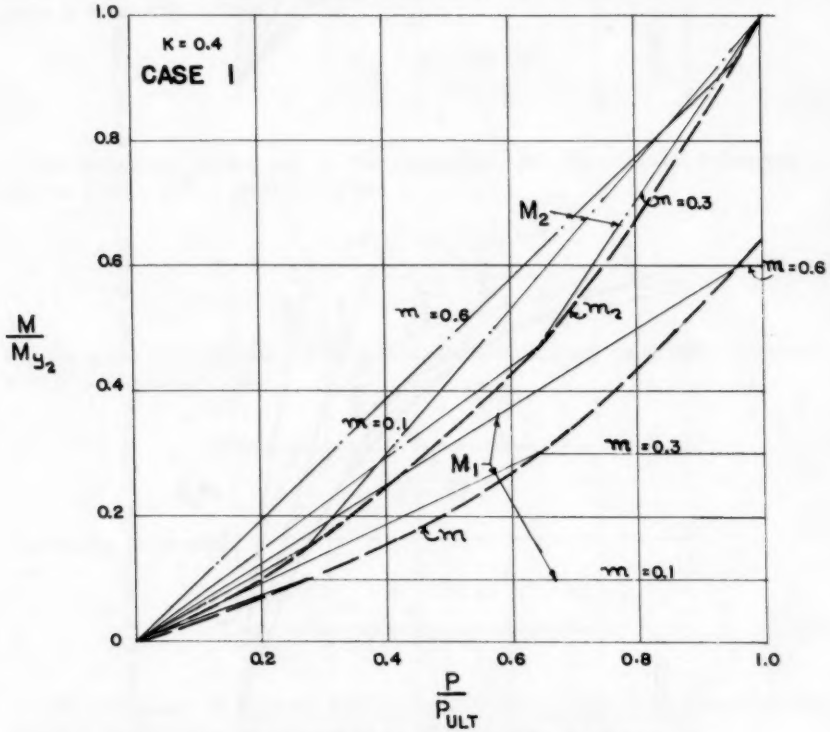

FIG. 4.—MOMENT RATIO VERSUS LOAD RATIO

be "carried" by the right hand part of the beam, BC (Fig. 1). The plastic hinge separates the two elastic parts of the beam, and is spread over some finite distance called the hinge length, H_L. Considering free body diagrams of the

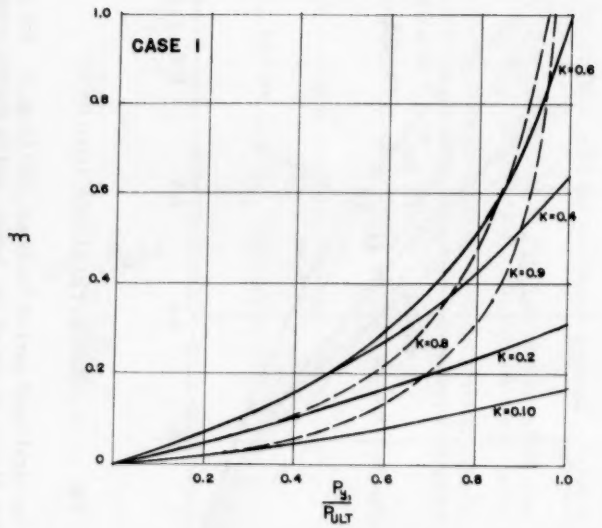

FIG. 5.—RATIO OF F.Y. MOMENTS VERSUS F.Y. LOAD RATIO

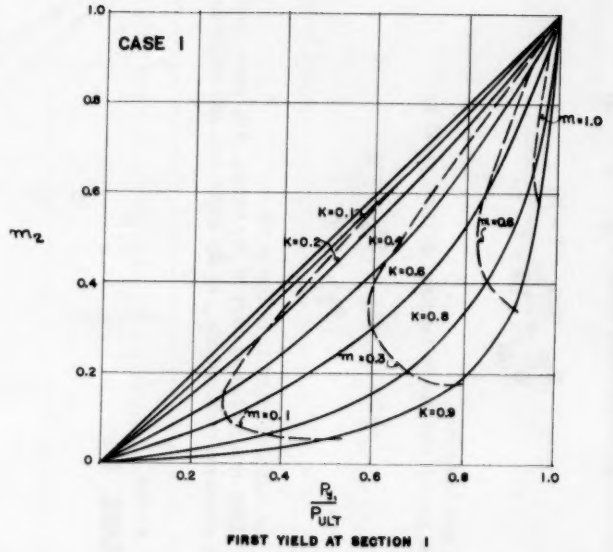

FIG. 6.—SECTION 2 MOMENT RATIO VERSUS F.Y. LOAD RATIO

two portions of the beam, Fig. 1, it can be seen that BC is now behaving as a cantilever with the differential load ($P_R = P_{y_1}$) at its free end. The increment of curvature at the hinge, over that at first yield, will be the total angle of rotation or the angle of discontinuity between the two elastic parts of the beam spread over the hinge length.

From Fig. 1, the increment of curvature at section 1 beyond that at first yield is

$$\theta_{i_1} = \frac{\theta_T}{H_L} = \frac{\theta_L + \theta_R}{H_L} \quad \ldots\ldots\ldots\ldots\ldots (14)$$

in which θ_T is the total rotation at the hinge, and θ_L and θ_R are the respective angles of rotation of the left and right portions of the beam.

Considering only the incremental load $\left(P_{ult} - P_{y_1}\right)$ acting on the cantilever B'C', and taking a new datum, θ_R, the angle between the tangent to the cantilever at B' and the new datum, is

$$\theta_R = \frac{\left(P_{ult} - P_{y_1}\right)(K\,L)^2}{2\,E\,I} \quad \ldots\ldots\ldots\ldots\ldots (15)$$

The deflection at the end of the cantilever, the incremental deflection at section 1 over that at first yield, is

$$\delta_{i_1} = \frac{\left(P_{ult} - P_{y_1}\right)(K\,L)^3}{3\,E\,I} \quad \ldots\ldots\ldots\ldots\ldots (16)$$

θ_L, the angle through which A'B' rotates as it undergoes rigid body movement with B' deflecting δ_{i_1} is

$$\theta_L = \frac{\delta_{i_1}}{(1 - K)\,L} \quad \ldots\ldots\ldots\ldots\ldots (17)$$

Combining these gives

$$\phi_{i_1} = \frac{\left(P_{ult} - P_{y_1}\right)(K\,L)^2\,(3 - K)}{6\,E\,I\,(1 - K)\,H_L} \quad \ldots\ldots\ldots\ldots\ldots (18)$$

The curvature at ultimate load is equal to the curvature at first yield (Eq. 13) plus the incremental curvature to ultimate (Eq. 18):

$$\frac{\phi_{ult_1}}{\phi_{y_1}} = 1 + \frac{\left(P_{ult} - P_{y_1}\right)(K\,L)^2\,(3 - K)}{6\,M_{y_1}\,(1 - K)\,H_L}$$

Rewriting in terms of K and m gives the rotation factor:

$$\left[\frac{\phi_{ult_1}}{\phi_{y_1}} - 1\right]\frac{H_L}{L} = \frac{K(3 - K) - m(2 - K)}{6\,m(1 - K)} \quad \ldots\ldots\ldots (19)$$

Case II.—The curvature due to moment at first yield is

$$\phi_{y_2} = \frac{M_{y_2}}{E\,I} \quad \ldots\ldots\ldots\ldots\ldots\ldots (20)$$

After the first hinge has formed at section 2, the beam acts as if simply supported, Fig. 8. Proceeding as before with a new datum for incremental loads only, the angle of discontinuity at the hinge is the angle between the tangent to beam A'C' at C' and the new datum:

$$\theta_R = \frac{\left(P_{ult} - P_{y_2}\right) K\,L^2\,(1 - K)\,(2 - K)}{6\,E\,I} \quad \ldots\ldots\ldots (21)$$

The increment of curvature at the hinge is

$$\phi_{i_2} = \frac{\left(P_{ult} - P_{y_2}\right) K\,L^2\,(1 - K)\,(2 - K)}{6\,E\,I\,H_L} \quad \ldots\ldots\ldots (22)$$

in which H_L is the hinge length at section 2 for the propped cantilever. The curvature at ultimate load is equal to the curvature at first yield (Eq. 20) plus the incremental curvature to ultimate (Eq. 22):

$$\frac{\phi_{ult_2}}{\phi_{y_2}} = 1 + \frac{\left(P_{ult} - P_{y_2}\right) K\,L^2\,(1 - K)\,(2 - K)}{6\,M_{y_2}\,H_L}$$

The rotation factor is then

$$\left[\frac{\phi_{ult_2}}{\phi_{y_2}} - 1\right]\frac{H_L}{L} = \frac{m(2 - K) - K(3 - K)}{6} \quad \ldots\ldots\ldots (23)$$

Fig. 9 is a very useful design tool. The left half of this diagram represents Case I failures. The rotation factor, given by Eq. 19, is plotted against the ratio of first yield to ultimate load, given by Eq. 7, for common values K and m. Similarly the right half represents Case II failures, with Eq. 23 plotted against Eq. 10, inverted.

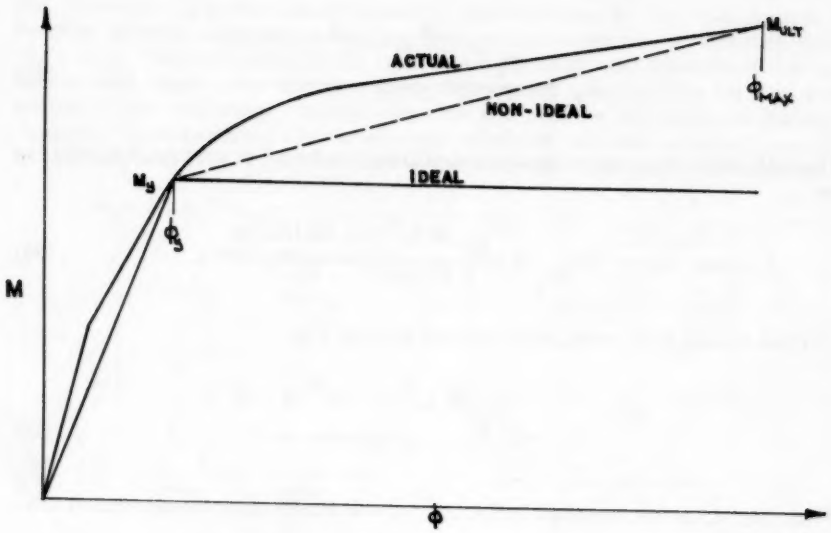

FIG. 7.—MOMENT-CURVATURE RELATIONSHIP

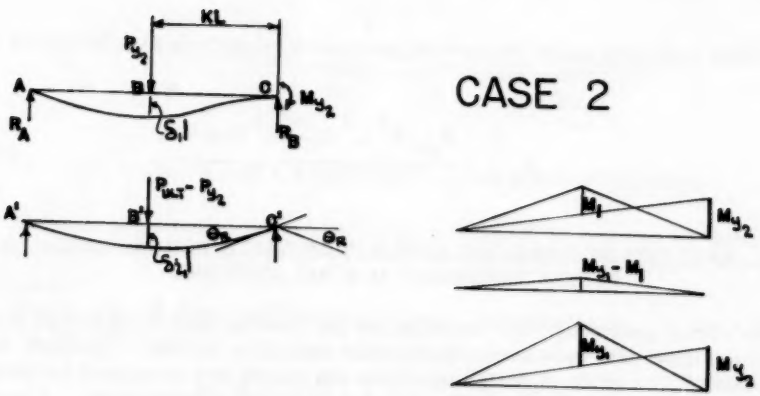

FIG. 8.—LOAD-CURVATURE RELATIONSHIP

Deflections.—
Case I.—At first yield, by elastic theory, the deflection at section 1 is

$$\delta_{y_1} = \frac{P_{y_1} (K L)^3 (1 - K)^2 (4 - K)}{12 E I} \quad \ldots\ldots\ldots\ldots (24)$$

The total deflection under the load at ultimate is found, from Eqs. 16 and 24 to be

$$\delta_{ult_1} = \frac{P_{ult} (K L)^3 (1 - K) (2 - m)}{6 E I (m + 1 - K)} \quad \ldots\ldots\ldots (25)$$

Case II.—At first yield, deflection at section 1 is

$$\delta_1 = \frac{P_{y_2} (K L)^3 (1 - K)^2 (4 - K)}{12 E I} \quad \ldots\ldots\ldots (26)$$

From Fig. 8, the incremental deflection for the simply supported beam at ultimate load is:

$$\delta_{i_1}\Big| = \frac{\left(P_{ult} - P_{y_2}\right) K^2 L^3 (1 - K)^2}{3 E I} \quad \ldots\ldots\ldots\ldots (27)$$

The total deflection under the load at ultimate is found from Eqs. 26 and 27 to be

$$\delta_{y_1}\Big| = \frac{P_{ult} K^2 L^3 (1 - K)^2 (2m - K)}{6 E I (m + 1 - K)} \quad \ldots\ldots\ldots (28)$$

ANALYSIS OF BEHAVIOR AFTER FIRST YIELD FOR ELASTIC-STRAIN HARDENING M-ϕ RELATIONSHIP

As stated previously, the expressions for loading conditions beyond first yield are dependent upon assumptions made regarding moment-curvature relationships. The group of design equations and charts just developed are based upon ideally simple elastic-plastic moment-curvature relationships. A more precise, though more complex, treatment will now be given, based upon a consideration of elastic-strain hardening moment-curvature characteristics (Fig. 7).

Behavior up to first yield is elastic and the expressions previously derived will apply. In the loading range, $P_{y_1} < P < P_M$ is the load at the formation of a collapse mechanism, there is yielding of tension reinforcement at section 1.

Increasing deformations will produce slightly higher resisting moments. Section 2 behaves elastically with increasing load until P_M is reached, when section 2 reaches its yield moment capacity. Behavior may be such that section 1 reaches ultimate resistance as first yield occurs at section 2, in which case $P_M = P_{ult}$. The load at which the mechanism forms is then taken to be the ultimate load capacity of the structure. Subsequent behavior may be such that section 1 has additional rotation capacity and reaches its ultimate moment capacity, while section 2 may or may not reach its ultimate moment capacity at ultimate load (Fig. 10). For Case II there are parallel stages of behavior.

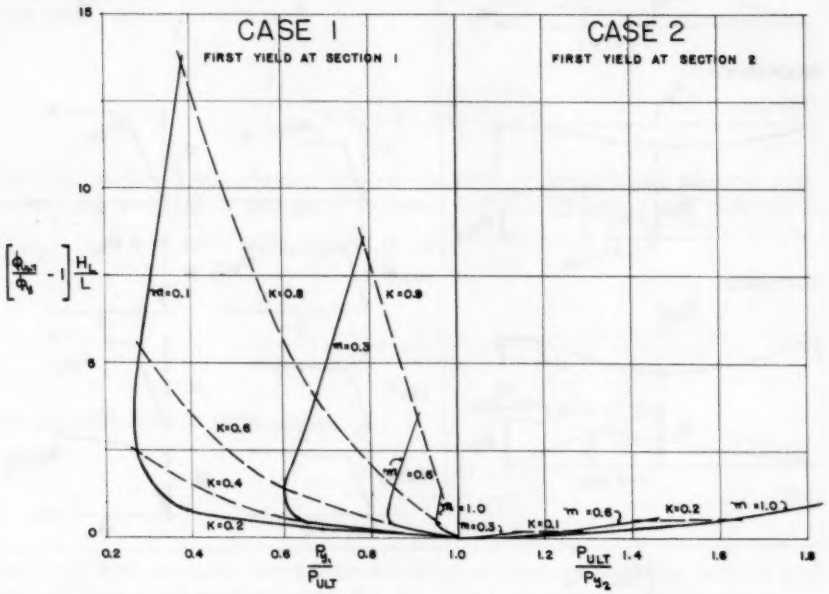

FIG. 9.—ROTATION FACTOR VERSUS FIRST YIELD LOAD RATIO

Moments and Loads.—It will be found convenient to express the moments and loads as ratios of M_{y_2} and P_M, respectively, in the expressions to be developed.

Case I.—Up to first yield the usual elastic equations apply. At the formation of the mechanism

$$P_M K (1 - K) L = M_{EP_1} + (1 - K) M_{y_2} \quad \ldots\ldots\ldots\ldots (29)$$

in which M_{EP_1} is such that $M_{y1} < M_{EP_1} < M_{ult_1}$

At ultimate load, ultimate failure at section 1 is assumed. However, there are three possible conditions of moment at section 2. From Fig. 10

$$P_{ult} K (1 - K) L = M_{ult_1} + (1 - K) M_2 \quad \ldots\ldots\ldots\ldots (30)$$

CASE I

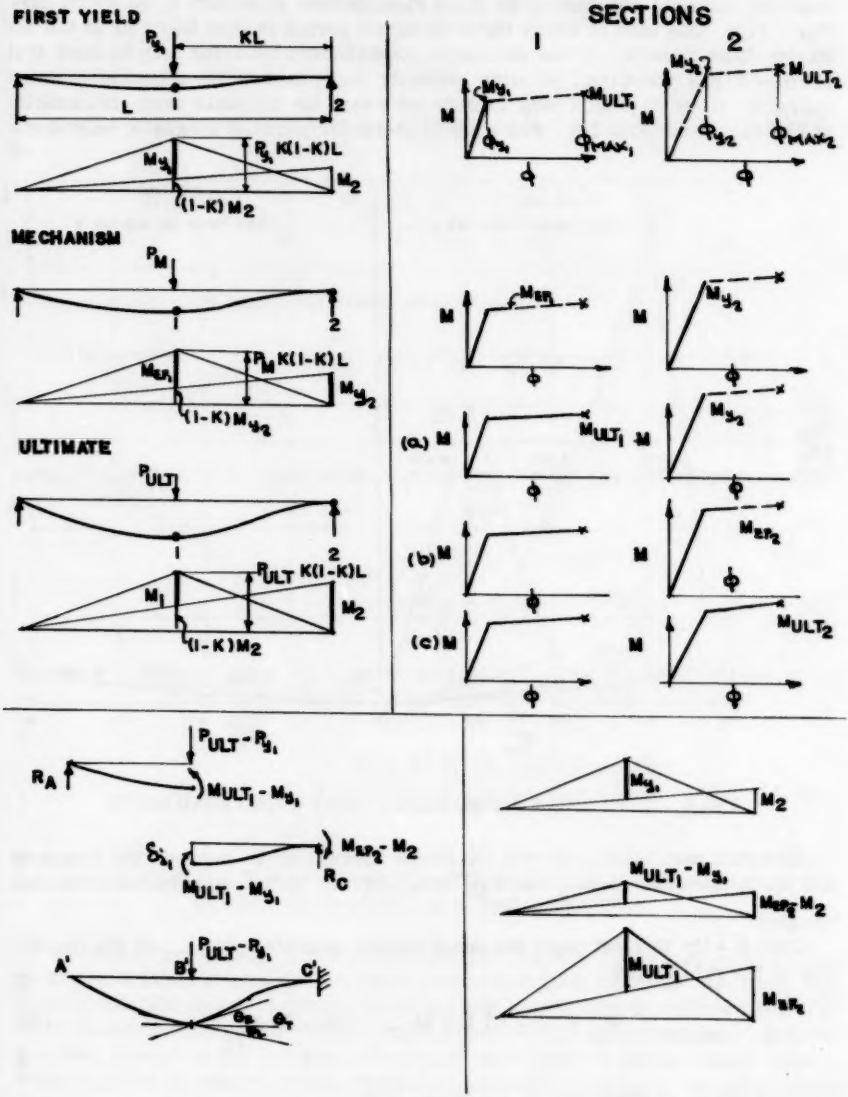

FIG. 10.—LOAD-MOMENT RELATIONSHIP (NON-IDEAL)

in which (i) $M_2 = M_{y_2}$, $P = P_M = P_{ult}$, (ii) $M_2 = M_{EP_2}$, $P = P_{ult}$, or (iii) $M_2 = M_{ult_2}$, $P = P_{ult}$. The following parameters are then defined:

$$\frac{M_{EP_1}}{M_{y_2}} = m_5, \quad \frac{M_{ult_1}}{M_{y_2}} = m_7, \quad \frac{M_{EP_2}}{M_{y_2}} = m_4, \text{ and } \frac{M_{ult_2}}{M_{y_2}} = m_6 \quad \ldots (31)$$

For (i), where ultimate moment at section 1 develops as section 2 reached first yield, the load ratio is:

$$\frac{P_{y_1}}{P_{ult}} = \frac{2\,m}{K\,(3 - K)\,(m_7 + 1 - K)} \quad \ldots\ldots\ldots\ldots (32)$$

For (ii), section 1 has greater rotation capacity before ultimate failure, permitting the moment at section 2 to reach the value M_{EP_2} $\left(M_{y_2} < M_{EP_2} < M_{ult_2}\right)$. The load ratio at first yield is then

$$\frac{P_{y_1}}{P_M} = \frac{2\,m}{K\,(3 - K)\,(m_5 + 1 - K)} \quad \ldots\ldots\ldots\ldots (33)$$

and the load ratio at ultimate is:

$$\frac{P_{ult}}{P_M} = \frac{m_7 + m_4\,(1 - K)}{(m_5 + 1 - K)} \quad \ldots\ldots\ldots\ldots\ldots (34)$$

For (iii), both sections reach ultimate moment capacity together, and the load ratio at first yield is as given by Eq. 33. The load ratio at ultimate is

$$\frac{P_{ult}}{P_M} = \frac{m_7 + m_6\,(1 - K)}{(m_5 + 1 - K)} \quad \ldots\ldots\ldots\ldots\ldots (35)$$

Considering now the moment ratios, Eqs. 4 and 8 apply at first yield as in the case of simple elastic-plastic behavior. At the formation of the mechanism the moment ratio at section 1, m_5, is by proportion from Fig. 11:

$$m_5 = m + (m_7 - m)\,\frac{\left(1 - P_{y_1}/P_M\right)}{\left(P_{ult}/P_M - P_{y_1}/P_M\right)} \quad \ldots\ldots\ldots (36)$$

Case II.—At first yield the elementary elastic equations apply. At the formation of the mechanism a derivation similar to that for Case I gives:

$$P_M\,K\,(1 - K)\,L = M_{y_1} + (1 - K)\,M_{EP_2} \quad \ldots\ldots\ldots (37)$$

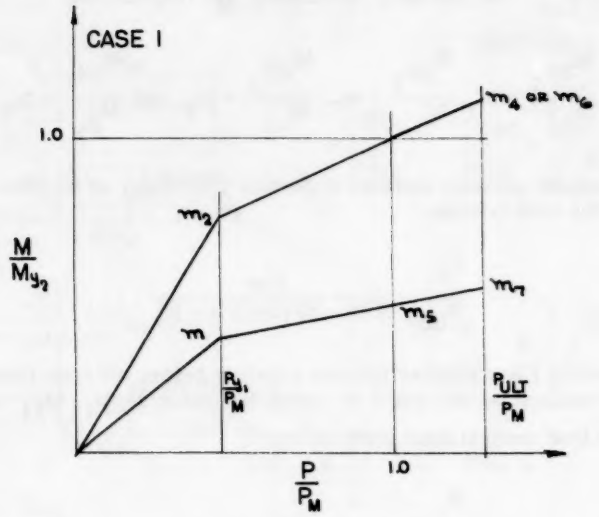

FIG. 11

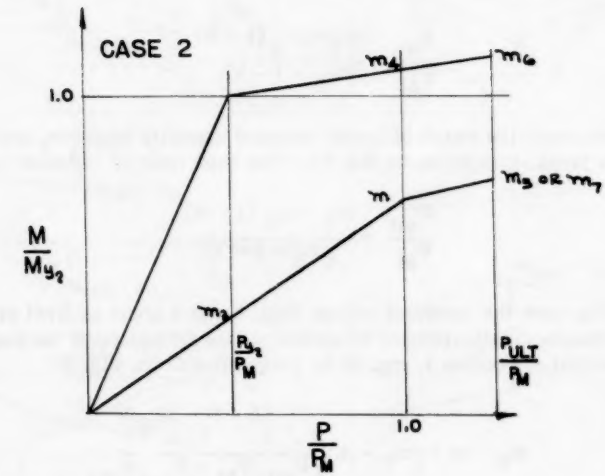

FIG. 12.—MOMENT VERSUS LOAD RATIO (NON-IDEAL)

At ultimate load, ultimate failure at section 2 is assumed. There are three conditions of moment at section 1:

$$P_{ult} K (1 - K) L = M_1 + (1 - K) M_{ult_2} \quad \ldots\ldots\ldots (38)$$

where, (i) $M_1 = M_{y_1}$, $P = P_M = P_{ult}$, (ii) $M_1 = M_{EP_1}$, $P = P_{ult}$ or (iii) $M_1 = M_{ult_1}$, $P = P_{ult}$.

The various load ratios are:

(i)

$$\frac{P_{y_2}}{P_{ult}} = \frac{2}{(2 - K)\left[m + m_6 (1 - K)\right]} \quad \ldots\ldots\ldots\ldots (39)$$

(ii) at first yield:

$$\frac{P_{y_2}}{P_M} = \frac{2}{(2 - K)\left[m + m_4 (1 - K)\right]} \quad \ldots\ldots\ldots\ldots (40)$$

and at ultimate:

$$\frac{P_{ult}}{P_M} = \frac{m_5 + m_6 (1 - K)}{m + m_4 (1 - K)} \quad \ldots\ldots\ldots\ldots\ldots (41)$$

and for (iii), at first yield Eq. 46 applies, and at ultimate:

$$\frac{P_{ult}}{P_M} = \frac{m_7 + m_6 (1 - K)}{m + m_4 (1 - K)} \quad \ldots\ldots\ldots\ldots\ldots (42)$$

The moment ratio at first yield is found from Eq. 11. At the formation of the mechanism, the moment ratio at section 2 is (from Fig. 12)

$$m_4 = 1.0 + \frac{(m_6 - 1)\left(1 - P_{y_2}/P_M\right)}{\left(P_{ult}/P_M - P_{y_2}/PM\right)} \quad \ldots\ldots\ldots\ldots (43)$$

Curvature.—The curvature relationships to be developed are for the critical hinge, which are the first to form, and are expressed in terms of the curvature at first yield.

Case I.—At first yield Eq. 13 applies. For the simple case in the loading range $P_{y_1} < P < P_M$, the moment at section 1 remained constant at M_{y_1}. Now there is an increase in the moment from M_{y_1} to some intermediate-value M_{EP_1}. The moment at section increases to value to M_{y_2}, when the mechanism is first formed.

Consider the beam action of B'C' in Fig. 10 to be made up of two parts: one, the pure cantilever, as for the ideal case, with the incremental load $\left(P = P_{y_1}\right)$ at B', its free end, and the other, a cantilever beam with the incremental moment $\left(M_{EP_1} - M_{y_1}\right)$ applied to its free end. Since B'C' is the completely elastic part of the beam to the right of the hinge, the two actions can be superimposed to achieve the actual behavior of B'C'.

The effect of this incremental moment is to decrease the angle of discontinuity of B' as well as to decrease the deflection at B'. A'B', the elastic part of the beam to the left of the hinge, is subjected to increased curvature as the moment at section 1 increases. The hinge length increases with increasing load, and its value can be determined from a study of the bending moment diagram.

At the formation of the mechanism, proceeding as in the simple case, the expressions for angles and deflections are:

$$\theta_R = \frac{\left(P_M - P_{y_1}\right)(K\,L)^2}{2\,E\,I} - \frac{\left(M_{EP_1} - M_{y_1}\right)K\,L}{E\,I} \quad \ldots\ldots\ldots (44)$$

$$\delta_{i_1} = \frac{\left(P_M - P_{y_1}\right)(K\,L)^3}{3\,E\,I} - \frac{\left(M_{EP_1} - M_{y_1}\right)(K\,L)^2}{2\,E\,I} \quad \ldots\ldots\ldots (45)$$

$$\theta_L = \frac{2\left(P_M - P_{y_1}\right)(K\,L)^3 - 3\left(M_{EP_1} - M_{y_1}\right)(K\,L)^2}{6\,E\,I\,(1 - K)\,L} \quad \ldots\ldots (46)$$

and the incremental curvature is

$$\phi_{i_1} = \frac{\left(P_M - P_{y_1}\right)(K\,L)^2\,(3 - K) - 3\left(M_{EP_1} - M_{y_1}\right)K\,L\,(2 - K)}{H_L\,6\,E\,I\,(1 - K)} \quad \ldots (47)$$

The curvature associated with M_{EP_1}, on the strain-hardening portion of the non-ideal, moment-curvature relationship in Fig. 7, can be thought of as being made up of an entirely elastic curvature due to moment alone, $M_{EP_1}/E\,I$, and a purely plastic hinge curvature.

The curvature ratio at the formation of the mechanism, expressed in terms of the parameters, is:

$$\frac{\phi_{M_1}}{\varphi_{y_1}} = \frac{m_5}{m} + \frac{L\left\{\left[K\,(3 - K)\left(m_5 + 1 - K\right) - 2\,m\right] - 3\left(m_5 - m\right)K\,(1 - K)\,(2 - K)\right\}}{6\,H_L\,(1 - K)^2\,m} \quad \ldots (48)$$

At ultimate load, the curvature ratio becomes:

$$\frac{\phi_{ult_1}}{\phi_{y_1}} - \frac{m_7}{m} + \frac{L\left\{\left[K\,(3-K)\left(m_7 + m_4\,(1-K)\right)\right] - 2\,m - 3\left(m_7 - m\right)K\,(1-K)\,(2-K)\right.}{6\,H_L\,(1-K)^2\,m} \quad \ldots (49)$$

in which $1.0 \leq m_4 \leq m_6$

Case II.—At first yield Eq. 20 applies. In the load range $P_{y_2} < P < P_M$ there is an increase in the resisting moment at the first hinge. Considering only the increment in load beyond that causing first yield, the beam behavior can be separated into two parts. First, as for the simple plastic case, is the simple beam with the differential load $\left(P - P_{y_2}\right)$. To this must be added the effect of the change in moment at the hinge, given by consideration of a simple beam with the differential moment $\left(M_{EP_2} - M_{y_2}\right)$ at its right support. The effect is of course to reduce the curvature and deflection of the beam.

At the formation of the mechanism, the expression for angle, curvature and curvature ratios are as follows:

$$\theta_R = \frac{\left(P_M - P_{y_2}\right)K\,L^2\,(1-K)\,(2-K)}{6\,E\,I} - \frac{\left(M_{EP_2} - M_{y_2}\right)L}{3\,E\,I} \quad \ldots\ldots (50)$$

$$\phi_{i_2} = \frac{\left(P_M - P_{y_2}\right)K\,L^2\,(1-K)\,(2-K) - 2\left(M_{EP_2} - M_{y_2}\right)L}{H_L\,3\,E\,I} \quad \ldots (51)$$

$$\frac{\phi_{M_2}}{\phi_{y_2}} = m_4 + \frac{L}{6\,H_L}\left\{(2-K)\left[m + m_4\,(1-K)\right] - 2\,m_4\right\} \quad \ldots\ldots (52)$$

At ultimate load the curvature ratio is:

$$\frac{\phi_{ult_2}}{\phi_{y_2}} = m_6 + \frac{L}{6\,H_L}\left\{(2-K)\left[m + m_6\,(1-K)\right] - 2\,m_6\right\} \quad \ldots\ldots (53)$$

in which $m \leq m_5 \leq m_7$

Deflections.—

Case I.—At first yield Eq. 24 applies. At the formation of the mechanism the total deflection under the load is found by combining Eq. 24 and Eq. 45:

$$\delta_{M_1} = \frac{4\,P_M\,(K\,L)^3 - P_{y_1}\,K\,(K\,L)^3\,(3-K)^2 - 6\left(M_{EP_1} - M_{y_1}\right)(K\,L)^2}{12\,E\,I} \quad \ldots (54)$$

At ultimate load, the total deflection under the load is δ_{ult_1}, for which an expression may be obtained by substituting $P_M = P_{ult}$ and $M_{EP_1} = M_{ult_1}$ in Eq. 54.

Case II.—At first yield Eq. 26 applies. At the formation of the mechanism, the incremental deflection under the load is the deflection for the simple beam with load $(P_M - P_{y_2})$, less the deflection of the simple beam due to the moment $(M_{EP_2} - M_{y_2})$.

$$\delta_{i_1}\Big| = \frac{(P_M = P_{y_2}) K^2 L^3 (1 - K)^2}{3 E I} - \frac{(M_{EP_2} - M_{y_2}) K L^2 (1 - K)(2 - K)}{6 E I} \quad . . (55)$$

The total deflection under the load is then:

$$\delta_{M_1}\Big| = \frac{4 P_M K^2 L^3 (1 - K)^2 - P_{y_2} K^2 L^3 (1 - K)^2 (2 - K)^2 - 2(M_{EP_2} - M_{y_2}) K L^2 (1 - K)(2 - K)}{12 E I} \quad . . (56)$$

At ultimate load, the total deflection under the load is $\delta_{ult_1}\Big|$ for which an expression may be obtained from Eq. 56 by substituting $P_M = P_{ult}$ and $M_{EP_2} = M_{ult_2}$.

MOMENT AND ROTATION CAPACITIES IN REINFORCED CONCRETE

Analysis of moment and rotation capacities are well established for reinforced concrete.[3,4,5,6,7] The following treatment is based on the usual assumptions:

(1) that concrete stress distribution may be described by the parameters shown in Figs. 13 and 14,
(2) that concrete has no tensile strength,
(3) that strains vary linearly across a section,
(4) that the steel reinforcement is perfectly bonded to the concrete,
(5) that the stress-strain relationship for the steel is known,
(6) that the concrete will crush when a strain ϵ_u, is reached, and the discussion is of course limited to under-reinforced sections.

---

3 "The Ultimate Load-Theory Applied to the Design of Reinforced and Prestressed Concrete Frames," by A. L. L. Baker, Concrete Publications, 1956.

4 "The Ultimate Strength and Deformation of Plastic Hinges in Reinforced Concrete Frameworks," by W. W. L. Chan, Magazine of Concrete Research, Vol. 7, No. 21, November, 1955.

5 "Plastic Hinging at the Intersection of Beams and Columns," by G. C. Ernst, ACI Journal, Vol. 28, No. 12, June, 1957, pp. 1119-1144.

6 "Ultimate Slopes and Deflections—A Brief for Limit Design," by G. C. Ernst, Proceedings, ASCE, Vol. 81, No. 583, January, 1955.

7 "Elastic-Plastic Design of Single Span Beams and Frames," by H. A. Sawyer, Proceedings, ASCE, Vol. 81, No. 851, December, 1955.

Tension Reinforcement Only.—From the usual elementary elastic theory

$$M_y = q_y\, b\, d^2\, f'_c \left(1 - \frac{a'}{3\,d}\right) \quad \ldots\ldots\ldots\ldots\ldots\ldots (57)$$

in which $q_y = \dfrac{p\, f_y}{f'_c}$, a parameter describing the effective percentage of steel,

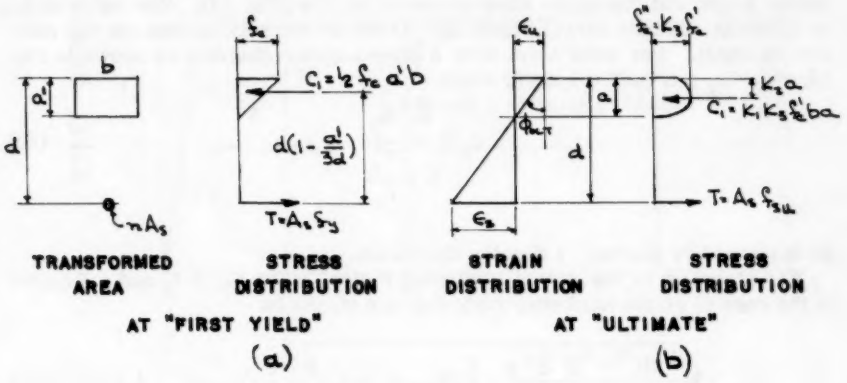

FIG. 13.—TENSION REINFORCEMENT

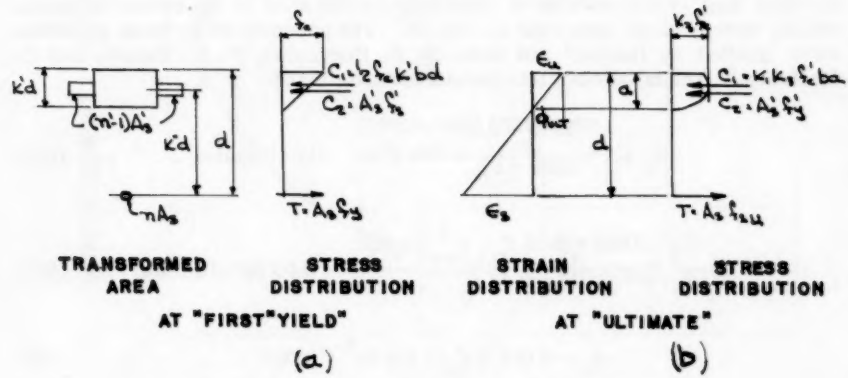

FIG. 14.—TENSION AND COMPRESSION REINFORCEMENT

and the other quantities are defined in Fig. 13. The curvature at the elastic limit is

$$\phi_y = \frac{M_y}{E\, I} \quad \ldots\ldots\ldots\ldots\ldots\ldots (58)$$

Analyses by J. R. Gaston,[8] have shown that the maximum or ultimate resistance of a reinforced concrete beam can be written as

$$M_{ult} = p f_{su} b d^2 \left[1 - \frac{K_2}{K_1 K_3} \cdot \frac{p f_{su}}{f'_c}\right] \quad \ldots\ldots\ldots\ldots (59)$$

in which K_1, K_2, and K_3 are parameters used to describe the concrete stress-strain curve and f_{su} is the steel stress at failure (Fig. 13). The value of f_{su} at ultimate depends largely upon the stress-strain relationship for the reinforcing steel. For mild steel with a stress-strain diagram as shown in Fig. 15, $F_{su} = f_y$ and $q_y \geq q \geq q_o$ in which

$$q_o = \frac{K_1 K_3}{1 + \frac{\epsilon'_o}{\epsilon_u}} \quad \ldots\ldots\ldots\ldots\ldots\ldots (60)$$

as developed by Gaston. ϵ denotes the strain.

For stresses in the strain-hardening region, when $f_{su} > f_y$ and $q < q_o$, or in the case of strain hardening material, the stress is:

$$f_{su} = \sqrt{\frac{E_{SH} K_1 K_3 f'_c \epsilon_u}{P} + \frac{1}{4}\left(E_{SH}\epsilon_u - f_o\right)^2} - \frac{1}{2}\left(E_{SH}\epsilon_u - f_o\right) \ldots\ldots (61)$$

in which E_{SH} is the modulus of elasticity for the steel in the strain hardening region and f_o is as indicated in Fig. 15. The parameters in these equations were studied by Gaston[8] and later by E. Hognestad, N. W. Hanson and D. McHenry.[9] The most complete results indicate that

$$K_1 K_3 = \frac{3900 + 0.35 f'_c}{3200 + f'_c} \approx 0.80 \quad \text{(at ultimate)} \quad \ldots\ldots\ldots (62a)$$

$$\frac{K_2}{K_1 K_3} = \frac{1600 + 0.46 f'_c - f'^2_c/80{,}000}{3900 + 0.35 f'_c} \approx 0.59 \text{ (at ultimate)} \ldots\ldots (62b)$$

$$\epsilon_u = 0.004 - f'_c/6.5 \times 10^6 \not< 0.003 \quad \ldots\ldots\ldots\ldots (63)$$

The curvature at ultimate is

$$\phi_{MAX} = \frac{\epsilon_S + \epsilon_u}{d} \quad \ldots\ldots\ldots\ldots\ldots\ldots (64)$$

---

8 "An Investigation of the Load-Deformation Characteristics of Reinforced Concrete Beams up to the Point of Failure," by J. R. Gaston, C. P. Siess, and N. M. Newmark, C. E. Studies, Univ. of Illinois, No. 40.

9 "Concrete Stress Distribution in Ultimate Strength Design," by E. Hognestad, N. W. Hanson, and D. McHenry, ACI Journal, Vol. 27, No. 4, December, 1955, pp. 455-479.

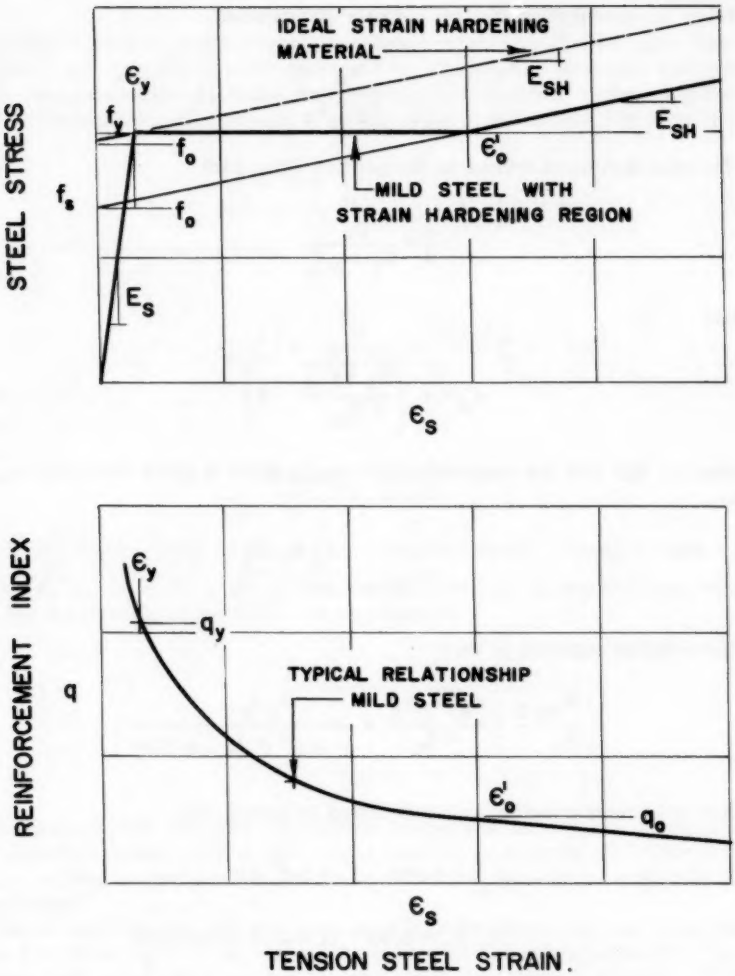

FIG. 15.—TYPICAL REINFORCEMENT CURVES

where ϵ_S and ϵ_u are strains in the steel and concrete, respectively. This, together with the previous expressions would enable ϕ_{MAX}, ϕ_y and their ratio to be determined, though perhaps not readily. For use in plastic design, a simpler approach is essential.

From the assumption of linear strain distribution

$$\frac{a}{d} = \frac{\epsilon_u}{\epsilon_S + \epsilon_u} \quad \ldots\ldots\ldots\ldots\ldots\ldots (65)$$

and for equilibrium of forces on the section (Fig. 13b)

$$\frac{a}{d} = \frac{p\, f_{Su}}{K_1\, K_3\, f'_c} \quad \ldots\ldots\ldots\ldots\ldots\ldots (66)$$

so that

$$\epsilon_S = \epsilon_u \left[\frac{K_1\, K_3\, f'_c}{p\, f'_{Su}} - 1 \right] \quad \ldots\ldots\ldots\ldots\ldots\ldots (67)$$

Introducing this into the expression for ϕ_{MAX} gives a more tractable expression:

$$\phi_{MAX} = \frac{\epsilon_u\, K_1\, K_3}{d\, q_u} \quad \ldots\ldots\ldots\ldots\ldots\ldots (68)$$

and the rotation capacity is then

$$\frac{\phi_{MAX}}{\phi_y} = \frac{\epsilon_u\, K_1\, K_3}{d\, q_u} \times \frac{E_c\, I_y}{q_y\, b\, d^2\, f'_c\, (1 - d/3\, d)} \quad \ldots\ldots\ldots\ldots (69)$$

which may be very considerably simplified by noting that

$$\epsilon_u \not< 0.003 \qquad I_y \approx b\, d^3/12$$

$$K_1\, K_3 \approx 0.80 \qquad (1 - a'/3\, d) \approx 0.875$$

$$E_c \approx 1000 f'_c \qquad q_u \approx q_y$$

thus giving

$$\frac{\phi_{MAX}}{\phi_y} = \frac{1}{4\, q_y^2} \quad \ldots\ldots\ldots\ldots\ldots\ldots (70)$$

For design, Eq. 59 may be approximated as

$$M_{ult} = q_y\, b\, d^2\, f'_c \left[1 - 0.59\, q_y\right] \quad \ldots\ldots\ldots\ldots (71)$$

Combined Tension and Compression Reinforcement.—In this case Gaston[8] has developed expressions for moments of resistance, stresses and strains which, though similar to those just described, are rather more complex and need not be reproduced in detail. The moments of resistance are (Fig. 14)

$$M_y = \frac{f_c\, K'\, b\, d^2}{2}\left[1 - \frac{K'}{3}\right] + A'_s\, f'_s\, K''\, d \quad \ldots\ldots\ldots (72)$$

and

$$M_{ult} = b\, d^2\, f'_c\, q'_u \left[1 - \frac{K_2}{K_1\, K_3}\, q'_u\right] + q'\, f'_y\, K''\, b\, d^2 \quad \ldots\ldots\ldots (73)$$

where

$$q'_u \frac{p\, f_{su} - p'\, f'_y}{f'_c} \quad \ldots\ldots\ldots\ldots\ldots\ldots (74)$$

and p', f'_y, A'_s, f'_s refer to compression reinforcement. Using the same procedure as in the case of simple tension reinforcing, an approximate expression for the curvature ratio may be established:

$$\frac{\phi_{MAX}}{\phi_y} = \frac{1}{5\, q_y\, q'_u} \quad \ldots\ldots\ldots\ldots\ldots (75)$$

TESTS

Outline.—A test program of limited scope was undertaken to supplement the analytical parts of the study. Eight tests were made in all. Two simply-supported single-span beams and six symmetrical two-span continuous beams were tested.

The beams all had a cross-section of 3 in. by 6½ in., and the span lengths were 4 ft. Properties of the various beams tested are given in detail in Table 1. Intermediate grade hi-bond reinforcing steel was used throughout. Tension tests on the steel showed a characteristic stress-strain relationship without a yield plateau, but rather with a tendency to commence strain-hardening immediately after yield. Fig. 16 shows a typical stress-strain curve for the reinforcing steel together with average characteristics for the different sizes used. High early strength Portland cement was used in fabricating the beams. Stress-strain characteristics for a typical concrete speciman are also shown in Fig. 16. Web reinforcement was designed to resist full shear at ultimate load and consisted of simple vertical stirrups made from 1/4-in.- diameter plain mild steel bars.

TABLE 1.—PROPERTIES OF BEAM CROSS SECTIONS

Beam No.	Section	K	b in.	d in.	Steel Tension Bars	Steel Comp. Bars	p	p'	n	n'	q_y	q_u	q_u'	F_c' psi	E_c psi x 10^6
1	1	0.31	3.05	5.21	2-#3	-	0.0143	-	6.85	-	0.100	0.124	-	6200	3.75
	2		3.05	5.55	2-#4	2-#3	0.0224	0.134	8.73	6.85	0.165	-	0.115		
2	1	0.60	3.09	5.46	1-#3	-	0.0068	-	6.00	-	0.052	0.058	-	5700	3.80
	2		3.08	5.50	2-#4	1-#3	0.0223	0.0068	7.40	6.00	0.179	-	0.158		
3	1	0.375	3.03	5.39	2-#3	2-#3	0.0141	0.0140	9.00	8.82	0.153	-	0.073	4000	3.05
	2		3.03	5.30	2-#3	2-#3	0.0140	0.0141	8.82	9.00	0.157	-	0.084		
4	1	0.80	3.08	4.83	3-#3	-	0.0229	-	5.15	-	0.214	0.332	-	4550	5.35
	2		3.05	5.43	3-#4	3-#3	0.0352	0.0206	5.95	5.15	0.343	-	0.215	5500	4.85
5	1	0.50	3.09	5.34	1-#3	-	0.007	-	9.22	-	0.140	0.172	-	2300	3.35
	2		3.07	5.50	2-#3	1-#3	0.0136	0.0070	7.55	9.80	0.183	-	0.156	3400	
6	1	0.75	3.07	5.20	3-#3	-	0.021	-	7.35	-	0.200	0.218	-	4900	3.78
	2		3.08	5.28	4-#3	3-#3	0.0278	0.0208	5.9	5.6	0.256	-	0.124	5000	4.95

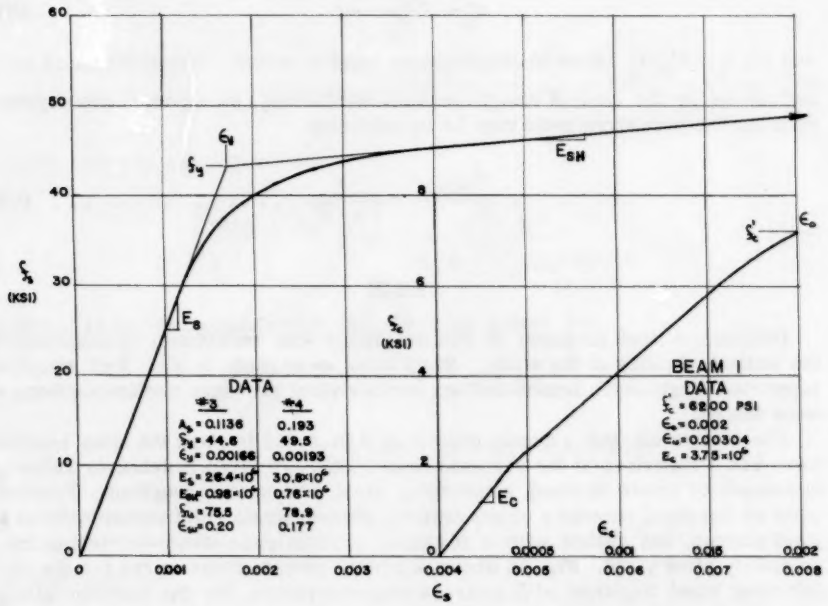

FIG. 16.—STRESS-STRAIN CURVES FOR REINFORCING STEEL AND CONCRETE MIX

The test beams and associated concrete cylinders were moist-cured until the day of their test. Stress-strain curves for the concrete cylinders were obtained with extensometers. In the tests of the continuous beams particular care had to be taken to avoid the introduction of secondary stresses due to uneven supports. In the beam tests the total applied load was measured, and the central reaction was weighed with a very stiff load cell. Strains were measured with gauges on the concrete, and on exposed portions of the reinforcing steel. Deflections were measured with direct-reading dial gauges.

Results.—A detailed study was made of the behavior and mode of failure of each beam. Analyses were made to show the variation with load of strain, curvature, deflection, and position of neutral axis. Figs. 17 and 18 show the results of such analyses for beam number 1, and in conjunction with the characteristics of the materials shown in Fig. 16 permit a precise determination of the mode of failure. Figs. 19 to 24 present comparisons of theoretically derived and observed moment and load ratios for the continuous beams at all stages up to failure. Table 2 provides additional comparative experimental and theoretical information.

A particular problem in the study was the determination of the flexural rigidity of the various cross sections. Computed values of curvature ratios and deflections are, of course, largely dependent on the accuracy of the EI determination. The flexural rigidity may be computed from either the product of the transformed section moment of inertia and the initial tangent modulus, or the gross effective moment of inertia ($b\,d^3/12$). Comparing these values with experimental determinations obtained from initial slopes of moment-curvature diagrams showed considerable scatter between computed and observed results. The analyses given are based entirely on the simple gross moment of inertia combined with the initial tangent modulus of elasticity for the concrete. Although less than entirely satisfactory this is a simple approach for the determination of curvature ratios and deflections, and appears to be as good as any method available.

Examination of the results in Figs. 19 to 24 and Table 2 show satisfactory agreement between derived and observed results. It appears that the theory based upon elastic-strain hardening behavior is more accurate than that based upon ideal elastic-plastic behavior. Results from both theories appear to be conservative, and the simpler theory would appear to be entirely satisfactory as a basis for design. The ability to estimate deflections at first yield seems fairly good, though there was a tendency to underestimate ultimate deflections. This is due in part to the ultimate loads being larger than anticipated. The use of $E\,I = E_c\,(b\,d^3/12)$ seemed also to be quite conservative in generally overestimating required curvature capacities.

APPLICATION OF THEORY

The analyses presented for the propped cantilever with a single concentrated load and the design expressions and charts developed using the ideal elastic-plastic, moment-curvature relationship represent the complete solution of one part of the general problem of a reinforced concrete continuous beam. Similar design expressions and charts can be evolved for other continuous of loading uniformly distributed or varying, for partially loaded spans and for other combinations of loadings.

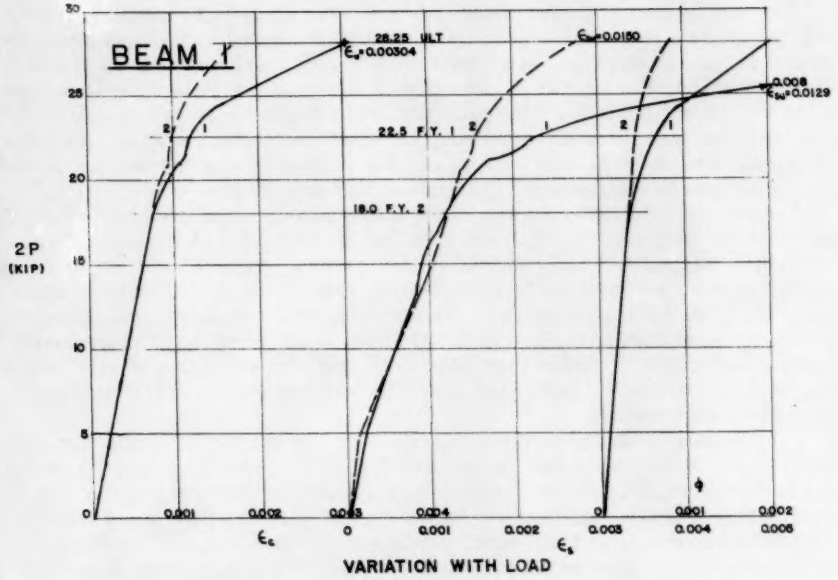

FIG. 17.—CONCRETE AND STEEL STRAIN, CURVATURE

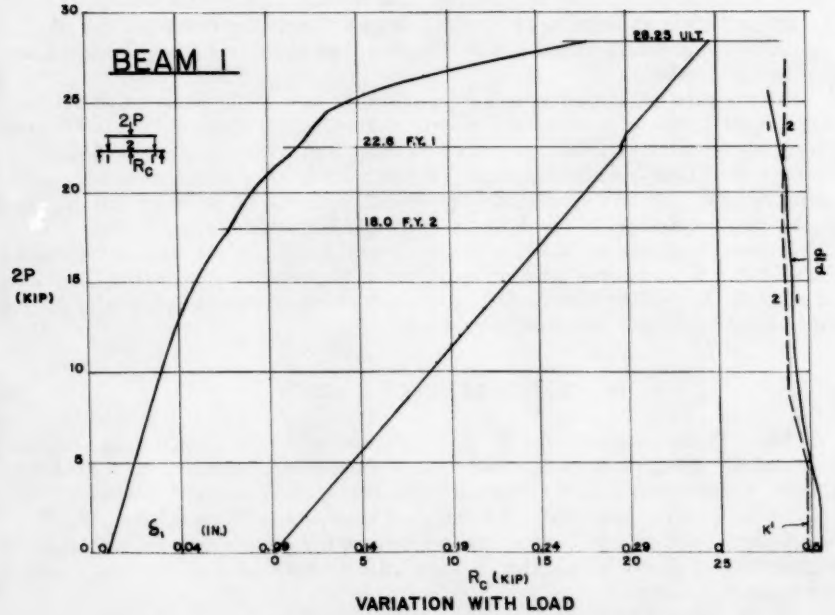

FIG. 18.—DEFLECTION AT 1, CENTER REACTION, AND LOCATION OF NEUTRAL AXIS

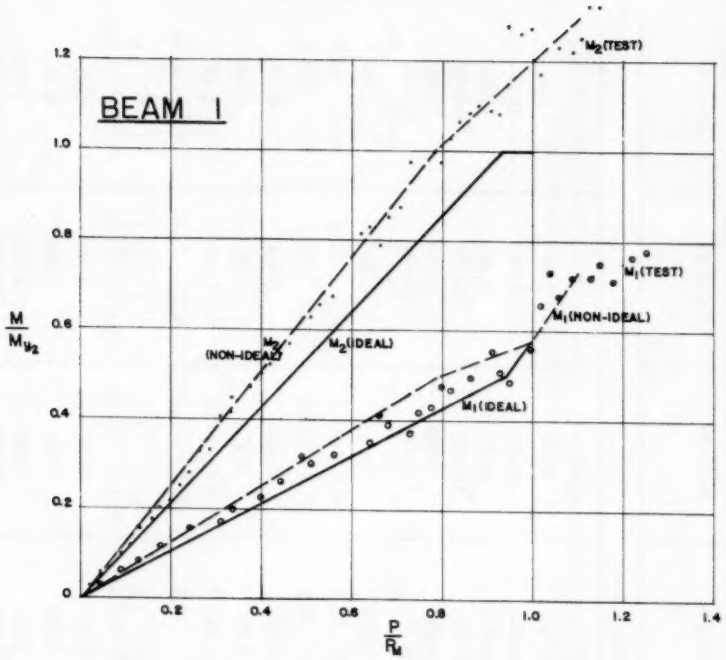

FIG. 19.—MOMENT RATIO VERSUS LOAD RATIO

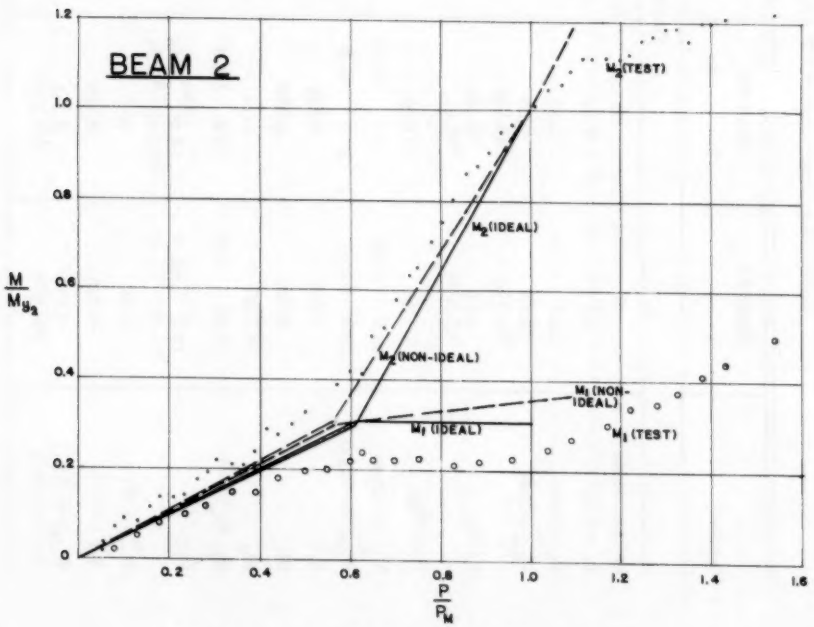

FIG. 20.—MOMENT RATIO VERSUS LOAD RATIO

TABLE 2.—COMPARISON OF EXPERIMENTAL AND THEORETICAL RESULTS

Section	Beam #1		Beam #2		Beam #3		Beam #4		Beam #5		Beam #6	
	1	2	1	2	1	2	1	2	1	2	1	2
Theoretical Results:												
Failure Mode	II		I		II		I		I		I	
P_y (Kips)	9.3		3.02		5.02		8.96		3.39		9.2	
P_M (Kips)	11.8		5.35		8.02		14.4		4.74		10.6	
P_{ult} (Kips)	12.73 [a](9.94)		5.85 [a](4.95)		9.8 [a](6.7)		14.9 [a](11.5)		5.43 [a](4.18)		11.1 [a](10.3)	
P_y/P_M	0.79 [a](0.935)		0.565 [a](0.61)		0.626 [a](0.75)		0.623 [a](0.78)		0.705 [a](0.80)		0.87 [a](0.89)	
P_{ult}/P_M	1.08		1.09		1.22		1.04		1.15		1.05	
M_y (in-Kips)	46.2	80.55	25.0	80.32	46.42	46.0	61.0	141.0	24.9	50.4	69.7	90.3
M_{ult} (in-Kips)	58.5	104.1	29.1	95.3	66.4	69.5	86.0	145.0	31.7	67.1	75.7	110.8
m	0.575		0.312		1.01		0.433		0.495		0.773	
m_7	0.728		0.363		1.45		0.61		0.63		0.84	
m_6	1.29		1.19		1.51		1.03		1.33		1.23	
ϕ_M/ϕ_y	1.16	1.22	12.6	3.3	1.7	2.4	9.0	3.4	2.2	1.7	2.7	1.75
ϕ_{ult}/ϕ_y	10.3 [a](1.2)	1.64 [a](1.4)	16.9 [a](12.8)	4.83 [a](3.3)	28.6 [a](1.7)	4.2 [a](3.0)	10.0 [a](24.8)	5.1 [a](3.4)	4.3 [a](4.1)	12.1 [a](1.7)	3.9 [a](3.9)	6.8 [a](1.75)
δ_{y_1} or δ_1 |	0.03		0.02		0.03		0.03		0.027		0.054	
δ_{M_1}	0.033		0.126		0.052		0.57		0.063		0.29	
δ_{ult_1} or δ_{y_1} |	0.049 [a](0.038)		0.151 [a](0.114)		0.084 [a](0.06)		0.64 [a](0.26)		0.100 [a](0.057)		0.330 [a](0.178)	

Experimental Results

Failure Mode	II	I	II	I	I	I
P_y (Kips)	9.0	3.5	5.75	10.0	3.10	10.0
P_M (Kips)	11.3	5.75	7.38	15.0	4.1	11.8
P_{ult} (Kips)	14.13	8.85	11.7	17.08	4.7	14.38
P_y/P_M	0.797	0.61	0.78	0.667	0.756	0.85
P_{ult}/P_M	1.25	1.54	1.59	1.14	1.15	1.22
M_y (in-Kips)	45.0 78.8	24.5 103.0	46.5 46.0	60.5 138.5	20.6 50.0	71.2 91.2
M_{ult} (in-Kips)	62.3 120.0	51.7 125.5	70.1 98.5	98.5 169.4	27.0 58.8	99.5 110.0
m	0.572	0.238	1.01	0.436	0.412	0.790
m_7	0.792	0.502	1.525	0.71	0.54	1.11
m_6	1.53	1.22	2.14	1.22	1.18	1.22
ϕ_M/ϕ_y	1.6 1.3	5.5 2.1	2.4 1.2	3.5 2.0	2.0 1.2	1.6 1.3
ϕ_{ult}/ϕ_y	2.5 2.5 [b](8.9) [b](10.6)	12.5 9.4 [b](100.0) [b](7.1)	11.6 6.3 (22.2)[b] (15.2)[b]	4.8 4.3 (5.5)[b] (2.7)[b]	3.8 2.2 (12.8)[b] (7.0)[b]	2.9 3.0 (6.3)[b] (6.3)[b]
δ_{y_1} or δ_1 [c]	0.07	0.04	0.05	0.08	0.044	0.09
δ_{M_1} (in)	0.110	0.104	0.08	0.24	0.077	0.129
δ_{ult_1} or δ_{y_1} [c]	0.27	0.45	0.455	0.48	0.125	0.285

[a] Ideal elastic-plastic, moment-curvature relationship. [b] Rotation capacities of cross sections. [c] Deflections in inches.

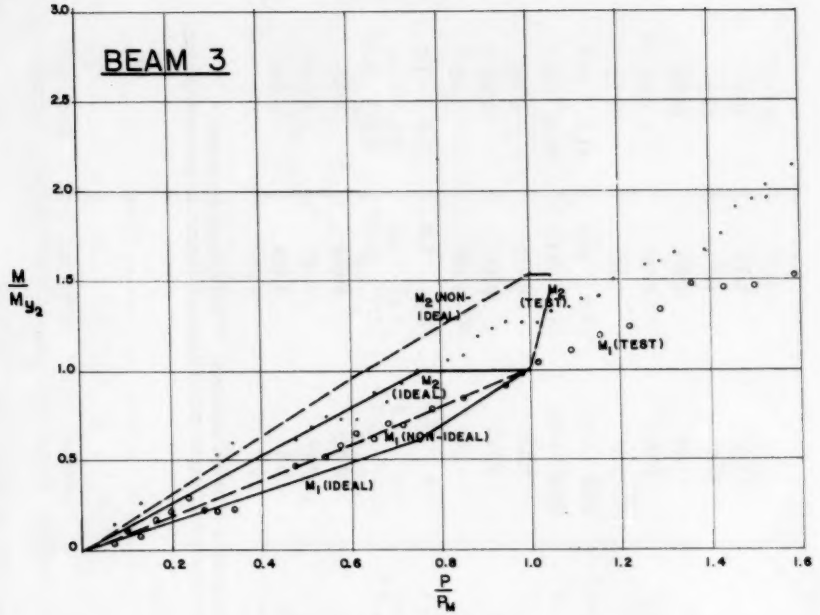

FIG. 21.—MOMENT RATIO VERSUS LOAD RATIO

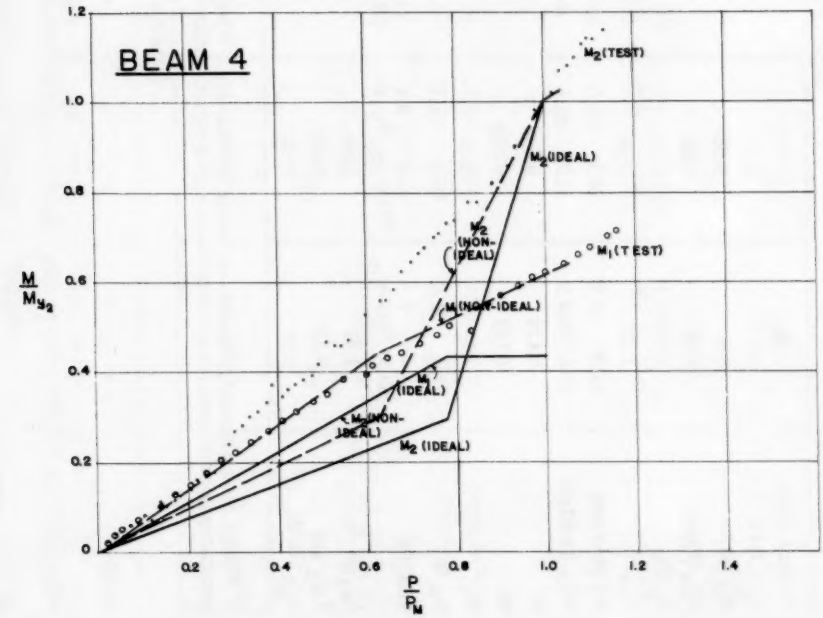

FIG. 22.—MOMENT RATIO VERSUS LOAD RATIO

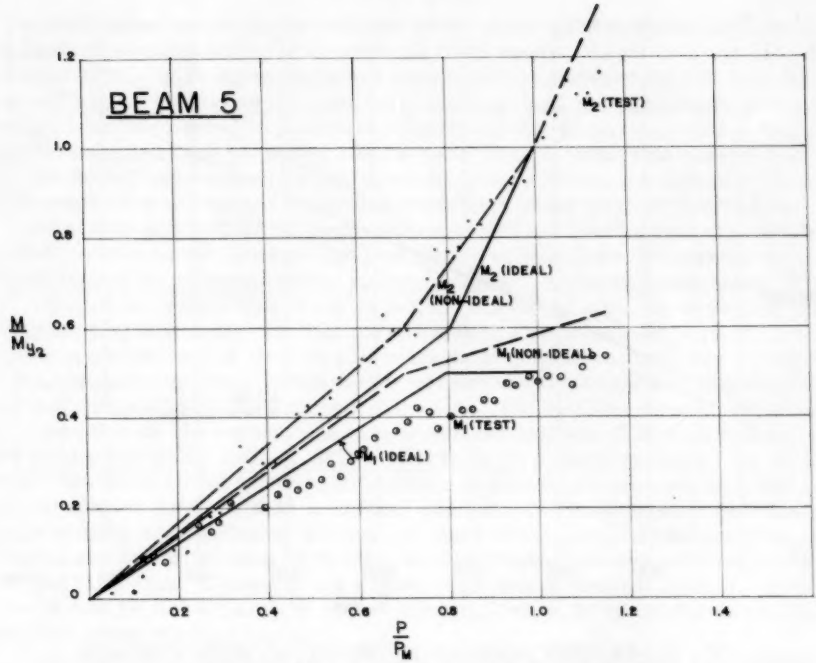

FIG. 23.—MOMENT RATIO VERSUS LOAD RATIO

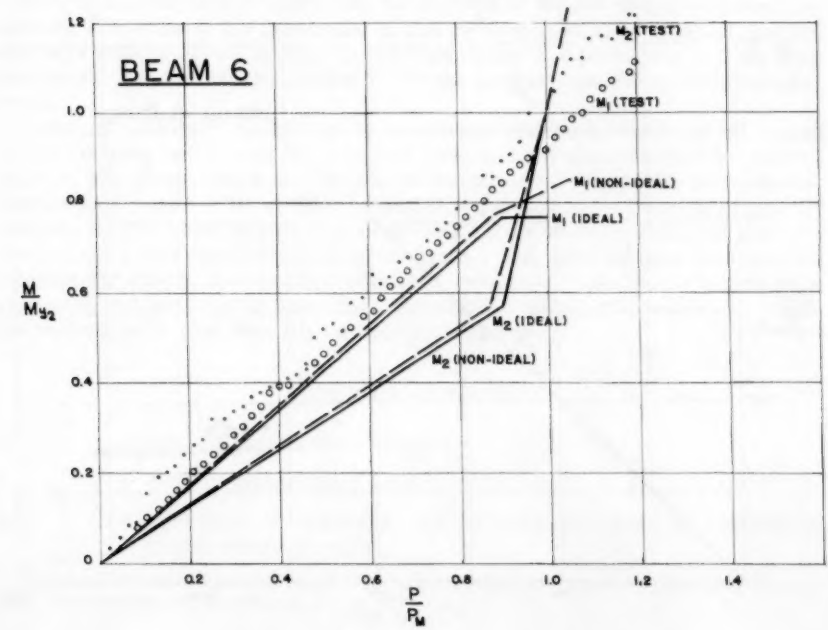

FIG. 24.—MOMENT RATIO VERSUS LOAD RATIO

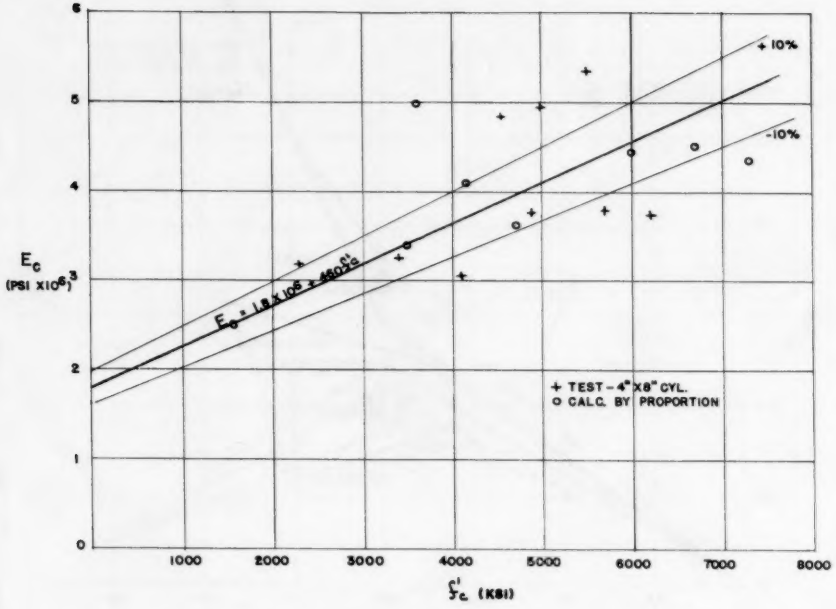

FIG. 25.—TANGENT MODULUS, E_c VERSUS CONCRETE STRENGTH

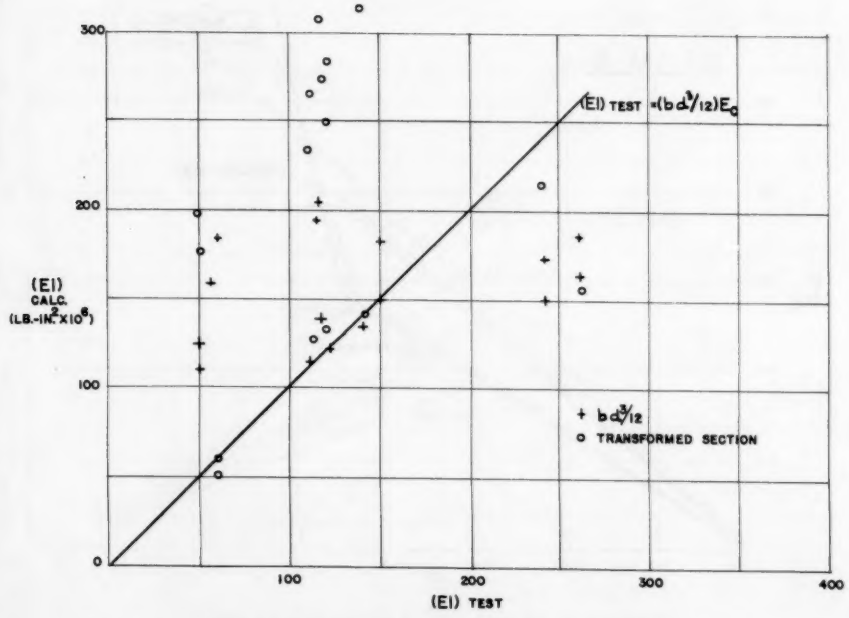

FIG. 26.—CALCULATED VERSUS EXPERIMENTAL FLEXURAL RIGIDITY

A continuous beam can be considered as made up of propped cantilevers (the exterior spans) and fixed or partially fixed beams (the interior spans). A parallel set of design expressions and charts can be developed for the most important loading conditions encountered in the fully fixed and partially fixed continuous beam segments. The design expressions for the fixed beam with a single concentrated load are presented elsewhere.[10] In each particular case of loading, the design expressions or charts would present a complete solution for all of the variables and for the particular continuous beam segment considered.

The design expressions for each beam segment and loading type considered include moment-load relationships that can be written from considerations of elasticity and the collapse bending moment diagram. A consideration of ductility is required to ensure that there is sufficient rotation capacity at each of the early forming hinges in order that the collapse mechanism can be formed. This requires a knowledge of the order in which the hinges are formed. For the case of the propped cantilever with a single concentrated load this simplifies to the critical section at which first yield will occur. The rotation capacity required is a function of the geometry of span length and position of load as well as of the parameter m, the ratio of yield moments at the critical sections. An additional consideration of apparent importance in reinforced concrete is a safety factor against first yield at a critical section. Flexural rigidity decreases quite rapidly as yielding of the tension steel takes place. From the point of view of service or working conditions, working loads should be sufficiently below the yield value to prevent any sudden reduction in flexural rigidity. There should also be some margin of safety against first yield occurring at critical sections under working loads.

The spans, load positions and values of working or design loads are normally known in a continuous beam design problem. The ultimate loads that the structure will be designed for can be arrived at by the use of suitable load factors. The value of the parameter m can be chosen so as to give any desired modes of failure. Thus, making use of Figs. 2 and 3, either Case I, Case II or Mechanism failure can be produced for the propped cantilever that was analyzed.

From a consideration of Fig. 9, or similar diagrams, the required values of the rotation factor and the ratio of first yield to ultimate load are determined. The first yield load can then be computed as well as the safety factor against first yield. The rotation capacity required can be computed from the rotation factor. For design the hinge length can be conservatively taken as being equal to the effective depth of the beam. The moment and rotation capacities for singly and doubly reinforced concrete cross sections have been presented and are used to proportion the critical sections for adequate yield-moment capacity, and ductility or rotation capacity.

APPENDIX—NOTATION

a' = depth of transformed area.

b = width of transformed area.

d = depth from compression face of beam to center of longitudinal tensile reinforcement.

---

10 "Application of Plastic Design Theory to Reinforced Concrete Continuous Beams," by C. Berwanger, M. Sc. Thesis, Queen's Univ., 1957.

E = modulus of elasticity.

E_{SH} = modulus of elasticity in strain hardening region.

f_{su} = steel stress at failure.

f_c = unit compressive stress in concrete.

H_L = hinge length.

I = moment of inertia.

K = increment of length parameter.

K_1, K_2, K_3 = parameters used to describe the concrete stress-strain curve.

L = span length.

M = moment of force.

m = ratio of yield capacities of critical sections.

P = point force.

P_M = load at the formation of a collapse mechanism.

q_y $= \frac{p f_y}{f'_c}$, a parameter describing the effective percentage of steel.

δ = deflection.

ϵ = deformation.

θ_T = total rotation of hinges.

θ_L = angle of rotation at left portion of beam.

θ_R = angle of rotation at right portion of beam.

ϕ = curvature.

Journal of the
STRUCTURAL DIVISION
Proceedings of the American Society of Civil Engineers

SECONDARY STRESSES IN PARALLEL WIRE SUSPENSION CABLES

By Thomas Alan Wyatt[1]

SYNOPSIS

The working stress in a parallel wire cable is normally based on the average stress across a section of the cable. This paper analyzes the variation of stress across the section, caused by deflection of the cable. The influences of clamping bands and of tensioned wire wrapping are considered. Numerical examples show that secondary stresses may be an important part of the effects of live loading.

INTRODUCTION

The advantages of the suspension bridge with parallel-wire cables for long spans are well known, and in a relatively short time considerable advances have been made in the methods of design and analysis. As in other fields this has been accompanied by an increase in the permissible stresses. One of the characteristics of this type of bridge is that the live load has relatively little effect on the tension in the cables which implies that the range of stress in service is low and also that an adequate load factor on the live load may be

Note.—Discussion open until December 1, 1960. To extend the closing date one month, a written request must be filed with the Executive Secretary, ASCE. This paper is part of the copyrighted Journal of the Structural Division, Proceedings of the American Society of Civil Engineers, Vol. 86, No. ST 7, July, 1960.

[1] Asst. Engr., Freeman, Fox and Partners, Cons. Engrs., London, England.

achieved while using a high value of total stress. Another characteristic however, is low stiffness, and the deflections may therefore be large, including, particularly, the change in slope near the supports. In this respect the live loading is proportionately more significant, and thus, the stresses induced in the cable due to bending are of enhanced interest to the designer.

When the cables are "spun" every effort is made to ensure that the stress in each wire is identical. Initially each wire behaves independently and, provided the cable is supported on saddles of suitable radius, the secondary stresses are small. The next stage of construction is to fit the bands to act as attachments for the deck suspenders or hangers. These clamp the wires together and this extra restraint leads to more serious secondary stresses as the dead load of the deck is built up.

Usually, the spun cable is wrapped with wire under tension, and although the transverse stresses set up between the wires are small, the friction stresses thus induced by deformation of the cables are very important. The loads causing deformation after wrapping include all the live load and possibly some part of the dead load.

The most significant feature of the deformation of the cable in respect to secondary stresses is the deflection angle, defined as the change of slope of the line of resultant cable tension. The deflection angle is clearly uniform throughout the length between two adjacent hangers, and it is found that the actual slope of the cable axis is very nearly equal to the slope of the cable tension line except within a very short distance from a hanger band or saddle. The angle between the cable axis and the tension line is, therefore, referred to as the local bending angle. It is convenient to consider the corresponding local bending stresses separately from other secondary effects, although the effect of the band clamping and wrapping on the local bending angle must be taken into account.

The worst conditions of secondary stress normally occur at the tower, probably in the side span if the backstays are loaded. The total secondary stress is then found by combining the effects of the deformation occurring before wrapping the cable (band clamping effect) with the stresses due to deformation of the wrapped cable, and including also the local bending stresses.

Notation.—The letter symbols adopted for use in this paper are defined where they first appear, in the illustrations or in the text, and are arranged alphabetically, for convenience of reference in Appendix I.

LOCAL BENDING STRESSES

The fundamental behavior of a tendon carrying a large axial tensile stress and subjected to bending at one end is shown in Fig. 1. The angle ψ_0 is the rotation of the tangent (say at a clamping band or at the saddle) relative to the direction of the resultant tension. Clearly at any section

$$M = E\,I\,\frac{d^2y}{dl^2} = T\,y$$

from which

$$y = A\,e^{gl} + B\,e^{-gl}$$

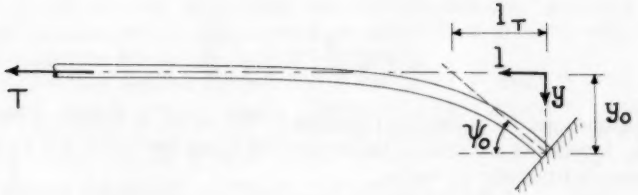

FIG. 1.—BENDING DEFLECTION OF A SIMPLE TENDON

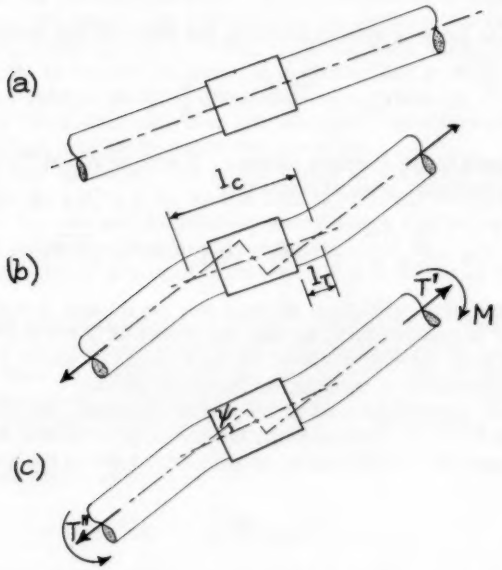

FIG. 2.—RESTRAINT CAUSED BY CLAMPING THE CABLE

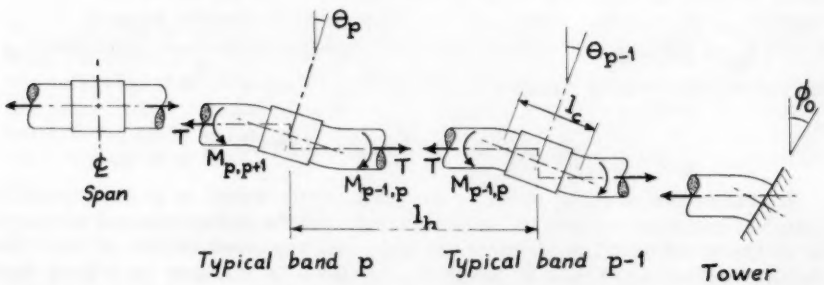

FIG. 3.—DEFLECTED FORM OF CABLE WITH CLAMPING BANDS

where

$$g = \sqrt{\frac{T}{E\,I}} = \frac{1}{k}\sqrt{\frac{f_T}{E}}$$

In these equations T is the total tension in the cable, k refers to the radius of gyration, l denotes the dimension measured along the cable and f_T is the tensile stress (a primary stress).

Determination of the constants from the end conditions shown in Fig. 1 gives

$$y = \frac{\psi_o}{g}\, e^{-gl} \quad \ldots\ldots\ldots\ldots\ldots\ldots (1)$$

and the maximum bending stress (writing the depth of the tendon as 2 h)

$$f_{B1} = \frac{M_o\, h}{I} = \psi_o\, \frac{h}{k}\, f_T\, E \quad \ldots\ldots\ldots\ldots\ldots\ldots (2)$$

in which f_B refers to the bending stress. It will be noted that $y_o = \psi_o/g$ and $l_r = 1/g$. For a circular wire of radius r,

$$g = \frac{2}{r}\sqrt{\frac{f_T}{E}} \qquad \text{and} \qquad f_{B1} = 2\,\psi_o\sqrt{E\,f_T}$$

For a circular wire with $f_T = 40$ tons per sq in. and E = 13,000 tons per sq in., g = 1/9 r approximately, so that for wires of 2 r = 0.196 in. the slope is reduced to 1% of the end value of ψ_o in a length of about 4 in., a distance that is very small indeed in relation to the panel length.

The deflection angle is largest at the end of the span, and the local bending stress is usually limited by supporting the cable on a curved saddle of radius R, say. The stress due to individual bending of a wire to the saddle is clearly

$$f_{B2} = E\,\frac{r}{R} \quad \ldots\ldots\ldots\ldots\ldots\ldots (3)$$

It will be seen that this maximum value does not change with live loading. However, there is a variation of stress to be taken into account when considering fatigue effects, due to the movement of the point where the cable is tangent to the saddle. Normally this movement is closely equal to $R\,\phi_L$, where ϕ_L is the live load deflection angle. Thus, at the farthest point touching the saddle, the bending stress varies from E (r/R) to $e^{-gr\phi_L}\,E\,(r/R)$.

CABLE BAND CLAMPING EFFECT

If there were no cable bands or wrapping, there would be no resistance to "slip" of any wire relative to those adjacent, and the deflections and stresses of all the wires would be identical. In that case, any cross section of the cable deflects without rotation. If, however, the cable is clamped by a band that prevents slip, the effect of the change of slope of the cable tension would be to exert a couple on the band as shown in Fig. 2(b). Some rotation of the band,

therefore, occurs so that the couple implicit in a uniform "primary" stress distribution is reduced and is balanced by redistribution of the axial stress, that is, by moments due to "secondary" stresses.

Owing to the load applied to the cable at the band, T' and T'' (Fig. 2(c) are not equal, and include a small angle. However, in any practical case the difference in magnitude is very small. The "primary" couple may be written, to a close approximation, as $T\ L_c\ \theta$, where θ is the mean of the values of ψ at the two sides of the bands. That is, θ is defined as the net rotation of the cable band relative to the bisector of the lines of cable tension in the adjacent panels. The effective length, l_c of the clamping band is seen to be increased by lengths l_T due to local bending. Thus, l_c = actual length of band plus $2/g$.

The analysis of cable band calmping for an unwrapped cable is most commonly required for the dead loading. As the dead load is usually almost uniform throughout the span, the deformation is uniform "curvature" with the deflection angle changing by $\phi_B = 2\ \phi_1$ (n-1) at each band, where ϕ_1 is the angular deflection in the end panels. It is convenient to write $\phi_o = n\ \phi_1$ (n-1) or $\phi_B = 2\ \phi_o/n$. The analysis is simplified by considering the deformation in two steps. It is found that each step has a linear load-deformation relation so that the total effect may be found by superposition.

Firstly, the end cross section of the cable at the tower is made to rotate through an angle $\phi_o = \phi_1 + \frac{1}{2}\ \phi_B$ as the load is applied. At this stage the relative rotation of the two end sections of every panel (including the end panels) is ϕ_B, so that there is a uniform sagging moment $M_s = -\ G\ \phi_B = -2\ G\ \phi_o/n$. There is no rotation of any band relative to the bisector of the directions of cable tension.

Secondly, the end of the cable is returned to its true attitude by applying an equal and opposite rotation ϕ_o without further deflection of the cable. The behavior in this stage is shown in Fig. 3, where, for clarity, the direction of the cable tension has been drawn horizontal throughout. The resultant action of the stress in a typical panel is represented by the tension T plus a moment $M_{p,p+1}$.

For the equilibrium of band p

$$T\ l_c\ \theta = M_{p-1,p} - M_{p,p+1}$$

From the relative rotation of the ends of the panel p-1,p

$$M_{p,p-1} = G\ (\theta_{p-1} - \theta_p)$$

The equations of this type for each panel may be solved as a recurrence relation. It is found in practice that the values of θ decrease rapidly away from the ends, and the influence of one end on the bending effect originating from the other end of the span is quite negligible. For example, the effective stiffness of the cable to the left of any band near the right hand end may, therefore, simply be defined by a coefficient S such that $M_{p,p+1} = S\ \theta_p$, from which

$$\left.\begin{aligned} T\ l_c\ \theta_p &= S\ \theta_{p-1} - S\ \theta_p \\ S\ \theta_{p-1} &= G\ \theta_{p-1} - G\ \theta_p \end{aligned}\right\} \quad \ldots\ldots\ldots\ldots\ (4)$$

Writing $\lambda \equiv \dfrac{T\ l_c}{2\ G} = \dfrac{f_T\ l_c\ l_h}{2\ E\ k^2}$ and $K \equiv \dfrac{\theta_p}{\theta_{p-1}}$

the solution obtained is

$$K = 1 + \lambda - \sqrt{\lambda\,(\lambda + 2)} \quad \ldots\ldots\ldots\ldots\ldots \quad (5)$$

For the first panel $\theta_o - \theta_1 = (1\text{-}K)\,\phi_o$. The maximum secondary strain is a $(\theta_o - \theta_1)/l_h$, from which the secondary stress, including the sagging deformation of the first step, is

$$f_{B4} = \left(1 - K - \frac{2}{n}\right)\frac{E\ a\ \phi_o}{l_h} \quad \ldots\ldots\ldots\ldots \quad (6)$$

With the normal order of numerical values the "damping" is very rapid ($K < \frac{1}{2}$) and the effect of the first step (the n term) is small, so that this solution could also be used for live load deformation of an unwrapped cable.

SLIP THROUGH HANGER BANDS

The difference between the stress in adjacent panels in each wire corresponding to the change of moment, $T\,l_c\theta$, is supplied by friction stresses action within the cable band length. It is assumed that due to the clamping pressure there is a limiting friction stress, $\mu_c\,P_c/a$, where P_c is the clamping force per unit length on each side of the band and μ_c is the coefficient of friction within the band. It is shown in Appendix II that there is thus a limiting maximum possible change of moment of approximately $6\,a\,l_c\,\mu_c\,P_c$.

The coefficient of friction, μ_c, in this expression is difficult to estimate because the effect of the local constriction of the cable is to increase the friction considerably above the normal value applicable when the transverse pressure is uniform over a large area (as for example in a wrapped length of cable). The value $\mu_c = 0.60$ has been suggested.

If there is no slip at the band the maximum change of moment is $(1\text{-}K)^2\,G\,\phi_o$ at the band nearest the tower. This value may, however, in a practical case, be as much as four times the limiting moment $6\,a\,l_c\,\mu_c\,P_c$. It is convenient to use a parameter υ defining the "effectiveness" of the band clamping, such that

$$\upsilon = \frac{6\ a\ l_c\ \mu_c\ P_c}{(1 - K)^2\ G\ \phi_o} \quad \ldots\ldots\ldots\ldots\ldots \quad (7)$$

The rotation relative to the line of tension of a section of the cable at the band farthest from the tower at which slip occurs may be written as $\upsilon^1\,\phi_o$, where clearly $\upsilon^1 \leq \upsilon$.

Treating the deformation in two stages as before, there is no tendency to slip in the first stage. In the second step the moment is applied to rotate the end section through an angle ϕ_o to return to its initial inclination. The moment thus caused in each panel of the cable is shown graphically in Fig. 4. The area of this diagram corresponds to the relative rotation of the cable cross-sections. Thus, because the tower and the farthest band at which slip occurs the change of rotation is $N\,(1\text{-}k)\,\upsilon^1\,\phi_o + \frac{1}{2}\,N\,(N+1)(1\text{-}K)^2\,\upsilon\,\phi_o$, which is by definition equal to $\phi_o - \upsilon^1\,\phi_o$. Therefore,

$$\upsilon^1\{1 + N(1 - K)\} + \upsilon \cdot \tfrac{1}{2}N(N+1)\ (1\text{-}K)^2 = 1 \quad \ldots\ldots\ldots \quad (8)$$

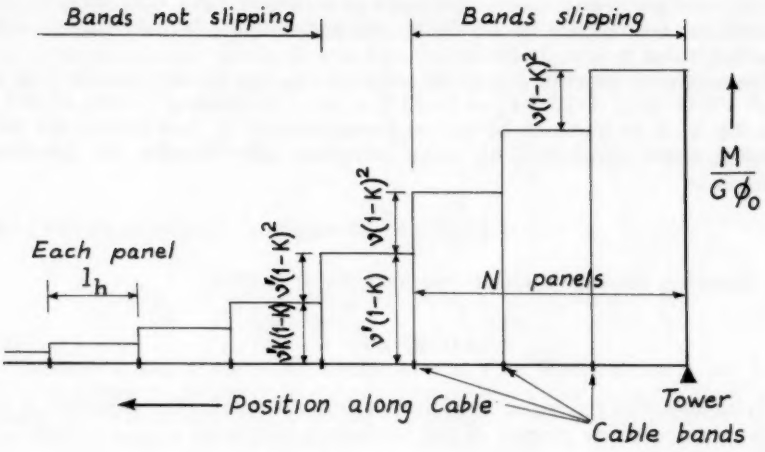

FIG. 4.—CABLE BAND CLAMPING EFFECT

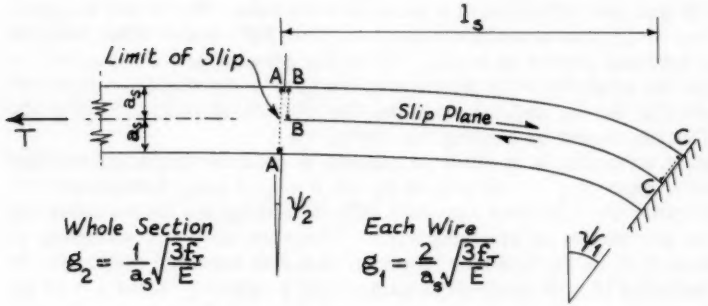

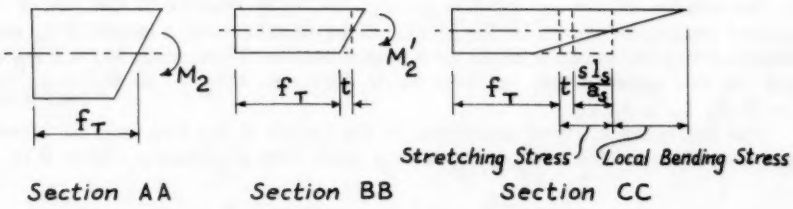

FIG. 5.—BENDING AND STRESS DIAGRAMS FOR SIMPLIFIED TWO-WIRE CABLE

In the above expressions N is the number of bands at which slip occurs, and is thus clearly an integer. The range of values of υ for each value of N is obtained by investigating the condition that an additional band is about to slip: namely, placing $\upsilon = \upsilon^1$ in Eq. 8.

The maximum moment due to the end effect ϕ_o is reduced from (1-K) G ϕ_o to $\{\upsilon^1 + N\,(1-K)\,\upsilon\}$ (1-K) G ϕ_o or (1-K) G ϕ_o say. Evaluating γ using υ^1 and N from Eq. 8, it is found to be almost independent of K (and thus of the band clamping effect parameter, λ), and a sufficient approximation for practical purposes is

$$\gamma = 1 \cdot 0 + 0 \cdot 27 \log_e \upsilon \quad \ldots\ldots\ldots\ldots\ldots \quad (9)$$

The maximum secondary stress (compare Eq. 6) is thus,

$$f_{B5} = \left\{ \gamma\,(1-K) - \frac{2}{n} \right\} \frac{E\,a\,\phi_o}{l_h} \quad \ldots\ldots\ldots\ldots\ldots \quad (10)$$

It will be seen that the reduction of stress is fairly small. For example, if the clamping force is one quarter of that necessary to prevent slip, $\gamma = 0.63$.

SECONDARY STRESSES DUE TO FRICTION BETWEEN WIRES

It is clear from the diagram illustrating the cable band clamping effect (Figs. 3 and 4) that the deflection of a parallel wire cable that is not wrapped, causes rotation of any cross section relative to the cable axis. Thus, there is slip between adjacent layers of wires. When the strands are compacted and bound together by wrapping with wire under tension, transverse stresses are set up between the wires, and the stresses due to friction radically alter the stress distribution caused by bending the cable.

The effect of wrapping is treated as causing a possible uniform, limiting friction-shear-stress of $s = 1.25\,\mu\,t_w/a\,d_w$ or $s = t_w/4\,a\,d_w$ assuming a coefficient of friction $\mu = 0.20$ (see Appendix III). d_w and t_w are the diameter and tension forces per strand of wrapping wire. The wire used for wrapping is commonly about 0.15 in. in diameter (9 gauge) in a soft annealed condition. In such a case the value of s is small—for example for a cable of radius a = 12 in. wrapped with wire, $d_w = 0.15$ in. at a tension of $t_w = 250$ lb. (stress about 7 tons per sq in.), the limiting friction shear stress s = 0.015 tons per sq in.

The analysis is best approached by considering a cable in which only one slip plane is allowed. For simplicity the cable is taken to be square made up of two similar rectangular wires each of size a_s by 2 a_s. The deformation due to the rotation of the end section through an angle relative to the line of resultant tension is shown in Fig. 5(a). Slips occurs over a length of l_s only, beyond which the cable behaves as a single tendon. Thus, at A, $M_2 = T\,\psi_2/g_2$, and in the upper wire, at section B adjacent, $M^1{}_2 = T\,\psi_2/8\,g_2$ and $t = 3\,\psi_2\,f_T/2\,a_s\,g_2$.

The deflected form of the wires in the length of the slip may be investigated similarly. The bending moment in each wire at distance l from B is

$$M_l = E\,I\,\frac{d^2y}{dl^2} = M_2^1 - s\,l\,a_s^2 + 2\,a_s^2\,f_T\,y,$$

where y is the deflection, since factors tending to cause bending of the two wires in opposing directions must be compensated for by transverse reactions between the wires, because the deflections are equal. These transverse forces are sufficiently small for their effect on the friction stress to be neglected.

By integration of the moment equation, writing $2\,a_s^2\,f_T/E\,I = g_1^2$,

$$y = C_1\,e^{g_1 l} + C_2\,e^{-g_1 l} - \frac{M_2^1}{2\,a_s^2\,f_T} + \frac{s\,l}{2\,f_T} \quad \ldots\ldots\ldots (11)$$

and from the conditions $\left(l = 0,\ y = 0,\ \frac{dy}{dl} = \psi_2\right)$ and $\left(l = l_s,\ \frac{dy}{dl} = \psi_1\right)$,

$$4\,\psi_1 = \left(3\psi_2 - \frac{s}{f_T}\right)e^{g_1 l_s} + \left(\psi_2 - \frac{s}{f_T}\right)e^{-g_1 l_s} + \frac{2}{f_T} \quad \ldots\ldots (12)$$

Between B and C the mean stress in each wire varies linearly due to the friction stress s, as shown in Fig. 5. The condition that B is the limit of the length over which slip occurs is that the strain of the middle fiber of the upper wire (relative to the lower wire) corresponds to the relative rotation $(\psi_1 - \psi_2)$ of the sections B and C. Thus,

$$\left(f_T + t + \frac{1}{2}\frac{s\,l_s}{a_s}\right)\frac{l_s}{E} - \left(f_T - t - \frac{1}{2}\frac{s\,l_s}{a_s}\right)\frac{l_s}{E} = a_s\,(\psi_1 - \psi_2)$$

whence, substituting for t and rearranging in terms of $g_1 l_s$,

$$\frac{s}{3\,f_T}\left(\frac{g_1\,l_s}{2}\right)^2 = \psi_1 - \psi_2\left(1 + \frac{g_1\,l_s}{2}\right) \quad \ldots\ldots\ldots\ldots (13)$$

Eliminating ψ_2 from Eqs. 12 and 13

$$\left\{3\,e^{g_1 l_s} + e^{-g_1 l_s}\right\}\left\{1 - \frac{s}{3\,f_T\,\psi_1}\left(\frac{g_1\,l_s}{2}\right)^2\right\}$$

$$= \frac{s}{f_T\,\psi_1}\left\{e^{g_1\,l_s} + e^{-g_1\,l_s} - 2\right\}\left\{1 + \frac{g_1\,l_s}{2}\right\} \quad \ldots\ldots (14)$$

This equation may be solved for l_s by successive approximation. However, if $g_1 l_s$ is a large number, first retaining the $e^{g_1 l_s}$ terms only,

$$1 + \frac{g_1\,l_s}{2} + \left(\frac{g_1\,l_s}{2}\right)^2 = \frac{3\,f_T\,\psi_1}{s}$$

and further

$$\frac{g_1\,l_s}{2} \doteq \frac{3\,f_T}{s} \qquad \text{or} \qquad l_s = a_s\sqrt{\frac{E\,\psi_1}{s}} \quad \ldots\ldots\ldots (15)$$

Thus great simplification is possible when $3\,f_T\,\psi_1/s$ is larger than approximately 100.

Examining the significance of these approximations it will be seen from Eq. 11 that the effect of the exponential or local bending terms is limited to very short regions at the two ends of the slipping length. From Eq. 12 the slope at the end of the slip (B) is $\psi_2 = s/3\ f_T$, whereas for the major part of the slipping region the slope is uniform $\frac{dy}{dl} = \frac{s}{2f_T}$. These angles are thus very small compared with the end deflection. Lastly, it will be seen that the greatest variation of stress where no slip occurs is also small compared with the stress changes along the slip. $\left(\frac{s\ l_s}{a_s}\right) \Big/ 2\ t = \frac{3\ f_T}{s}$

The secondary stress may be regarded as the sum of the "stretching" stress (Fig. 5b)

$$f_{B6} = \frac{s\ l_s}{a_s} = \sqrt{s\ E\ \psi_1} \quad \ldots\ldots\ldots\ldots\ldots\ldots (16)$$

plus the local bending stress for each wire due to rotation ψ_1, determined separately as previously described.

MULTI-WIRE WRAPPED CABLE

These simplifications may now be applied to a cable of square section (side $2\ a_s$) made up of 2q layers of wire each of thickness $2\ r$ and effective area $2\ r\ 2a_s\ j$, as shown in Fig. 6.

A typical element of this cable at l_p from the end is shown in Fig. 7. 2rp is the depth of the region over which slip is not occurring and, thus, between A and B the stress is uniform. Since slip is taking place to the right of B, equal and opposite forces act on both faces of layer $(p + 1)$ and the stress remains the same as on section AB. The stress on section CD, and thus in layer (p) to the right of D, is greater however due to the friction force of $\left[2\ a_s \left(l_p - l_{p-1}\right) S\right]$ on the slip surface between B and D.

The difference in stress between layer (p) and layer $(p + 1)$ is thus

$$\delta f = \frac{2\ a_s \left(l_p - l_{p-1}\right) s}{2\ a_s\ 2r\ j\ p}$$

The corresponding difference between the extension of the middle fibers of these layers must be equivalent to the end rotation ψ_1. Thus,

$$\frac{\left(l_p - l_{p-1}\right)s}{2\ r\ j\ p} \quad \frac{\left(l_p + l_{p+1}\right)}{2} \quad \frac{1}{E} = 2\ r\ \psi_1$$

$$l_p^2 = l_{p-1}^2 + 8\ p\ r^2\ j\ E\ \psi_1/s \quad \ldots\ldots\ldots\ldots (17)$$

This equation applies for all values of p from 1 to (q-1). For the center layers it can similarly be shown that $l_q^2 = l_{q-1}^2 + 4\ p\ r^2\ E\ j\ \psi_1/s$.

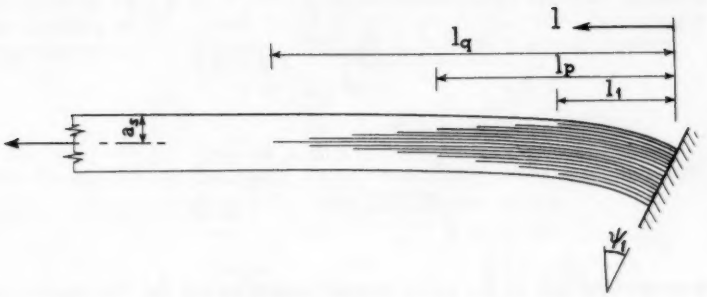

FIG. 6.—BENDING OF MULTI-WIRE CABLE

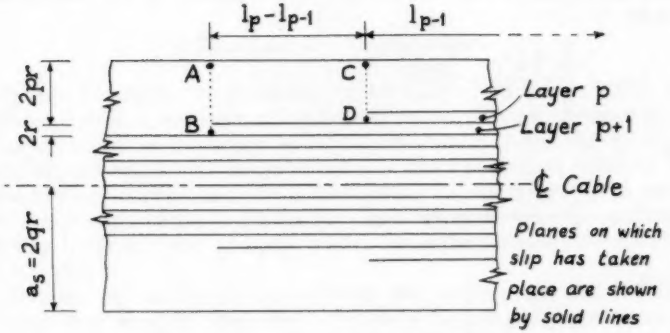

FIG. 7.—TYPICAL ELEMENT OF MULTI-WIRE CABLE

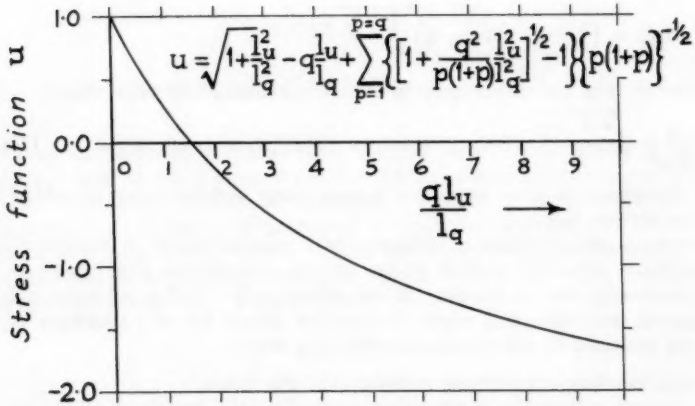

FIG. 8.—REDUCTION OF STRESS BY OMISSION OF WRAPPING FROM THE REGION ADJACENT TO THE TOWER

The solution of these equations is thus

$$l_q^2 = \frac{4\,r^2\,E\,j\,\psi_1}{s}\left\{\sum_{p=1}^{p=q} 2\,p - q\right\}$$

$$l_q^2 = \frac{a_s^2\,E\,j\,\psi_1}{s}\left\{q\,(q+1) - q\right\}$$

$$l_q = a_s\sqrt{\frac{E\,j\,\psi_1}{s}} \qquad \ldots\ldots\ldots\ldots\ldots\ldots \quad (18)$$

It will be noted that this is the same overall length as for the two-layer cable.

The secondary "stretching" stress is obtained as the sum of the changes of stress from layer to layer, starting from the central layers of the cable. Thus, the maximum stretching stress, which occurs in the outermost layer, is given by

$$f_{B7} = \sum_{q}^{1} \frac{s\left(l_p - l_{p-1}\right)}{2\,j\,r\,p}$$

in which

$$l_p^2 = \frac{a_s^2}{q^2}\,\frac{E\,j\,\psi_1}{s}\,p\,(p+1)$$

Therefore,

$$f_{B7} = \frac{s\,E\,\psi_1}{j}\left\{\sum_{1}^{q}\left(\sqrt{1+\frac{1}{p}} - \sqrt{1-\frac{1}{p}}\right) - \left(\sqrt{1+\frac{1}{q}} - 1\right)\right.$$

Thus,

$$f_{B7} = \left(1 \cdot 02 + \log_e q\right)\sqrt{\frac{s\,E\,\psi_1}{j}} \qquad \ldots\ldots\ldots\ldots\ldots\ldots \quad (19)$$

The error in this approximation to the sum required is very small, being of order $\frac{1}{16\,q^2}\sqrt{\frac{s\,E\,\psi_1}{j}}$ when q is large. The "local bending" stress (Eq. 2 or Eq. 3 if allowance is to be made for a supporting saddle) must be added to the stretching stress f_{B7}.

A check on the accuracy of this analysis may be made by considering the deflected form actually implied by the stress distribution previously derived. The strain energy due to bending of the wires to this deflected form may then be compared with the total work done on the cable due to secondary effects. Terms not included in the above analysis are due to

(a) local bending originating at the end of the cable,
(b) a smooth curvature of the cable throughout the length of slip, and
(c) local bending originating at the end of the slip.

Item (a) is allowed for by separate computation of a local bending stress that is then added to the stretching stress. Item (b) corresponds to strain energy

due to bending $U_2 = E\, a_s^4\, s^2/96\, j\, l_q\, f_T$. Item (c) may be regarded as similar to the bending at the end of the slip included in the two-layer analysis and leading to stress f, and corresponds approximately to strain energy

$$U_3 = \frac{3\ E\ j\ a_s^4\ \psi_1^2}{4\ l_q} \left\{ \frac{s}{3\ j\ f_T\ \psi_1} \right\}^{3/2}$$

The work done on the cable due to secondary effects as included in the analysis is $U_0 \doteq 2\ E\ a_s^4\ j \psi_1^2 / l_q$. The comparison is thus

$$\frac{U_2}{U_0} = \frac{3}{64} \left(\frac{s}{3\ j\ f_T\ \psi_1} \right)^2 \quad \text{and} \quad \frac{U_3}{U_0} = \frac{3}{8} \left(\frac{s}{3\ j\ f_T\ \psi_1} \right)^{3/2}$$

With typical values $s/3\ j\ f_T\ \psi_1$ is of the order 1/200, so that the accuracy of the analysis may be expected to be satisfactory.

CIRCULAR SECTION CABLE

Results are required, in practice, to be applied to the circular section cable. The analysis is, however, considerably more difficult because the trace of the slip surfaces on the cross section (more strictly defined by the lines joining wires between which there is no slip and which thus form an elastic layer) are curved, convex away from the horizontal diameter. The geometry of the circle is also more complicated, and because the two slip surfaces bounding any layer are not of equal width, the stress changes throughout the length of the layer.

An indication of the difference between the rectangular and the circular sections can, however, be obtained by considering a regular octagonal section, for which a solution may be obtained by arithmetical integration. It must be assumed that the slip surfaces remain plane but this should not cause serious error for the octagon. The results obtained are

$$\text{maximum stress;} \quad f_B = \left(1 \cdot 10 + \log_e q\right) \sqrt{\frac{s\ E\ \psi_1}{j}}$$

$$\text{total length of slip;} \quad l_q = 0 \cdot 86\ a_o \sqrt{\frac{E\ j\ \psi_1}{s}}$$

where $2\ a_o$ is the depth of the section, across flats. The stress is thus very nearly the same as for a square section having the same number of slip surfaces (q). The length of slip is, however, reduced in roughly the proportion that is simply predicted by considering a typical slip plane mid-way between the center of the cable and the top. It is therefore suggested that Eqs. 15 and 16 may be used with sufficient accuracy for the circular cable, taking for the size of the equivalent square cable in Eq. 15,

$$a_s = 0.85\ a \qquad \ldots\ldots\ldots\ldots\ldots\ldots\ (20)$$

INITIAL LENGTH OF CABLE LEFT UNWRAPPED

The maximum secondary stress is reduced if a length of cable adjacent to the tower (l_u for example) is left unwrapped. This case may be analyzed by

the same method. The total length of slip (including the unwrapped length) is given by l_v,

$$l_v = \sqrt{l_u^2 + l_q^2} \quad \ldots\ldots\ldots\ldots\ldots\ldots (21)$$

where $l_q = a_s \sqrt{\frac{E\ j\ \psi_1}{s}}$ as before. It is found that the stress may be expressed as

$$f_{B8} = \left(u + \log_e q\right) \sqrt{\frac{s\ E\ \psi_1}{j}} \quad \ldots\ldots\ldots\ldots\ldots (22)$$

where the factor u is dependent principally on the parameter $q\ l_u/l_q$ as shown on Fig. 8; the line drawn represents a close approximation for any value $l_u < \frac{1}{3}\ l_q$.

EFFECT OF REVERSAL OF DEFORMATION

It has been shown that the behavior of the wrapped cable is governed by $\psi_1^{\frac{1}{2}}$. Successive deformations cannot be treated by superposition and it is also clear that the stretching stresses do not return to zero on removal of the load causing deformation. As the deflection angle is decreased from its maximum value, slip in the reverse direction occurs, starting from the end of the cable. The change of friction stress where the slip is reversed is 2 s, and the previous analysis may be used substituting twice the normal limiting friction stress. If the deflection is varied from ψ_1 to $-\psi_1$ the deflection angle for the reverse slip is $2\ \psi_1$, and it can thus be shown that the reverse slip just covers the initial slip, and that the bending stress also is exactly reversed.

CABLE BAND EFFECT ON WRAPPED CABLE

The rotation ψ_1 of the end cross section of the cable, relative to the cable axis, has been considered without allowance for deformation applied to other points on the cable or for the clamping effect of the bands. In many cases an adequate description of the secondary effects at the tower is thus obtained. However, if the predicted length of slip is longer than about two panel lengths, a modified method of analysis must be used.

A typical panel subjected to bending at the ends causing slip in the same direction is shown in Fig. 9. For simplicity in analysis the stresses, bending moments, and deformation angles are written in non-dimensional form, that is, respectively,

$$f' = \frac{a_s\ j}{l_h\ s}\ f\ , \quad M' = \frac{1}{l_h\ a_s^2\ s}\ M\ , \quad \psi' = \frac{a_s^2\ E\ j}{l_h^2\ s}\ \psi \quad \ldots\ldots (23)$$

The boundary of the slip zone is defined by $z\ a_s$, $d\ a_s$ as shown, so that z and d are also non-dimensional. The definition of ψ_1' is such that in the previous

analysis $l_s = l_h \sqrt{\psi'}$, or $\frac{z\ a_s}{l} = \frac{a_s}{l_h \sqrt{\psi'}}$ (very nearly). Thus, for the point D,

$$d\sqrt{\psi'_R} = 1 - d\sqrt{\psi'_L} \quad \ldots\ldots\ldots\ldots\ldots (24)$$

In the central region, slip extends throughout the panel, so that (for the square cable) the stress in any wire is constant. An example is, at the limiting layer passing through D,

$$f_d = \frac{E\ a_s}{l_h} (1 - d) \left(\psi_R - \psi_L\right)$$

and, using Eq. 24,

$$f'_d = (1 - d)\left(\psi'_R - \psi'_L\right) = \frac{1 - d}{d^2} \left(1 - 2\ d\sqrt{\psi'_L}\right) \quad \ldots\ldots\ldots (25)$$

The stresses outside the central core at the left and right hand ends of the penel respectively (in the upper part of the cable) are approximately

$$f'_L = f'_d - \sqrt{\psi'_L} \log \frac{d}{z}$$

$$f'_R = f'_d + \sqrt{\psi'_R} \log \frac{d}{z}$$

These expressions do not apply for very small z, but the error introduced in the subsequent moment integrals is negligible.

The total moments corresponding to these stress distributions are

$$M'_L = F_1 \left(1 - 2\ d\sqrt{\psi'_L}\right) - d\ (4 - d)\sqrt{\psi'_L} = F_1 - F_2\sqrt{\psi'_L} \ldots\ldots (26)$$

$$M'_R = F_1 \left(1 - 2\ d\sqrt{\psi'_L}\right) + d\ (4 - d)\sqrt{\psi'_R} = M'_L + 4 - d \ldots\ldots (27)$$

where F_1 and F_2 are functions of d only

$$F_1 = \frac{2\ (1 - d)}{d^2} \left(2 + 2\ d - d^2\right), \qquad F_2 = 2\ d\ F_1 + d\ (4 - d) \ldots (28)$$

These equations completely describe the relation between moments and deformation of a typical panel (p). The relation to the next panel to the right (p+1) is

$$_{p+1}\psi'_L = {}_p\psi'_R + \phi'_B \quad \ldots\ldots\ldots\ldots\ldots\ldots (29)$$

$$\left.\begin{aligned} {}_{p+1}M_L &= {}_pM_R + T\ l_c \left({}_p\psi_R + \tfrac{1}{2}\ \phi_B\right) \\ \text{or} \\ {}_{p+1}M'_L &= {}_pM'_R + \frac{4\ f_T\ l_h\ l_c}{E\ a_s^2} \left({}_p\psi'_R + \tfrac{1}{2}\ \phi'_B\right) \end{aligned}\right\} \ldots\ldots\ldots (30)$$

assuming no slip takes place through the band, where ϕ_B is the change in angle between the two panels due to the load applied after wrapping.

Angles ψ_L and ψ_R clearly decrease away from the tower. Provided the friction stress is sufficiently large, in relation to the deformation originating from the hanger loads (that is, compared with ϕ_B), there will be sections of cable over which no slip occurs in the panels remote from the tower. Denoting the panel nearest to the tower for which this is true as panel 1, the bending through angle ψ_R at the end nearer the lower is not affected by deformation of the cable farther from the tower.

Using any trial value for ${}_1\psi'_R$, ${}_1M'_R = 3\sqrt{{}_1\psi'_R}$ (d = 1 in Eq. 27), whence ${}_2M'_L$ may be obtained from Eq. 30 and also ${}_2\psi'_L$ from Eq. 29. The value d_2 for panel 2 is found by solution of Eq. 26 and ${}_2M'_R$ from Eq. 27. The procedure is repeated in succeeding panels until a value of ${}_n\psi_R$ is obtained which exceeds the given end deflection ψ'_1 for which the solution is required. The

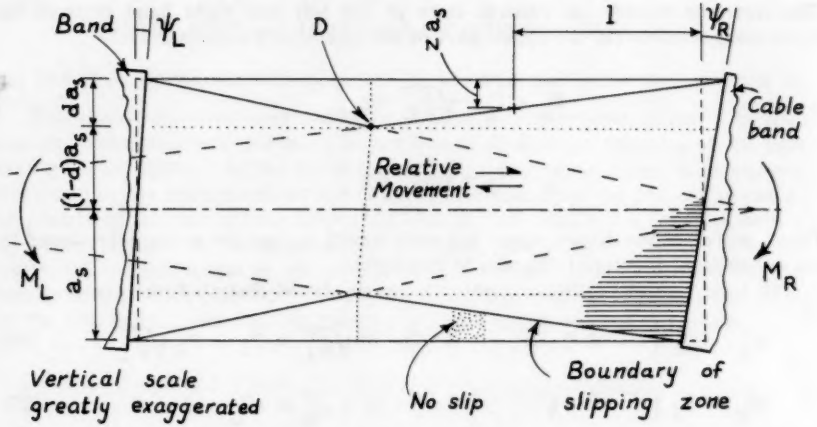

FIG. 9.—LENGTH OF WRAPPED CABLE BETWEEN TWO CLAMPING BANDS

choice of the starting value ${}_1\psi'_R$ may then be improved to obtain the true solution.

The slip regions at the bands that are remote from the tower are increased as the deflection angle at these bands is increased in relation to the friction stress. The method described cannot be strictly applied when there is no starting section at which the cable is entirely unaffected by slip. The analysis of a panel subjected to secondary bending in opposite directions at the ends becomes very difficult if the deformation is so large that the two zones, slipping in opposite senses, meet, because the slip boundaries cannot then simply be defined. It is found, however, that the relation between stress and deformation at the tower is very little affected by conditions three or four panels distant, as would be anticipated from the "exponential decay" nature of the disturbance. If analysis is started from the panel nearest the tower using a trial value for d it is found that the moments or displacements predicted by working away from the tower in successive panels become absurd unless d

(and thus the maximum stress) is correctly chosen within an extremely narrow range. It is, however, easier to work towards the tower, and, in the practical case, any reasonable value of ${}_1M'_R$ can be combined with the trial value of ${}_1\psi'_R$ without invalidating the results.

The maximum stress is obtained from the previous equation for f'_R, modified to apply to the top wire layer. Thus,

$$f'_{B9} = \left(1 - d_n\right)\left({}_n\psi'_R - {}_n\psi'_L\right) + \left(1 \cdot 0 + \log_e d_n\right) q \sqrt{{}_n\psi'_R}$$

which may be written as

$$f_{B9} = \left(1 \cdot 0 \log_e q\right) \sqrt{\frac{s\ E\ \psi_1}{j}} + \frac{l_h\ s}{a_s\ j} f'_c \quad \ldots\ldots\ldots\ldots (31)$$

in which

$$f'_c = \left(1 - d_n\right)\left({}_n\psi'_R - {}_n\psi'_L\right) + \sqrt{{}_n\psi'_R}\ \log_e d_n$$

Thus the increase in stress due to the cable bands is given by f'_c, which is shown plotted against ψ'_1 on Fig. 10 for various values of the band clamping

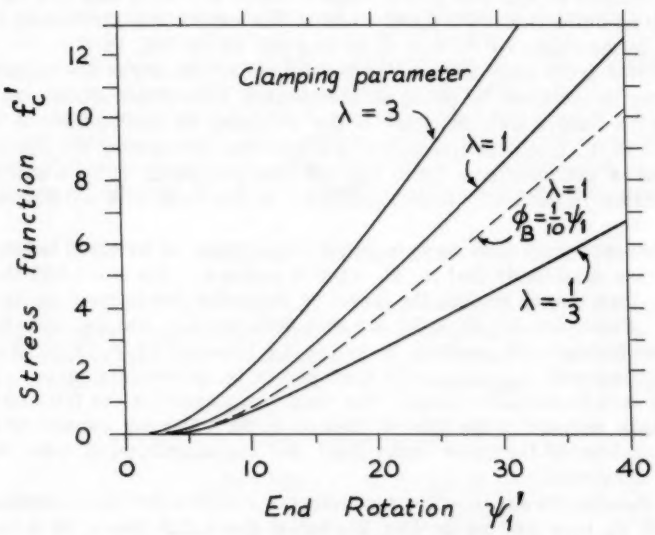

FIG. 10.—INCREASE OF STRESS IN WRAPPED CABLE DUE TO BAND CLAMPING EFFECT

parameter $\lambda = 3\ f_T\ l_h l_c / 2\ E\ a_s^2$. The effect of deformation at the loaded cable bands is indicated by the dotted line, which shows f'_c when the concave-upwards deflection angle at each band is 1/10 of the end deflection (ψ_1 downwards, $\lambda = 1$).

NUMERICAL EXAMPLES

The relative importance of the secondary effects may be shown by reference to a typical long-span bridge with a main span of 3,000 ft and suspended side spans of 1,200 ft each. With two 24 in. cables made up of 0.194-in.-diam wire, the quantities governing the secondary stresses may be taken as: $a = 12$ in., $a_s = 10$ in., $E = 13{,}000$ tons per sq in., $f_T = 35$ tons per sq in. due to dead load or 40 tons per sq in. maximum, $j = 0.8$, $r = 0.097$ in., $q = 60$, and the panel length, $l_h = 60$ ft $= 720$ in.

The analysis will be applied to the side span, for an end deflection due to dead load $\phi_1 = 0.050$ radians (after fixing the clamping bands) plus deflections after wrapping due to live loads and temperature changes of 0.020 radians downwards or 0.015 radians upwards.

Cable Band Clamping Effect.—If the band length, $l_c = 40$ in., the clamping parameter $\lambda = 1.1$ and $K = 0.255$ (Eq. 5), the maximum stress is then $f_{B4} = 7\frac{1}{2}$ tons per sq in. (Eq. 6). The total clamping force $2\, l_c\, P_c$ necessary to prevent slip is 310 tons, determined by placing $\upsilon = 1$ in Eq. 7 (for $\mu_c = 0.6$). It is likely that the actual clamping force would be of this order, since the bands are normally designed for a conservative value of μ_c. If, however, the clamping force is reduced by half, $\upsilon = 0.5$ and $\gamma = 0.8$, the stress is reduced to $f_{B5} = 6$ tons per sq in. (Eq. 9).

Wrapped Cable.—In normal practice the wrapping tension is such that the limiting friction stress s is in the range $0.005 < s < 0.03$ tons per sq. in. For the live load deflection $\psi_1 = 0.020$ radians the respective stretching stresses would be in the range $6\frac{1}{2} < f_{B7} < 16$ tons per sq in. (Eq. 19).

Protection from corrosion in the region where the wires are tangent to the saddle may be obtained by using an independent articulated sheath, as for example on the Golden Gate bridge. If the wrapping is omitted for a distance $l_u = 8$ ft $= 96$ in. from the tower, for $s = 0.03$ the parameter $q\, l_u/l_q = 7$ and the stress is reduced from 16 to $f_{B8} = 8$ tons per sq in. (Fig. 8 and Eq. 22). The reduction is naturally less significant in the case of $s = 0.005$ tons per sq in.

The stresses may also be calculated if the cable is wrapped before application of the dead load; that is, $\psi_1 = 0.070$ radians. For $s = 0.005$ the length of slip is then large, so that the effect of the cable bands must be taken into account. From Eq. 23, $\psi_1' = 29$, so that with $\lambda = 1.1$ and $\phi_B = \psi_1/10$ the stress (excluding local bending) is $f_{B9} = 15\frac{1}{2}$ tons per sq in. (Fig. 13 and Eq. 31), compared with $f_{B4} + f_{B7} = 14$ tons per sq in. previously given. The increase is seen to be quite small. The final value used for the friction stress, s, must take account of the loss of tension in the wrapping caused by the lateral contraction of the cable under load, but the magnitude of this reduction is rather uncertain.

Local Bending Stresses.—The fundamental equation for local bending gives $f_{B1} = 1440\, \psi_o$ tons per sq in. (Eq. 2); but if the cable bears on a saddle of radius R = 20 ft, the stress is limited to $f_{B2} = 5$ tons per sq in. (Eq. 3). It will be noted that $1/g \div 9\, r = 0.9$ in. so that the local bending stress is reduced by a factor of 10 in each 2 in. along the wire. Local bending may also be significant at the first cable band. In the previous example the rotation of the first band, if no slip occurs, is $K\, \phi_o = 0.013$ radians, which, together with the possible coexistant local deformation due to the load at that band, could cause a stress of $f_{B1} = 25$ tons per sq in.

CONCLUSIONS

Secondary Stresses due to Dead Load.—These examples show that the dead load stresses are quite large. The stresses would be considerably reduced by over 40% in the example given) if the band nearest the end of the span was relèased after the remaining bands were loaded. Some relief may occur in this way due to slip caused by the loss of clamping force as the cable contracts laterally on loading: the bolts clamping the bands are normally retightened after most of the load has been applied. A similar reduction would be obtained if the erection procedure was such that the end band was actually fitted while the cable was deflected towards its final position. The local bending effect at the end band may also be counteracted by a relieving radius similar in function to the saddle radius.

Secondary Stresses due to Live Load.—The live load secondary stresses may be of additional importance, since, due to repeated application, their effect on the ultimate strength of the cable may be relatively greater than their actual magnitude, whereas the converse would normally be true of the dead load stresses. For the example considered, taking a typical value for the wrapping s = 0.015 tons per sq in., the maximum stress is 40 + 24 = 64 tons per sq in. (primary and total secondary stresses respectively). The change of "stretching" stress due to the change of deflection from 0.020 radians downwards to 0.015 radians upwards is 20 tons per sq in., and the maximum coexistant change of local bending stress is very nearly 5 tons per sq in. (by the saddle). Allowing also for a 5 tons per sq in. change of primary stress, the total stress may be expressed as $f_1 = 49 \pm 15$ tons per sq in. For a hard-drawn wire of 100 tons per sq in., ultimate tensile stress, this corresponds to a factor of safety of the order of 1.5 against failure due to fatigue. Alternatively, considered in terms of load factor, applying a factor of 1.1 to the dead load primary stresses (which are predictable to a high standard of accuracy), the factor on live loading approaches 2.0 even after application of an additional "factor of ignorance" of 1.5 applied to all the secondary stresses.

ACKNOWLEDGMENTS

The author would like to express his appreciation to the Royal Military College of Science, Shrivenham, England, whose staff he was on at the time this paper was written. It was at the request of Gilbert Roberts, M. ASCE, that the research leading to the preparation of this paper was carried out.

APPENDIX I.—NOTATION

a	radius of cable.
a_s	half length of side of equivalent square section.
E	Youngs Modulus.
f_T	tensile stress (primary stress).
f_B	bending stress (secondary stress).

G flexural stiffness of one panel of cable.

g $= \frac{1}{k}\sqrt{\frac{f_T}{E}} = \sqrt{\frac{\text{Axial force}}{\text{Bending stiffness}}}$.

j ratio of net area to gross area of cable section.

k radius of gyration.

l dimension measured along cable.

l_h panel length: that is, distance along cable between hangers.

L span + $n\ l_h$.

n number of panels.

q $= \frac{a}{2\ r}$

r radius of individual wires of cable.

R radius of saddle at ends of span.

T total tension in cable.

ϕ deflection angle.

ϕ_1 deflection angle in the end panel.

ϕ_o $\phi_1\ n/(n-1)$

ϕ_B difference between the deflection angles in two adjacent panels.

ψ local bending angle.

ψ_1 deflection angle in the end panel due to load applied after wrapping.

θ rotation of cable band relative to tension line (see definition in text description of Fig. 3).

Band Clamping Analysis.

K $= \theta_p/\theta_{p-1}$, factor by which effect diminishes in each panel.

l_c effective length of clamping band (Fig. 3b).

P_c clamping force per unit length each side of band.

λ $= \frac{T\ l_c}{2\ G} = \frac{f_T\ l_c\ l_h}{2\ E\ k^2}$, band clamping parameter.

μ_c coefficient of friction within band.

υ, γ parameters for effect of slip through bands.

Wrapped Cable Analysis.

d_w, t_w diameter and tension force per strand of wrapping wire.

f'_c stress factor for effect of clamping bands.

l_q length of slip.

l_s length of slip in simple two-layer cable.

l_u length of cable adjacent to tower without wrapping.

s equivalent limiting shear stress.

u stress factor for effect of unwrapped length at tower.

μ coefficient of friction in wrapped cable.

APPENDIX II

SLIP THROUGH HANGER BAND

The difference between the stresses in the wires in adjacent panels is supplied by friction within the cable b band length. Considering the forces on the wires indicated by stippling in Fig. 11(a), the change in tension between the ends of the band is denoted by $F_{TA} + F_{TB}$, due to change of the total cable tension and to the secondary stresses respectively, and is equal to the friction force F_S.

The total change in primary tension is W sin β (see Fig. 11(b) where W is the hanger load and sin β is the inclination of the cable to the horizontal. Thus,

$$F_{TA} = W \sin \beta \cdot (\alpha - \sin \alpha \cos \alpha)/\pi .$$

The change in moment is $m = T\, l_c\, \theta$, and as the stress varies linearly across the section,

$$F_{TB} = m \frac{a}{I} \int_{-\alpha}^{+\alpha} j\, a^2 \sin^2 \alpha \cos \alpha \, d\alpha = \frac{8\,m}{3\,a} \sin^3 \alpha$$

It is assumed that clamping the band causes a uniform transverse pressure of P_c/a so that the limiting friction stress may be written $\mu_c P_c/a$. Thus, for slip to occur on the boundary as indicated (that is, with a plane lower surface)

$$F_S = \frac{\mu_c P_c}{a} 2\, a\, l_c\, (\alpha + \sin \alpha) = \frac{W \sin \beta}{\pi} (\alpha - \sin \alpha \cos \alpha) + \frac{8\,m}{3\,a} \sin^3 \alpha$$

The critical boundary is determined by the condition $\frac{dm}{d\alpha} = 0$. In normal practice the factor of safety (C) against slip due to primary forces alone is quite large, and a good approximate solution is then

$$m = a\, l_c\, \mu_c\, P_c \left\{ 5 \cdot 8 - \frac{3 \cdot 2}{C} \right\}$$

in which

$$C = 2\, \pi\, l_c\, \mu_c\, P_c / W \sin \beta$$

This value of m is a slight over-estimate because slip would occur first on a boundary with the lower face convex downwards, but the error is small since

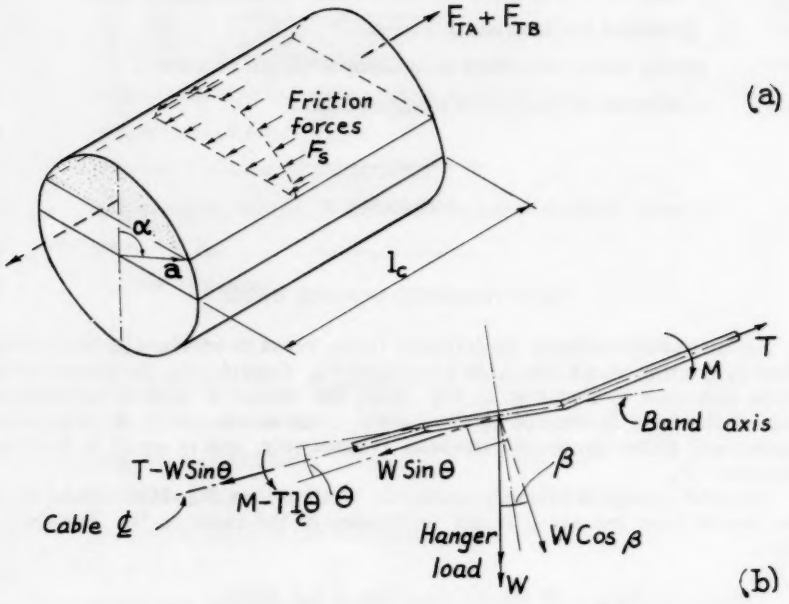

FIG. 11.—FORCES ACTING ON PART OF CABLE WITHIN A CLAMPING BAND

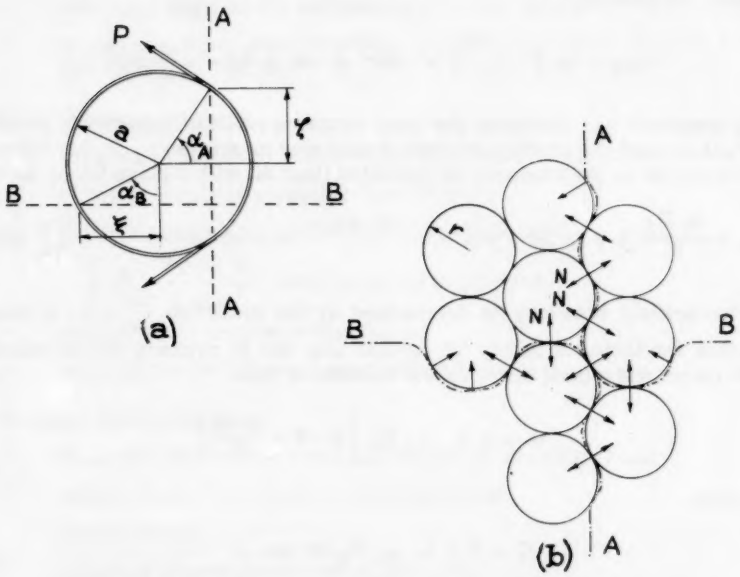

FIG. 12.—TRANSVERSE FORCES BETWEEN WIRES CAUSED BY WRAPPING.

the boundary is shown to be in a region where the stress change in each wire is small.

If the applied moment, M, is greater, some increase of m can still occur. Considering the change of moment as the force transferred across neutral axis (m) times the lever arm, if the stress distribution were to remain linear with the maximum possible force transferred across the axis

$$m = (\pi + 2)\, l_c\, \mu_c\, P_c\, \frac{3}{8}\pi\, a = 6 \cdot 1\, a\, l_c\, \mu_c\, P_c$$

Thus, a reasonable approximation to the behavior of the band is given by the simple relation, that under increasing deflection of the cable the moment change at the band increases linearly with increasing band rotation, θ, up to a limiting value $m = 6\, a l_c\, \mu_c\, P_c$ and thereafter remains constant.

APPENDIX III

LIMITING SHEAR STRESS IN A WRAPPED CABLE

Fig. 12 (a) shows a cable wrapped with a single layer of wire of diameter d_w at a tension t_w. The tangential tension force per unit length of cable is thus $P = t_w/d_w$. The ideal wire packing is shown in Fig. 12 (b).

Considering the vertical section AA, and resolving horizontally,

$$2\, n_A\, N \cos 30° = 2\, P \sin \alpha_A = 2\, P\, \zeta/a$$

where M_A is the number of wires on the section.

The limiting longitudinal friction force on AA is $\mu\, 2\, n_A\, N$, whence the limiting stress is

$$s_A = \frac{1}{2\,\xi}\ \mu \frac{2\, P\, \xi}{a \cos 30} = \frac{2}{\sqrt{3}}\frac{\mu\, P}{a}$$

Similarly for the section BB,

$$s_B = \frac{1}{2\,\xi}\ \mu \cdot \frac{4\, P\, \xi}{a\,(1 + \sin 30)} = \frac{4}{\sqrt{3}}\frac{\mu\, P}{a}$$

The cable with ideal packing is thus slightly anisotropic in this respect. In the practical cable there are also variations of the forces between the wires due to irregular packing. It may be noted that the distance between successive planes of type BB (on which s is a maximum) is larger than between planes of type AA.

Journal of the
STRUCTURAL DIVISION
Proceedings of the American Society of Civil Engineers

VARIOUS INSTABILITY MODES OF THE FIXED BASE COLUMN

By D. A. Sawyer,[1] J.M. ASCE

SYNOPSIS

Equations are presented for the critical buckling load of a column, fixed at its base and loaded at its upper end, under a variety of conditions. The case of the column loaded at its upper end through a frictionless roller is believed to be presented here for the first time. A column loaded at its upper end through a pinned link has appeared rather obscurely in the literature. This case is developed and expanded for comparison with the similar case of loading through a roller. The columns of a lift-slab operation are loaded by hanging links. Equations that have possible application in this field are derived.

INTRODUCTION

The fixed base column exhibits various modes of instability depending on the loading and support conditions at the upper end. Two classic examples are (1) the column fixed at the base and simply supported at the upper, loaded end, and (2) the column fixed at the base and free to translate at the upper, loaded end. Solutions to both of these cases have been known since Euler's time. Timoshenko,[2] as well as many others, has presented complete derivations of the controlling differential equations. The first of these problems leads to a transcendental equation,

Note.—Discussion open until December 1, 1960. To extend the closing date one month, a written request must be filed with the Executive Secretary, ASCE. This paper is part of the copyrighted Journal of the Structural Division, Proceedings, of the American Society of Civil Engineers, Vol. 86, No. ST 7, July, 1960.

[1] Asst. Prof., Dept. of Civ. Engrg., Univ. of Florida, Gainesville, Fla.

[2] "Theory of Elastic Stability," by S. Timoshenko, McGraw-Hill Book Co., Ind., New York, 1936.

$$\tan k\,L = k\,L \quad \ldots\ldots\ldots\ldots\ldots\ldots \quad (1)$$

which has the smallest root, k L = 4.493. The resulting primary buckling load is:

$$P_{cr} = \frac{20.19\,E\,I}{L^2} \quad \ldots\ldots\ldots\ldots\ldots\ldots \quad (2)$$

The second problem has as the solution to its differential equation the relationship:

$$\cos k\,L = 0 \quad \ldots\ldots\ldots\ldots\ldots\ldots \quad (3)$$

This equation has as its smallest root $k\,L = \frac{\pi}{2}$ and the resulting primary buckling load is:

$$P_{cr} = \frac{\pi^2\,E\,I}{4\,L^2} \quad \ldots\ldots\ldots\ldots\ldots\ldots \quad (4)$$

In design-office practice, the situation is sometimes encountered where the use of one or the other of these basic buckling loads is ostensibily required. One such situation is that involving the columns in a lift-slab operation. Another case might arise in a design problem where it is advantageous or necessary to support the expansion end of a bridge girder, or similar structure, on a free-standing column. It is probable that some designers would consider the design quite conservative, if the columns of either condition above were proportioned using the buckling load given by Eq. 4 and modified by some reasonable factor of safety, such as 1.71. Actually, the resulting design may be either grossly conservative or dangerously light, depending on some rather subtle differences in the construction details.

As a first consideration, the free-standing column supporting the expansion end of a structure will be examined. It is considered that the far end of the girder or structure is either simply supported or otherwise fixed against translation. The expansion detail may be a simple sliding plate or, more generally, a detailed sector of a circle. Conceivably, some designers might consider a simple link as the equivalent of the sector of a circle because in many situations the action of a link and a roller are almost identical for small movements. A poorly designed "roller" such as that shown in Fig. 1 might be used here. The sliding plate will not be considered further and attention will be focused on the roller or link designs.

COLUMN SUPPORTING A ROLLER

Fig. 2 shows a fixed-base column supporting a roller of radius m L where L is the length of the column and m is a decimal number, which is usually small. The load is applied vertically through the center of the roller and is restrained by the far-end support conditions of the structure so that it always remains on the same vertical axis. The significance of this is that the load is unable to follow the column laterally if the buckling load causes deflection. Contrast this with the assumptions made in the derivation of the equations leading to Eq. 4. The roller will be assumed ideal and frictionless so that the contact force between the roller and the column head will be on a line that is normal to the plane of contact, that is, it will always be radial to the roller.

In considering the possible buckling modes, it is apparent that the column cannot buckle in a single half wave such as the classic free-standing column.

FIG. 1.—EXAMPLE OF A POORLY DESIGNED ROCKER.

FIG. 2.—THE ROLLER-SUPPORTING COLUMN IN ITS UNDEFLECTED POSITION.

FIG. 3.—THE ROLLER-SUPPORTING COLUMN DEFLECTED IN THE SHAPE OF THE FUNDAMENTAL MODE.

If such an initial deflection occurred, all induced moments would be of a sense to return the column to its straight position. The assumed fundamental buckling shape is that shown in Fig. 3. The contact force between the roller and the column head can be broken into two components—one parallel to the column axis and the other perpendicular to it.

For small deflections, $\cos \phi = 1$ and $\sin \phi = \phi$, approximately. Thus, the force parallel to the column axis is approximated by the vertical force P, whereas the force perpendicular to the axis is approximately $P \phi$. The angle ϕ is the rotation of the roller during buckling and is equal to the slope of the elastic curve at the column head, that is,

$$\phi = - dy/dx \text{ at } x = L \quad \ldots\ldots\ldots\ldots\ldots\ldots \quad (5)$$

Coordinate axes are taken as shown in Fig. 3. The two components of force induce moments in the column as follows:

$$M_x = P (y - R \phi) - P \phi (L - x) \quad \ldots\ldots\ldots\ldots \quad (6)$$

Thus, using small deflection theory, the differential equation is

$$E I \frac{d^2 y}{dx^2} = - M_x = P (R \phi - y) + P \phi (L - x) \quad \ldots\ldots\ldots \quad (7)$$

Letting

$$\frac{P}{E I} = k^2$$

the solution to this differential equation can be written as

$$y = A \cos k x + B \sin k x - \phi x + R \phi + L \phi \quad \ldots\ldots\ldots\ldots \quad (8)$$

The boundary conditions are

$$y = 0, \text{ at } x = 0 \quad \ldots\ldots\ldots\ldots\ldots\ldots \quad (9)$$

$$dy/dx = 0, \text{ at } x = 0 \quad \ldots\ldots\ldots\ldots\ldots\ldots \quad (10)$$

$$y = \delta, \text{ at } x = L \quad \ldots\ldots\ldots\ldots\ldots\ldots \quad (11)$$

$$dy/dx = - \phi, \text{ at } x = L \quad \ldots\ldots\ldots\ldots\ldots\ldots \quad (12)$$

Substitution of boundary conditions 9 and 10 and either 11 or 12 leads to the transcendental equation

$$\tan k L = - \frac{1}{k L (m + 1)} \quad \ldots\ldots\ldots\ldots\ldots\ldots \quad (13)$$

in which $R = m L$.

The roots to this equation vary with the value of m. The critical buckling load is given by

$$P_{cr} = \frac{(k L)^2 E I}{L^2} \quad \ldots\ldots\ldots\ldots\ldots\ldots \quad (14)$$

The value of $(k L)^2 = N$, for various magnitudes of m, is plotted on Fig. 4. It is interesting that the buckling load for this condition varies from 3.17 to 3.29 times the buckling load for the classic free-standing column (Eq. 4) for a range of m values from 0 to 0.14.

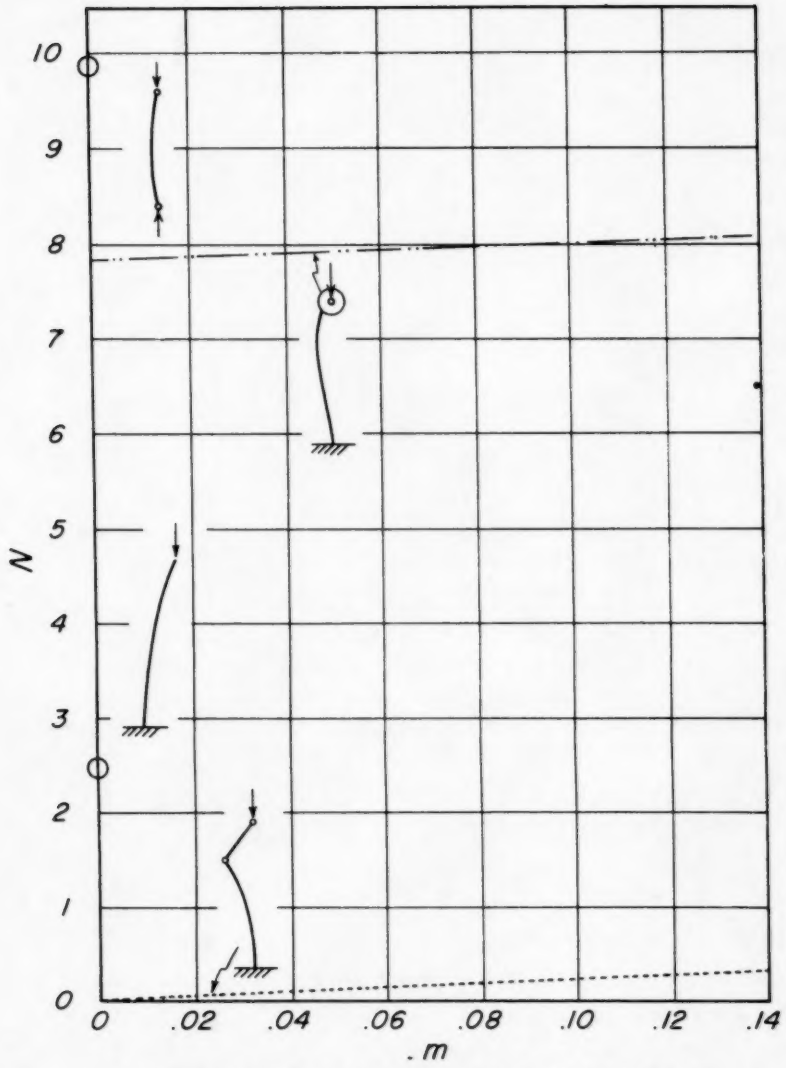

FIG. 4.—COMPARISON OF ROLLER AND LINK-SUPPORTING COLUMNS WITH CLASSIC CASES.

INITIAL ECCENTRIC LOADING BY A ROLLER

Because of an expansion or contraction in the superstructure, the roller may move laterally with respect to the original position by an amount e and

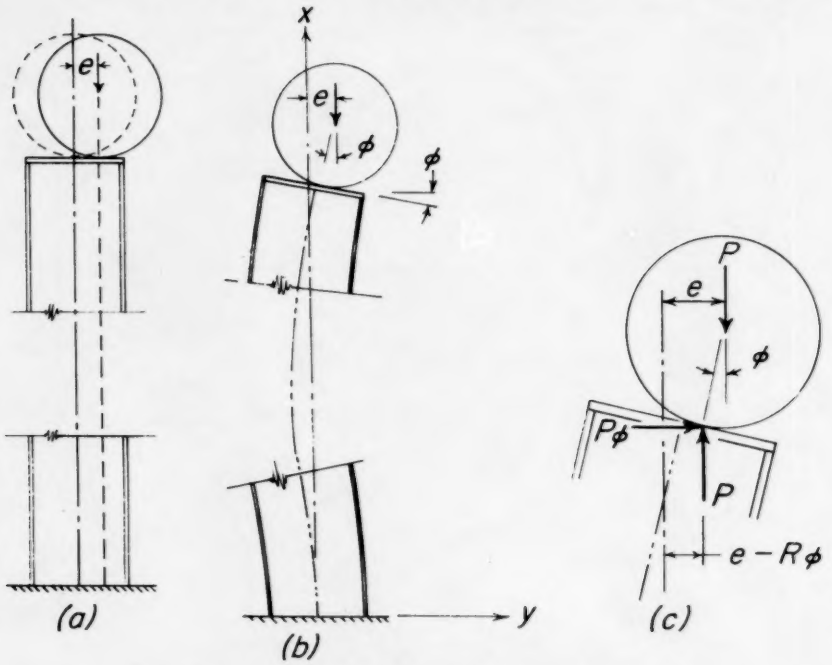

FIG. 5.—COLUMN SUPPORTING AN ECCENTRIC ROLLER.

thereafter remain along this new vertical axis. The conditions then are those shown in Fig. 5. The moment equation can be written

$$M_x = - P (e - R \phi - y) + P \phi (L - x) \quad \ldots\ldots\ldots\ldots (15)$$

The resulting differential equation is

$$E I \frac{d^2y}{dx^2} = - M_x = P (e - R \phi - y) - P \phi (L - x) \quad \ldots\ldots\ldots (16)$$

The solution to this equation is

$$y = A \cos k x + B \sin k x + \phi x + (e - R \phi - L \phi) \quad \ldots\ldots\ldots\ldots (17)$$

The boundary conditions are

$$y = 0, \text{ at } x = 0 \quad \ldots\ldots\ldots\ldots\ldots\ldots (18)$$

$$dy/dx = 0, \text{ at } x = 0 \quad \ldots\ldots\ldots\ldots\ldots\ldots (19)$$

$$dy/dx = \phi, \text{ at } x = L \quad \ldots\ldots\ldots\ldots\ldots\ldots (20)$$

Substitution of these boundary conditions leads to the following expression for ϕ:

$$\phi = \frac{k\, e \tan k\, L}{k\, L\, (m+1) \tan k\, L + 1} \quad \ldots\ldots\ldots\ldots (21)$$

The resultant eccentricity e' is equal to

$$e' = e - y - m\, L\, \phi \quad \ldots\ldots\ldots\ldots\ldots\ldots (22)$$

The bending moment equation is

$$M_x = -P\,(e - y - m\, L\, \phi) + P\, \phi\, (L - x)$$

so that the maximum bending moment occurs where $dM/dx = 0$. Thus,

$$dM/dx = 0 = -0 + 0 + P\,(dy/dx) + 0 - P\,\phi \quad \ldots\ldots\ldots\ldots (23)$$

Therefore, the maximum moment occurs where $dy/dx = \phi$. This locates the point of maximum moment at the head of the column. Substitution of the expression for y evaluated at x = L into Eq. 22, permits the calculation of e'/e for various values of P/P_{cr}. This computation has been made and the results shown on Fig. 6 for several values of m. Note the interesting response of this type of column when the eccentric load P is increased from zero to P_{cr}. For values of P/P_{cr} up to approximately 0.33, the eccentric effect of the vertical component of force is sufficient to cause the column to deflect toward the load axis somewhat and cause a reduction in effective eccentricity. For larger values of P/P_{cr}, the horizontal component of force plays a more important role and finally causes the column to be forced out laterally away from the load axis.

For design purposes, a set of curves similar to the familiar secant formula curves may be developed. For an eccentrically loaded column, the maximum stress occurs at the extreme fiber and may be computed by the conventional short column formula, provided that the maximum eccentricity that occurs throughout the column length is used. In the present case,

$$\sigma_{max.} = \frac{P}{A} + \frac{P\, e'\, c}{I} \quad \ldots\ldots\ldots\ldots\ldots\ldots (24)$$

in which c is the distance to the extreme fiber and e' is the maximum eccentricity that occurs as determined by Eq. 22 or as located on Fig. 6. Eq. 24 can be rearranged in the form

$$\frac{P}{A} = \frac{\sigma_{max}}{1 + \dfrac{e'\, c}{r^2}} \quad \ldots\ldots\ldots\ldots\ldots\ldots (25)$$

where r is the radius of gyration of the column section. Let P take on arbitrary values $\gamma\, P_{cr}$, $(0 \leq \gamma < 1)$, for curve plotting purposes. Then Eq. 25 can be written as

$$\gamma\, \frac{P_{cr}}{A} = \frac{\sigma_{max}}{1 + \dfrac{e'\, c}{r^2}} = \frac{\gamma\, N\, E}{\left(\dfrac{L}{r}\right)^2} \quad \ldots\ldots\ldots\ldots (26)$$

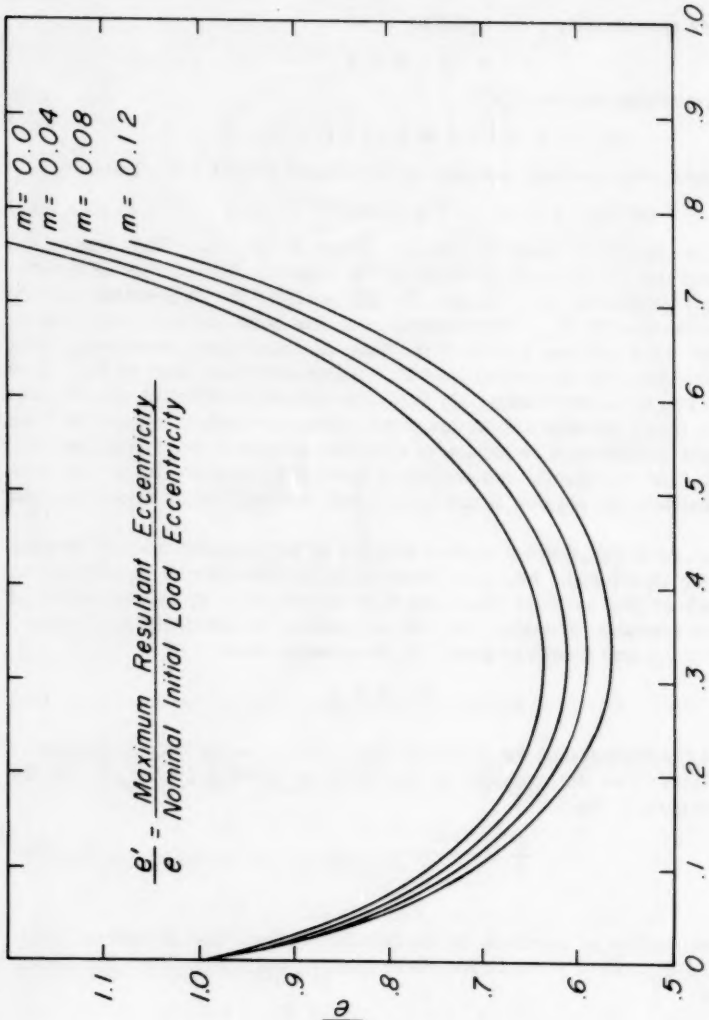

FIG. 6.—RESPONSE OF ROLLER-SUPPORTING COLUMN TO ECCENTRIC LOAD.

in which N is the critical buckling factor obtained from Fig. 4 for the particular value of m desired, or N may be computed exactly by the solution of Eq. 13. Rearrange Eq. 26 in the form

$$\left(\frac{L}{r}\right)^2 = \frac{\gamma\, N\, E\left(1 + \frac{e'\, c}{r^2}\right)}{\sigma_{max}} \quad \ldots\ldots\ldots\ldots\ldots (27)$$

To plot the design curves for a particular value of m and initial eccentricity e, arbitrary values of γ are chosen and corresponding values of e' and N are computed. Then with a particular value of σ_{max} specified, Eq. 27 is solved for $(L/r)^2$. This value of $(L/r)^2$ may be used to compute the nominal value of P/A that caused the stress σ_{max} by substitution in Eq. 26. Finally, the nominal value of P/A found can be divided by a suitable factor of safety.

A sample set of curves of this kind for m = 0, σ_{max} = 32.0 ksi, and the factor of safety = 1.71 are shown in Fig. 7. This procedure is not advocated as the best possible way to treat column stresses but it does reflect the philosophy of existing codes.

COLUMN LOADED THROUGH A LINK

Although the free-standing column supporting a roller of radius m L proved to be considerably stiffer than the classic free-standing column, the substitution of a link of length m L will result in a catastrophic reduction in load-carrying capacity. As in the case of the roller, the upper end of the link, where the load is to be applied, is assumed to be restrained so that this point must remain along a fixed vertical axis. The lower end of the link can also apply both a vertical and horizontal component of force. However, in this case, the contact force is not required to be normal to the head of the column. The resulting components of force and the deflected configuration are shown in Fig. 8. Coordinate axes are taken as shown. The moment equation is

$$M_x = -P(\delta - y) - \frac{P\,\delta}{m\,L}(L - x) \quad \ldots\ldots\ldots (28)$$

The resulting differential equation is

$$E\,I\,\frac{d^2y}{dx^2} = -M_x = -P\,y - \frac{P\,\delta\,x}{m\,L} + \frac{P\,\delta}{m} + P\,\delta \quad \ldots\ldots\ldots (29)$$

The solution to this differential equation is

$$y = A\cos k\,x + B\sin k\,x - \frac{\delta\,x}{m\,L} + \left(\frac{1+m}{m}\right)\delta \quad \ldots\ldots\ldots (30)$$

The boundary conditions are

$$y = 0, \text{ at } x = 0 \quad \ldots\ldots\ldots\ldots\ldots (31)$$

$$dy/dx = 0, \text{ at } x = 0 \quad \ldots\ldots\ldots\ldots\ldots (32)$$

$$y = -\delta, \text{ at } x = L \quad \ldots\ldots\ldots\ldots\ldots (33)$$

Substitution of these boundary conditions in Eq. 30 leads to the following transcendental equation

$$\tan k\,L = (1 + m)\,k\,L \quad \ldots\ldots\ldots\ldots\ldots (34)$$

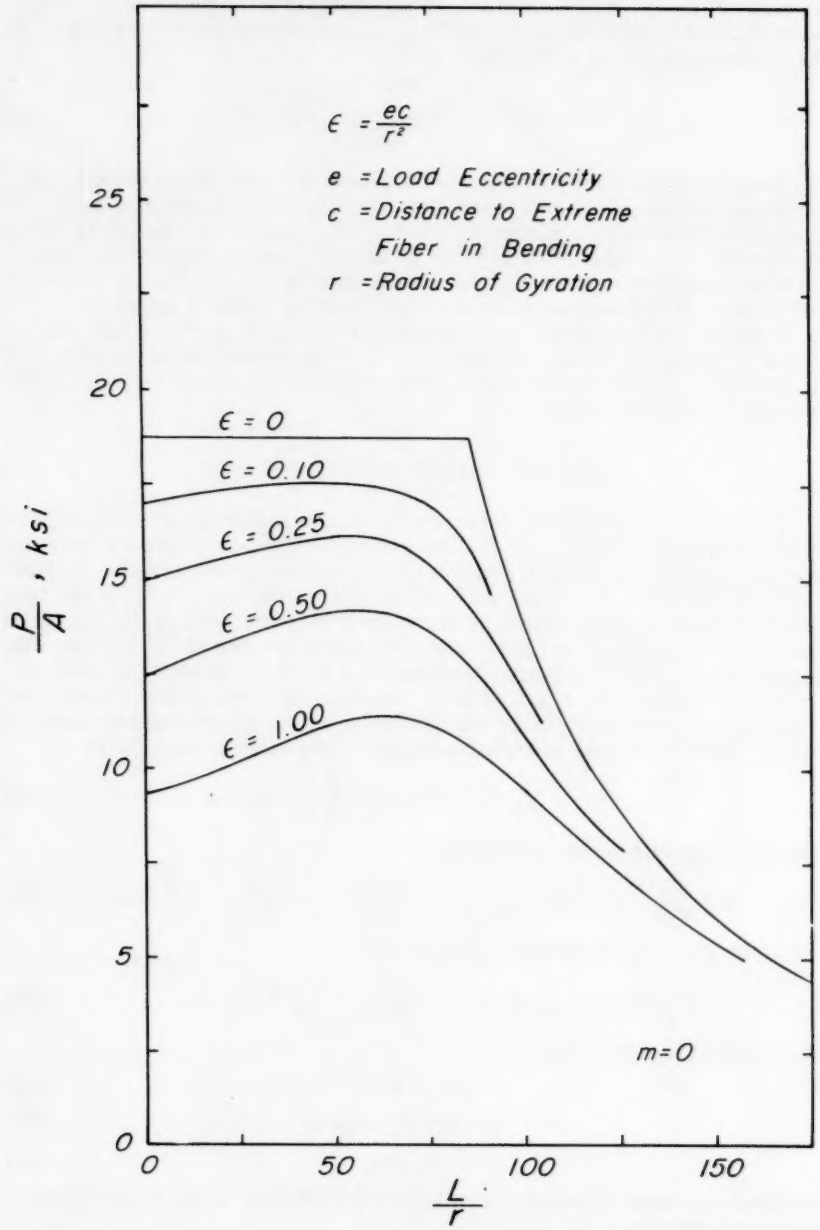

FIG. 7.—DESIGN CURVES FOR COLUMN SUPPORTING AN ECCENTRIC ROLLER

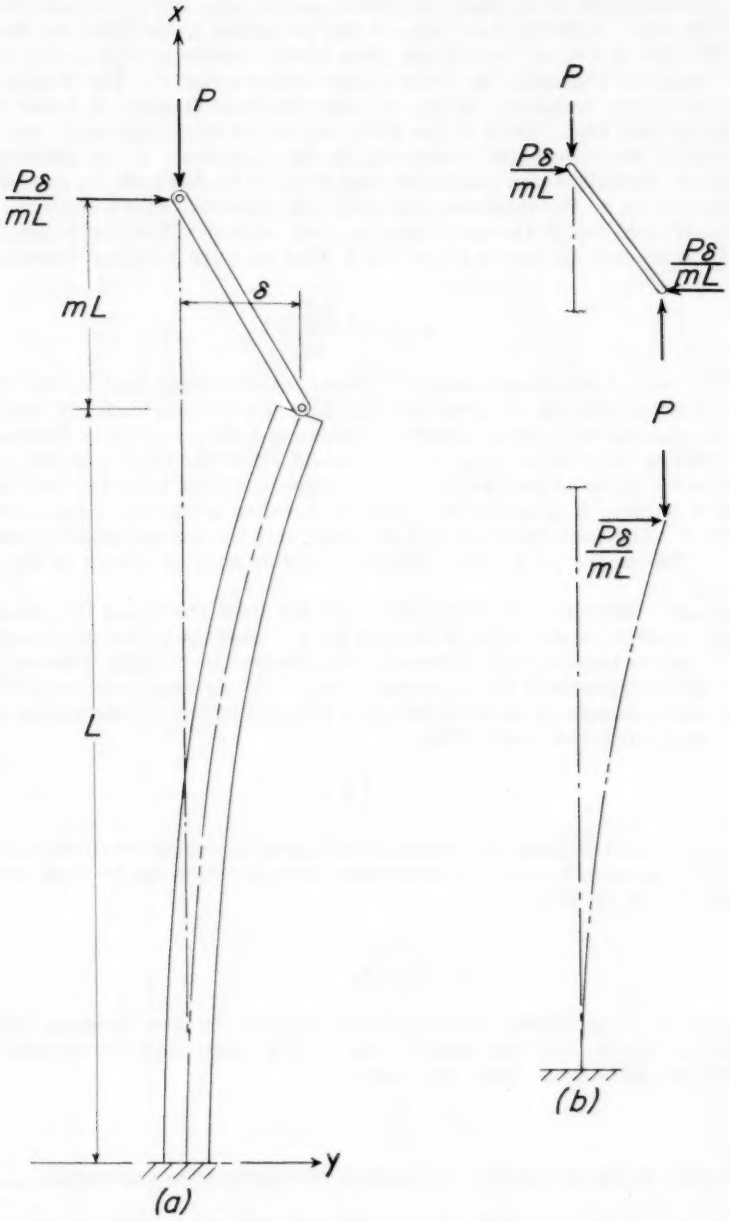

FIG. 8.—COLUMN SUPPORTING A LINK WITH POSITIVE m.

Note that with the exception of the term (1 + m) Eq. 34 is identical to Eq. 1 for the column fixed at the base and pinned at the top. For m = 0 the equations are identical. Both Eq. 1 and Eq. 34 can be solved graphically as shown in Fig. 9. For m = 0, both equations have trivial solutions at k L = 0. In fact, both equations represent the same column action since, if a link of zero length were to buckle completely as Eq. 34 indicates, then at worst it would lie flat on the column head. Since it has zero length and since the top of the link is restrained from sidewise movement by the conditions of the problem, the boundary conditions are converted immediately to those of the problem described by Eq. 1. For finite lengths of the link, however, real non-trivial roots of Eq. 34 exist which are quite close to zero. For m = 0.10, for example, the smallest non-trivial root is k L = 0.518. This fixes the smallest buckling load as

$$P_{cr} = \frac{0.268\ E\ I}{L^2} \quad \ldots\ldots\ldots\ldots\ldots\ldots (35)$$

This load is only about one-ninth the critical buckling load for the classic free-standing column or about one-thirtieth the critical buckling load for a similar column supporting a roller of radius m L = 0.10 L. It is doubtful that the buckling of a link of length 0.10 L would allow the top of the link to rest upon the top of the column as in the m = 0 case and, thus, force the next highest mode of failure. It is more likely that the buckling of the link would force the column from beneath the supported structure with a resulting catastrophic collapse. The danger of a poorly designed roller, such as shown in Fig. 1, is obvious.

Eq. 34 is difficult to solve quickly since the slope of the line (1 + m) k L is almost identical to the slope of the line tan k L near the points of interest. A very accurate approximate solution to this problem is possible, however. The horizontal component of force causes the top of the column to deflect laterally in the same manner as the deflection of a simple cantilever beam loaded at the end by a concentrated load, Thus,

$$\delta = \frac{F\ L^3}{3\ E\ I} \quad \ldots\ldots\ldots\ldots\ldots\ldots (36)$$

Since the column is under the simultaneous action of the vertical component of force, an approximate correction for beam-column action can be made by multiplying Eq. 36 by the factor

$$\frac{1}{1 - P_{cr}/P_e} \quad \ldots\ldots\ldots\ldots\ldots\ldots (37)$$

The term P_e is the classic Euler buckling load for the free-standing column, as given by Eq. 4. The horizontal force F is a function of the vertical load P_{cr} and the deflection. Thus, for small δ,

$$F = \frac{P_{cr}\ \delta}{m\ L} \quad \ldots\ldots\ldots\ldots\ldots\ldots (38)$$

Substitution of Eq. 38 into Eq. 36 leads to the approximate expression

$$P_{cr} = \frac{3\ m\ E\ I}{\left(1 + \frac{12\ m}{\pi^2}\right) L^2} \quad \ldots\ldots\ldots\ldots\ldots\ldots (39)$$

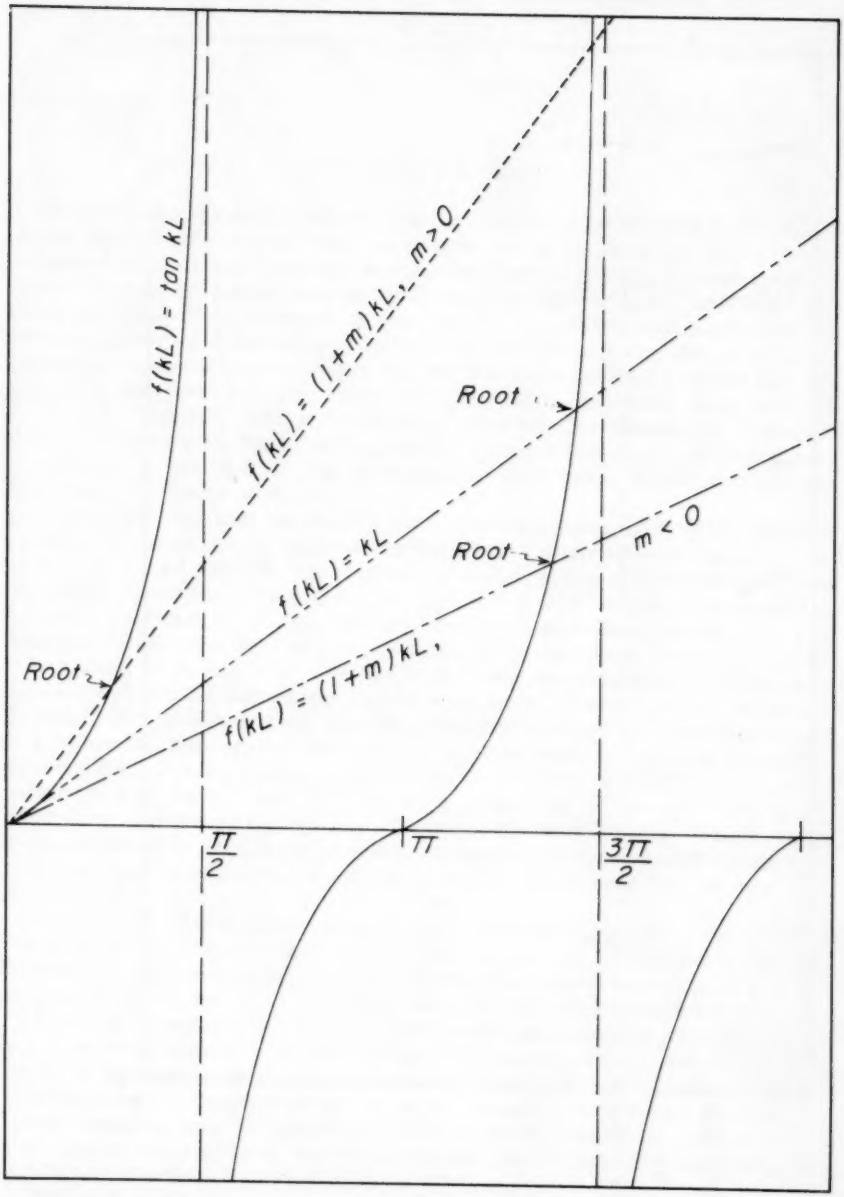

FIG. 9.—GRAPHICAL SOLUTION OF TRANSCENDENTAL EQUATIONS.

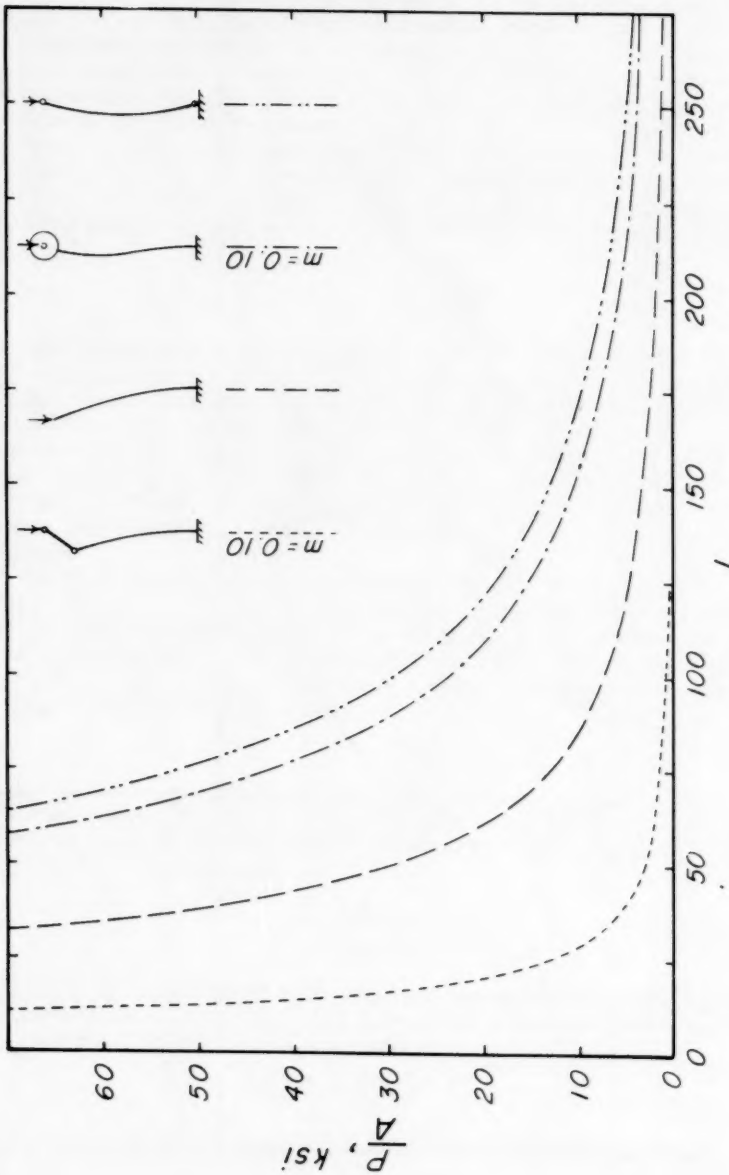

FIG. 10.—EULER-TYPE CURVES FOR FOUR COLUMN CASES.

Substitution of m = 0.10 into Eq. 39 gives, as the critical buckling load

$$P_{cr} = \frac{0.2675\ E\ I}{L^2} \quad \ldots\ldots\ldots\ldots\ldots\ldots (40)$$

Compare this with Eq. 35.

NEGATIVE LINKS

Neither of the foregoing support conditions are compatible with those existing for the columns of a lift-slab operation. These columns are more nearly subjected to a loading condition wherein the load is applied through inverted links. That is, the loaded ends of the links (the links being the jack rods) are below the tops of the columns. If the conditions of this problem are used to set up a governing differential equation with the link lengths given as m L, the resulting transcendental equation will be the same as Eq. 34 except that the sign of m will be reversed. This signifies that the inverted link acts in the sense of a "negative" link. A graphical solution for this equation is shown on Fig. 9, together with the preceding cases. Again, a link of minus-zero length is identical to the link of plus-zero length. Both cases degenerate into the conditions expressed by Eq. 1.

It is noteworthy that the buckling load for the column, with either positive or negative values of m, approaches that of the classic free-standing column as m approaches infinity. For positive values of m the critical buckling load increases from $P_{cr} = 0$ for m = 0 to $P_{cr} = (\pi^2\ E\ I)/(4\ L^2)$ for m approaching infinity. That is, the classic buckling load is approached from below. For negative values of m the critical buckling load decreases from $P_{cr} = 20.19\ E\ I\ L^2$ at m = 0 to $P_{cr} = (\pi^2\ E\ I)/(4\ L^2)$ at m approaching infinity. In this case, the classic buckling load is approached from above. Positive values of m may be considered as defining a region of instability wherein the potential energy is a maximum. Conversely, negative values of m define a region of instability wherein the potential energy is a minimum. If a link of length m L could be constructed so that it would function as a normal or as an inverted link, an interesting phenomena could occur. Starting with the link in the "normal" position so that m is considered positive, a load could be applied until the critical load was approached. This would be a rather small load for any moderate value of m.

At this critical load, buckling would occur with the column head being thrust sideways by an amount equal to the length of the link. If the link were constructed as supposed previously, the column head could then snap back to its original position, but now the link is below so that m is considered negative.

Thus, the structure has passed from a state of maximum potential energy to a state of minimum potential energy at a corresponding position where m = - m. In this new position, the load may be increased further until the higher buckling load for negative values of m is reached. The manner in which the classic buckling load is approached from above and below for various values of m, and an illustration of the "snap-through" phenomenon for a typical case, m = 1, are shown on Fig. 11.

The case of negative values of m has practical application in the field of lift-slab operations. At the beginning of a lift-slab operation the jack rods extend the full length of the column so that they function as a link with m = - 1.

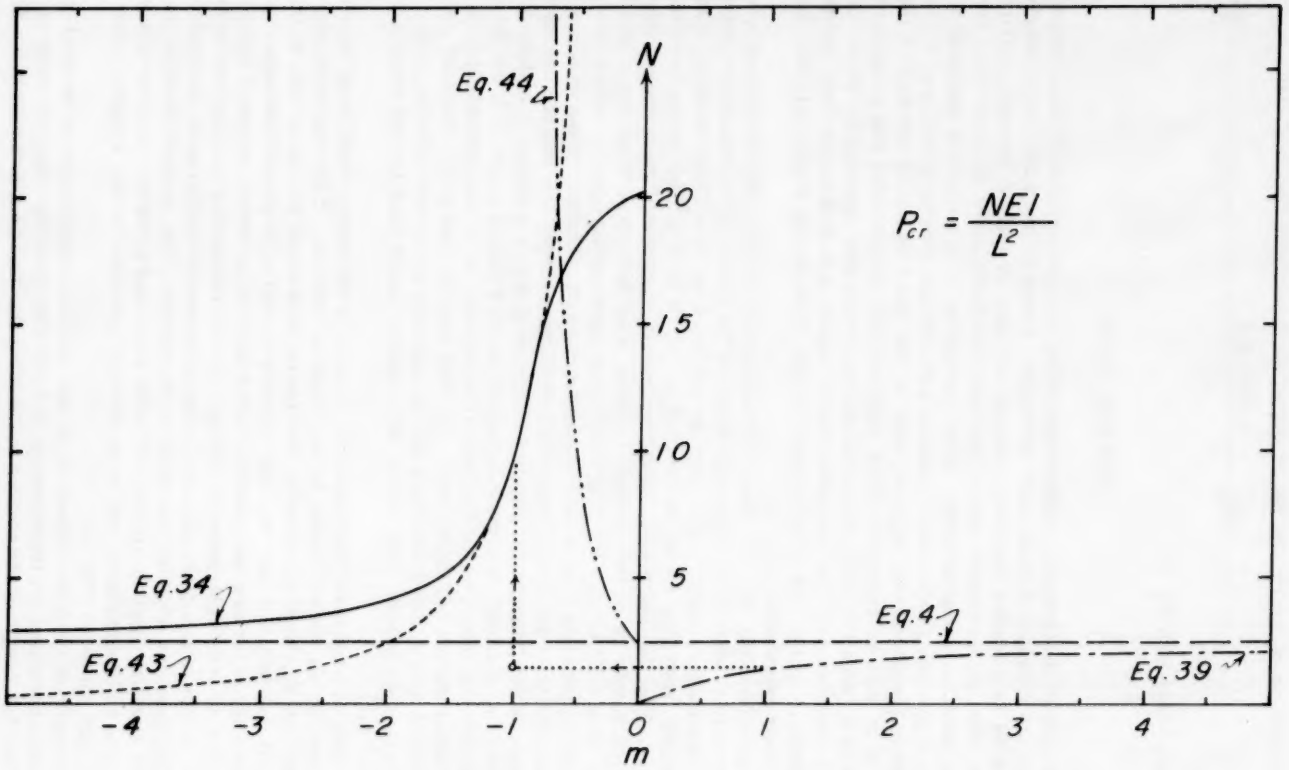

FIG. 11.—CHARACTERISTIC CURVES FOR COLUMN SUPPORTING VARIOUS LINKS.

Thus, at this value of m the root of the governing equation is k L = π, so that the column has a buckling strength equal to that of classic Euler pin-ended column, namely

$$P_{cr} = \pi^2 E I/L^2 \quad \ldots\ldots\ldots\ldots\ldots\ldots (41)$$

If the slab were restrained from sidesway by diagonal cables or other suitable external bracing, the strength of the column would increase as the lift proceeded because of the decrease in the length of the link. With the slab at the full height of the column, m = 0, and the critical buckling load would be that given by Eq. 2.

In most cases, it may not be practical to brace the slab against sidesway. Consequently, the column will act in a somewhat different manner with the column itself acting as a partial bracing system for part of the lift. This bootstrap-like action can be explained by reference to Fig. 12. Consider the column to be in neutral equilibrium with a slightly buckled shape. The top of the column, which supports the upper end of the link, will be deflected laterally by the amount Δ. At the level of the slab where the lower end of the link is loaded by the weight of the slab, the column is deflected by an amount δ. Because of the slight difference in the lateral deflection of the two points, the link will be inclined at a small angle so that there exists a horizontal component equal to

$$f(P) = P \frac{(\Delta - \delta)}{m L} \quad \ldots\ldots\ldots\ldots\ldots\ldots (42)$$

This horizontal component loads the column as a pair of forces separated by a distance m L, so as to cause a couple equal to P (Δ - δ). At the level of the slab, the vertical component P causes a moment equal to - P (Δ - δ), so that the sum of the couple formed by the two horizontal components and the couple caused by the vertical component is identically zero. Hence, the part of the column above the slab level is loaded as a pin-ended column of length m L and has as its critical buckling load:

$$P_{cr} = \frac{\pi^2 E I}{(m L)^2} \quad \ldots\ldots\ldots\ldots\ldots\ldots (43)$$

That part of the column below the slab level acts as the classic free-standing column of length (1 + m) L, where m < 0, and has as its critical buckling load:

$$P_{cr} = \frac{\pi^2 E I}{(4 + 8 m + m^2) L^2} \quad \ldots\ldots\ldots\ldots\ldots\ldots (44)$$

Thus, the column loaded in this manner will buckle at the load given by Eqs. 34, 43 or 44, whichever gives the smallest value. Eqs. 43 and 44 are plotted on Fig. 11 with the previous results. Eq. 43 is tangent to the curve defined by Eq. 34 at the point m = - 1. For - 1 < m < 0, Eq. 43 lies above the curve for Eq. 34 and, thus, never controls the buckling load for practical values of m. Between the values m = - 0.65 and m = 0, Eq. 44 controls. Thus, in the final phases of a lift, the free-standing columns act in the classic manner.

Note that the phase of the lift from m = - 1 to m = - 0.50 is characterized by columns having a buckling strength equal to or greater than pin-ended columns of equal length. External bracing on the slab could surely provide enough stability to assure this strength throughout the entire lift.

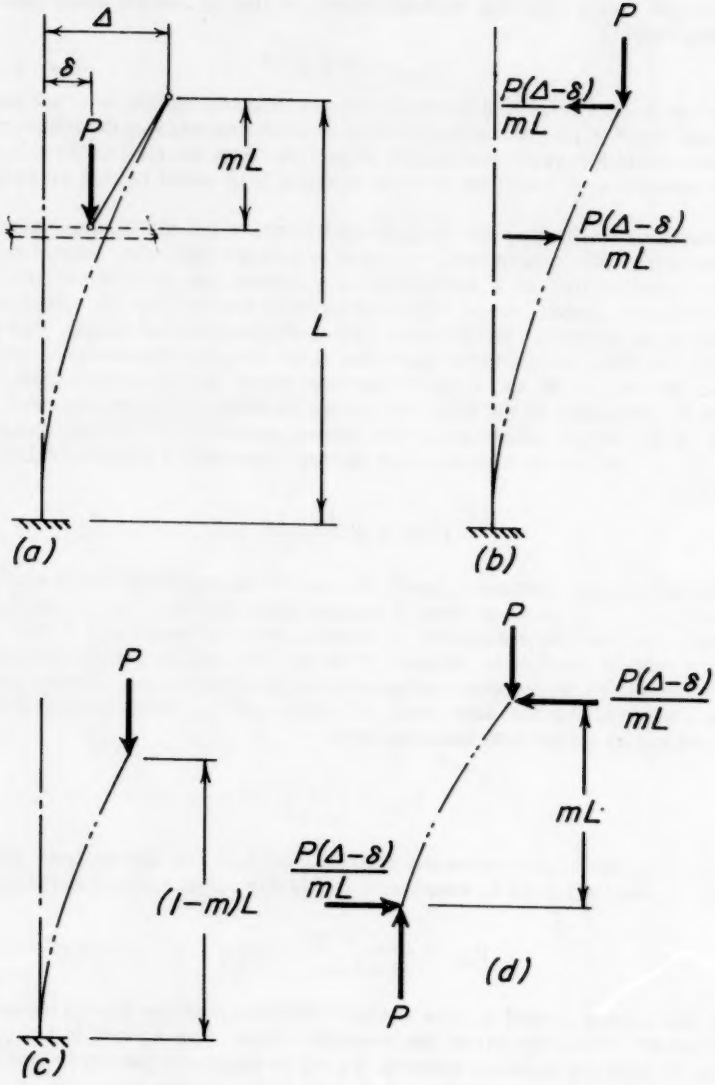

FIG. 12.—THE LIFT-SLAB COLUMN.

SUMMARY

These few comments have shown that two basic equations for buckling, namely Eq. 2 and Eq. 4, are only special cases of a general column problem, the buckling load for which is given by the roots to the transcendental equation, Eq. 34.

Eq. 2 results when m takes on the value of zero, whereas Eq. 4 is the consequence of letting m approach infinity. A problem involving a column supporting a roller of radius m L is shown to be a separate and distinct structure from the column supporting the link of length m L, in spite of their nominal similarity. Characteristic curves for all of the cases considered are shown in Figs. 4 and 10 for comparison.

ACKNOWLEDGMENT

The ideas presented in this paper first occurred to the author during the graduate lectures given at the University of Florida, by Bruce G. Johnston, Professor of Structural Engineering, University of Michigan, while on sabbatical leave from that institution. The development of Eq. 39 was taken directly from those lectures.

The suggestion of L. E. Grinter, Dean of the Graduate School, University of Florida, that these ideas might be of interest to other engineers encouraged the author to present this paper.

ADDITIONAL READING REFERENCES

1. "Multistory Lift-Slab Construction," by W. Sefton, Journal, American Concrete Inst., Vol. 27, No. 7, January, 1958, p. 579.
2. "Terminal's Prestressed Steel Roof is Umbrella for Jet Passengers," by Z. Levinton, Engineering News-Record, March, 1959, p. 30.

Journal of the
STRUCTURAL DIVISION
Proceedings of the American Society of Civil Engineers

DYNAMIC RESPONSE OF ELASTO-PLASTIC FRAMES[a]

By Joseph Penzien[1], A. M. ASCE

SYNOPSIS

This paper presents the results of an analytical investigation involving a single mass system that has an idealized elasto-plastic resistance deformation relationship and that is subjected to the ground motion measured by the United States Coast and Geodetic Survey during the May 1940 El Centro earthquake. The basic parameters that are varied in this investigation are the natural period, ultimate strength, and damping of the system. All results are presented in the form of graphs showing the maximum dynamic response of the system during the simulated earthquake input plotted against natural period for various combinations of ultimate strength and damping.

INTRODUCTION

The philosophy of the design of structures to withstand strong motion earthquakes has changed appreciably in recent years due to a better understanding of the true dynamic behavior of structures during an earthquake. However, in the past there has been an apparent wide gap between analytical results based on elastic behavior and the results of observation. This difference has been due to the extreme difficulty, in general, in setting up a proper mathematical model to be used in any dynamic analysis.

Note.—Discussion open until December 1, 1960. To extend the closing date one month, a written request must be filed with the Executive Secretary, ASCE. This paper is part of the copyrighted Journal of the Structural Division, Proceedings, of the American Society of Civil Engineers, Vol. 86, No. ST 7, July, 1960.

[a] Presented at the February 1959 ASCE Convention in Los Angeles, Calif.

[1] Assoc. Prof. of Civ. Engrg., Univ. of California, Berkeley, Calif.

Such a model should simulate the true resistance-deformation characteristics of the structure throughout the history of deformation imposed by the earthquake and should also simulate the true damping of the structure. For the conventional structure, where its stiffness, strength, and damping properties are greatly influenced by the existence of secondary structural elements such as filler walls, partitions, stairwells, etc., and are also influenced by foundation conditions, a proper mathematical model is difficult to establish. However, considerable progress has been made by engineers and researchers in recent years in this direction and, as a result, the gap between the theoretical and true behaviors of structures subjected to strong motion earthquakes is gradually closing.

While there have been many papers that have contributed to a better understanding of the response of structures subjected to earthquakes, the writer would like to mention two that are particularly pertinent. A report[2] by J. L. Alford, G. W. Housner, and R. R. Martel has greatly advanced the understanding of the dynamic response of structures subjected to earthquakes and has had a considerable influence on present day seismic codes. A paper[3] by J. A. Blume has contributed a great deal in explaining the differences existing between the dynamic behavior of structures, as predicted by the usual methods of analysis, and the true behavior that has been observed.

It is the purpose of this paper to present the results of a spectrum analysis similar to those presented by Alford, Housner, and Martel except that varying degrees of plastic deformation are allowed in the structural system. These results show quantitatively the importance of plastic deformation in limiting the dynamic response of structural systems. This effect was described[3] qualitatively by Blume.

METHOD OF ANALYSIS

Equation of Motion.—The single mass system used in this investigation is represented by the simple frame shown in Fig. 1 in which the quantity u represents the displacement of the mass relative to its moving base, u_t represents the total displacement of the mass relative to a fixed reference position, u_g represents the ground displacement, Q represents the total resisting force offered by the frame (not including damping), and c represents a viscous damping coefficient.

The equation of motion of mass M can be written as follows:

$$M\ddot{u}_t + c\dot{u} + Q = 0 \quad \ldots\ldots\ldots\ldots (1)$$

However,

$$u_t = u_g + u \quad \ldots\ldots\ldots\ldots\ldots\ldots (2)$$

Therefore, Eq. 1 can be written as

$$M\ddot{u} + c\dot{u} + Q = -M\ddot{u}_g \quad \ldots\ldots\ldots\ldots (3)$$

This equation of motion shows that any analysis to determine the frame displacement, u, can be carried out assuming a fixed base. However, a forcing

---

2 "Spectrum Analyses of Strong-Motion Earthquakes," by J. L. Alford, G. W. Housner, and R. R. Martel, Office of Naval Research Contract N6 ONR-244, August, 1951.

3 "Structural Dynamics in Earthquake-Resistant Design," by John A. Blume, Proceedings, ASCE, Vol. 84, No. ST 4, July, 1958.

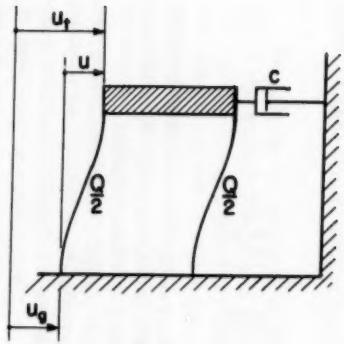

FIG. 1.—SIMPLE FRAME

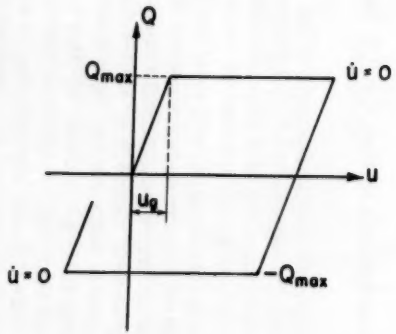

FIG. 2.—RESISTANCE-DEFORMATION RELATIONSHIP

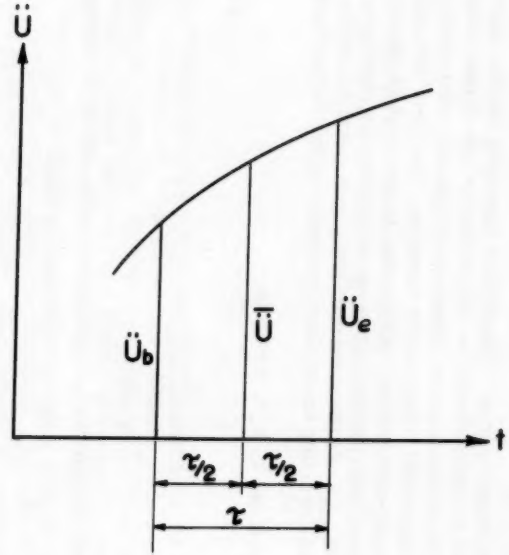

Known: $\ddot{U}_b, \dot{U}_b, U_b$

FIG. 3

function is applied to the mass equal to the negative product of the mass times the ground acceleration.

If the response of the frame is to be determined assuming elastic behavior, the frame resistance Q would simply be the product of the frame elastic spring constant times the displacement u. However, if plastic deformation is allowed, this term becomes considerably more complex. For this investigation an idealized resistance-deformation relationship is assumed as shown in Fig. 2. This relationship limits the total force developed in the structure to some maximum value (Q_{max}). As the mass oscillates back and forth during an earthquake, the frame may be acting as an elastic element during certain intervals of time.

If one defines the quantities U, θ, λ, and T as

$$U = u/u_y \quad \ldots\ldots\ldots\ldots\ldots\ldots (4a)$$

$$\theta = \frac{Q_{max}}{-M\,g} \quad \ldots\ldots\ldots\ldots\ldots\ldots (4b)$$

$$\lambda = c/c_c \quad \ldots\ldots\ldots\ldots\ldots\ldots (4c)$$

in which $c_c = \frac{4\,\pi\,M}{T}$ (critical damping), and T is the elastic period of vibration, then the quantities Q_{max}, u_y and c can be expressed as shown by Eqs. 5.

$$Q_{max} = \theta\,M\,g \quad \ldots\ldots\ldots\ldots\ldots\ldots (5a)$$

$$u_y = \frac{\theta\,g\,T^2}{4\,\pi^2} \quad \ldots\ldots\ldots\ldots\ldots\ldots (5b)$$

$$c = \frac{4\,\pi\,M\,\lambda}{T} \quad \ldots\ldots\ldots\ldots\ldots\ldots (5c)$$

Using relationships of Eqs. 4 and 5, the equation of motion (Eq. 3) may be written as

$$\dot{U} = -\left(\frac{4\,\pi^2}{\theta\,g\,T^2}\right) \ddot{u}_g - \left(\frac{4\,\pi^2}{\theta\,g\,T^2}\right) \frac{Q}{M} - \left(\frac{4\,\pi\,\lambda}{T}\right) \dot{U} \quad \ldots\ldots\ldots (6)$$

Solution of this equation will yield the time history of the dimensionless ratio U. The three dimensionless parameters T, θ, and λ appearing in this equation have been varied over a considerable range in this general investigation.

Integration of Equation of Motion.—Due to the complications imposed by allowing plastic deformation, Eq. 6 has been solved using a numerical step-by-step integration procedure. By this procedure the duration of the earthquake is divided into equal small intervals of time (τ). Assuming the quantities U, $\dot{U}$, and $\ddot{U}$ are known at the beginning of any interval, these same quantities are determined at the end of that interval using the so-called "mid-acceleration" method.

Let $\ddot{U}_b$, $\dot{U}_b$, and U_b represent the known values of $\ddot{U}$, $\dot{U}$, and U, respectively, at the beginning of any interval. The mid-interval values of $\ddot{U}$ and $\dot{U}$ ($\bar{U}$ and $\bar{\dot{U}}$, respectively) are determined by the simple relations.

$$\left.\begin{aligned} \overline{U} &= U_b + \dot{U}_b\,\tau/2 \\ \overline{\dot{U}} &= \dot{U}_b + \ddot{U}_b\,\tau/2 \end{aligned}\right\} \quad \ldots\ldots\ldots\ldots\ldots\ldots (7)$$

Knowing $\overline{U}$ and $\overline{\dot{U}}$, the mid-value of $\ddot{U}$ ($\overline{\ddot{U}}$) is obtained using Eq. 6. Having $\overline{\ddot{U}}$, the magnitudes of U and $\dot{U}$ at the end of the interval are obtained using Eqs. 8

$$\left.\begin{aligned} U_e &= U_b + \dot{U}_b\,\tau + \overline{\ddot{U}}\,\tau^2/2 \\ \dot{U}_e &= \dot{U}_b + \ddot{U}\,\tau \end{aligned}\right\} \quad \ldots\ldots\ldots\ldots\ldots\ldots (8)$$

Substituting the values of U_e and $\dot{U}_e$ just obtained into Eq. 6, the magnitude of $\ddot{U}_e$ is determined. The known end values U_e, $\dot{U}_e$, and $\ddot{U}_e$ are now used as the beginning values for the next time interval. Thus the calculations proceed through all time intervals in a similar manner. In starting the calculations at the first time interval the initial values of U and $\dot{U}$ are zero.

The code for the digital computer used in this investigation was written so that one could obtain either the maximum dynamic response during the earthquake input or the complete time history of response. The latter, however, requires considerable machine time for printing of results and, therefore, was carried out for special cases only.

Ground Motion Used in Analysis.—The ground acceleration $\ddot{u}_g$ (E-W component) measured by the United States Coast and Geodetic Survey (USC & GS) during the May 18, 1940 El Centro, Calif. earthquake was used throughout this investigation. Fig. 4 shows this ground acceleration plotted against time.

In carrying out the numerical integration of Eq. 6 using this ground motion, a time interval τ equal to 0.01986 sec. was used.

ANALYTICAL RESULTS

The maximum dynamic response of the single mass system during the period of the earthquake was of primary concern in this investigation. Therefore, all results are presented by plotting a dimensionless displacement ratio against the elastic period of vibration of the system for various combinations of damping and yield strength.

This dimensionless displacement ratio is defined as the ratio of the maximum dynamic displacement occurring during the simulated earthquake to the static displacement produced by a 1g load on the system. It is assumed, however, in computing the latter displacement that the system has infinite strength, that is, no yielding will take place. Therefore, the dimensionless strength parameter, θ, effects only the maximum dynamic displacement in the above ratio.

All basic results of the investigation are shown in Figs. 5 through 12. In these figures, the dimensionless strength parameter θ ranges from 0.05 to 1.00, the stiffness parameter T ranges from 0.2 sec to 2.4 sec, and the damping ratio ranges from 0% to 15%.

The dashed curve which is repeated in each of these figures refers to the purely elastic case with zero damping and therefore can be used as a basis for

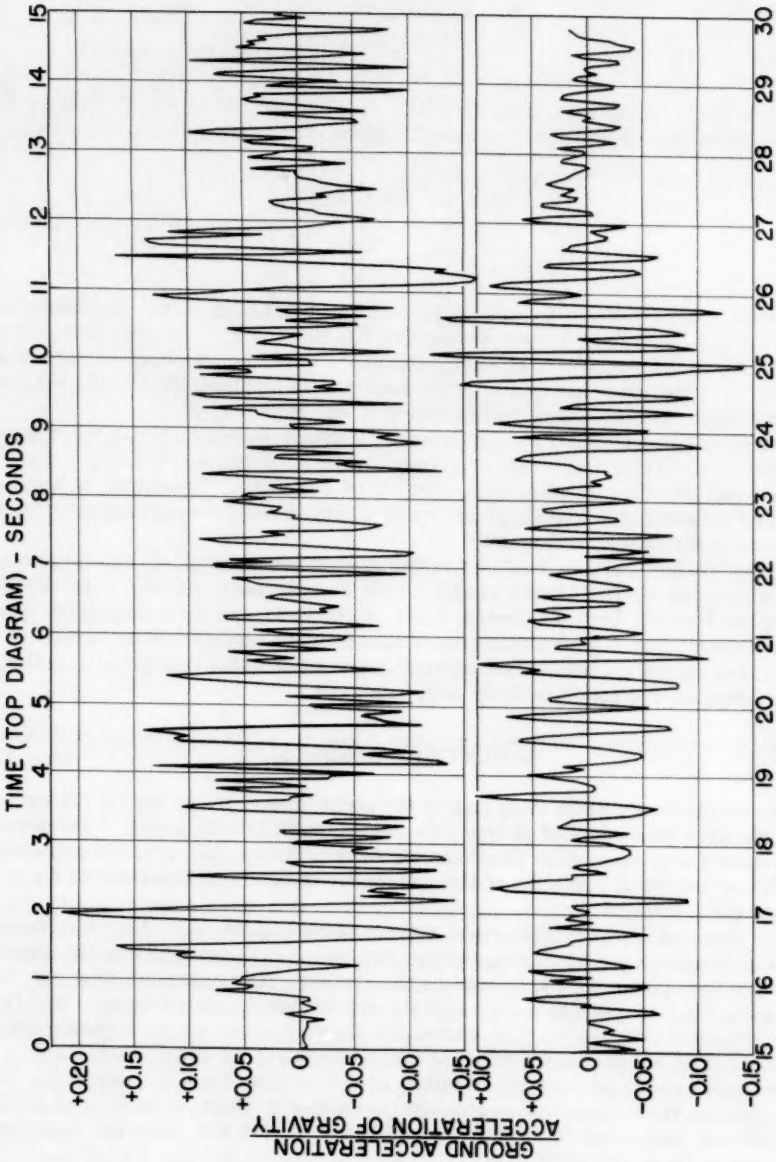

FIG. 4.—ACCELEROGRAM FOR EL CENTRO, CALIFORNIA EARTHQUAKE OF MAY 18, 1940 COMPONENT E-W

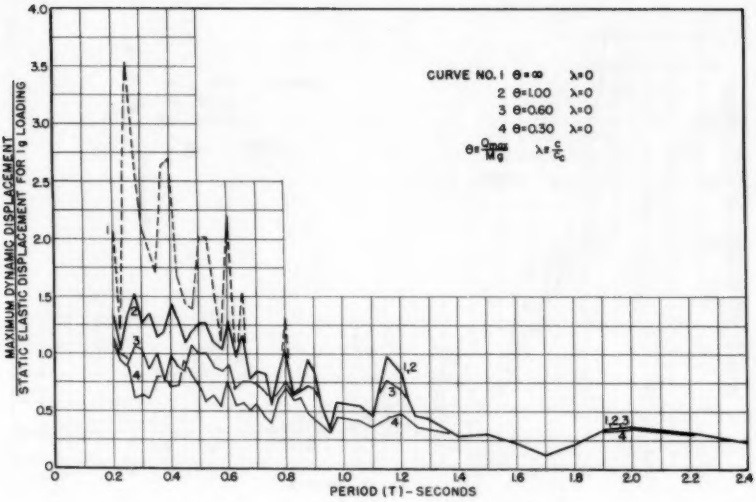

FIG. 5.—MAXIMUM DYNAMIC RESPONSE FOR EL CENTRO, CALIFORNIA EARTHQUAKE OF MAY 18, 1940 E-W COMPONENT

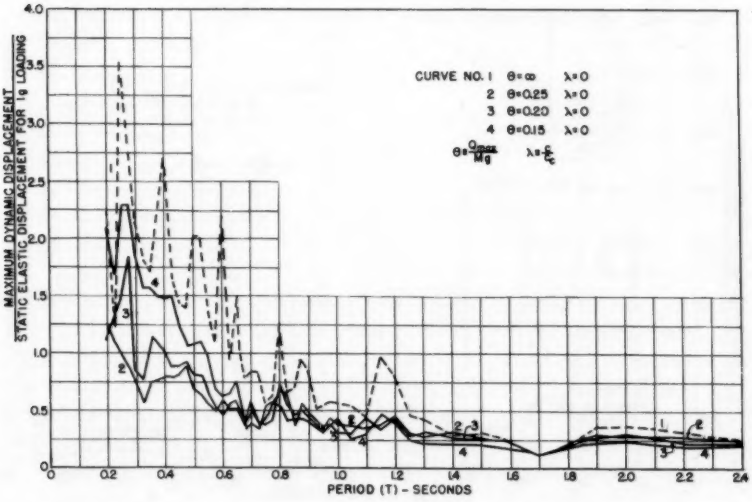

FIG. 6.—MAXIMUM DYNAMIC RESPONSE FOR EL CENTRO, CALIFORNIA EARTHQUAKE OF MAY 18, 1940 E-W COMPONENT

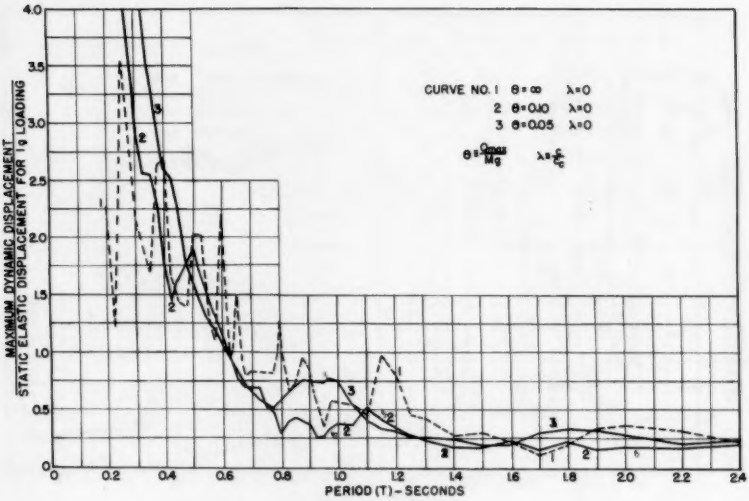
CURVE NO. 1 θ = ∞ λ = 0
2 θ = 0.10 λ = 0
3 θ = 0.05 λ = 0
θ = Qmax/Mg λ = ξ/ξc
MAXIMUM DYNAMIC DISPLACEMENT / STATIC ELASTIC DISPLACEMENT FOR 1g LOADING
PERIOD (T) - SECONDS

FIG. 7.—MAXIMUM DYNAMIC RESPONSE FOR EL CENTRO, CALIFORNIA EARTHQUAKE OF MAY 18, 1940 E-W COMPONENT

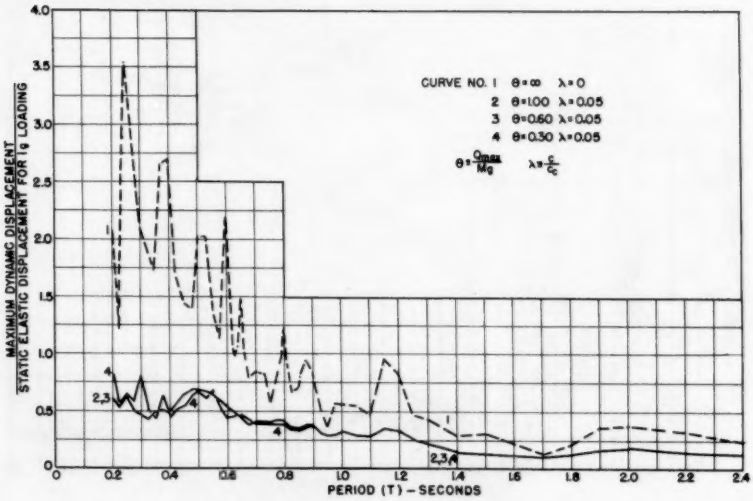
CURVE NO. 1 θ = ∞ λ = 0
2 θ = 1.00 λ = 0.05
3 θ = 0.60 λ = 0.05
4 θ = 0.30 λ = 0.05
θ = Qmax/Mg λ = ξ/ξc
MAXIMUM DYNAMIC DISPLACEMENT / STATIC ELASTIC DISPLACEMENT FOR 1g LOADING
PERIOD (T) - SECONDS

FIG. 8.—MAXIMUM DYNAMIC RESPONSE FOR EL CENTRO, CALIFORNIA EARTHQUAKE OF MAY 18, 1940 E-W COMPONENT

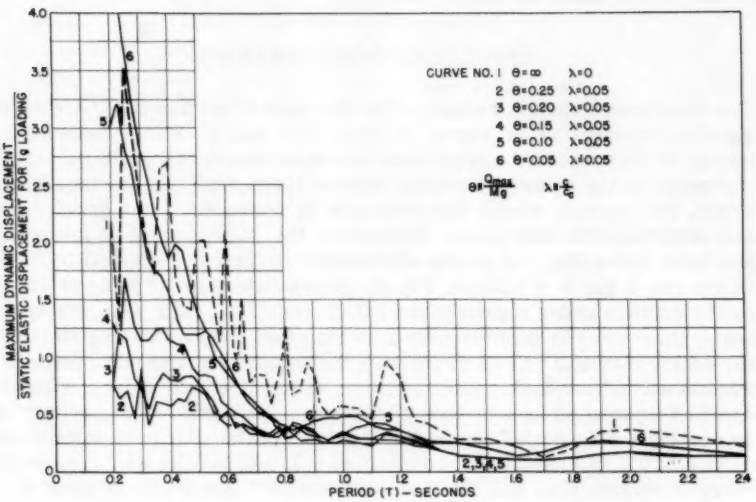
CURVE NO. 1 θ=∞ λ=0
2 θ=0.25 λ=0.05
3 θ=0.20 λ=0.05
4 θ=0.15 λ=0.05
5 θ=0.10 λ=0.05
6 θ=0.05 λ=0.05
θ=Qmax/Mg λ=c/cc
MAXIMUM DYNAMIC DISPLACEMENT / STATIC ELASTIC DISPLACEMENT FOR 1g LOADING
PERIOD (T) – SECONDS

FIG. 9.—MAXIMUM DYNAMIC RESPONSE FOR EL CENTRO, CALIFORNIA EARTHQUAKE OF MAY 18, 1940 E-W COMPONENT

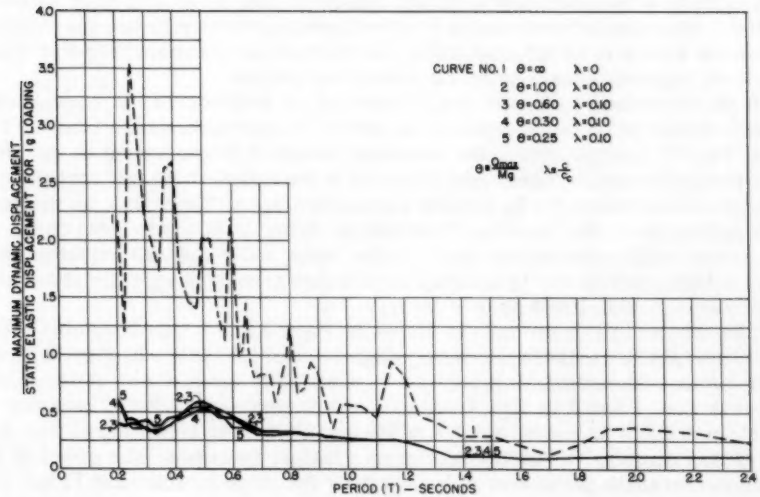
CURVE NO. 1 θ=∞ λ=0
2 θ=1.00 λ=0.10
3 θ=0.60 λ=0.10
4 θ=0.30 λ=0.10
5 θ=0.25 λ=0.10
θ=Qmax/Mg λ=c/cc
MAXIMUM DYNAMIC DISPLACEMENT / STATIC ELASTIC DISPLACEMENT FOR 1g LOADING
PERIOD (T) – SECONDS

FIG. 10.—MAXIMUM DYNAMIC RESPONSE FOR EL CENTRO, CALIFORNIA EARTHQUAKE OF MAY 18, 1940 E-W COMPONENT

comparison. The ordinates of this curve correspond to the usual acceleration spectrum curve based on elastic behavior.

RESULTS OF COMPUTATIONS

The maximum dynamic response for the case of no damping ($\lambda = 0$) except by plastic deformation is shown in Figs. 5, 6, and 7. For periods where the ordinates of curve No. 1 (elastic case) are less than the strength parameter θ, the response of the system is purely elastic throughout the earthquake input. However, for periods where the ordinates of curve No. 1 are greater than θ, plastic deformations take place. Therefore, the solid curves in these figures depart from curve No. 1 at points where their ordinates are equal to θ.

Curve No. 2 for $\theta = 1.00$, in Fig. 5, shows that plastic deformations take place for periods under approximately 0.66 sec. The total dynamic response shown by this curve is considerably less than that shown for the purely elastic case. As the strength (θ) is decreased the maximum dynamic response also decreases until θ reaches some optimum value at which point a further decrease in θ results in an increase of maximum response. Comparison of the curves in Figs. 5 through 7 shows this optimum value of θ to be approximately equal to 0.3, 0.2, 0.1, and 0.05 at periods of 0.3, 0.6, 0.9, and 1.2, respectively. For larger periods than 1.2, the optimum value of θ generally is about 0.10 but curves for additional values of θ would probably show it to be somewhat less than 0.10.

After observation of these results and the ground motion shown in Fig. 4, it would seem that the optimum θ for any period is approximately equal to the amplitude (expressed as a fraction of gravity) of the component of ground acceleration having this same period. Therefore, for increasing values of θ greater than this optimum value, the maximum dynamic response is due more and more to a resonant condition that builds up over an appreciable increment of time; whereas, for decreasing θ values less than this optimum, the maximum response seems to be affected more and more by the transient response resulting from separate single ground acceleration pulses.

It should be noted that the rapid increase in ordinate of all curves where plastic deformation is involved as the period T approaches zero (curves 2 and 3, of Fig. 7) does not mean the maximum dynamic displacement is increasing in a similar manner. This rapid increase is due mainly to the fact that the static elastic displacement for 1g loading approaches zero. Therefore, as the period approaches zero, the numerator (maximum dynamic displacement) in the displacement ratio approaches some finite value while the denominator (static elastic displacement for 1g loading) approaches zero; consequently, the dynamic displacement ratio itself goes to infinity.

The dynamic response curves shown in Figs. 8 and 9 have been obtained for conditions similar to those previously discussed for the curves in Figs. 5 through 7 except that 5% viscous damping has been added to the system. A comparison of curve Nos. 1 and 2 in Fig. 8, both of which represent elastic behavior but which represent damping factors of 0% and 5% respectively, shows the large effect that damping has on the maximum dynamic response. The effect of lowering the strength parameter θ is generally the same for this case (Figs. 8, 9) as it was for the previously discussed case involving no viscous damping (Figs. 5, 6, 7) that is, the response reduces with decreasing θ to a certain point and then increases.

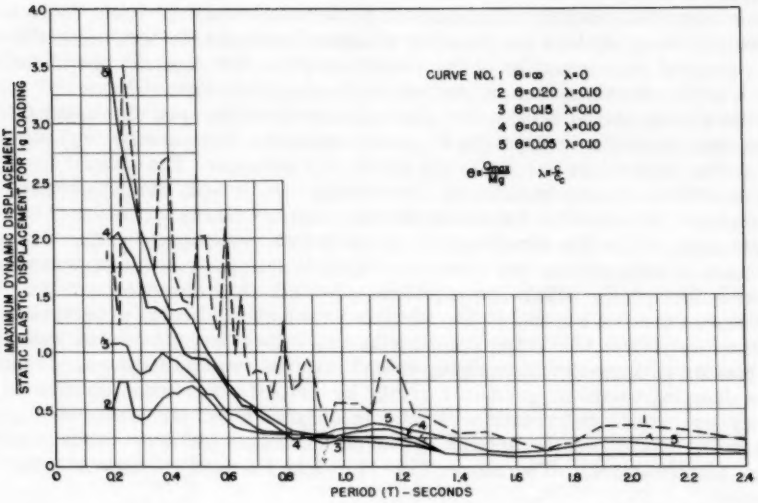
CURVE NO. 1 θ=∞ λ=0
2 θ=0.20 λ=0.10
3 θ=0.15 λ=0.10
4 θ=0.10 λ=0.10
5 θ=0.05 λ=0.10
θ=Qmax/Mg λ=ξ/ξc
MAXIMUM DYNAMIC DISPLACEMENT / STATIC ELASTIC DISPLACEMENT FOR 1g LOADING
PERIOD (T) - SECONDS

FIG. 11.—MAXIMUM DYNAMIC RESPONSE FOR EL CENTRO, CALIFORNIA EARTHQUAKE OF MAY 18, 1940 E-W COMPONENT

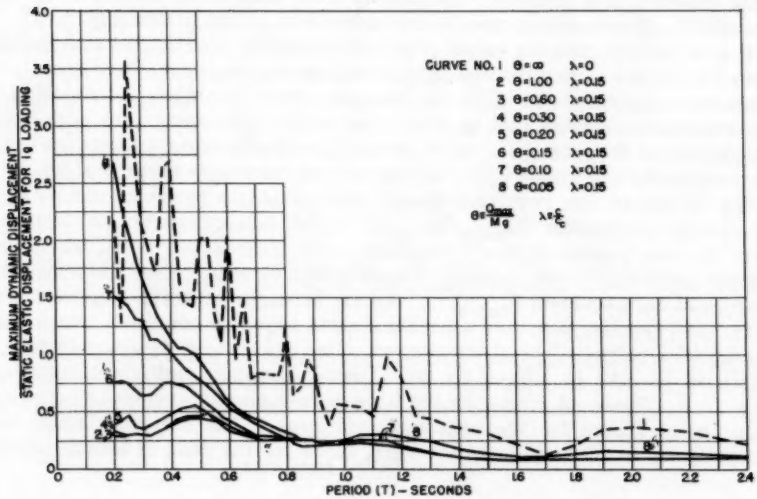

FIG. 12.—MAXIMUM DYNAMIC RESPONSE FOR EL CENTRO, CALIFORNIA EARTHQUAKE OF MAY 18, 1940 E-W COMPONENT

Figs. 10 and 11 show similar dynamic response curves for the case of 10% damping and Fig. 12 shows the response for 15% damping. While dynamic response shows a general reduction with an increase in damping coefficient, this reduction becomes less and less for continued increases in damping coefficient.

A general interpretation of the results in Figs. 5 through 12 would indicate that a stiff structure, that is periods up to approximately 0.8 sec for the El Centro earthquake, must be strengthened considerably over the more flexible structures in order to limit the dynamic response. This usually is the case as the stiffer structures are generally inherently stronger. The usual-type building has filler walls, partitions, stairwells, and so on, which considerably strengthen the structure for small displacements.[3] However, since these elements also stiffen the structure to a great extent, one should use this increased stiffness in interpreting any dynamic response data such as those presented in Figs. 5 through 12. While the resistance-deformation characteristics of such structures are not similar to the idealized case used herein, nevertheless, in general, the effect of forcing the structure to deform beyond its ultimate capacity results in appreciable damping which limits the maximum dynamic response. This damping would be produced partly by velocity dependent conditions and partly by plastic deformations in the structural steel elements. A damping factor (λ) of 15% would, perhaps, not be unreasonable for such cases involving large displacements. Therefore, Fig. 12 might be used to estimate this response.

For the "modern-type" structure, in which the structural frame is not assisted by the secondary elements previously mentioned, a damping factor of 5% would be more reasonable. Fig. 9 might therefore be used in this case. The reader should keep in mind that the dynamic response data in Figs. 5 through 12 are maximum values during the period of the earthquake and not the final values. Therefore, the permanent plastic deformations remaining at the end of the earthquake period are in general considerably less than those indicated by Figs. 5 through 12. These values may be considered as upper limits only.

In general the damping effect produced by plastic deformation is appreciable under conditions where the maximum dynamic response results primarily from a resonant condition. To show the damping effect of plastic deformation for a true resonant condition, that is, where the natural frequency (ω) of the system is equal to the frequency (p) of the ground forcing function, a sinusoidal ground acceleration of amplitude $\ddot{u}_{go}$ was imposed on the single mass system.

Fig. 13 shows the resulting steady state dynamic response plotted against the strength parameter ($Q_{max}/M\,\ddot{u}_{go}$). As this strength parameter approaches zero, the steady state dynamic response ratio approaches unity, which means that the amplitude of the dynamic displacement u_d approaches the amplitude of the ground displacement (u_{go}/ω^2). As the strength parameter approaches infinity, the response becomes a purely elastic resonant condition which results in infinite amplitudes of displacement. The equivalent damping factor (λ_e) plotted in Fig. 13 is difined as the viscous damping coefficient required to limit the amplitude of displacement for a purely elastic system to those shown in this same figure for the elasto-plastic case. This damping factor varies from 50% for the case of zero strength, to 0% for the case of infinite strength.

CONCLUSIONS

Based on the results of this investigation using the El Centro earthquake of May 1940, the following general conclusions are deduced.

(1) Buildings designed under present-day code requirements depend a great deal on damping to limit their dynamic response during the period of a strong motion earthquake. Because much of this damping is provided by plastic deformations, it is important that structures be designed to withstand large displacements without ultimate collapse.

(2) The maximum dynamic-elasto-plastic response of a structure decreases with a decrease in lateral yield strength until this strength reaches some optimum value at which point a further decrease in strength results in an increase in dynamic response.

(3) The optimum lateral strength in limiting the maximum dynamic response is of the order of 0.1 gravity or less for tall flexible buildings that have long periods of vibration and is of the order of 0.2 gravity for low stiff buildings that have short periods of vibration.

(4) The damping obtained from inelastic deformations, along with the increased strength and stiffness provided by secondary components such as walls, partitions, stairwells, and so on, are primarily responsible for the apparent ability of many existing structures to withstand strong-motion earthquakes.

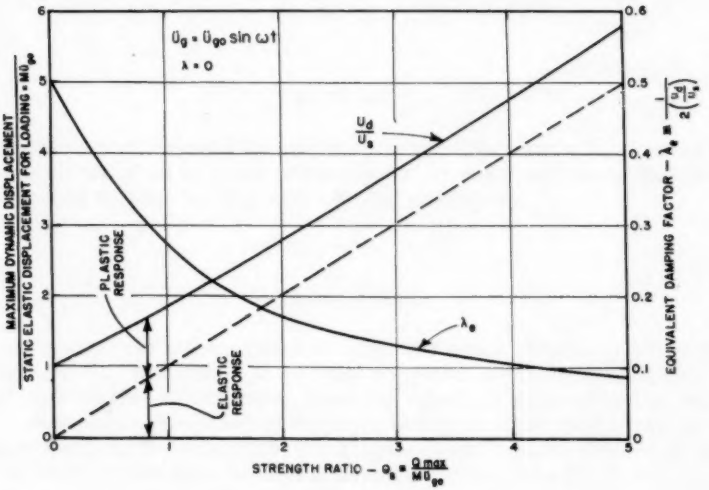
$\ddot{U}_g = \ddot{U}_{go} \sin \omega t$
$\lambda = 0$
$\frac{U_o}{U_s}$
λ_e
PLASTIC RESPONSE
ELASTIC RESPONSE
MAXIMUM DYNAMIC DISPLACEMENT / STATIC ELASTIC DISPLACEMENT FOR LOADING = $M\ddot{U}_{go}$
EQUIVALENT DAMPING FACTOR — $\lambda_e = \frac{1}{2}\left(\frac{U_d}{U_s}\right)$
STRENGTH RATIO — $\theta_s = \frac{Q_{max}}{M\ddot{U}_{go}}$

FIG. 13.—STEADY STATE DYNAMIC RESPONSE FOR SINUSIODAL GROUND ACCELERATION OF AMPLITUDE $\ddot{U}_{go}$

While conclusions 1 and 4 are perfectly general, conclusions 2 and 3 are based on the May 1940 El Centro earthquake and, therefore, may not necessarily show this same behavior for another earthquake of somewhat different characteristics.

ACKNOWLEDGMENTS

The author wishes to express his appreciation to the University of California (Berkeley, Calif.) Computer Center for the use of their IBM 701 computer in carrying out the computations for this investigation. He also wishes to thank

Leonard Housner for his help in writing the computer code and R. W. Clough for his suggestions and comments in the preparation of this paper.

ADDITIONAL REFERENCES

1. "United States Earthquakes," U. S. Coast and Geodetic Surbey, Govt. Printing Office, Washington, D. C.
2. "Computations on the Response of One-Mass Undamped Structures to the El Centro Acceleragraph Record," by E. C. Robison, Watson Scientific Computing Lab., Columbia Univ., New York, N. Y.
3. "Methods of Analysis for Structures Subjected to Dynamic Loading," by N. M. Newmark, Report to Directorate of Intelligence Hdqtrs., U. S. Air Force, Washington, D. C., December, 1950.

Journal of the
STRUCTURAL DIVISION
Proceedings of the American Society of Civil Engineers

MATRIX ANALYSIS OF PLANE RIGID FRAMES

By Fernando Venancio Filho[1]

SYNOPSIS

The problem of plane rigid frames is formulated in matrix form, using the principle of virtual work with displacements or forces as unknowns. The method is especially suitable for highspeed digital computers.

INTRODUCTION

The matrix form of the equations of plane redundant structures by the displacement and force methods is derived following ideas developed by J. H. Argyris[2] and making an adaptation from the equations deduced by that author for plane structures composed of rigid joints and straight bars with constant transverse section. The extension of the method to structures with curved bars and/or variable transverse section is obvious and immediate. By the matrix formulation, one finds the joints equilibrium equations of the displacement method or the elastic compatibility equations of the force method. It will be seen, however, that for the structures analyzed, in terms of the matrix formulation, the displacement method has a great advantage over the force method. The equations are solved by matrix methods, the final results being in the form of a matrix of the internal forces at the ends of the bars.

Note.—Discussion open until December 1, 1960. To extend the closing date one month, a written request must be filed with the Executive Secretary, ASCE. This paper is part of the copyrighted Journal of the Structural Division, Proceedings, of the American Society of Civil Engineers, Vol. 86, No. ST 7, July, 1960.

[1] Asst. Prof., Structures Dept., Instituto Tecnologico de Aeronautica Sao Jose dos Campos, Sao Paulo, Brasil.

[2] "Energy Theorems and Structural Analysis," by J. H. Argyris, part I, General Theory, Aircraft Engineering, Vol. 27, Nos. 2 and 3, February and March, 1955.

DISPLACEMENT METHOD

In this method the linear displacements x and y and the angular displacement θ of each joint are chosen as redundants.

Consider any bar ik of the structure, bounded by the joints i and k, Fig. 1. Let α_{ik} be the inclination from the bar axis in relation with the x axis and the system of orthogonal axis x' and y', the x' axis lying along the bar axes ik. Express the displacements of the joints i and k in the system x' y' in terms of the ones in the system xy:

$$\begin{bmatrix} \theta_1^{(ik)} \\ x_i'^{(ik)} \\ y_i'^{(ik)} \\ \theta_k^{(ik)} \\ x_k'^{(ik)} \\ y_k'^{(ik)} \end{bmatrix} = \begin{bmatrix} 1 & 0 & 0 & 0 & 0 & 0 \\ 0 & \cos\alpha_{ik} & \sin\alpha_{ik} & 0 & 0 & 0 \\ 0 & -\sin\alpha_{ik} & \cos\alpha_{ik} & 0 & 0 & 0 \\ 0 & 0 & 0 & 1 & 0 & 0 \\ 0 & 0 & 0 & 0 & \cos\alpha_{ik} & \sin\alpha_{ik} \\ 0 & 0 & 0 & 0 & -\sin\alpha_{ik} & \cos\alpha_{ik} \end{bmatrix} \begin{bmatrix} \theta_i \\ x_i \\ y_i \\ \theta_k \\ x_k \\ y_k \end{bmatrix} \quad \ldots (1)$$

Assume the whole structure to be composed of n/6 bars, then

$$[\Delta] = [a]\,[x] \quad \ldots\ldots\ldots\ldots\ldots\ldots \quad (2)$$

in which $[\Delta]$ is a column matrix whose n elements are the displacements $\theta_1^{(12)}, x_1'^{(12)}, y_1'^{(12)}, \theta_2^{(12)}, x_2'^{(12)}, y_2'^{(12)} \ldots \theta_i^{(ik)}, x_i'^{(ik)}, y_i'^{(ik)}, \theta_k^{(ik)}, x_k'^{(ik)}, y_k'^{(ik)} \ldots$ of the joints of the bars 12, . . . ik . . . taken, respectively, in each bar axis system; [X] is a column matrix the p elements of which are the unknown displacements of each joint; consequently, [a] will be an (n x p) matrix, which, multiplied by [X], will result in $[\Delta]$. The matrix [a] has an aspect similar to the first matrix on the right hand side of Eq. 1. It depends only upon the geometry of the structure and it can be found by simple inspection. Geometrically, its elements are the joint displacements referred to the bar axes, due to unit joint displacements referred to the x, y axes. The internal forces $M_i^{(ik)}, F_{x_i'}^{(ik)}, F_{y_i'}^{(ik)}, M_k^{(ik)}, F_{x_k'}^{(ik)}, F_{y_k'}^{(ik)}$, Fig. 2, can now be expressed as functions of the displacements $\theta_i^{(ik)}, x_i'^{(ik)}, y_i'^{(ik)}, \theta_k^{(ik)}, x_k'^{(ik)}, y_k'^{(ik)}$, Fig. 3, and the external loads.

In fact, if l_{ik}, A_{ik}, and I_{ik}, are, respectively, the span, the area and the moment of inertia of the transverse section, and E is Young's Modulus of the material, the parts from these internal forces due to the joint displacements

will be in order:

$$E\left(\frac{4\,I_{ik}}{l_{ik}}\,\theta_i^{ik} + \frac{6\,I_{ik}}{l^2_{ik}}\,y_i'^{(ik)} + \frac{2\,I_{ik}}{l_{ik}}\,\theta_k^{(ik)} - \frac{6\,I_{ik}}{l^2_{ik}}\,y_k'^{(ik)}\right)$$

$$E\left(\frac{A_{ik}}{l_{ik}}\,x_i'^{(ik)} - \frac{A_{ik}}{l_{ik}}\,x_k'^{(ik)}\right)$$

$$E\left(\frac{6\,I_{ik}}{l^2_{ik}}\,\theta_i^{(ik)} + \frac{12\,I_{ik}}{l^3_{ik}}\,y_i'^{(ik)} + \frac{6\,I_{ik}}{l^2_{ik}}\,\theta_k^{(ik)} - \frac{12\,I_{ik}}{l^3_{ik}}\,y_k'^{(ik)}\right)$$

$$E\left(\frac{2\,I_{ik}}{l_{ik}}\,\theta_i^{(ik)} + \frac{6\,I_{ik}}{l^2_{ik}}\,y_i'^{(ik)} + \frac{4\,I_{ik}}{l_{ik}}\,\theta_k^{(ik)} - \frac{6\,I_{ik}}{l^2_{ik}}\,y_k'^{(ik)}\right)$$

$$E\left(-\frac{A_{ik}}{l_{ik}}\,x_i'^{(ik)} + \frac{A_{ik}}{l_{ik}}\,x_k'^{(ik)}\right)$$

and

$$E\left(-\frac{6\,I_{ik}}{l^2_{ik}}\,\theta_i^{(ik)} - \frac{12\,I_{ik}}{l^3_{ik}}\,y_i'^{(ik)} - \frac{6\,I_{ik}}{l^2_{ik}}\,\theta_k^{(ik)} + \frac{12\,I_{ik}}{l^3_{ik}}\,y_k'^{(ik)}\right)$$

Calling $m_i^{(ik)}$, $f_{x_i}'^{(ik)}$, $f_{y_i}'^{(ik)}$, $m_k^{(ik)}$, $f_{x_k}'^{(ik)}$, $f_{y_k}'^{(ik)}$, the parts from $M_i^{(ik)}$, $F_{x_i}'^{(ik)}$, $F_{y_i}'^{(ik)}$, $M_k^{(ik)}$, $F_{x_k}'^{(ik)}$, $F_{y_k}'^{(ik)}$, due to the external loads, one can write under matrix form:

$$\begin{bmatrix} M_i^{(ik)} \\ F_{x_i}'^{(ik)} \\ F_{y_i}'^{(ik)} \\ M_k^{(ik)} \\ F_{x_k}'^{(ik)} \\ F_{y_k}'^{(ik)} \end{bmatrix} = E \begin{bmatrix} \frac{4\,I_{ik}}{l_{ik}} & 0 & \frac{6\,I_{ik}}{l^2_{ik}} & \frac{2\,I_{ik}}{l_{ik}} & 0 & -\frac{6\,I_{ik}}{l^2_{ik}} \\ 0 & \frac{A_{ik}}{l_{ik}} & 0 & 0 & -\frac{A_{ik}}{l_{ik}} & 0 \\ \frac{6\,I_{ik}}{l^2_{ik}} & 0 & \frac{12\,I_{ik}}{l^3_{ik}} & \frac{6\,I_{ik}}{l^2_{ik}} & 0 & -\frac{12\,I_{ik}}{l^3_{ik}} \\ \frac{2\,I_{ik}}{l_{ik}} & 0 & \frac{6\,I_{ik}}{l^2_{ik}} & \frac{4\,I_{ik}}{l_{ik}} & 0 & -\frac{6\,I_{ik}}{l^2_{ik}} \\ 0 & -\frac{A_{ik}}{l_{ik}} & 0 & 0 & +\frac{A_{ik}}{l_{ik}} & 0 \\ \frac{6\,I_{ik}}{l^2_{ik}} & 0 & -\frac{12\,I_{ik}}{l^3_{ik}} & -\frac{6\,I_{ik}}{l^2_{ik}} & 0 & \frac{12\,I_{ik}}{l^3_{ik}} \end{bmatrix} \begin{bmatrix} \theta_i^{(ik)} \\ x_i'^{(ik)} \\ y_i'^{(ik)} \\ \theta_k^{(ik)} \\ x_k'^{(ik)} \\ y_k'^{(ik)} \end{bmatrix} + \begin{bmatrix} m_i^{(ik)} \\ f_{x_i}'^{(ik)} \\ f_{y_i}'^{(ik)} \\ m_k^{(ik)} \\ f_{x_k}'^{(ik)} \\ f_{y_k}'^{(ik)} \end{bmatrix} \quad \ldots(3)$$

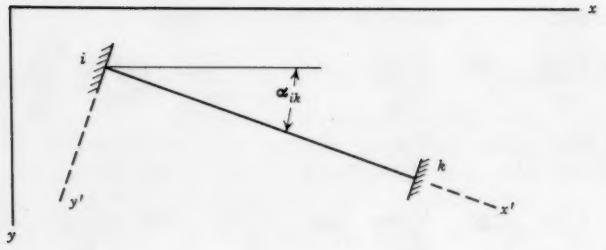

FIG. 1

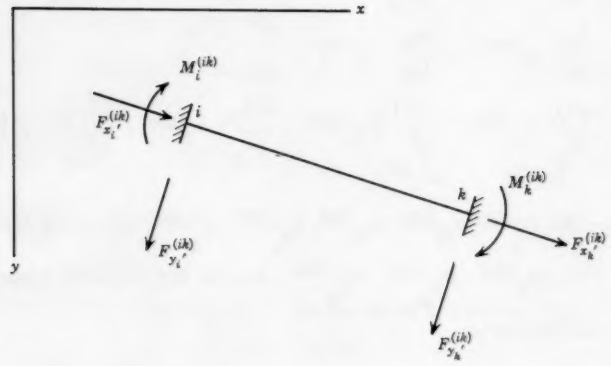

FIG. 2

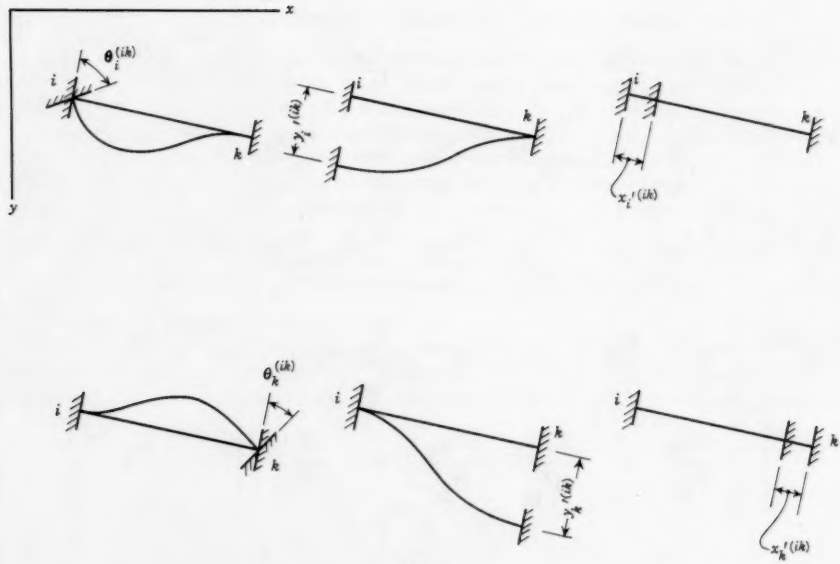

FIG. 3

If a bar is pinned at end k, the equation analogous to Eq. 3 is:

$$\begin{bmatrix} M_i^{(ik)} \\ F_{x_i}^{'(ik)} \\ F_{y_i}^{'(ik)} \\ F_{x_k}^{'(ik)} \\ F_{y_k}^{'(ik)} \end{bmatrix} = E \begin{bmatrix} \frac{3\,I_{ik}}{l_{ik}} & 0 & \frac{3\,I_{ik}}{l^2_{ik}} & 0 & -\frac{3\,I_{ik}}{l^2_{ik}} \\ 0 & \frac{A_{ik}}{l_{ik}} & 0 & -\frac{A_{ik}}{l_{ik}} & 0 \\ \frac{3\,I_{ik}}{l^2_{ik}} & 0 & \frac{3\,I_{ik}}{l^3_{ik}} & 0 & -\frac{3\,I_{ik}}{l^3_{ik}} \\ 0 & -\frac{A_{ik}}{l_{ik}} & 0 & \frac{A_{ik}}{l_{ik}} & 0 \\ -\frac{3\,I_{ik}}{l^2_{ik}} & 0 & -\frac{3\,I_{ik}}{l^2_{ik}} & 0 & \frac{3\,I}{l^3_{ik}} \end{bmatrix} \begin{bmatrix} \theta_i^{(ik)} \\ x_i^{'(ik)} \\ y_i^{'(ik)} \\ x_k^{'(ik)} \\ y_k^{'(ik)} \end{bmatrix} + \begin{bmatrix} m_i^{'(ik)} \\ f_{x_i}^{'(ik)} \\ f_{y_i}^{'(ik)} \\ f_{x_k}^{'(ik)} \\ f_{y_k}^{'(ik)} \end{bmatrix} \quad \ldots (3a)$$

The (6 x 6) matrix from Eq. 3 or the (5 x 5) one from Eq. 3a is the so called stiffness matrix from the ik bar, and it be designated by $[r_{ik}]$. The (n x n) matrix,

$$[r] = \begin{bmatrix} [r_{12}] & & & \\ & \ddots & & \\ & & [r_{ik}] & \\ & & & \ddots \end{bmatrix} \quad \ldots\ldots\ldots\ldots\ldots (4)$$

in which the elements of the principal diagonal are the stiffness matrices of each bar and the elements outside the principal diagonal are zero matrices, is the stiffness matrix of the complete structure.

Referring to Eqs. 2, 3 and 4, Eq. 5 can be written, for the whole structure.

$$[S] = [r]\,[a]\,[X] + [s] \quad \ldots\ldots\ldots\ldots\ldots (5)$$

in which [S] is a column matrix representing the total internal forces at the ends of the bars. The latter can be obtained by placing successively, one below the other, the matrices, of which that on the left hand side of Eq. 3 is typical. The term [s] is also a column matrix obtained in like manner from the column matrix on the extreme right hand side of Eq. 3, and represents the internal forces at the ends of the bars due to the external loads only.

The joint equilibrium equations will be obtained by the use of the virtual work principle, in matrix form. Referring to a force system F_1, $F_2 \ldots F_n$,

represented by the column matrix:

$$[F] = \begin{bmatrix} F_1 \\ F_2 \\ \cdot \\ \cdot \\ \cdot \\ F_n \end{bmatrix} \quad \ldots\ldots\ldots\ldots\ldots\ldots \quad (6)$$

and to the displacements of its points of application in its directions, δ_1, δ_2 $\ldots$ δ_n, represented by the column matrix:

$$[\delta] = \begin{bmatrix} \delta_1 \\ \delta_2 \\ \cdot \\ \cdot \\ \cdot \\ \delta_n \end{bmatrix} \quad \ldots\ldots\ldots\ldots\ldots\ldots \quad (7)$$

the work from the F forces corresponding to the δ displacements can be expressed in matrix form as,

$$T = [\delta]^*[F] \quad \ldots\ldots\ldots\ldots\ldots\ldots \quad (8)$$

in which the matrix with (*) is the transpose matrix. In fact:

$$[\delta]^*[F] = \begin{bmatrix} \delta_1 \delta_2 \ldots \delta_n \end{bmatrix} \begin{bmatrix} F_1 \\ F_2 \\ \cdot \\ \cdot \\ \cdot \\ F_n \end{bmatrix} = F_1 \delta_1 + F_2 \delta_2 + \ldots F_n \delta_n = T$$

The equilibrium conditions from the joints can be expressed then, by the vanishing of the work of the forces of matrix [S] from Eq. 5 through the displacements from matrix [a], Eq. 2, thus,

$$[a]^*[S] = 0 \quad \ldots\ldots\ldots\ldots\ldots\ldots \quad (9)$$

or, substituting from Eq. 5 the value of [S]:

$$[a]^*[r]\,[a]\,[X] + [a]^*[s] = 0 \quad \ldots\ldots\ldots\ldots\ldots\ldots (10)$$

The matrix [X] of the unknowns will be found by multiplying both members of Eq. 10 by $\left\{[a]^*[r]\,[a]\right\}^{-1}$, the reciprocal of $[a]^*[r]\,[a]$:

$$[X] = -\left\{[a]^*[r]\,[a]\right\}^{-1}[a]^*[s] \quad \ldots\ldots\ldots\ldots\ldots\ldots (11)$$

Substituting in Eq. 5 the value of [X] from Eq. 11, the problem of finding the internal forces at the ends of the bars is completely solved:

$$[S] = \left\{[E] - [r]\,[a]\left\{[a]^*[r]\,[a]\right\}^{-1}[a]^*\right\}[s] \quad \ldots\ldots\ldots\ldots\ldots (12)$$

in which [E] is the identity matrix.

From the perusal of Eq. 12, the following conclusions can be reached: (1) Matrix [S], giving the internal forces at the ends of the bars, is the solution of the problem and is obtained by matrix operations on matrices [r], [a] and [s], as indicated by Eq. 12; (2) Matrices [a] and [r] depend on the geometric and elastic properties of the structure, and matrix [s] depends on the external loads; (3) Once the matrix, which is to be multiplied by [s] in Eq. 12, is obtained, several cases of loading can be solved, simply by introducing the proper [s] matrix; (4) The order of the matrix $[a]^*[r][a]$, which is the matrix to be inverted, is equal to p, the number of unknown displacements; (5) This form of attack of the problem is particularly suitable for the use of electronic digital computers. With a matrix interpretive program, the matrix operations indicated in Eq. 12 are conveniently performed.

Consider, as a simple application example, the structure in Fig. 4. Let all the bars have the same transverse section of moment of inertia I and the external loads as indicated. The bar extensions will be neglected so that it is not necessary to consider the area of the transverse section. The unknowns, in this problem, will be the rotations θ_2 and θ_4 of joints 2 and 4 and the horizontal sidesway δ.

Let, $X_1 = \theta_2$, $X_2 = \theta_4$, and $X_3 = \delta$.

Equation 2 will be, for this particular case:

$$\begin{bmatrix} \theta_1^{(12)} \\ \theta_2^{(12)} \\ y_2'^{(12)} \\ \theta_3^{(34)} \\ \theta_4^{(34)} \\ y_4'^{(34)} \\ \theta_2^{(24)} \\ \theta_4^{(24)} \end{bmatrix} = \begin{bmatrix} 0 & 0 & 0 \\ 1 & 0 & 0 \\ 0 & 0 & 1 \\ 0 & 0 & 0 \\ 0 & 1 & 0 \\ 0 & 0 & 1 \\ 1 & 0 & 0 \\ 0 & 1 & 0 \end{bmatrix} \begin{bmatrix} X_1 \\ X_2 \\ X_3 \end{bmatrix} \quad \ldots\ldots\ldots (13)$$

Equation 5 will be:

$$\begin{bmatrix} M_1^{(12)} \\ M_2^{(12)} \\ F_{y_2'}^{(12)} \\ M_3^{(34)} \\ M_4^{(34)} \\ F_{y_4'}^{(34)} \\ M_2^{(24)} \\ M_4^{(24)} \end{bmatrix} = EI \begin{bmatrix} \frac{4}{l_{12}} & \frac{2}{l_{12}} & -\frac{6}{l_{12}^2} & 0 & 0 & 0 & 0 & 0 \\ \frac{2}{l_{12}} & \frac{4}{l_{12}} & -\frac{6}{l_{12}^2} & 0 & 0 & 0 & 0 & 0 \\ -\frac{6}{l_{12}^2} & -\frac{6}{l_{12}^2} & \frac{12}{l_{12}^3} & 0 & 0 & 0 & 0 & 0 \\ 0 & 0 & 0 & \frac{4}{l_{34}} & \frac{2}{l_{34}} & -\frac{6}{l_{34}^2} & 0 & 0 \\ 0 & 0 & 0 & \frac{2}{l_{34}} & \frac{4}{l_{34}} & -\frac{6}{l_{34}^2} & 0 & 0 \\ 0 & 0 & 0 & -\frac{6}{l_{34}^2} & -\frac{6}{l_{34}^2} & \frac{12}{l_{34}^3} & 0 & 0 \\ 0 & 0 & 0 & 0 & 0 & 0 & \frac{4}{l_{24}} & \frac{2}{l_{24}} \\ 0 & 0 & 0 & 0 & 0 & 0 & \frac{2}{l_{24}} & \frac{4}{l_{24}} \end{bmatrix} \begin{bmatrix} 0 & 0 & 1 \\ 1 & 0 & 0 \\ 0 & 0 & 1 \\ 0 & 0 & 0 \\ 0 & 1 & 0 \\ 0 & 0 & 1 \\ 1 & 0 & 0 \\ 0 & 1 & 0 \end{bmatrix} \begin{bmatrix} X_1 \\ X_2 \\ X_3 \end{bmatrix} + \begin{bmatrix} 0 \\ 0 \\ -H \\ 0 \\ 0 \\ 0 \\ -\frac{p\,l_{24}^3}{12} \\ \frac{p\,l_{24}^3}{12} \end{bmatrix} \quad \ldots\ldots (14)$$

The equilibrium condition, Eq. 10, will be:

$$\begin{bmatrix} 0&1&0&0&0&0&1&0 \\ 0&0&0&0&1&0&0&1 \\ 1&0&1&0&0&1&0&0 \end{bmatrix} EI \begin{bmatrix} \frac{4}{l_{12}} & \frac{2}{l_{12}} & -\frac{6}{l_{12}^2} & 0 & 0 & 0 & 0 & 0 \\ \frac{2}{l_{12}} & \frac{4}{l_{12}} & -\frac{6}{l_{12}^2} & 0 & 0 & 0 & 0 & 0 \\ -\frac{6}{l_{12}^2} & -\frac{6}{l_{12}^2} & \frac{12}{l_{12}^3} & 0 & 0 & 0 & 0 & 0 \\ 0 & 0 & 0 & \frac{4}{l_{34}} & \frac{2}{l_{34}} & -\frac{6}{l_{34}^2} & 0 & 0 \\ 0 & 0 & 0 & \frac{2}{l_{34}} & \frac{4}{l_{34}} & -\frac{6}{l_{34}^2} & 0 & 0 \\ 0 & 0 & 0 & -\frac{6}{l_{34}^2} & -\frac{6}{l_{34}^2} & \frac{12}{l_{34}^2} & 0 & 0 \\ 0 & 0 & 0 & 0 & 0 & 0 & \frac{4}{l_{24}} & \frac{2}{l_{24}} \\ 0 & 0 & 0 & 0 & 0 & 0 & \frac{2}{l_{24}} & \frac{4}{l_{24}} \end{bmatrix} \begin{bmatrix} 0&0&1 \\ 1&0&0 \\ 0&0&1 \\ 0&0&0 \\ 0&1&0 \\ 0&0&1 \\ 1&0&0 \\ 0&1&0 \end{bmatrix} \begin{bmatrix} X_1 \\ X_2 \\ X_3 \end{bmatrix} +$$

$$+ \begin{bmatrix} 0&1&0&0&0&0&1&0 \\ 0&0&0&0&1&0&0&1 \\ 1&0&1&0&0&1&0&0 \end{bmatrix} \begin{bmatrix} 0 \\ 0 \\ -H \\ 0 \\ 0 \\ 0 \\ \frac{p\,l_{24}^2}{12} \\ \frac{p\,l_{24}^2}{12} \end{bmatrix} = 0 \quad \ldots\ldots\ldots\ldots\ldots (15)$$

After making the indicated operations there results:

$$EI\left(\frac{4}{l_{24}} + \frac{4}{l_{14}}\right)X_1 + EI\frac{2}{l_{24}}X_2 - EI\frac{6}{l_{12}^3}X_3 - \frac{p\,l_{24}^2}{12} = 0 \ldots . (16a)$$

$$EI\frac{2}{l_{24}}X_1 + EI\left(\frac{4}{l_{34}} + \frac{4}{l_{24}}\right)X_2 - EI\frac{6}{l_{34}^2}X_3 + \frac{p\,l_{24}^2}{12} = 0 \ldots . (16b)$$

and

$$-EI\frac{6}{l_{12}^2}X_1 - EI\frac{6}{l_{34}^2}X_2 + EI\left(\frac{12}{l_{12}^3} + \frac{12}{l_{34}^3}\right)X_3 - H = 0 \ldots . (16c)$$

two joint and one sidesway equilibrium equations which could be obtained by the usual way.

FORCE METHOD

The matrix formulation by the force method can be made in a similar manner to the displacement method for structures in which it is convenient to take as redundants the bending moments at the ends of the bars, as in the continuous beam problem. The force method, nevertheless, shows its greatest potentiality when the so called group loadings are used and, in this case, the redundants are not, generally, bending moments at the ends of the bars.

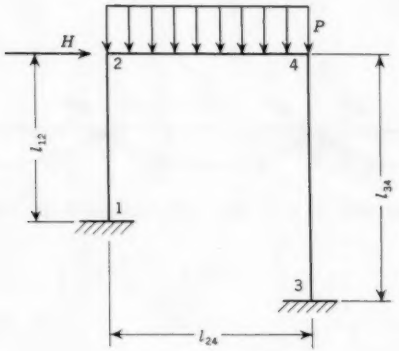

FIG. 4

Consider the continuous beam from Fig. 5, with constant transverse section area of moment of inertia I and with any vertical external load.

The basic statically determinate system will be obtained placing hinges on supports 2 and 3 and the redundants will be the bending moments in the beam at these supports. Thus,

$$\begin{bmatrix} M_1^{(12)} \\ M_2^{(12)} \\ M_2^{(23)} \\ M_3^{(23)} \\ M_3^{(34)} \\ M_4^{(34)} \end{bmatrix} = \begin{bmatrix} 0 & 0 \\ 1 & 0 \\ 1 & 0 \\ 0 & 1 \\ 0 & 1 \\ 0 & 0 \end{bmatrix} \begin{bmatrix} X_1 \\ X_2 \end{bmatrix} \quad \ldots\ldots\ldots\ldots\ldots (17)$$

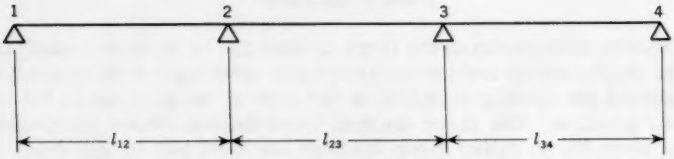

FIG. 5

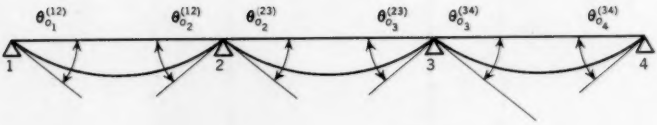

FIG. 6

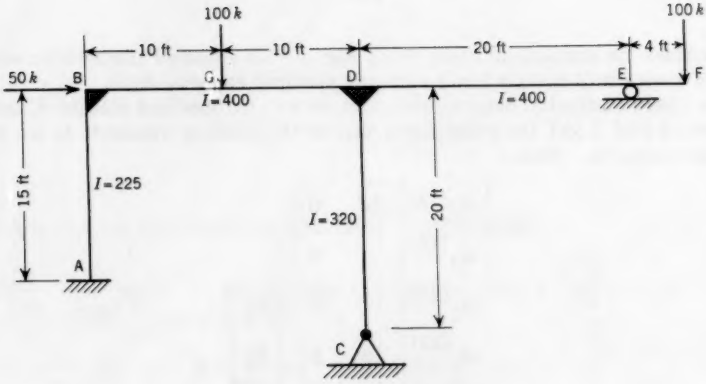

FIG. 7

or,

$$[M] = [b]\,[X] \quad \ldots\ldots\ldots\ldots\ldots\ldots (18)$$

in which [M] is the column matrix of six elements representing the bending moments at the ends of the spans; [X] is the column matrix formed by the two redundants and [b] is a (6 x 2) matrix which when multiplied by [X] results in [M]. It shall be noted that the elements of [b] are bending moments at the ends of the spans due to unit values of the redundants.

For any bar, 12, for instance, the slopes at the ends of the spans will be given by:

$$\begin{bmatrix} \theta_1^{(12)} \\ \theta_2^{(12)} \end{bmatrix} = \frac{1}{E\,I} \begin{bmatrix} \frac{l_{12}}{3} & \frac{l_{12}}{6} \\ \frac{l_{12}}{6} & \frac{l_{12}}{3} \end{bmatrix} \begin{bmatrix} M_1^{(12)} \\ M_2^{(12)} \end{bmatrix} + \begin{bmatrix} \theta_{o_1}^{(12)} \\ \theta_{o_2}^{(12)} \end{bmatrix} \quad \ldots\ldots (19)$$

The matrix:

$$\left[f_{12}\right] = \frac{1}{E\,I} \begin{bmatrix} \frac{l_{12}}{3} & \frac{l_{12}}{6} \\ \frac{l_{12}}{6} & \frac{l_{12}}{3} \end{bmatrix} \quad \ldots\ldots\ldots\ldots\ldots (20)$$

is the flexibility matrix of the bar 12. The (6 x 6) matrix:

$$[f] = \begin{bmatrix} \left[f_{12}\right] & & \\ & \left[f_{23}\right] & \\ & & \left[f_{34}\right] \end{bmatrix} \quad \ldots\ldots\ldots\ldots\ldots\ldots (21)$$

in which the elements of the principal diagonal are the flexibility matrices of each bar and the other elements are zero matrices, is the flexibility matrix of the whole structure. Therefore, following Eqs. 17 and 19,

$$\begin{bmatrix} \theta_1^{(12)} \\ \theta_2^{(12)} \\ \theta_2^{(23)} \\ \theta_3^{(23)} \\ \theta_3^{(34)} \\ \theta_4^{(34)} \end{bmatrix} = \frac{1}{EI} \begin{bmatrix} \frac{l_{12}}{3} & \frac{l_{12}}{6} & 0 & 0 & 0 & 0 \\ \frac{l_{12}}{6} & \frac{l_{12}}{3} & 0 & 0 & 0 & 0 \\ 0 & 0 & \frac{l_{23}}{3} & \frac{l_{23}}{6} & 0 & 0 \\ 0 & 0 & \frac{l_{23}}{6} & \frac{l_{23}}{3} & 0 & 0 \\ 0 & 0 & 0 & 0 & \frac{l_{34}}{3} & \frac{l_{34}}{6} \\ 0 & 0 & 0 & 0 & \frac{l_{34}}{6} & \frac{l_{34}}{3} \end{bmatrix} \begin{bmatrix} 0 & 0 \\ 1 & 0 \\ 1 & 0 \\ 0 & 1 \\ 0 & 1 \\ 0 & 0 \end{bmatrix} \begin{bmatrix} X_1 \\ X_2 \end{bmatrix} + \begin{bmatrix} \theta_{o_1}^{(12)} \\ \theta_{o_2}^{(12)} \\ \theta_{o_2}^{(23)} \\ \theta_{o_3}^{(23)} \\ \theta_{o_3}^{(34)} \\ \theta_{o_4}^{(34)} \end{bmatrix} \quad \ldots\ldots (22)$$

in which the second part of the right hand side of Eq. 22, is a matrix formed by the slopes at the ends of the spans in the basic system, due to the external loads, Fig. 6.

Concisely, Eq. 12 can be written

$$[\theta] = [f]\,[b]\,[X] + \left[\theta_o\right] \quad \ldots\ldots\ldots\ldots\ldots (23)$$

The elastic compatibility equations at the supports can be formulated by the condition of the vanishing of the work of the bending moments of matrix [b], Eq. 18, through the slopes from $[\theta]$, Eq. 23:

$$[b]^*[f][b][X] + [b]^*\left[\theta_o\right] = 0 \quad \ldots\ldots\ldots\ldots (24)$$

Multiplying both members by $\left\{[b]^*[f][b]\right\}^{-1}$:

$$[X] = -\left\{[b]^*[f][b]\right\}^{-1}[b]^*\left[\theta_o\right] \quad \ldots\ldots\ldots\ldots (25)$$

The final solution will be found by substituting Eq. 25 in Eq. 18:

$$[M] = -[b]\left\{[b]^*[f][b]\right\}^{-1}[b]^*\left[\theta_o\right] \quad \ldots\ldots\ldots\ldots (26)$$

Eq. 24, when written out in full, gives the three moment equations of the given continuous beam. In fact,

$$\begin{bmatrix} 0 & 1 & 1 & 0 & 0 & 0 \\ 0 & 0 & 0 & 1 & 1 & 0 \end{bmatrix} \frac{1}{E\,I} \begin{bmatrix} \frac{l_{12}}{3} & \frac{l_{12}}{6} & 0 & 0 & 0 & 0 \\ \frac{l_{12}}{6} & \frac{l_{12}}{3} & 0 & 0 & 0 & 0 \\ 0 & 0 & \frac{l_{23}}{3} & \frac{l_{23}}{6} & 0 & 0 \\ 0 & 0 & \frac{l_{23}}{6} & \frac{l_{23}}{3} & 0 & 0 \\ 0 & 0 & 0 & 0 & \frac{l_{34}}{3} & \frac{l_{34}}{6} \\ 0 & 0 & 0 & 0 & \frac{l_{34}}{6} & \frac{l_{34}}{3} \end{bmatrix} \begin{bmatrix} 0 & 0 \\ 1 & 0 \\ 1 & 0 \\ 0 & 1 \\ 0 & 1 \\ 0 & 0 \end{bmatrix} \begin{bmatrix} X_1 \\ X_2 \end{bmatrix} +$$

$$+ \begin{bmatrix} 0 & 1 & 1 & 0 & 0 & 0 \\ 0 & 0 & 0 & 1 & 1 & 0 \end{bmatrix} \begin{bmatrix} \theta_{o_1}^{(12)} \\ \theta_{o_2}^{(12)} \\ \theta_{o_2}^{(23)} \\ \theta_{o_3}^{(23)} \\ \theta_{o_3}^{(34)} \\ \theta_{o_4}^{(34)} \end{bmatrix} = 0 \quad \ldots\ldots\ldots (27)$$

After making the operations, the following moment equations are found:

$$\frac{1}{E\,I}\left(\frac{l_{12}}{3} + \frac{l_{23}}{3}\right)X_1 + \frac{1}{E\,I}\,\frac{l_{23}}{6}\,X_2 + \left(\theta_{o_2}^{(12)} + \theta_{o_2}^{(23)}\right) = 0 \ldots (28a)$$

and

$$\frac{1}{E\,I}\,\frac{l_{23}}{6}\,X_1 + \frac{1}{E\,I}\left(\frac{l_{23}}{3} + \frac{l_{34}}{3}\right)X_2 + \left(\theta_{o_3}^{(23)} + \theta_{o_3}^{(34)}\right) = 0 \quad \ldots \quad (28b)$$

NUMERICAL EXAMPLE

Consider the structure[3] of Fig. 7. The influence of axial forces is neglected, as habitually. For computational convenience assume 2 E = 0.1.

Matrices [a], [r], and [s] are

$$[a] = \begin{bmatrix} 0 & 0 & 0 \\ 1 & 0 & 0 \\ 0 & 0 & 1 \\ 1 & 0 & 0 \\ 0 & 1 & 0 \\ 0 & 1 & 0 \\ 0 & 0 & 1 \\ 0 & 1 & 0 \end{bmatrix} \quad [r] = \begin{bmatrix} 3 & 1.5 & -0.3 & 0 & 0 & 0 & 0 & 0 \\ 1.5 & 3 & -0.3 & 0 & 0 & 0 & 0 & 0 \\ -0.3 & -0.3 & 0.04 & 0 & 0 & 0 & 0 & 0 \\ 0 & 0 & 0 & 4 & 2 & 0 & 0 & 0 \\ 0 & 0 & 0 & 2 & 4 & 0 & 0 & 0 \\ 0 & 0 & 0 & 0 & 0 & 2.4 & -0.12 & 0 \\ 0 & 0 & 0 & 0 & 0 & -0.12 & 0.006 & 0 \\ 0 & 0 & 0 & 0 & 0 & 0 & 0 & 3 \end{bmatrix} \quad [s] = \begin{bmatrix} 0 \\ 0 \\ -25 \\ -250 \\ 250 \\ 0 \\ -25 \\ 200 \end{bmatrix}$$

Matrix $[a]^*[r]\,[a]$ is

$$\begin{bmatrix} 7 & 2 & -0.30 \\ 2 & 9.4 & -0.12 \\ -0.30 & -0.12 & 0.046 \end{bmatrix}$$

The inverse of this matrix is $\left\{[a]^*[r]\,[a]\right\}^{-1}$

$$\begin{bmatrix} 0.20491 & -0.02746 & 1.26481 \\ -0.02746 & 0.11373 & 0.11754 \\ 1.26481 & 0.11754 & 30.29385 \end{bmatrix}$$

---

3 "Digital Computation for Stiffness Matrix Analysis," by J. S. Archer, Proceedings, ASCE, Vol. 84, No. ST 6, October, 1958.

Finally matrix $[E] - [r][a]\{[a]^*[r][a]\}^{-1}[a]^*$ is

$$\begin{bmatrix}
1 & 0.07208 & 7.19105 & 0.07208 & 0.07645 & 0.07645 & 7.19105 & 0.07645 \\
0 & 0.76471 & 5.29384 & -0.23529 & 0.11764 & 0.11764 & 5.29384 & 0.11764 \\
0 & 0.01088 & 0.16769 & 0.01088 & -0.01294 & -0.01294 & -0.83231 & -0.01294 \\
0 & -0.76472 & -5.29432 & 0.23528 & -0.11762 & -0.11762 & -5.29432 & -0.11762 \\
0 & 0.29998 & -2.99978 & -0.29998 & 0.60000 & -0.40000 & -2.99878 & -0.40000 \\
0 & 0.21768 & 3.35317 & 0.21768 & -0.25885 & 0.74115 & 3.35317 & -0.25885 \\
0 & -0.01088 & -0.16766 & -0.01088 & 0.01294 & 0.01294 & 0.83234 & 0.01294 \\
0 & 0.08238 & -0.35262 & 0.08238 & -0.34119 & -0.34119 & -0.35262 & 0.65881
\end{bmatrix}$$

Multiplying this matrix by the external load matrix [s], matrix [S] will be:

$$[S] = \begin{bmatrix} M_1^{(12)} \\ M_2^{(12)} \\ F_{y_2'}^{(12)} \\ M_2^{(23)} \\ M_3^{(23)} \\ M_3^{(53)} \\ F_{y_3'}^{(53)} \\ M_3^{(34)} \end{bmatrix} = \begin{bmatrix} -343.17 \\ -152.93 \\ 8.07 \\ +152.97 \\ 294.98 \\ -338.56 \\ -8.07 \\ 43.50 \end{bmatrix}$$

Journal of the
STRUCTURAL DIVISION
Proceedings of the American Society of Civil Engineers

METHOD FOR ANALYSIS OF MULTIBEAM BRIDGES

By John E. Duberg,[1] Narbey Khachaturian,[2] M. ASCE,
and Raul E. Fradinger,[3] A.M. ASCE

SYNOPSIS

A general method for the analysis of multibeam bridges is presented. Expressions for moment, shear, and torque in each beam element, due to a concentrated load acting at any point on the multibeam bridge, are derived. The method developed is applied in calculating the vertical moments in beam elements of solid square section constituting a multibeam bridge. Influence lines for vertical moment in multibeam bridges having two, three, and ten beam elements of solid square section are developed.

A METHOD FOR ANALYSIS OF MULTIBEAM BRIDGES

Notation.—The letter symbols adopted for use in this paper are defined where they first appear in the text, and are arranged alphabetically for convenience of reference in the Appendix.

Note.—Discussion open until December 1, 1960. To extend the closing date one month, a written request must be filed with the Executive Secretary, ASCE. This paper is part of the copyrighted Journal of the Structural Division, Proceedings of the American Society of Civil Engineers, Vol. 86, No. ST 7, July, 1960.

[1] Formerly, Prof. of Civ. Engrg., Univ. of Illinois; now with Langley Research Center, Langley Field, Natl. Aeronautics and Space Admin., Va.
[2] Assoc. Prof. of Civ. Engrg., Univ. of Illinois, Urbana, Ill.
[3] Research Asst., Civ. Engrg., Univ. of Illinois, Urbana, Ill.

Assumptions.—In the development of a theory for analysis of multibeam bridges as presented herein, the structure is idealized with the following assumptions.

It is assumed that the bridge consists of beam elements placed side by side and connected to each other along the span by hinges at the corners of the cross section at the level of top fiber. For convenient reference, the hinge defining the point of connection of any two adjacent beam elements will be called a joint.

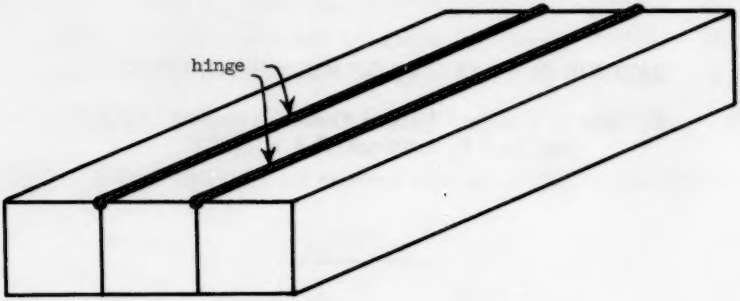

(a) A Perspective View of the Idealized Structure

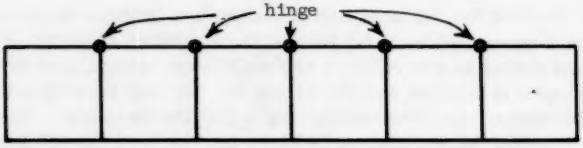

(b) Cross-Section of the Idealized Structure

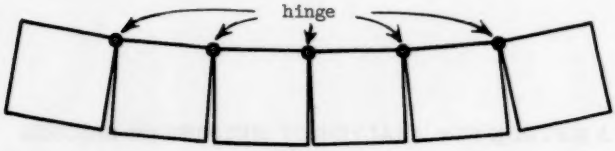

(c) Deflected Shape of the Idealized Structure Due to Downward Loads

FIG. 1.—IDEALIZED STRUCTURE

Evidently, this assumption implies that, although the joints move, all the components of movement and the rotation of each element at a joint are equal to those of the adjacent element at the same joint. Furthermore, according to this assumption, as the bridge is subjected to downward loads, the beam elements deflect downward and rotate about the hinges causing a separation of elements at all points except at the hinge. Fig. 1(a) shows a perspective view of the idealized structure in which the elements are shown to have solid square

sections. The cross-sectional view is shown in Fig. 1(b) while the lateral deflected shape of the cross section is shown in Fig. 1(c).

In addition, the following assumptions are made in this study.

1. The beam elements are made up of a homogeneous, isotropic, and elastic material.
2. The shear strains are small and can be neglected.
3. The cross section of each element is rigid, that is, the relative deformation of the parts forming the beam element is small in comparison with the deformation of the beam element as a whole.
4. All beam elements have the same cross-sectional properties and are of the same material.
5. Each beam element is simply-supported over the abutments or piers.
6. The beam elements are prismatic.
7. The external forces are concentrated loads and act vertically down.

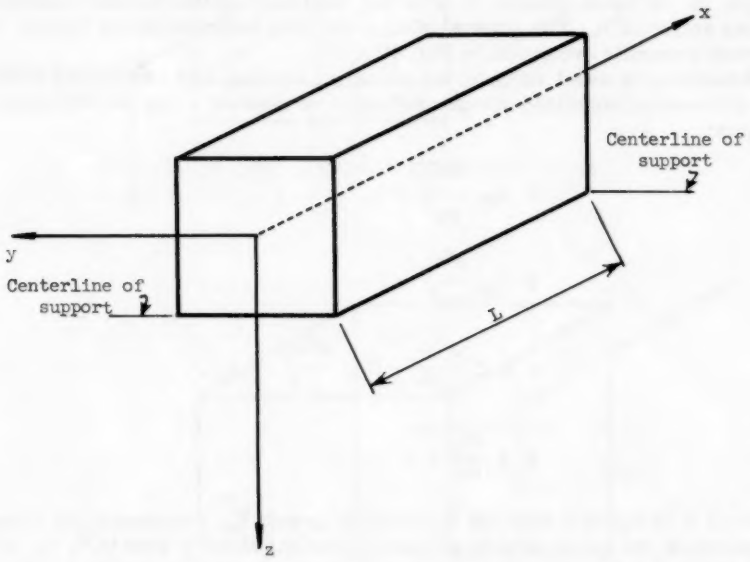

FIG. 2.—COORDINATE AXES

The Coordinate Axes.—The coordinate axes are taken as shown in Fig. 2. The x-axis is in the direction of the span passing through the center of gravity of any beam element. The y-axis is the horizontal axis which is in the transverse direction of the span. The z-axis is the vertical axis which, in this study, is parallel to the external loads. The origin of the coordinate axes is taken at the center of an end support.

The positive direction of z-axis is downward—in the direction of acting loads. The positive direction of x and y axes are as shown in Fig. 2.

Deformations of Each Beam Element.—Let j designate an intermediate beam element between elements j-1 and j+1. For convenience, the joints to the positive direction of y-axis of element j will also be designated as j.

The beam element j is subjected to the external load P_j as well as to statically indeterminate distributed forces which act on the element at Joints j and j-1. The lateral position of the given force P_j is defined by e_j, which is the lateral distance of the point of action of P_j from the centerline of the beam element. Figure 3(a) shows a small length dx of element j subjected to the concentrated load P_j which acts at a distance of e_j from the center of elements. The internal shears are also indicated on the same figure. It should be emphasized that P_j is the only load acting on the element j. For convenience, the internal moments are shown in Fig. 3(b).

The statically indeterminate forces acting on beam element j at joint j are q_j, r_j, and s_j and at joint j-1 are q_{j-1}, r_{j-1}, and s_{j-1}. The distributed forces q_j and q_{j-1}, which are parallel to x-axis, are opposite in sign and act on element j at joints j and j-1, respectively. The distributed forces r_j and r_{j-1} are opposite in sign and act on element j at joints j and j-1 parallel to y axis. Similarly, the distributed forces s_j and s_{j-1} act parallel to z axis, are opposite in sign, and act on element j at joints j and j-1. Fig. 4(a) shows a small length dx of beam element j with the statically indeterminate distributed forces acting on it. The internal shears are also indicated in the figure. The internal moments are shown in Fig. 4(b).

According to usual engineering theory of bending and restrained torsion, the differential equations for the deflection of element j can be expressed as follows:

$$E\, I_{xy} \frac{d^4 w_j}{dx^4} = p_j \quad \ldots\ldots\ldots\ldots\ldots\ldots \quad (1)$$

$$E\, I_{zx} \frac{d^4 v_j}{dx^4} = 0 \quad \ldots\ldots\ldots\ldots\ldots\ldots \quad (2)$$

$$-E\, C \frac{d^4 \phi_j}{dx^4} + G\, J \frac{d^2 \phi_j}{dx^2} = -t_j \quad \ldots\ldots\ldots\ldots \quad (3)$$

and

$$E\, A \frac{du_j}{dx} = 0 \quad \ldots\ldots\ldots\ldots\ldots\ldots \quad (4)$$

in which E is Young's modulus of elasticity in psi; I_{xy} represents the moment of inertia of the cross section of beam element j about y axis $in.^4$; w_j is the total vertical deflection of beam element j in in.; p_j represents the distributed load acting parallel to z axis in lb. per in.; I_{zx} is the moment of inertia of the cross section of beam element j about the axis parallel to z axis, in $in.^4$; v_j denotes the total horizontal deflection of beam element j in in.; C is the torsion-bending constant, in $in.^6$; ϕ_j represents the total rotation of beam element j in radians; G is the shear modulus of elasticity in psi; J is the torsion constant in $in.^4$; t_j denotes the acting torque in in.-lb per in.; A is the gross cross-sectional area of each beam element in $in.^2$; and u_j represents the axial deformation at centroid of beam element j in in.

It should be pointed out that Eqs. 1 through 4 are applicable to beam elements of any cross-sectional shape. In beam elements of solid or hollow square section, C is small or zero so that the first term on the left side of Eq. 3 can be neglected.

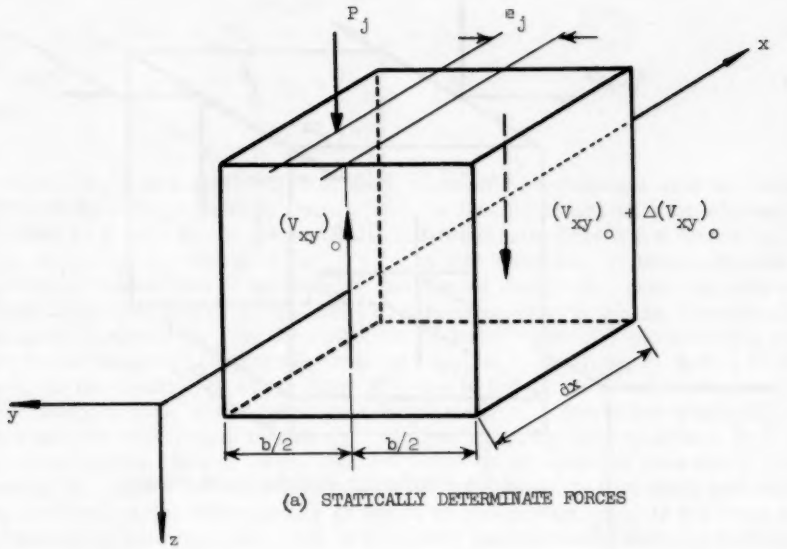

(a) STATICALLY DETERMINATE FORCES

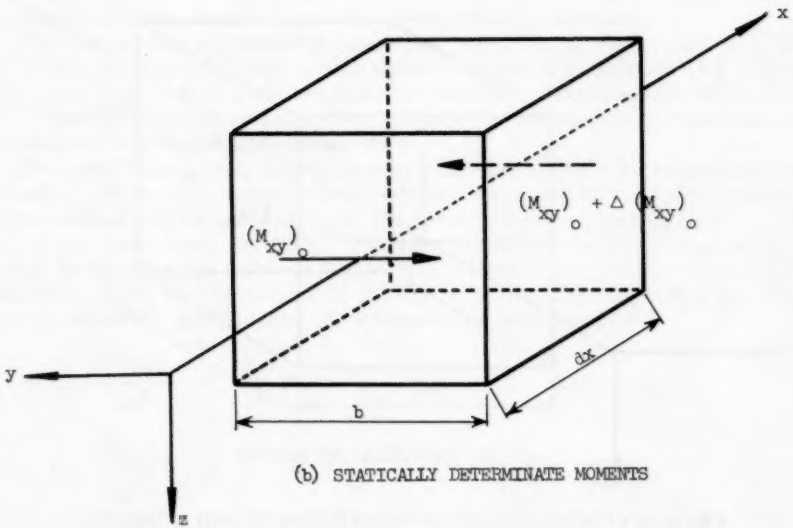

(b) STATICALLY DETERMINATE MOMENTS

FIG. 3.—STATICALLY DETERMINATE FORCES AND MOMENTS ACTING ON A SMALL ELEMENT

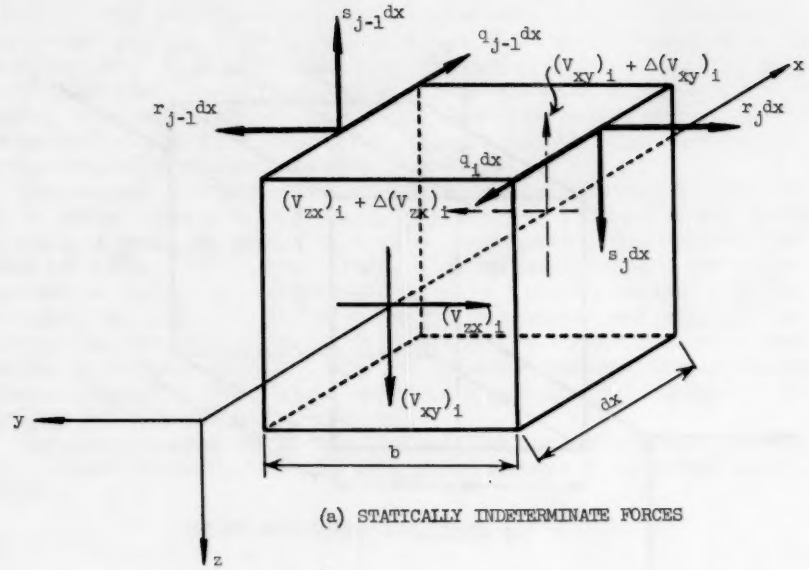

(a) STATICALLY INDETERMINATE FORCES

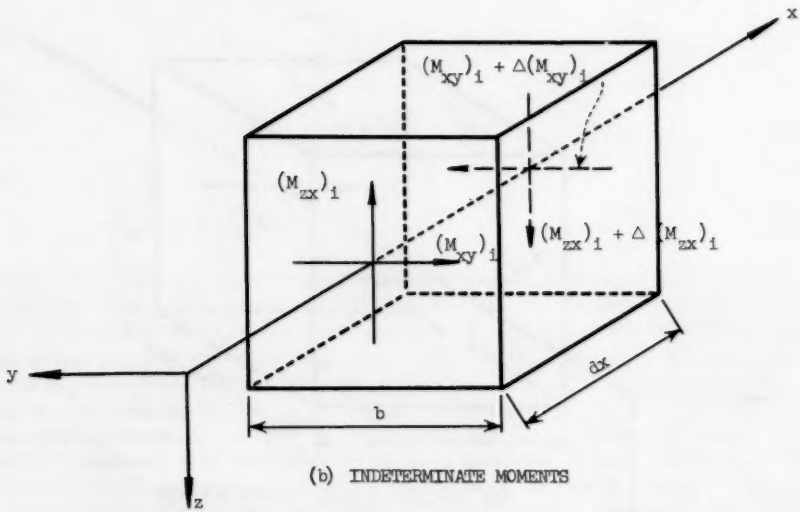

(b) INDETERMINATE MOMENTS

FIG. 4.—STATICALLY INDETERMINATE FORCES AND MOMENTS ACTING ON A SMALL ELEMENT.

The quantities w_j, v_j, ϕ_j, and u_j can be expressed in the following form:

$$w_j = (w_j)_o + (w_j)_i \quad \ldots\ldots\ldots\ldots\ldots\ldots \quad (5)$$

$$v_j = (v_j)_o + (v_j)_i \quad \ldots\ldots\ldots\ldots\ldots\ldots \quad (6)$$

$$\phi_j = (\phi_j)_o + (\phi_j)_i \quad \ldots\ldots\ldots\ldots\ldots\ldots \quad (7)$$

and

$$u_j = (u_j)_o + (u_j)_i \quad \ldots\ldots\ldots\ldots\ldots\ldots \quad (8)$$

in which $(w_j)_o$ is the deflection of beam element J parallel to z axis due to the external distributed load p_j in in.; $(w_j)_i$ is the deflection of beam element j parallel to y axis due to the statically indeterminate distributed forces q_{j-1}, r_{j-1}, s_{j-1}, q_j, r_j, and s_j in in.; $(v_j)_o$ is the deflection of beam element j parallel to y axis, due to an external distributed load in in. (Since the only external loads considered in this study are those parallel to z axis, this quantity is equal to zero); $(v_j)_i$ is the deflection of beam element j parallel to y axis due to the statically indeterminate forces q_{j-1}, r_{j-1}, s_{j-1}, q_j, r_j, and s_j in in.; $(\phi_j)_o$ is the rotation of beam element j due to the external distributed torque t in radians; $(\phi_j)_i$ is the rotation of beam element j due to the statically indeterminate distributed forces q_{j-1}, r_{j-1}, s_{j-1}, q_j, r_j, and s_j in in., $(u_j)_o$ is the axial deformation of beam element j due to an external concentric axial load in in. (Since the only external loads considered in this study are those parallel to z axis, this quantity is equal to zero); and $(u_j)_i$ is the axial deformation of beam element j due to statically indeterminate distributed forces q_{j-1}, r_{j-1}, s_{j-1}, q_j, r_j, and s_j in in.

The quantities w_j, v_j, ϕ_j and u_j are the total deflections, rotation and deformation of beam element j and have been defined previously.

For convenient reference the quantities $(w_j)_o$, $(v_j)_o$, $(\phi_j)_o$, and $(u_j)_o$ will be called the statically determinate deflections, while quantities $(w_j)_i$, $(v_j)_i$, $(\phi_j)_i$, and $(u_j)_i$ will be referred to as the statically indeterminate deflections.

In the following paragraphs, the statically determinate and indeterminate deflections will be discussed separately.

Statically Determinate Deflections of Beam Element j.—As mentioned previously, only vertical concentrated loads are taken into account. The only external load acting on beam element j is the concentrated load P_j which is acting at any point along the span. The lateral position of P_j is defined by e_j which is the distance between the point of action of P_j and the center of the element. If P_j is represented by a Fourier Series, the differential equations for the statically determinate deflections of element j will be

$$E\,I_{xy}\,\frac{d^4(w_j)_o}{dx^4} = \sum \frac{2\,P_j}{L}\,\sin\frac{n\,\pi\,c}{L}\,\sin\frac{n\,\pi\,x}{L} \quad \ldots\ldots\ldots\ldots\ldots \quad (9)$$

$$E\,I_{zx}\,\frac{d^4(v_j)_o}{dx^4} = 0 \quad \ldots\ldots\ldots\ldots\ldots\ldots\ldots\ldots\ldots\ldots \quad (10)$$

$$-\,E\,C\,\frac{d^4(\phi_j)_o}{dx^4} + G\,J\,\frac{d^2(\phi_j)_o}{dx^2} = -\sum \frac{2\,P_j\,e_j}{L}\,\sin\frac{n\,\pi\,c}{L}\,\sin\frac{n\,\pi\,x}{L} \quad \ldots \quad (11)$$

and

$$E\,A\,\frac{d(u_j)_o}{dx} = 0 \quad \ldots\ldots (12)$$

in which L is the length of simply-supported span in in.; c represents the distance from the point of action of P_j to the origin in in.; and n denotes a number.

All other terms have been defined previously.

Integration of Eqs. 9 through 12 will result in the following expressions:

$$(w_j)_o = \frac{2\,P_j\,L^3}{\pi^4\,E\,I_{xy}} \sum_n \frac{1}{4} \sin\frac{n\,\pi\,c}{L} \sin\frac{n\,\pi\,c}{L} \quad \ldots\ldots (13)$$

$$(v_j)_o = 0 \quad \ldots\ldots (14)$$

$$(\phi_j)_o = \frac{2\,P_j\,e_j\,L^3}{\pi^2} \sum \frac{1}{E\,C\,n^4\,\pi^2 + G\,J\,n^2\,L^2} \sin\frac{n\,\pi\,c}{L} \sin\frac{n\,\pi x}{L} \quad \ldots (15)$$

and

$$(u_j)_o = 0 \quad \ldots\ldots (16)$$

The preceding expressions for $(w_j)_o$, $(v_j)_o$, $(\phi_j)_o$, and $(u_j)_o$ satisfy the following boundary conditions:

1. The deflections of element j in the y and z direction are equal to zero at the supports, that is, for x = 0 and x = L.

$$(w_j)_o = 0 \quad \ldots\ldots (17a)$$

$$(v_j)_o = 0 \quad \ldots\ldots (17b)$$

2. Rotation due to torque is zero at the supports, that is, for x = 0 and x = L.

$$(\phi_j)_o = 0 \quad \ldots\ldots (18)$$

3. Stresses due to bending and due to torsion bending are equal to zero at the supports, that is, for x = 0 and x = L.

$$\frac{\partial^2(w_j)_o}{\partial x^2} = 0 \quad \ldots\ldots (19a)$$

$$\frac{\partial^2(v_j)_o}{\partial x^2} = 0 \quad \ldots\ldots (19b)$$

and

$$\frac{\partial^2(\phi_j)_o}{\partial x^2} = 0 \quad \ldots\ldots (19c)$$

4. Stresses due to axial forces are zero at the support, that is, for $x = 0$ and $x = L$.

$$\frac{\partial u}{\partial x} = 0 \quad \ldots\ldots\ldots\ldots\ldots\ldots\ldots (20)$$

Statically Indeterminate Deflections of Beam Element j.—As shown in Fig. 4, beam element j is subjected to statically indeterminate distributed forces which are exerted by the adjacent elements. As indicated before, the forces q_j and q_{j-1} act parallel to x-axis as joints j and j-1, respectively. The forces r_j and r_{j-1} act parallel to y-axis, the former at joint j and the latter at joint j-1. The forces s_j and s_{j-1}, which act at joint j and j-1, are parallel to z-axis. As shown in Fig. 4(a), q_j, r_j, and s_j have the same direction as the positive direction of the coordinate axes, while the direction of q_{j-1}, r_{j-1}, and s_{j-1} oppose the positive direction of the coordinate axes.

Referring to Fig. 4, it can be shown that the following relations are correct:

$$E\, I_{xy} \frac{d^4(w_j)_i}{dx^4} = (s_j - s_{j-1}) - \frac{d}{dx}(q_j - q_{j-1})\,\bar{z} \quad \ldots\ldots\ldots\ldots (21)$$

$$E\, I_{zx} \frac{d^4(v_j)_i}{dx^4} = (r_j - r_{j-1}) + \frac{d}{dx}(q_j + q_{j-1})\,\frac{b}{2} \quad \ldots\ldots\ldots\ldots (22)$$

$$-E\,C \frac{d^4(\phi_j)_i}{dx^4} + G\,J \frac{d^2(\phi_j)_i}{dx^2} = -(s_j + s_{j-1})\,\frac{b}{2} - (r_j - r_{j-1})\,\bar{z} \ldots (23)$$

and

$$E\,A \frac{d^2(u_j)_i}{dx^2} = -(q_j - q_{j-1}) \quad \ldots\ldots\ldots\ldots\ldots\ldots\ldots (24)$$

in which $\bar{z}$ is the distance of the joint from the shear center of the cross section of a beam element, in in.; and b is the width of the beam element in in. All other terms have been defined previously.

The distributed forces q_j, r_j, and s_j can be expressed in a form of series as follows:

$$q_j = \sum q_{jn} \cos \frac{n\,\pi\,x}{L} \quad \ldots\ldots\ldots\ldots\ldots (25)$$

$$r_j = \sum r_{jn} \sin \frac{n\,\pi\,x}{L} \quad \ldots\ldots\ldots\ldots\ldots (26)$$

and

$$s_j = \sum s_{jn} \sin \frac{n\,\pi\,x}{L} \quad \ldots\ldots\ldots\ldots\ldots (27)$$

Similarly

$$q_{j-1} = \sum q_{(j-1)n} \cos \frac{n\,\pi\,x}{L} \quad \ldots\ldots\ldots\ldots\ldots (28)$$

$$r_{j-1} = \sum r_{(j-1)n} \sin \frac{n \pi x}{L} \quad \ldots\ldots\ldots\ldots\ldots (29)$$

and

$$s_{j-1} = \sum s_{(j-1)n} \sin \frac{n \pi x}{L} \quad \ldots\ldots\ldots\ldots\ldots (30)$$

in which q_{jn}, r_{jn}, s_{jn}, $q_{(j-1)n}$, $r_{(j-1)n}$ and $s_{(j-1)n}$ represent the amplitudes of the nth Fourier component.

Substituting the preceding expressions in Eqs. 9 through 12 the following will be obtained:

$$E I_{xy} \frac{d^4(w_j)_i}{dx^4} = \sum \left[s_{jn} - s_{(j-1)n}\right] \sin \frac{n \pi x}{L} + \frac{\pi}{L} \bar{z} \sum n \left[q_{jn} - q_{(j-1)n}\right] \sin \frac{n \pi x}{L} \quad \ldots (31)$$

$$E I_{zx} \frac{d^4(v_j)_i}{dx^4} = \sum \left[r_{jn} - r_{(j-1)n}\right] \sin \frac{n \pi x}{L} - \frac{\pi b}{2 L} \sum n \left[q_{jn} + q_{(j-1)n}\right] \sin \frac{n \pi x}{L} \quad \ldots (32)$$

$$- E C \frac{d^4(\phi_j)_i}{dx^4} + G J \frac{d^2(\phi_j)_i}{dx^2} = \frac{b}{2} \sum \left[s_{jn} + s_{(j-1)n}\right] \sin \frac{n \pi x}{L} - z \sum \left[r_{jn} - r_{(j-1)n}\right] \sin \frac{n \pi x}{L} \quad \ldots (33)$$

and

$$E A \frac{d^2(u_j)_i}{dx^2} = - \sum \left[q_{jn} - q_{(j-1)n}\right] \cos \frac{n \pi x}{L} \quad \ldots\ldots\ldots\ldots\ldots (34)$$

Integration of the preceding equations will result in the following expressions:

$$(w_j)_i = \frac{L^4}{\pi^4 E I_{xy}} \sum n^{\frac{1}{4}} \left[s_{jn} - s_{(j-1)n}\right] \sin \frac{n \pi x}{L} + \frac{L^3 \bar{z}}{\pi^3 E I_{xy}} \sum n^{\frac{1}{3}} \left[q_{jn} - q_{(j-1)n}\right] \sin \frac{n \pi x}{L} \quad \ldots\ldots\ldots (35)$$

$$(v_j)_i = \frac{L^4}{\pi^4 E I_{zx}} \sum n^{\frac{1}{4}} \left[r_{jn} - r_{(j-1)n}\right] \sin \frac{n \pi x}{L} - \frac{L^3 b}{2 \pi^3 E I_{zx}} \sum n^{\frac{1}{3}} \left[q_{jn} + q_{(j-1)n}\right] \sin \frac{n \pi x}{L} \quad \ldots\ldots\ldots (36)$$

$$(\phi_j)_i = \frac{L^4\, b}{2\,\pi^2} \sum \frac{1}{E\,C\,n^4\,\pi^2 + G\,J\,n^2\,L^2} \left[s_{jn} + s_{(j-1)n}\right] \sin \frac{n\,\pi\,x}{L}$$

$$+ \frac{L^4\,\bar{z}}{\pi^2} \sum \frac{1}{E\,C\,n^4\,\pi^2 + G\,J\,n^2\,L^2} \left[r_{jn} - r_{(j-1)n}\right] \sin \frac{n\,\pi\,x}{L} \quad \ldots (37)$$

and

$$(u_j)_i = \frac{L^2}{\pi^2\,E\,A} \sum \frac{1}{n^2} \left[q_{jn} - q_{(j-1)n}\right] \cos \frac{n\,\pi\,x}{L} \quad \ldots\ldots\ldots (38)$$

Evidently Eqs. 35 to 38 also satisfy the boundary conditions mentioned in the preceding section.

Substitution of Eqs. 35 to 38 and Eqs. 13 through 16 in Eqs. 5 through 8 will result in the total deflections of beam element j as follows:

$$w_j = (w_j)_o + (w_j)_i = \frac{2\,P_j\,L^3}{\pi^4\,E\,I_{xy}} \sum \frac{1}{n^4} \sin \frac{n\,\pi\,c}{L} \sin \frac{n\,\pi\,x}{L}$$

$$+ \frac{L^4}{\pi^4\,E\,I_{xy}} \sum \frac{1}{n^4} \left[s_{jn} - s_{(j-1)n}\right] \sin \frac{n\,\pi\,x}{L}$$

$$+ \frac{L^3\,\bar{z}}{\pi^3\,E\,I_{xy}} \sum \frac{1}{n^3} \left[q_{jn} - q_{(j-1)n}\right] \sin \frac{n\,\pi\,x}{L} \quad \ldots\ldots\ldots (39)$$

$$v_j = (v_j)_o + (v_j)_i = (v_j)_i = \frac{L^4}{\pi^4\,E\,I_{zx}} \sum \frac{1}{n^4} \left[r_{jn} - r_{(j-1)n}\right] \sin \frac{n\,\pi\,x}{L}$$

$$- \frac{L^3\,b}{2\,\pi^3\,E\,I_{zx}} \sum \frac{1}{n^3} \left[q_{jn} + q_{(j-1)n}\right] \sin \frac{n\,\pi\,x}{L} \quad \ldots\ldots\ldots (40)$$

$$\phi_j = (\phi_j)_o + (\phi_j)_i = \frac{2\,P_j\,e_j\,L^3}{\pi^2} \sum \frac{1}{E\,C\,n^4\,\pi^2 + G\,J\,n^2\,L^2} \sin \frac{n\,\pi\,c}{L} \sin \frac{n\,\pi\,c}{L}$$

$$+ \frac{L^3\,b}{\pi^2} \sum \frac{1}{E\,C\,n^4\,\pi^2 + G\,J\,n^2\,L^2} \left[s_{jn} + s_{(j-1)n}\right] \sin \frac{n\,\pi\,x}{L}$$

$$+ \frac{L^2\,\bar{z}}{\pi^2} \sum \frac{1}{E\,C\,n^4\,\pi^2 + G\,J\,n^2\,L^2} \left[r_{jn} - r_{(j-1)n}\right] \sin \frac{n\,\pi\,x}{L} \quad \ldots (41)$$

$$u_j = (u_j)_o + (u_j)_i = (u_j)_i$$

$$= \frac{L^2}{\pi^2\,E\,A} \sum \frac{1}{n^2} \left[q_{jn} - q_{(j-1)n}\right] \cos \frac{n\,\pi\,x}{L} \quad \ldots\ldots\ldots (42)$$

Eqs. 39 to 42 are for the total deflection of beam element j. Evidently, similar expressions can be derived for elements j-1 and j+1.

Continuity.—In order to satisfy continuity at joint j, the following requirements must be met.

1. Vertical deflection of element j at joint j is equal to the vertical deflection of element j+1 at joint j.
2. The horizontal deflection of element j at joint j is equal to the horizontal deflection of element j+1 at joint j.
3. The axial deformation of element j at joint j is equal to the axial deformation of joint j+1 at joint j.

The preceding requirements for continuity can be expressed mathematically as follows:

$$w_j + \frac{b}{2}\phi_j = w_{j+1} - \frac{b}{2}\phi_{j+1} \quad \ldots\ldots\ldots\ldots\ldots (43)$$

$$v_j + \bar{z}\,\phi_j + v_{j+1} + \bar{z}\,\phi_{j+1} \quad \ldots\ldots\ldots\ldots\ldots (44)$$

$$u_j + \bar{z}\frac{\partial w_j}{\partial x} - \frac{b}{2}\frac{\partial v_j}{\partial x} + \bar{\Omega}\frac{\partial \phi_j}{\partial x} = u_{j+1} + \bar{z}\frac{\partial w_{j+1}}{\partial x} + \frac{b}{2}\frac{\partial v_{j+1}}{\partial x} - \bar{\Omega}\frac{\partial \phi_{j+1}}{\partial x} \quad \ldots\ldots (45)$$

in which $\bar{\Omega}$ is the axial deformation per unit rotation of element j at joint due to torsion warping in in. per radian per in.

The quantities w_{j+1}, v_{j+1}, ϕ_{j+1}, and u_{j+1} are vertical deflection, horizontal deflection, rotation and axial deformation of beam element j+1, respectively, as the subscript j+1 indicates.

The coefficient $\bar{\Omega}$, which appears in the last term of each side of Eq. 45, is generally small for closed box sections. It can be shown that for such box sections the terms containing $\bar{\Omega}$ have the same order of magnitude as the shearing deformations associated with bending which have been neglected in this study. These terms, therefore, can be neglected when the beam elements are closed box sections.

In beam elements of open section, however, it is a better approximation to include the terms containing $\bar{\Omega}$, even though the shearing deformations associated with bending are ignored. In beam elements of channel section, the terms containing $\bar{\Omega}$ should be taken into account.

Substituting Eqs. 39 through 42 for total deflections of element j, and similar expressions for the total deflections of element j+1 in Eqs. 43 through 45, the continuity relations for each n will become

$$-\frac{2(P_j - P_{j+1})L^3}{n^2\pi^2 E I_{xy}}\sin\frac{n\pi c}{L} - \frac{(P_j e_j + P_{j+1})e_{j+1} L^3 b}{E C n^2\pi^2 + G J L^2}\sin\frac{n\pi c}{L}$$

$$= -\frac{L^3\bar{z}}{n\pi E I_{xy}}\left[q_{(j-1)n} - 2q_{jn} + q_{(j+1)n}\right]$$

$$-\frac{L^4\bar{z}\,b}{2(E C n^2\pi^2 + G J L^2)}\left[r_{(j-1)n} - r_{(j+1)n}\right]$$

$$-\frac{L^4}{n^2\pi^2 E I_{xy}}\left[s_{(j-1)n} - 2s_{jn} + s_{(j+1)n}\right]$$

$$+\frac{L^4 b^2}{4(E C n^2\pi^2 + G J L^2)}\left[s_{(j-1)n} + 2s_{jn} + s_{(j+1)n}\right] \quad \ldots\ldots\ldots (46)$$

$$- \frac{2\left(P_j\, e_j - P_{j+1}\, e_{j+1}\right) L^3\, \bar{z}}{E\, C\, n^2\, \pi^2 + G\, J\, L^2} \sin \frac{n\, \pi\, c}{L}$$

$$= \frac{L^3\, b}{2\, n\, \pi\, E\, I_{xy}} \left[q_{(j-1)n} - q_{(j+1)n}\right]$$

$$- \left(\frac{L^4}{n^2\, \pi^2\, E\, I_{zx}} + \frac{L^4\, \bar{z}^2}{E\, C\, n^2\, \pi^2 + G\, J\, L^2} \right) \left[r_{(j-1)n} - 2r_{jn} + r_{(j+1)n}\right]$$

$$+ \frac{L^4\, \bar{z}\, b}{2\left(E\, C\, n^2\, \pi^2 + G\, J\, L^2\right)} \left[s_{(j-1)n} - s_{(j+1)n}\right] \quad \ldots\ldots\ldots\ldots\ldots\ldots (47)$$

$$- \frac{2\left(P_j - P_{j+1}\right) L^2\, \bar{z}}{n^2\, \pi^2\, E\, I_{xy}} \sin \frac{n\, \pi\, c}{L} + \frac{2\left(P_j\, e_j + P_{j+1}\, e_{j+1}\right) L^2\, \bar{\Omega}}{E\, C\, n^2\, \pi^2 + G\, J\, L^2} \sin \frac{n\, \pi\, c}{L}$$

$$= - \left(\frac{L^2}{n\, \pi\, E} \frac{1}{A} + \frac{\bar{z}^2}{I_{xy}} - \frac{b^2}{4\, I_{zx}} \right) \left[q_{(j-1)n} + q_{(j+1)n}\right]$$

$$+ \frac{2\, L^2}{n\, \pi\, E} \left(\frac{1}{A} + \frac{\bar{z}^2}{I_{xy}} + \frac{b^2}{4\, I_{zx}} \right) q_{jn}$$

$$+ \frac{L^3\, b}{2\, n^2\, \pi^2\, E\, I_{zx}} + \frac{L^3\, \bar{z}\, \bar{\Omega}}{E\, C\, n^2\, \pi^2 + G\, J\, L^2} \left[r_{(j-1)n} - r_{(j+1)n}\right]$$

$$- \frac{L^3\, \bar{z}}{n\, \pi\, E\, I_{xy}} + \frac{L^3\, b\, \bar{\Omega}}{2\left(E\, C\, n^2\, \pi^2 + G\, J\, L^2\right)} \left[s_{(j-1)n} + s_{(j+1)n}\right]$$

$$+ \frac{2\, L^3\, \bar{z}}{n^2\, \pi^2\, E\, I_{xy}} - \frac{L^3\, b\, \bar{\Omega}}{E\, C\, n^2\, \pi^2 + G\, J\, L^2}\, s_{jn} \quad \ldots\ldots\ldots\ldots\ldots\ldots (48)$$

Eqs. 46, 47, and 48 are three simultaneous equations in q_{jn}, r_{jn}, and s_{jn} derived on the basis of the continuity requirements at joint j. Evidently, equations similar to Eqs. 46, 47, and 48 can be derived for each joint in the multibeam structure relating the three forces in the joint. Each joint contains three unknowns q_n, r_n, and s_n.

If the multibeam structure consists of only two beam elements, there will be only one joint j with the three unknowns q_{jn}, r_{jn}, and s_{jn}. In this case, however, all the terms containing unknown forces in joints other than j will vanish. Generally, if the bridge contains m joints, there will be 3m unknown forces in each joint, and 3m equations available for their solution.

Once the unknown forces in each joint are determined, the analysis of a multibeam structure becomes possible. Shears and moments as well as stresses in each element, due to concentrated loads acting at various points on the bridge, can be calculated.

Derivation of Expressions for Moments, Shears, and Torque in Element j.— In order to determine the normal and shearing stresses in each element, it is necessary to calculate the moments, shears, and torque which are carried by each element.

The following expressions are consistent with the ordinary theory of bending and torsion:

$$(M_j)_{xy} = - E I_{xy} \frac{d^2 w_j}{dx^2} \quad \ldots\ldots\ldots\ldots\ldots\ldots (49)$$

$$(M_j)_{zx} = - E I_{zx} \frac{d^2 v_j}{dx^2} \quad \ldots\ldots\ldots\ldots\ldots\ldots (50)$$

$$(V_j)_{xy} = - E I_{xy} \frac{d^3 w_j}{dx^3} \quad \ldots\ldots\ldots\ldots\ldots\ldots (51)$$

$$(V_j)_{zx} = - E I_{zx} \frac{d^3 v_j}{dx^3} \quad \ldots\ldots\ldots\ldots\ldots\ldots (52)$$

and

$$T_j = - E C \frac{d^3 \phi_j}{dx^3} + G J \frac{d\phi_j}{dx} \quad \ldots\ldots\ldots\ldots (53)$$

in which $(M_j)_{xy}$ denotes the bending moment in element j about the neutral plane xy in in-lb; $(M_j)_{zx}$ represents the bending moment zx in element j about the neutral plane zx in in-lb; $(V_j)_{xy}$ is the shear in element j corresponding to $(M_j)_{xy}$ in-lb; $(V_j)_{zx}$ is the shear in element j corresponding to $(M_j)_{zy}$ in-lb; and T_j is the torque in element j in in-lb.

Substituting Eqs. 39, 40, and 41 for w_j v_j and ϕ_j in Eqs. 49 to 53 and differentiating, for each n the following will be obtained:

$$(M_j)_{xy} = \frac{2 P_j L}{n^2 \pi^2} \sin \frac{n \pi c}{L} - \frac{L \bar{z}}{n \pi} \left[q_{(j-1)n} - q_{jn}\right] - \frac{L^2}{n^2 \pi^2} \left[s_{(j-1)n} - s_{jn}\right] \ldots (54)$$

$$(M_j)_{zx} = - \frac{L b}{2 n \pi} \left[q_{(j-1)n} + q_{jn}\right] - \frac{L^2}{n^2 \pi^2} \left[r_{(j-1)n} - r_{jn}\right] \ldots\ldots\ldots (55)$$

$$(V_j)_{xy} = \frac{2 P_j}{n \pi} \sin \frac{n \pi c}{L} - \bar{z} \left[q_{(j-1)n} - q_{jn}\right] - \frac{L}{n \pi} \left[s_{(j-1)n} - s_{jn}\right] \ldots (56)$$

$$(V_j)_{zx} = - \frac{b}{2} \left[q_{(j-1)n} + q_{jn}\right] - \frac{L}{n \pi} \left[r_{(j-1)n} - r_{jn}\right] \ldots\ldots\ldots\ldots (57)$$

$$T_j = \frac{2 P_j e_j n \pi E C}{E C n^2 \pi^2 + G J L^2} \sin \frac{n \pi c}{L} + \frac{2 P_j e_j G J L^2}{\pi \left(E C n^3 \pi^2 + G J L^2\right)} \sin \frac{n \pi c}{L}$$

$$- \left[\frac{\bar{z} n L \left(\pi E C + L^2 G J\right)}{E C n^2 \pi^2 + G J L^2}\right] \left[r_{(j-1)n} - r_{jn}\right]$$

$$+ \left[\frac{b n L \left(\pi E C + L^2 G J\right)}{2 E C n^2 \pi^2 + G J L^2}\right] \left[s_{(j-1)n} + s_{jn}\right] \ldots\ldots\ldots\ldots (58)$$

Clearly, the preceding expressions for $(M_j)_{xy}$, $(M_j)_{zx}$, $(V_j)_{xy}$, $(V_j)_{zx}$, and T_j are functions of distributed indeterminate forces $q_{(j-1)n}$, $r_{(j-1)n}$, $s_{(j-1)n}$, q_{jn}, r_{jn}, and s_{jn} which act in the two joints on each side of element j. In order to calculate the preceding quantities, it is necessary to calculate these indeterminate distributed forces from Eqs. 46, 47, and 48, the continuity equations for joint j, and similar continuity equations for the other joints.

The quantity $(M_j)_{xy}$ presented by Eq. 54 seems to be the most significant quantity in this particular study, for it is through the study of this quantity that the lateral distribution of load in a multibeam bridge can be defined.

The quantity of $(M_j)_{zx}$ presented by Eq. 55 is generally small. However, for an accurate calculation of normal stress in a beam element this quantity may be necessary. The quantities $(V_j)_{xy}$, $(V_j)_{zx}$, and T_j, although not used in this study, may be used in the calculation of shear stresses in a beam element.

Determination of Normal Stresses in Each Beam Element.—The normal stresses in beam element j caused by $(M_j)_{xy}$ and $(M_j)_{zx}$ can be expressed as follows:

$$(\sigma_j)_1 = \frac{(M_j)_{xy}}{I_{xy}} z \quad \ldots\ldots\ldots\ldots\ldots\ldots (59)$$

and

$$(\sigma_j)_2 = \frac{(M_j)_{zx}}{I_{zx}} y \quad \ldots\ldots\ldots\ldots\ldots\ldots (60)$$

in which $(\sigma_j)_1$ represents the stress in element j due to $(M_j)_{xy}$ at a distance z from the xy-plane in psi; z is the distance of the point under consideration from the xy-plane in in.; $(\sigma_j)_2$ denotes the normal stress in element j due to $(M_j)_{zx}$ at a distance y from the zx-plane in psi; and y is the distance of the point under consideration from the zx-plane in in.

Substituting Eqs. 54 and 55 for $(M_j)_{xy}$ and $(M_j)_{zx}$ in Eqs. 59 and 60, $(\sigma_j)_1$ and $(\sigma_j)_2$ for each n will be

$$(\sigma_j)_1 = \frac{2 P_j L z}{n^2 \pi^2 I_{xy}} \sin \frac{n \pi c}{L} - \frac{L \bar{z} z}{n \pi I_{xy}} \left[q_{(j-1)n} - q_{jn}\right] - \frac{L^2 z}{n^2 \pi^2 I_{xy}} \left[s_{(j-1)n} - s_{jn}\right] \quad \ldots\ldots\ldots\ldots (61)$$

and

$$(\sigma_j)_2 = - \frac{L b y}{2 n \pi I_{zx}} \left[q_{(j-1)n} + q_{jn}\right] - \frac{L^2 y}{n^2 \pi^2 I_{zx}} \left[r_{(j-1)n} + r_{jn}\right] \ldots (62)$$

The uniformly distributed normal stress $(\sigma_j)_3$ caused by axial load is

$$(\sigma_j)_3 = E \frac{du_j}{dx} \quad \ldots\ldots\ldots\ldots\ldots\ldots (63)$$

Substituting the differential of Eq. 42 in terms of x in Eq. 63, the value of $(\sigma_j)_3$ for each n will be

$$(\sigma_j)_3 = \frac{L}{n\,\pi\,A}\left[q_{(j-1)n} - q_{jn}\right] \quad \ldots\ldots\ldots\ldots (64)$$

In addition to the normal stresses caused by $(M_j)_{xy}$, $(M_j)_{zx}$ and axial load, element j is subjected to normal stresses due to restrained torsional warping. The normal stresses due to this effect can be presented by the following expression:

$$(\sigma_j)_4 = E\,\Omega\,\frac{d^2\phi_j}{dx^2} \quad \ldots\ldots\ldots\ldots\ldots\ldots (65)$$

in which $(\sigma_j)_4$ is the normal stress in element j due to restrained warping caused by torsion psi; and Ω is the axial deformation of the point under consideration per unit rotation due to warping in in. per radians per in.

Substituting the second differential of Eq. 41 in terms of x in Eq. 65 and rearranging the value of $(\sigma_j)_4$ for each n will be

$$(\sigma_j)_4 = -\frac{2\,P_j\,e_j\,L\,E\,\Omega}{E\,C\,n^2\,\pi^2 + G\,J\,L^2}\sin\frac{n\,\pi\,c}{L} + \frac{L^2\,z\,E\,\Omega}{E\,C\,n^2\,\pi^2 + G\,J\,L^2}\left[r_{(j-1)n} - r_{jn}\right]$$

$$- \frac{L^2\,b\,E\,\Omega}{2\left(E\,C\,n^2\,\pi^2 + G\,J\,L^2\right)}\left[s_{(j-1)n} + s_{jn}\right] \quad \ldots\ldots\ldots\ldots\ldots (66)$$

The total normal stress in element j, σ_j can be obtained by the addition of Eqs. 61, 62, 64, and 66 as follows:

$$\begin{aligned}
\sigma_j &= (\sigma_j)_1 + (\sigma_j)_2 + (\sigma_j)_3 + (\sigma_j)_4 \\
&= \frac{2\,P_j\,L\,z}{n^2\,\pi^2\,I_{xy}} - \frac{2\,P_j\,e_j\,L\,E\,\Omega}{E\,C\,n^2\,\pi^2 + G\,J\,L^2}\sin\frac{n\,\pi\,c}{L} \\
&\quad - \left[\frac{L\,\bar{z}\,z}{n\,\pi\,I_{xy}} + \frac{L\,b\,y}{2\,n\,\pi\,I_{zx}} - \frac{L}{n\,\pi\,A}\right] q_{(j-1)n} \\
&\quad + \left[\frac{L\,\bar{z}\,z}{n\,\pi\,I_{xy}} - \frac{L\,b\,y}{2\,n\,\pi\,I_{zx}} - \frac{L}{n\,\pi\,a}\right] q_{jn} \\
&\quad - \left[\frac{L\,y}{n^2\,\pi^2\,I_{zx}} - \frac{L^2\,\bar{z}\,E\,\Omega}{E\,C\,n^2\,\pi + G\,J\,L^2}\right] r_{(j-1)n} \\
&\quad - \left[\frac{L\,y}{n^2\,\pi^2\,I_{zx}} + \frac{L^2\,z\,E\,\Omega}{E\,C\,n^2\,\pi + G\,J\,L^2}\right] r_{jn} \\
&\quad - \left[\frac{L^2\,z}{n^2\,\pi^2\,I_{xy}} + \frac{L^2\,b\,E\,\Omega}{2\left(E\,C\,n^2\,\pi^2 + G\,J\,L^2\right)}\right] s_{(j-1)n} \\
&\quad + \left[\frac{L^2\,z}{n^2\,\pi^2\,I_{xy}} - \frac{L^2\,b\,E\,\Omega}{2\left(E\,C\,n^2\,\pi^2 + G\,J\,L^2\right)}\right] s_{jn} \quad \ldots\ldots\ldots (67)
\end{aligned}$$

Eq. 67 presents accurately the normal stress at any point in beam element j. From a practical point of view, the important part of the total normal stress is provided by $(\sigma_j)_1$ or the stress due to $(M_j)_{xy}$. In practice $(\sigma_j)_2$, $(\sigma_j)_3$, and $(\sigma_j)_4$ are neglected. The quantity of $(\sigma_j)_4$ may be important for channel sections.

In order to solve Eq. 67 it is necessary to determine the distributed indeterminate forces $q_{(j-1)n}$, $r_{(j-1)n}$, $s_{(j-1)n}$, q_{jn}, r_{jn}, and s_{jn}. Simultaneous Eqs. 46, 47, and 48 for the continuity of joint j and similar equations for the continuity of other joints provide sufficient equations for the solution of these distributed indeterminate forces.

Shearing Stresses in Each Beam Element.—Shearing stresses in beam element j may be calculated from the shear forces and torque given by Eqs. 56, 57, and 58.

The shearing stresses caused by each of $(V_j)_{xy}$, $(V_j)_{zx}$, and T_j values are proportional to these values, and the constant of proportionality can be derived from the geometry of the particular section.

Since, in this study, no use has been made of shearing stresses, and it is inconvenient to present them so that they may be applicable to any shape of section, their derivation has been omitted.

Convergence.—The equations derived in this section are developed for any value of n. In order to get fairly accurate results, solutions for three or four values of n will be necessary. The total results will be the summation of results for each n.

It should be pointed out that Eqs. 46, 47, and 48 for the continuity of joint j and similar equations for other joints do not yield convergent results for successive values of n. Consequently, an actual solution for the distributed indeterminate forces q_r, r_n, s_r is not possible by Eqs. 46, 47, and 48.

However, from an analytical point of view, the moments, shears, torque, and stresses represented by Eqs. 54 through 67 are the quantities generally needed. These equations give convergent results for successive values of n.

In this particular study, the value of $(M_j)_{xy}$ is the quantity used for the determination of the lateral distribution of load. For the determination of this quantity, only the summation of three terms corresponding to three values of n have been used—namely n = 1, 3 and 5.

MULTIBEAM BRIDGES WITH BEAM ELEMENTS HAVING A SOLID SQUARE CROSS SECTION

General Expression for Continuity and $(M_j)_{xy}$.—In order to show the application of the method developed in the preceding section in calculating $(M_j)_{xy}$ in each element, the simplest case will be considered. It will be assumed that the multibeam bridge consists of beam elements having a solid square cross section.

In solid square sections the following expressions are correct: $I_{xy} = I_{zy} = \frac{b^4}{12}$, $J = 0.141\ b^4$; $A = b^2$; $\bar{z} = \frac{b}{2}$; $C \simeq 0$; $\Omega \simeq 0$; and $\frac{G}{E} = 0.50$ for $\mu = 0$.

Substituting the preceding expressions in Eqs. 46, 47, and 48, the continuity equations as joint f for each n become:

$$-\frac{1}{2\,n\,\pi}\,\frac{L}{b}\left[q_{(j-1)n}-2\,q_{jn}+q_{(j+1)n}\right]-0.296\left[r_{(j-1)n}-r_{(j+1)n}\right]$$

$$+0.296\left[s_{(j-1)n}+2\,s_{jn}+s_{(j+1)n}\right]-\frac{1}{n^2\,\pi^2}\left(\frac{L}{b}\right)^2\left[s_{(j-1)n}-2\,s_{jn}+s_{(j+1)n}\right]$$

$$=-\left[\frac{\left(P_j-P_{j+1}\right)}{L}\,\frac{2}{n^2\,\pi^2}\left(\frac{L}{b}\right)^2+0.591\,\frac{P_j\,\frac{2\,e_j}{b}+P_{j+1}\,\frac{2\,e_{j+1}}{b}}{L}\right]\sin\frac{n\,\pi\,c}{L}\quad\ldots\ (68)$$

$$-\frac{1}{2\,\pi\,n}\,\frac{L}{b}\left[q_{(j-1)n}-q_{(j+1)n}\right]-\left[\frac{1}{n^2\,\pi^2}\left(\frac{L}{b}\right)^2+0.296\right]\left[r_{(j-1)n}-2\,r_{jn}\right.$$

$$\left.+\,r_{(j+1)n}\right]+0.296\left[s_{(j-1)n}-s_{(j+1)n}\right]$$

$$=-0.591\,\frac{\left(P_j\,\frac{2\,e_j}{b}-P_{j+1}\,\frac{2\,e_{j+1}}{b}\right)}{L}\sin\frac{n\,\pi\,c}{L}\quad\ldots\ (69)$$

$$-\frac{1}{3}\left[q_{(j-1)n}-2\,q_{jn}+q_{(j+1)n}\right]+\frac{1}{4}\left[q_{(j-1)n}+2\,q_{jn}+q_{(j+1)n}\right]$$

$$+\frac{1}{2\,n\,\pi}\,\frac{L}{b}\left[r_{(j-1)n}-r_{(j+1)n}\right]-\frac{1}{2\,n\,\pi}\,\frac{L}{b}\left[s_{(j-1)n}-2\,s_{jn}+s_{(j+1)n}\right]$$

$$=-\frac{\left(P_j-P_{j+1}\right)}{L}\,\frac{1}{\pi\,n}\,\frac{L}{b}\sin\frac{n\,\pi\,c}{L}\quad\ldots\ (70)$$

The expression for $M_{j\,xy}$ for beam elements with a solid square section from Eq. 54 becomes

$$\left(M_j\right)_{xy}=\frac{2\,P_j\,L}{n^2\,\pi^2}\sin\frac{n\,\pi\,c}{L}-\frac{L\,b}{2\,n\,\pi}\left[q_{(j-1)n}-q_{jn}\right]$$

$$-\frac{L^2}{n^2\,\pi^2}\left[s_{(j-1)n}-s_{jn}\right]\quad\ldots\ (71)$$

Two-Element Structures.—This type of structure consists only of two solid square section elements connected by means of a hinge. The joint will be designated j, the left element will be referred to as j and the right element as

j+1. Evidently, in this case $q_{(j-1)} = 0$; $r_{(j-1)} = 0$; $s_{(j-1)} = 0$; $q_{(j+1)} = 0$; $r_{(j+1)} = 0$; and $s_{(j+1)} = 0$. Eqs. 68, 69, and 70 can be written as follows:

$$-\frac{2\left(P_j - P_{j+1}\right)}{L}\frac{L^2}{n^2\,\pi^2\,b^2}\sin\frac{n\,\pi\,c}{L} - 0.591\frac{\left(P_j\,\frac{2\,e_j}{b} + P_{j+1}\,\frac{2\,e_{j+1}}{b}\right)}{L}\sin\frac{n\,\pi\,c}{L}$$

$$= \frac{L}{n\,\pi\,b}\,q_{jn} + 2\left(0.296 + \frac{L^2}{n^2\,\pi^2\,b^2}\right)s_{jn} \quad \ldots\ldots\ldots\ldots\ldots\ldots\ldots\ldots (72)$$

$$-\frac{0.591\left(P_j\,\frac{2\,e_j}{b} - P_{j+1}\,\frac{2\,e_{j+1}}{b}\right)}{L}\sin\frac{n\,\pi\,c}{L}$$

$$= 2\left(\frac{L^2}{n^2\,\pi^2\,b^2} + 0.296\right)r_{jn} \quad \ldots\ldots\ldots\ldots\ldots\ldots\ldots\ldots\ldots\ldots (73)$$

$$-\frac{\left(P_j - P_{j+1}\right)}{L}\frac{L}{n\,\pi\,b}\sin\frac{n\,\pi\,c}{L} = \frac{7}{6}\,q_{jn} + \frac{L}{n\,\pi\,b}\,s_{jn} \quad \ldots\ldots\ldots\ldots\ldots (74)$$

A simultaneous solution of Eqs. 72, 73, and 74 yields the following expressions for q_{jn}, r_{jn}, and s_{jn}, respectively:

$$q_{jn} = -\frac{0.857\,P_j\left[\frac{1}{n\pi}\frac{L}{b}\,1 - \frac{2\,e_j}{b}\right] - 0.857\,P_{j+1}\frac{1}{n\pi}\frac{L}{b}\left[1 + \frac{2\,e_{j+1}}{b}\right]}{L\left[1 + 1.934\,\frac{1}{\pi^2\,n^2}\left(\frac{L}{b}\right)^2\right]}\sin\frac{n\,\pi\,c}{L} \quad \ldots\ldots (75)$$

$$r_{jn} = -\frac{1}{1 + \frac{3.384}{\pi^2\,n^2}\left(\frac{L}{b}\right)^2}\left(\frac{P_j\,\frac{2\,e_j}{b} - P_{j+1}\,\frac{2\,e_{j+1}}{b}}{L}\right)\sin\frac{n\,\pi\,c}{L} \quad \ldots\ldots (76)$$

$$s_{jn} = -\frac{P_j\left[\frac{1.934}{\pi^2\,n^2}\left(\frac{L}{b}\right)^2 + \frac{2\,e_j}{b}\right]P_{j+1}\left[\frac{1.934}{\pi^2\,n^2}\left(\frac{L}{b}\right)^2 - \frac{2\,e_{j+1}}{b}\right]}{L\left[1 + \frac{1.934}{\pi^2\,n^2}\left(\frac{L}{b}\right)^2\right]}\sin\frac{n\,\pi\,c}{L} \quad \ldots\ldots (77)$$

Since two-element structures are of academic interest, and they are discussed merely to show the application of the theory to solution of actual problems, an average value of $L/b = 20$ is taken in the solution of $(M_j)_{xy}$.

It can be shown that, in this case, L/b has a comparatively small effect on $(M_j)_{xy}$.

For $L/b = 20$ of the influence lines of $(M_j)_{xy}$ is drawn for a unit load that moves transversely from left to right at the midspan section.

In order to obtain the ordinates to the influence line for $(M_j)_{xy}$, the values of q_{jn} and s_{jn} from Eqs. 75 and 77 are substituted in Eq. 71 assuming $q_{(j-1)n} = 0$, $s_{(j-1)n} = 0$ and $c = L/2$.

The ordinates to the influence line have been tabulated as coefficients of L for each n value in Table 1. Three values of n have been used, namely 1, 3, and 5. Evidently, the even values of n result in zero values for q_{jn}, r_{jn}, and s_{jn}, since in this study it is assumed that c = L/2. Summation of moments for each n value results in the total moment. The total moments for various loadings are presented in the last column from the left in Table 1. More accurate values of $(M_j)_{xy}$ may be obtained by taking additional terms in the series representing q_{jn}, r_{jn}, and s_{jn}. By adding the component of $(M_j)_{xy}$ for n = 7 to

TABLE 1

ORDINATES TO THE INFLUENCE LINE OF $(M)_{xy}$ AT MIDSPAN FOR TWO ELEMENT STRUCTURES IN WHICH L/b = 20

Position	Solution	(M_{xy})/L carried by element	
		I	II
Point 1	n=1	0.1027	0.0999
	n=3	0.0126	0.0100
	n=5	0.0052	0.0028
	Σ	0.1205	0.1127
Point 2	n=1	0.1020	0.1006
	n=3	0.0119	0.0107
	n=5	0.0046	0.0034
	Σ	0.1185	0.1147
Point 3	n=1	0.1013	0.1013
	n=3	0.0113	0.0113
	n=5	0.0040	0.0040
	Σ	0.1166	0.1166

the total moments listed in Table 1, the accuracy may be somewhat improved. It can be shown that error in the quantities shown in Table 1 is in the neighborhood of 7%. The influence line for $(M_j)_{xy}$ is shown in Fig. 7.

Three-Element and Ten-Element Structures.—Eqs. 68, 69 and 70 can be rewritten in a form allowing their immediate use for the solution of any number of elements simply by isolating the coefficients of the unknowns. The m-element-structure leads to the solution of the linear matrix equation:

$$[A]_n\ [x]_n = [B]_n \quad \ldots\ldots\ldots\ldots\ldots\ldots\ (78)$$

[A] = matrix of order 3m-3
[B] = matrix of size m x p

The matrices $[A]_n$ and $[B]_n$ are the stiffness and load matrices, respectively, for each n. The $[x]_n$ values obtained are used in the evaluation of the moment carried by each element as given by Eq. 54.

The matrix $[x]_n$ has been evaluated on the Illiac, the electronic digital computer of the University of Illinois, using a standard library routine.

The solutions obtained for $(M)_{xy}$ values in three-element structure have been summarized in Table 2. For convenience, the beam elements have been designated as I, II, and III beginning from the left. The ordinate to influence

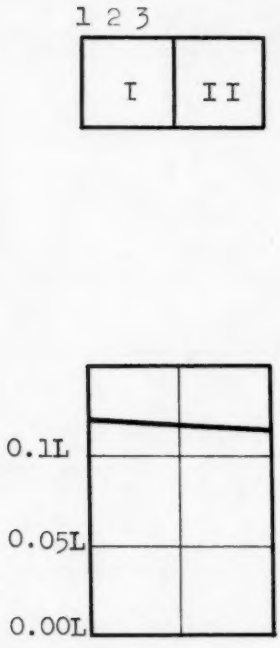

FIG. 5.—INFLUENCE LINE FOR $(M)_{xy}$ IN ELEMENT I WHEN A UNIT LOAD MOVES TRANSVERSELY AT MIDSPAN, TWO-ELEMENT STRUCTURE

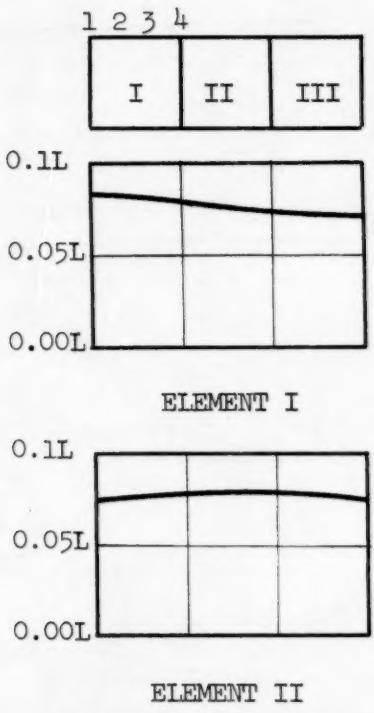

FIG. 6.—INFLUENCE LINES FOR $(M)_{xy}$ IN ELEMENTS I AND II WHEN A UNIT LOAD MOVES TRANSVERSELY AT MIDSPAN, THREE-ELEMENT STRUCTURES

lines are listed in terms of L for each n value corresponding to a particular position of load. As before, the solution is based on three values of n, namely, 1, 3, and 5. The sum of components of moment for each n is also shown in Table 2.

The solution for the three-element structure is based upon L/b = 20. This value of L/b is an average value and it has been chosen, since L/b ratio has a comparatively small effect upon the moments.

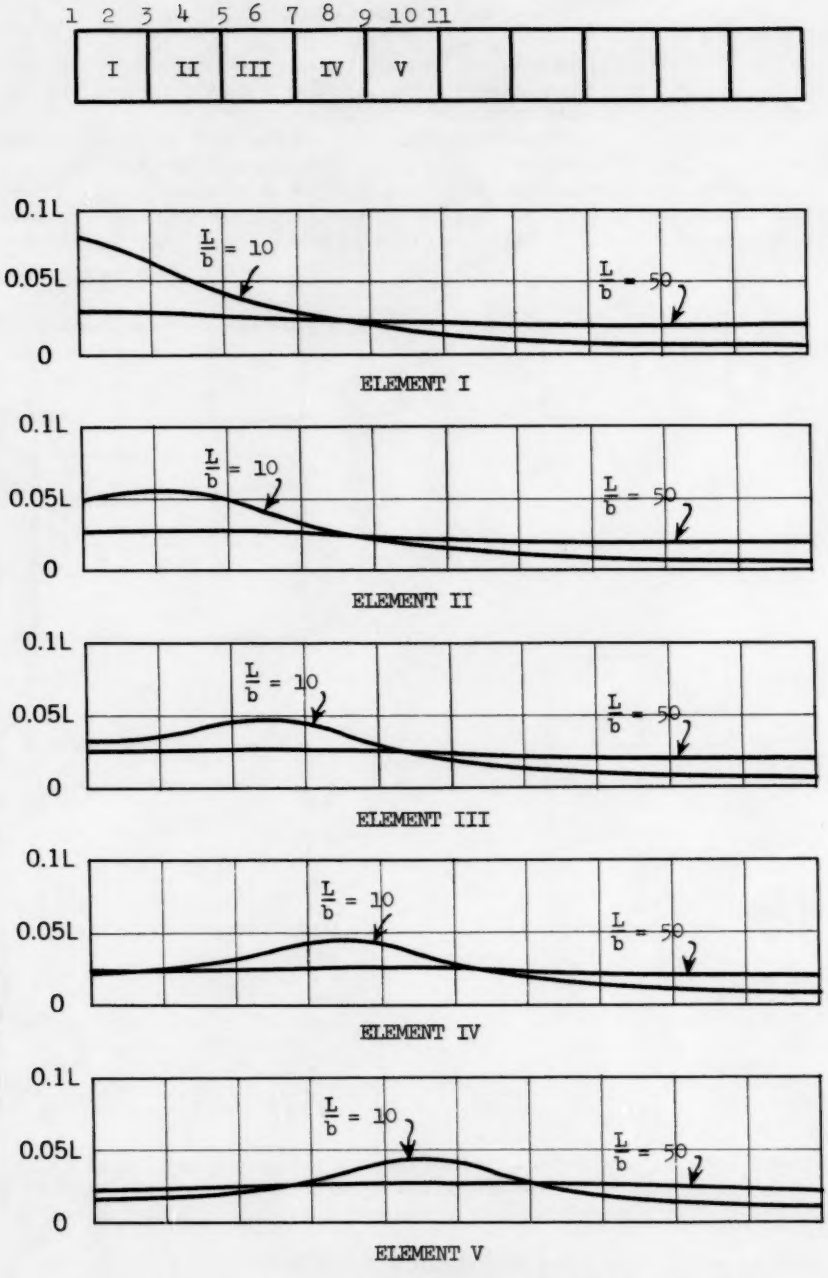

FIG. 7.—INFLUENCE LINE OF $(M)_{xy}$ IN EACH ELEMENT WHEN A UNIT LOAD MOVES TRANSVERSELY AT MIDSPAN.

Fig. 6, shows the influence line for (M_{xy}) in Elements I, II, and III. The ordinates are given in terms of L.

The solutions obtained for $(M)_{xy}$ values in a ten-element structure are listed in Tables 3 and 4 for L/b = 10, L/b = 50, respectively. For convenience the elements are designated as I through X. The solutions are based on three

TABLE 2

ORDINATES TO THE INFLUENCE LINE OF $(M)_{xy}$ AT MIDSPAN

FOR THREE ELEMENT STRUCTURE IN WHICH L/b = 20

Position	Solution	$10\ (M)_{xy}/L$ carried by element		
		I	II	III
Point 1	n=1	0.7074	0.6690	0.6500
	n=3	0.1016	0.0690	0.0546
	n=5	0.0460	0.0218	0.0123
	Σ	0.8560	0.7598	0.7169
Point 2	n=1	0.6978	0.6738	0.6548
	n=3	0.0935	0.0736	0.0581
	n=5	0.0407	0.0257	0.0147
	Σ	0.8320	0.7731	0.7276
Point 3	n=1	0.6882	0.6788	0.6595
	n=3	0.0853	0.0781	0.0618
	n=5	0.0343	0.0296	0.0171
	Σ	0.8078	0.7865	0.7384
Point 4	n=1	0.6738	0.6788	0.6738
	n=3	0.0741	0.0781	0.0741
	n=5	0.0251	0.0297	0.0251
	Σ	0.7730	0.7866	0.7730

values of n, namely 1, 3, and 5. The results given in Tables 3 and 4 are similar to those in Table 2.

Fig. 7 shows the influence lines of $(M)_{xy}$ in elements I through V for two values of L/b, 10 and 50. For convenience in this case, the ordinates are given in terms of L.

TABLE 3

ORDINATES TO INFLUENCE LINE TO $(M)_{xy}$ AT MIDSPAN FOR TEN ELEMENT STRUCTURE IN WHICH $\frac{L}{b} = 10$

Position of load	Solution	$10(M)_{xy}/L$ carried by element									
		I	II	III	IV	V	VI	VII	VIII	IX	X
	n=1	0.5856	0.4174	0.2980	0.2134	0.1537	0.1118	0.0831	0.0640	0.0524	0.0469
Point 1	n=3	0.1411	0.0527	0.0197	0.0074	0.0027	0.0010	0.0004	0.0001	-	-
	n=5	0.0635	0.0180	0.0001	-	-	-	-	-	-	-
	Σ	0.7902	0.4881	0.3178	0.2208	0.1564	0.1128	0.0835	0.0641	0.0524	0.0469
	n=1	0.5435	0.4296	0.3067	0.2196	0.1581	0.1151	0.0855	0.0659	0.0539	0.0483
Point 2	n=3	0.1190	0.0665	0.0249	0.0093	0.0035	0.0013	0.0005	-	-	-
	n=5	0.0513	0.0250	0.0041	0.0011	-	-	-	-	-	-
	Σ	0.7138	0.5211	0.3357	0.2300	0.1616	0.1164	0.0860	0.0659	0.0539	0.0483
	n=1	0.5015	0.4418	0.3154	0.2258	0.1626	0.1184	0.0879	0.0677	0.0555	0.0497
Point 3	n=3	0.0969	0.0804	0.0300	0.0112	0.0042	0.0016	0.0006	-	-	-
	n=5	0.0387	0.0331	0.0080	0.0017	-	-	-	-	-	-
	Σ	0.6371	0.5553	0.3534	0.2387	0.1558	0.1200	0.0885	0.0677	0.0555	0.0497
	n=1	0.4296	0.4206	0.3425	0.2452	0.1766	0.1285	0.0955	0.0736	0.0602	0.0539
Point 4	n=3	0.0665	0.0773	0.0510	0.0190	0.0071	0.0027	0.0010	-	-	-
	n=5	0.0245	0.0329	0.0196	0.0042	0.0003	-	-	-	-	-
	Σ	0.5206	0.5308	0.4131	0.2684	0.1840	0.1312	0.0965	0.0736	0.0602	0.0539
	n=1	0.3577	0.3995	0.3696	0.2646	0.1906	0.1387	0.1030	0.0794	0.0650	0.0582
Point 5	n=3	0.0362	0.0742	0.0719	0.0269	0.0100	0.0037	0.0014	0.0005	-	-
	n=5	0.0082	0.0325	0.0325	0.0063	0.0014	0.0001	-	-	-	-
	Σ	0.4021	0.5062	0.4740	0.2983	0.2020	0.1425	0.1044	0.0799	0.0650	0.0582

	n=1	0.3067	0.3425	0.3591	0.2995	0.2156	0.1570	0.1166	0.0898	0.0736	0.0659
Point 6	n=3	0.0249	0.0500	0.0715	0.0488	0.0182	0.0068	0.0025	0.0010	-	-
	n=5	0.0051	0.0200	0.0320	0.0194	0.0041	0.0008	0.0001	-	-	-
	Σ	0.3367	0.4135	0.4626	0.3677	0.2379	0.1646	0.1192	0.0908	0.0736	0.0659
	n=1	0.2557	0.2855	0.3487	0.3343	0.2407	0.1752	0.1302	0.1003	0.0821	0.0735
Point 7	n=3	0.0135	0.0277	0.0710	0.0707	0.0264	0.0099	0.0037	0.0014	0.0005	-
	n=5	0.0017	0.0068	0.0319	0.0326	0.0068	0.0014	0.0003	-	-	-
	Σ	0.2709	0.3200	0.4516	0.4376	0.2739	0.1865	0.1342	0.1017	0.0826	0.0735
	n=1	0.2196	0.2452	0.2995	0.3295	0.2798	0.2037	0.1513	0.1166	0.0955	0.0855
Point 8	n=3	0.0093	0.0190	0.0488	0.0706	0.0485	0.0181	0.0068	0.0026	0.0010	-
	n=5	0.0011	0.0041	0.0193	0.0319	0.0199	0.0041	0.0009	0.0002	-	-
	Σ	0.2300	0.2683	0.3676	0.4320	0.3482	0.2259	0.1590	0.1194	0.0965	0.0855
	n=1	0.1835	0.2049	0.2503	0.3248	0.3190	0.2322	0.1725	0.1329	0.1088	0.0975
Point 9	n=3	0.0050	0.0104	0.0265	0.0706	0.0705	0.0264	0.0099	0.0037	0.0014	0.0007
	n=5	0.0004	0.0014	0.0062	0.0319	0.0319	0.0068	0.0014	0.0003	-	-
	Σ	0.1889	0.2167	0.2830	0.4273	0.4214	0.2654	0.1838	0.1369	0.1102	0.0982
	n=1	0.1581	0.1766	0.2156	0.2798	0.3176	0.2742	0.2037	0.1570	0.1285	0.1151
Point 10	n=3	0.0035	0.0071	0.0182	0.0485	0.0705	0.0484	0.0181	0.0068	0.0027	0.0013
	n=5	0.0002	0.0009	0.0041	0.0199	0.0319	0.0193	0.0041	0.0009	0.0002	-
	Σ	0.1618	0.1346	0.2379	0.3482	0.4200	0.3419	0.2259	0.1647	0.1314	0.1164
	n=1	0.1328	0.1482	0.1810	0.2349	0.3162	0.3162	0.2349	0.1810	0.1482	0.1328
Point 11	n=3	0.0019	0.0039	0.0099	0.0264	0.0705	0.0705	0.0264	0.0099	0.0039	0.0019
	n=5	0.0001	0.0005	0.0014	0.0068	0.0319	0.0319	0.0068	0.0014	0.0005	0.0001
	Σ	0.1348	0.1526	0.1923	0.2681	0.4186	0.4186	0.2681	0.1923	0.1526	0.1348

TABLE 4 ORDINATES TO INFLUENCE LINE TO $(M)_{xy}$ AT MIDSPAN FOR TEN ELEMENT STRUCTURE IN WHICH $\frac{L}{b} = 50$

Position of Load	Solution	$\frac{M_{xy}}{L}$ x 10 carried by element									
		I	II	III	IV	V	VI	VII	VIII	IX	X
Point 1	n=1	0.2287	0.2203	0.2129	0.2066	0.2011	0.1967	0.1931	0.1904	0.1887	0.1878
	n=3	0.0432	0.0356	0.0294	0.0245	0.0207	0.0176	0.0154	0.0138	0.0127	0.0122
	n=5	0.0234	0.0167	0.0120	0.0085	0.0061	0.0045	0.0033	0.0026	0.0021	0.0019
	Σ	0.2953	0.2726	0.2543	0.2396	0.2279	0.2188	0.2118	0.2068	0.2035	0.2019
Point 2	n=1	0.2266	0.2205	0.2132	0.2068	0.2014	0.1969	0.1934	0.1907	0.1889	0.1881
	n=3	0.0413	0.0360	0.0298	0.0248	0.0209	0.0178	0.0155	0.0139	0.0128	0.0123
	n=5	0.0217	0.0172	0.0122	0.0088	0.0063	0.0046	0.0034	0.0026	0.0022	0.0019
	Σ	0.2896	0.2737	0.2552	0.2404	0.2286	0.2193	0.2123	0.2072	0.2039	0.2023
Point 3	n=1	0.2245	0.2207	0.2134	0.2070	0.2016	0.1972	0.1936	0.1909	0.1892	0.1883
	n=3	0.0394	0.0363	0.0301	0.0251	0.0211	0.0180	0.0157	0.0140	0.0130	0.0124
	n=5	0.0201	0.0177	0.0126	0.0090	0.0065	0.0047	0.0034	0.0028	0.0022	0.0020
	Σ	0.2840	0.2737	0.2561	0.2411	0.2292	0.2199	0.2127	0.2977	0.2044	0.2027
Point 4	n=1	0.2205	0.2192	0.2142	0.2078	0.2023	0.1973	0.1943	0.1916	0.1898	0.1885
	n=3	0.0360	0.0352	0.0310	0.0258	0.0218	0.0186	0.0162	0.0145	0.0134	0.0128
	n=5	0.0172	0.0168	0.0137	0.0098	0.0071	0.0053	0.0038	0.0029	0.0024	0.0022
	Σ	0.2737	0.2712	0.2589	0.2434	0.2312	0.2217	0.2143	0.2090	0.2056	0.2035
Point 5	n=1	0.2166	0.2176	0.2149	0.2085	0.2030	0.1985	0.1949	0.1923	0.1905	0.1896
	n=3	0.0325	0.0339	0.0319	0.0266	0.0224	0.0190	0.0167	0.0149	0.0138	0.0132
	n=5	0.0143	0.0160	0.0148	0.0106	0.0076	0.0056	0.0041	0.0032	0.0026	0.0023
	Σ	0.2634	0.2675	0.2616	0.2457	0.2330	0.2232	0.2157	0.2104	0.2069	0.2051

	n=1	0.2132	0.2142	0.2140	0.2096	0.2042	0.1997	0.1961	0.1934	0.1916	0.1907
Point 6	n=3	0.0298	0.0310	0.0311	0.0280	0.0235	0.0201	0.0175	0.0157	0.0145	0.0139
	n=5	0.0122	0.0137	0.0144	0.0120	0.0086	0.0063	0.0046	0.0036	0.0029	0.0026
	Σ	0.2552	0.2589	0.2595	0.2496	0.2363	0.2261	0.2182	0.2127	0.2090	0.2072
	n=1	0.2097	0.2107	0.2127	0.2109	0.2054	0.2008	0.1972	0.1945	0.1927	0.1918
Point 7	n=3	0.0270	0.0281	0.0304	0.0293	0.0247	0.0211	0.0184	0.0164	0.0152	0.0146
	n=5	0.0102	0.0114	0.0139	0.0134	0.0096	0.0070	0.0052	0.0040	0.0033	0.0029
	Σ	0.2469	0.2502	0.2570	0.2536	0.2397	0.2289	0.2208	0.2149	0.2112	0.2093
	n=1	0.2068	0.2078	0.2096	0.2102	0.2071	0.2024	0.1988	0.1960	0.1943	0.1934
Point 8	n=3	0.0248	0.0258	0.0280	0.0289	0.0263	0.0225	0.0196	0.0175	0.0162	0.0155
	n=5	0.0098	0.0098	0.0120	0.0132	0.0112	0.0081	0.0060	0.0047	0.0038	0.0034
	Σ	0.2404	0.2434	0.2496	0.2523	0.2446	0.2330	0.2244	0.2182	0.2143	0.2123
	n=1	0.2038	0.2048	0.2067	0.2096	0.2086	0.2040	0.2004	0.1976	0.1958	0.1949
Point 9	n=3	0.0226	0.0235	0.0255	0.0285	0.0280	0.0239	0.0208	0.0186	0.0172	0.0165
	n=5	0.0074	0.0082	0.0100	0.0130	0.0128	0.0093	0.0069	0.0053	0.0044	0.0039
	Σ	0.2338	0.2365	0.2422	0.2511	0.2494	0.2372	0.2281	0.2215	0.2174	0.2153
	n=1	0.2014	0.2023	0.2042	0.2071	0.2085	0.2061	0.2024	0.1997	0.1978	0.1969
Point 10	n=3	0.0209	0.0218	0.0235	0.0263	0.0278	0.0258	0.0225	0.0201	0.0186	0.0178
	n=5	0.0063	0.0070	0.0086	0.0112	0.0127	0.0110	0.0082	0.0063	0.0051	0.0046
	Σ	0.2286	0.2311	0.2363	0.2446	0.2490	0.2429	0.2331	0.2261	0.2215	0.2193
	n=1	0.1989	0.1998	0.2017	0.2045	0.2083	0.2083	0.2045	0.2017	0.1998	0.1989
Point 11	n=3	0.0192	0.0200	0.0216	0.0241	0.0277	0.0277	0.0241	0.0216	0.0200	0.0192
	n=5	0.0053	0.0059	0.0072	0.0094	0.0126	0.0126	0.0094	0.0072	0.0059	0.0053
	Σ	0.2234	0.2257	0.2305	0.2380	0.2486	0.2486	0.2380	0.2305	0.2257	0.2234

From Tables 2, 3, and 4 it can be shown that for three values of n, $(M)_{xy}$ values for three-and ten-element structures are roughly within 7% of the static values. It may be said that the errors, in this case, are of the same order of magnitude as those in two-element structures.

Interpretation of Results.—A study of influence lines for $(M)_{xy}$ in two-element and three-element multibeam structures, as shown in Figs. 5 and 6, indicates the load is distributed almost uniformly among the elements. It should be pointed out that the influence lines in these figures are drawn for L/b = 20. For L/b values greater than 20, the influence lines may tend to become horizontal. For L/b values less than 20 it is possible that the loaded element may carry somewhat more load than the others.

From the shape of the influence lines and the pattern of lateral load distribution, one may conclude that in two-element and three-element structures the lateral distribution of load is uniform. In this case, as one element is loaded all elements in the bridge deflect almost the same amount. It is true that two-element and three-element structures have no practical significance, nevertheless, their study contributes to the understanding of the problem.

A study of Fig. 7 indicates that the lateral distribution of load in a ten-element structure depends on the L/b value. Fig. 7 is prepared for two values of L/b, 10 and 50. From the figure it may be observed that for L/b = 50, the structure is similar to two-element or three-element structures. For L/b = 10, however, the loaded element carries a greater percentage of the load, and the structure is more rigid.

It should be pointed out that the range of L/b, as selected in this study, is unreasonably high. From a practical point of view, it is very seldom that L/b exceeds about 30. It may be concluded, therefore, that, generally, in ten-element structures a greater percentage of the load is carried by the loaded element.

APPENDIX. NOTATION

A = gross cross-sectional area of a beam element, in sq in.;

b = width of a beam element in in.;

C = torsion-bending constant, in $in.^6$;

c = distance between the point of action of concentrated load P_j from the support of the beam assumed origin, in in.;

E = Young's modulus of elasticity, in psi;

e = eccentricity, that is, the transverse distance between the point of action of external load and the center of beam element, in in.;

G = shearing modulus of elasticity, in psi;

h = overall depth of a beam element, in in.;

I_{xy} = moment of inertia of the cross section of a beam element about the axis parallel to y axis, in $in.^4$;

I_{zx} = moment of inertia of the cross section of a beam element about the axis parallel to z axis, in $in.^4$;

J = torsion constant of the cross section of a beam element, in $in.^4$;

j = a letter designating a typical beam element and the joint immediately to the right of the element;

L = length of simply-supported span, in in.;

$(M_j)_{xy}$ = total bending moment in element j about the neutral plane xy, in in.-lb;

$(M_{xy})_o$ = bending moment about the neutral plane zx due to the statically determinate external forces, in in.-lb;

$(M_{xy})_i$ = bending moment about the neutral plane zx due to the statically indeterminate forces q, r, and s, in in.-lb;

$(M_j)_{zx}$ = total bending moment in element j about the neutral plane zx, in in.-lb;

$(M_{zx})_o$ = bending moment about the neutral plane zx due to the statically determinate external forces, in in.-lb.;

$(M_{zx})_i$ = bending moment about the neutral plane zx due to the statically indeterminate forces q, r, and s, in in.-lb.;

n = a number designating number of terms in the Fourier Series;

P_j = concentrated load acting parallel to z axis on element j in.-lb;

p_j = distributed load acting parallel to z axis on element j, in lb per in.;

q_j = each of the indeterminate distributed loads which are equal in magnitude and opposite in sign and which act parallel to x axis on elements j and j+1 at joint j, in lb per in.;

q_{jn} = amplitude of the distributed load q_j corresponding to the nth Fourier component, in lbs per in.;

r_j = each of the indeterminate distributed loads which are equal in magnitude and opposite in sign and which act parallel to z axis on elements j and j+1 at joint j, in lbs per in.;

r_{jn} = amplitude of the distributed load r_j corresponding to the nth Fourier component, in lbs per in.;

s_j = each of the indeterminate distributed loads which are equal in magnitude and opposite in sign and which act parallel to z axis on elements j and j+1 at joint j, in lbs per in.;

s_{jn} = amplitude of the distributed load s_j corresponding to the nth Fourier component, in lbs per in.;

T_j = total torque, in in.-lb;

t_j = distributed torque acting on beam element j, in in.-lb per in.;

u_j = total axis deformation of element j, in in.;

$(u_j)_o$ = axial deformation of element j due to statically determinate external axial forces, in in.;

$(u_j)_i$ = axial deformation of element j due to statically indeterminate distributed loads q_{j-1}, r_{j-1}, s_{j-1}, q_j, r_j and s_j, in in.;

$(V_j)_{xy}$ = total shear in element j corresponding to $(M_j)_{xy}$, in lb;

$(V_{xy})_o$ = shear corresponding to $(M_{xy})_o$, in lb;

$(V_{xy})_i$ = shear corresponding to $(M_{xy})_i$, in lb;

$(V_j)_{zx}$ = total shear in element j corresponding to $(M_j)_{zx}$, in lb;

$(V_{zx})_o$ = shear corresponding to $(M_{zx})_o$, in lb;

$(V_{zx})_i$ = shear corresponding to $(M_{zx})_i$, in in.;

v_j = total deflection of element j, in in.;

$(v_j)_o$ = deflection of element j parallel to y axis due to the statically determinate external loads, in in.;

$(v_j)_i$ = deflection of element j parallel to y axis due to the statically indeterminate distributed forces q_{j-1}, r_{j-1}, s_{j-1}, q_j, r_j, and s_j in lb;

w_j = total deflection of element j parallel to z axis, in in.;

$(w_j)_o$ = deflection of element j parallel to z axis due to the statically determinate external loads, in in.;

$(w_j)_i$ = deflection of element j parallel to z axis due to the statically indeterminate distributed forces q_{j-1}, r_{j-1}, s_{j-1}, q_j, r_j and s_j, in in.;

y = distance of any point in the cross section of a beam element from the zx plane, in in.;

z = distance of any point in the cross section of a beam element from the xy plane, in in.;

$\bar{z}$ = distance of the joint from the shear center of a beam element, in in.;

ϕ_j = total normal stress in element j, in psi;

$(\sigma_j)_1$ = normal stress in element j due to $(M_j)_{xy}$ at a distance z from the xy plane, in psi;

$(\sigma_j)_2$ = normal stress in element j due to $(M_y)_{zx}$ at a distance y from the zx plane, in psi;

$(\sigma_j)_3$ = normal stress caused by axial load, in psi;

$(\sigma_j)_4$ = normal stress due to torsional warping, in psi;

ϕ_j = total rotation of element j, in radians;

$(\phi_j)_o$ = rotation of element j due to statically determinate external loads, in radians;

$(\phi_j)_i$ = rotation of element j due to statically indeterminate distributed forces q_{j-1}, r_{j-1}, s_{j-1}, q_j, r_j and s_j, in radians;

Ω = axial deformation per unit rotation due to warping, in in. per radians per in.; and

$\overline{\Omega}$ = axial deformation per unit rotation due to warping at level of the joint, in in. per radians per in.

Journal of the
STRUCTURAL DIVISION
Proceedings of the American Society of Civil Engineers

BASIC COLUMN STRENGTH

By Lynn S. Beedle,[1] F. ASCE, and Lambert Tall,[2] A. M. ASCE

FOREWORD

The papers that form the ASCE-CRC Symposium on Metal Compression Members are representative of all phases of Column Research Council activities. Several papers represent summaries of both past and current research, prepared specifically to assist in the preparation of the "Guide to Design Criteria for Metal Compression Members." Also included are reports on recently completed research on pony truss bridges and on plate girders.

In the January 1960 Journal of the Structural Division Bruce G. Johnston documented the inception of the CRC and the many activities undertaken by the Council.

Thomas C. Kavanagh, in the February 1960 Journal of the Structural Division, reviewed the state of knowledge concerning the effective length of framed columns.

In the April 1960 Journal of the Structural Division, Robert M. Barnoff and William G. Mooney studied the effect of floor-system participation on pony truss bridges.

Bruce G. Johnston presented a digest of the "Guide" in the April 1960 Journal of the Structural Division.

Note.—Discussion open until December 1, 1960. Separate discussions should be submitted for the individual papers in this symposium. To extend the closing date one month, a written request must be filed with the Executive Secretary, ASCE. This paper is part of the copyrighted Journal of the Structural Division, Proceedings of the American Society of Civil Engineers, Vol. 86, No. ST 7, July, 1960.

[1] Chmn., Struct. Metals Div., Fritz Engrg. Lab., Lehigh Univ., Bethlehem, Pa.
[2] Research Assoc., Lehigh Univ., Bethlehem, Pa.

SYNOPSIS

A summary is presented of a theoretical and experimental investigation of the strength of centrally loaded columns as influenced by residual stresses and variations in the yield-stress level. It is shown that the basic strength of structural steel columns containing residual stresses may be expressed in terms of the tangent modulus. Approximations suitable for design use are suggested. Information on both the yield stress level and the magnitude and distribution of residual stress in structural members is presented.

INTRODUCTION

A research project on the "Influence of Residual Stress on Column Strength and the Mechanical Properties of Rolled Shapes" has been in progress at Lehigh University under the guidance of Research Committee A of the Column Research Council. This Committee was assigned the task of determining the relationship between material properties and the strength of columns, and the first pronouncement of the Council (based on the recommendation of Committee A) was issued in 1952.[3] This memorandum states that the critical or ultimate failure load of a column is given by

$$\sigma_{cr} = \frac{\pi^2 E_t}{\left(\frac{K L}{r}\right)^2} \quad \ldots\ldots\ldots\ldots\ldots\ldots (1)$$

in which σ_{cr} is the applied average maximum stress on a column, E_t denotes the tangent modulus, L is the total length of a pin-end column, r represents the radius of gyration, and K L/r is the effective slenderness ratio.

Eq. 1 cannot be applied to steel columns if the stress-strain relationship is determined from a small coupon cut from the section. Early work clearly showed this to be true, and in later studied completed prior to the time that this general investigation was started it was shown that residual stresses might account for differences in column strength of as much as 30% below that which would be inferred from coupon tests.

The column curve depends on the stress-strain relationship. The latter, in turn, is dependent on two important factors; these are: (a) the magnitude and distribution of residual stresses, and (b) the basic yield stress level of the material. Therefore, the objectives of the investigation were: (1) to determine the magnitude and distribution of residual stresses in columns, and (2) to develop methods of predicting the influence of these residual stresses on column strength. As a necessary parallel study, the program included a determination of the basic yield stress level of the material of which columns would be fabricated.

The program included tests of coupons of the type performed in the mill, tests of stub columns (short lengths of full cross-sectional area), and column tests. For the same shapes, residual stresses were measured by the sectioning technique. Theories were developed for predicting column strength, and

[3] "The Basic Column Formula," Column Research Council, Tech. Memorandum No. 1, May, 1952.

from the measurements made it was possible to obtain a correlation with the theory. Maximum strength columns formulas could then be written.

It is the purpose of this paper to summarize the findings of the investigation to date and to discuss the significance thereof. Reference is made, throughout, to the various progress reports that contain the detailed experimental and theoretical work. This paper is concerned primarily with rolled wide-flange shapes of ASTM Designation A7 structural steel. A brief discussion of built-up columns (welded and riveted) and of low-allow high-strength steel columns is included. The scope is limited to centrally loaded columns.

RESIDUAL STRESSES

Formation.—Residual stresses are formed in a structural member as a result of plastic deformations. In rolled shapes these deformations always occur during the process of cooling from the rolling temperature to air temperature; the plastic deformations result from the fact that some parts of the shape cool much more rapidly than others causing inelastic deformations in the slower cooling portions. (The flange tips of a wide-flange shape, for example, would cool more rapidly than the juncture of flange and web.) The mechanism by which residual stresses are formed has been described.[4,5,6]

Residual stresses also are formed as a result of fabrication operations. The process of cold-bending that is required in the straightening operation and the process of cambering both introduce residual stresses due to plastic deformation.[5,6] Residual stresses are also introduced during the welding operation as a result of the localized heat input and resultant plastic deformation.[7]

Thus, plastic deformations are necessary in order that residual stresses be formed. In hot-rolled or welded members, the part to cool last is usually in a state of tensile residual stress.

Magnitude and Distribution.—Methods for determining cooling residual stresses in plates and for obtaining a qualitative estimate of stresses in wide-flange shapes are available.[5] The magnitude and distribution of these stresses depend on the shape of cross section, initial temperature, cooling conditions, and material properties.

The measurement of residual stresses confirms the trends predicted theoretically. A considerable number of such measurements have been made and they permit a good estimate to be made of the magnitude and distribution of residual stresses likely to be encountered in hot-rolled wide-flange members.[5,8] For the purpose of making these measurements shapes were selected with widely differing geometry. Fig. 1 presents some of the measured results, showing the magnitude and distribution of stresses across the flange and web. While the variation is considerable, the general pattern in the flange is similar. The residual stresses were determined by the "method of sectioning" described elsewhere.[4]

---

4 "Residual Stress and the Compressive Strength of Steel," by A. W. Huber and L. S. Beedle, Final Report on Pilot Program, Welding Journal, Vol. 33, No. 12, December, 1954, p. 589-s.

5 "Residual Stresses in Wide-Flange Beams and Columns," by A. W. Huber, Lehigh Univ., Fritz Lab. Report No. 220A.25, July, 1959 (to be published in Proceedings, ASCE).

6 "Residual Stress and the Yield Strength of Steel Beams," by C. H. Yang, L. S. Beedle, and B. G. Johnston, Welding Journal, Vol. 31, No. 4, April, 1952, p. 205-s.

7 "Built-Up Column Strength," by Y. Fujita, Dissertation, Lehigh Univ., August, 1956.

8 "The Magnitude and Distribution of Residual Stress," by Y. Fujita, Lehigh Univ., Fritz Lab. Report 220A.20, June, 1955.

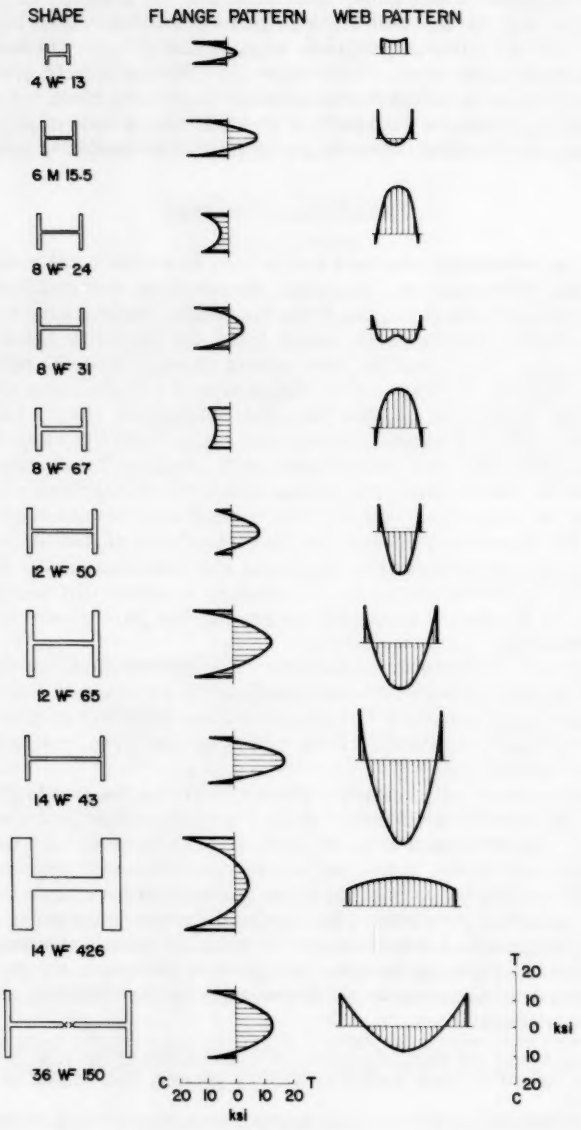

FIG. 1.—RESIDUAL STRESS DISTRIBUTION IN WIDE-FLANGE SHAPES

The magnitude and distribution of residual stresses in the flanges also may be estimated from the results of a stub-column test.[4,9]

Table 1 contains a listing of all shapes studied thus far. It also contains a summary of all the measurements made in the program. Table 2 presents the average value of the residual stress at different positions in the cross section and gives the variation as well. Insofar as columns are concerned, the most important of the stresses are those at the flange tips (σ_{rc}) and from this program of tests the average compressive stress σ_{rc} is 12.8 ksi with a maximum of 18.7 ksi and a minimum of 7.7 ksi.

The magnitude of the residual stress at the flange tips may also be determined indirectly from a stub-column test, and is the difference between the yield stress level and the proportional limit. This value has been found to be approximately 12.0 ksi which agrees well with the measured value of 12.8 ksi noted previously.[5]

Variation.—In addition to average values, Table 2 gives the maximum and minimum values of measured residual stresses. Fig. 2(a) gives the frequency distribution of flange-tip stress as determined by actual sectioning.[5] Fig. 2(b) shows the same information as determined indirectly from the proportional limit obtained for the same group of "stub-column" tests.[5]

The variation of residual stress within material from one ingot is relatively small, but larger variations may exist between material from different lots.[4]

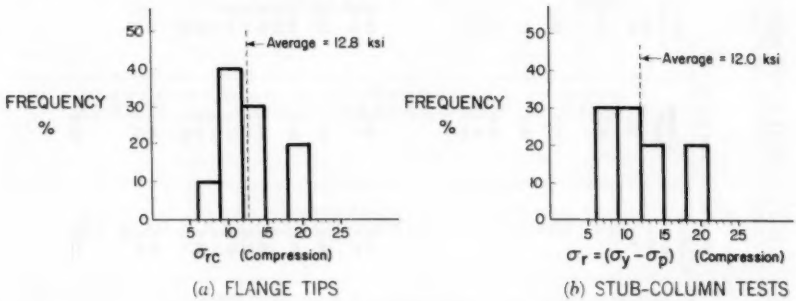

FIG. 2.—MEASURED RESIDUAL STRESS

Theoretical studies show that cooling residual stresses are constant along the member except for a distance approximately equal to the larger cross-sectional dimension at the ends. This is due to the uniformity of the shape and its manufacture. Measurements are in agreement with the theory as shown in Fig. 3.[5] While a trend may exist for the variation of residual stress as a function of the geometry of the cross-sectional shape, it has not been possible, as yet, to show a precise relationship.

Influence on the Apparent Stress-Strain Relationship.—As implied previously, residual stresses affect the average stress-strain relationship of the complete cross section. Fig. 4 is presented to show this influence diagrammatically. Fig. 4(a) shows a short length of a wide-flange shape with a simplified linear distribution of residual stress in the flanges. The cutting of a

[9] "The Influence of Residual Stress on the Instability of Axially Loaded Columns," by A. W. Huber, L. Tall, and L. S. Beedle, Lehigh Univ., Fritz Lab. Report 220A.26 (in preparation).

TABLE 1.—TEST RESULTS

Test No.	Shape	Yield Stress Level (σ_y)				Proportional limit, σ_p, Stub-column Test	Residual Stress, σ_{rc}	Column Test	
		Mill test	Simulated mill test	Coupon test[a]	Stub-column test			σ_{cr}/σ_y	L/r
(1)	(2)	(3)	(4)	(5)	(6)	(7)	(8)	(9)	(10)[b]
T-0	8WF31	43.3		41.4	37.3	25.6	-13.9		
205A-T18	8WF31							0.99	28(x)
205A-T15	8WF31							0.905	42(x)
T-1	8WF31			37.0	36.2	28.0	-11.5		
205A-T11	8WF31							0.935	56(x)
T-2	8WF31	43.3		40.2	37.8	25.2	-12.5		
205A-T25	8WF31							0.74	82(y)
T-3	8WF31[c]			36.0[d]	33.4	26.0			
T-4	8WF31	43.3		40.1[d]	36.7	27.0	- 9.0	0.815	58(y)
T-5	8WF31[c]			33.9[d]	31.4	31.0			
T-5 a	8WF31[c]							0.925	82(y)
T-5 b	8WF31[c]							0.98	58(y)
T-6 a	8WF31						-16.1		
T-6 b	8WF31						(Aver-		
T-6 c	8WF31						age)		
T-7	8WF24	39.8	40.7	36.1	35.0	26.4	-10.2	0.73	84(y)
T-8 a	8WF67	43.0	37.5	31.4	31.4	25.4	- 9.5	0.815	85(y)
T-8 b	8WF67						- 8.0		
T-9 a	12WF50	42.6	41.3	37.6	35.8	24.0	- 5.5		
T-9 b	12WF50							0.81	80(y)
T-10	12WF65	39.7	40.7	38.3	36.6	22.0	-18.7	0.76	81(y)
205E-D1	10WF33	42.9			34.4	25.8			
205E-D2	8WF24	39.8	40.4	34.2	33.4				
205E-D3	10W 39	41.2	41.0	35.6	35.9				
205E-D4	12WF50	42.6	42.0	37.2	36.3				
205E-D5	8WF35	40.0	40.8	37.6	36.7				
205E-D6	10WF21	46.9	48.1	41.6	37.2				
205A-T25	4WF13			41.1	39.8		-10.0	0.78	91(x)
205A-T28	4WF13							0.49	118(x)
T-11	6WF15.5	44.0	41.0	36.4	43.0	20.7		0.73	87(y)
T-12 a	5WF18.5		36.6	33.8	36.7	27.5	- 7.7	0.81	78(y)
T-12 b	5WF18.5	42.2						0.78	80(y)
T-12 c+	5WF18.5						-10.6	0.95	78(y)
T-12 d	5WF18.5								
T-13	14WF426	35.9	31.5	28.6			-17.8		
T-14	6WF15.5	49.1					-15.1		
T-15 a	14WF43	41.6					- 8.5		

T-15 b	14WF43	41.6					- 8.5		
T-16	36WF150	47.0					-10.8		
T-17	12Jr14	50.4					- 4.1		
T-19	6WF25	36.7	42.2	35.0					
T-22	10WF66	46.8	38.8	32.4	33.2	22.0		0.82	72(x)
T-23	10WF66	43.9		35.5					
T-24	5WF18.5	48.8	44.7	41.3	38.7	32.3			
T-25	14WF111	45.0	39.4	32.7	33.0	22.8			
T-26 a	14WF111		43.8	33.9	35.5	16.3	-14.0	0.73	60(y)
T-26 b	14WF111							0.58	99(y)
T-27	6WF15.5	51.1	52.1	43.3	43.0	19.7			
T-28	8WF24	47.4	48.5	37.8	39.4	15.0			
T-29	8WF31	44.4	48.8	37.9	36.1	29.5			
T-30	8WF35	48.3	44.7	35.3	35.9	20.0			
T-31	8WF67	33.5	34.7	26.3	26.4	17.5			
T-32	10WF33	52.0	44.3	34.3	32.4	21.3			
T-33	10WF39	41.9	44.7	34.7	37.2				
T-34	12WF50	42.2	43.1	34.4	32.9	16.4			
T-35	12WF65	44.3	38.6	33.8	32.6	18.0			
T-36	12WF53	44.9	46.3	34.4	35.0	21.7			
T-37	12WF53	35.1	40.4	35.2	35.0	22.7			
T-38	12WF92	45.7	41.4	33.6	34.4	14.6			
T-40	12WF190	34.1	32.9	26.8	24.6	12.5			
T-41	12WF190	39.6	39.2	30.9	30.2	18.9			
T-42	14WF53	37.1	36.9	29.6					
T-44	14WF61	44.3	35.7	30.6					
T-45	14WF61	44.2	42.7	36.3	36.7	27.6			
T-46	14WF78	38.4	33.6	29.2	29.4	19.2			
T-47	14WF78	42.3	44.2	35.1	35.8	21.0			
T-48	14WF142	37.1	38.9	29.3	30.7	18.7			
T-49	14WF142	51.2	45.2	38.0	38.7	20.6			
T-50	14WF228	38.2	35.2		25.8	16.3			
T-52	14WF320	38.5	26.4	22.7					
T-54	14WF426	38.2	34.1						
T-56	16WF88	42.3	38.3	31.4	31.4	12.8			
T-57	16WF88	41.6	39.8	34.3	34.4	11.1			
T-58	18WF105	43.1	40.6	30.4	29.8	17.0			
T-59	18WF105	37.7	38.0	32.8	33.0	19.6			
249-R1					35.3	23.7		0.86	80(x)
249-R2	Built-			36.7[d]	37.3	22.5		0.89	60(y)
249-R3								0.80	79(x)
249-W1	up				34.3	13.7		0.62	74(x)
249-W2					32.7	12.5	-21.0	0.64	55(y)
249-W3	Column			31.7[d]				0.50	98(y)

[a] Coupon tests were for static yield stress. [b] (x) denotes buckling about strong axis, (y) represents buckling about weak axis. [c] Annealed material, all others "as delivered." [d] Weighted average value of compression tests, all others are of tension tests.

coupon from the flange of the member would relieve the residual stresses that were present in the coupon prior to sectioning, and the stress-strain relationship determined from this coupon would be as shown by the dashed line in Fig. 4(b). If, now, the load is considered as being applied to the entire cross section containing its residual stresses, it is evident that when the applied stress becomes equal to the difference between σ_y and σ_{rc}, then yielding will commence at the flange tips. Thus,

$$\sigma_p = \sigma_y - \sigma_{rc} \quad \ldots\ldots\ldots\ldots\ldots\ldots\ldots (2)$$

in which σ_p is the yield stress at the proportional limit and σ_y denotes the yield stress level. The superposition of stresses at the "proportional limit"

TABLE 2.—RESIDUAL STRESSES IN WIDE-FLANGE SHAPES DUE TO COOLING

	Flange Edge, σ_{rc}			Flange Center, σ_{ro}			Web Center, σ_{rw}		
	Maximum	Average	Minimum	Maximum	Average	Minimum	Maximum	Average	Minimum
Columns $d/b \leq 1.5$	-7.7	-12.8	-18.7	+16.5	+ 4.7	-4.1	+18.2	+ 8.0	-15.5
Beams $d/b > 1.5$	-4.1	- 7.5	-10.8	+24.2	+15.1	+8.3	- 8.8	-21.8	-41.0

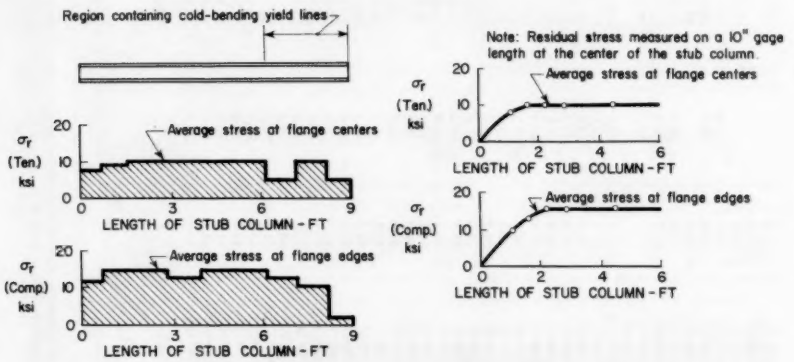
Region containing cold-bending yield lines
Average stress at flange centers
Average stress at flange edges
σr (Ten) ksi
σr (Comp.) ksi
LENGTH OF STUB COLUMN - FT
Note: Residual stress measured on a 10" gage length at the center of the stub column.

(a) ALONG 8 WF 31 BEAM (b) WITH STUB-COLUMN LENGTH

FIG. 3.—VARIATION OF RESIDUAL STRESS

is shown in Fig. 4(c). Yielding occurs when the flange tip residual stress σ_{rc} plus the applied stress σ_p is equal to σ_y.

When more load is applied, the average stress and average strain are no longer proportional to one another and a non-linear stress-strain relationship results for the section as a whole. Fig. 4(d) shows a wide-flange shape with flanges partially yielded (shown shaded) and the corresponding stress distribution for $\sigma_{avg} > \sigma_p$. Above the proportional limit and below the yield stress the strain is given by

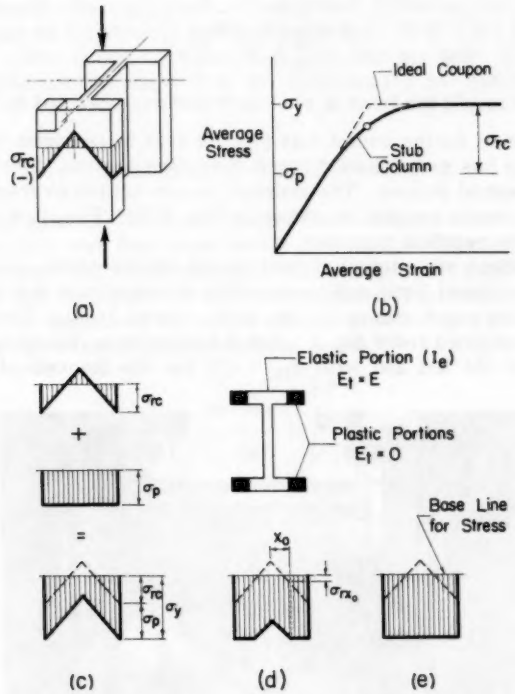

FIG. 4.—INFLUENCE OF RESIDUAL STRESS ON STRESS-STRAIN CURVE

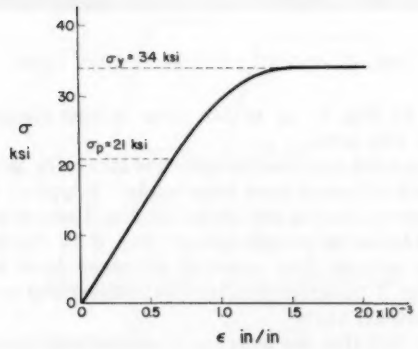

FIG. 5.—STRESS-STRAIN CURVE FOR ASTM A7 COLUMNS BASED ON MEASURED RESIDUAL STRESSES

$$\epsilon = \frac{1}{E}\left(\sigma_y - \sigma_{rx_o}\right) \quad \ldots\ldots\ldots\ldots\ldots\ldots (3)$$

in which E is Young's modulus of elasticity and σ_{rx_o} defined in Fig. 4(c).[4] The stress distribution for the completely yielded section is shown in Fig. 4(e). As soon as yielding has progressed across the entire section, there is no further influence of residual stress. The average stress versus average strain curve for the entire cross section is shown in Fig. 4(b). The yield stress level is unaffected by the residual stresses.

Thus, the effect of residual stress on the stress-strain relationship is to lower the proportional limit and to cause the stress-strain diagram to be non-linear beyond that point and up to the yield stress level. The proportional limit may be computed from Eq. 2. For a typical wide-flange column (A_f/A_w = 3.0) with σ_y = -34 ksi and with σ_{rc} = -13 ksi the theoretical stress-strain

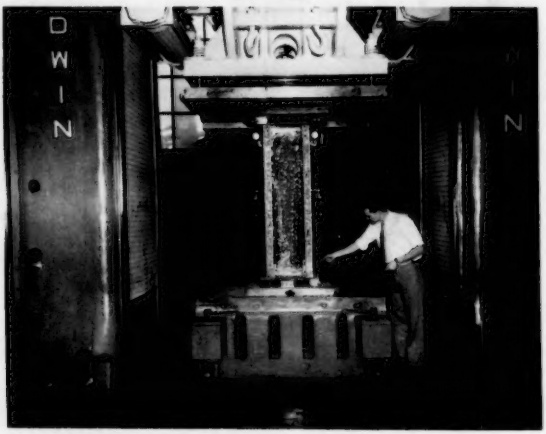

FIG. 6.—TYPICAL STUB-COLUMN TEST

curve is as shown in Fig. 5; A_f is the area of both flanges of a wide-flange shape and A_w is the web area.

To obtain experimental correlation with the foregoing predictions, tests and measurements of stub columns have been made. A typical stub column test is shown in Fig. 6. Typical results are shown in Fig. 7 which also shows the contrast with the curve based on coupon tests. Fig. 8 is the stress-strain curve of an annealed stub column (the residual stresses have been removed); the comparison with Fig. 7 clearly verifies the influence of residual stresses on the average stress-strain curve.

Of interest is the fact that the average stress-strain curve, Fig. 5, is nearly identical with the average stress-strain curve determined from stub column tests (Fig. 18, to be presented subsequently).

Cold-Bending Residual Stresses.—Residual stresses due to cold bending can be predicted with reasonable accuracy,[5] assuming certain initial cooling stresses and the extent of deformation. Some measurements are shown in

Fig. 9. In general, the maximum and minimum stresses are of the same order of magnitude as the cooling residual stresses. While the influence on the stress-strain curve might be predicted, this has not been done as studies (described subsequently) show it to be unnecessary for the purposes of this present study.

MECHANICAL PROPERTIES

Proportional Limit.—The general effect of residual stresses on the stress-strain relationship was discussed under the heading "Residual Stresses: Influence on the Apparent Stress-Strain Relationship." The proportional limit is reduced below that obtained in coupon tests, and may be computed either from Eq. 2 or may be measured in a stub column test. Fig. 7 clearly shows this effect, and further comparisons have been made.[4,5]

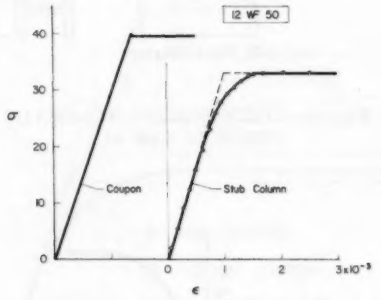

FIG. 7.—STUB COLUMN STRESS-STRAIN CURVE FOR AS-DELIVERED MATERIAL

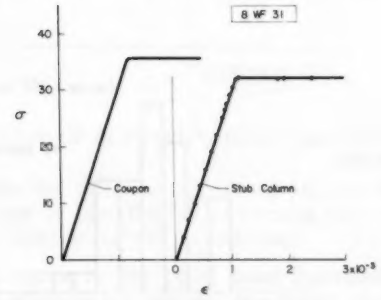

FIG. 8.—STUB COLUMN STRESS-STRAIN CURVE FOR ANNEALED MATERIAL

The average value of the proportional limit is 21.7 ksi as determined indirectly by residual-stress measurements in this program of tests. The average value determined by the offset method from stub column tests is 20.7 ksi, and the frequency distribution curve for these 40 specimens is shown in Fig. 10. Since the offset method was used to determine the proportional limit, the actual value is even lower than 20.7 ksi. It is to be expected that the stub

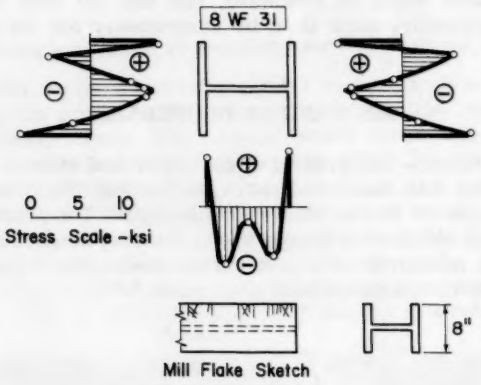

FIG. 9.—COLD-BENDING RESIDUAL STRESS IN 8 WF 31

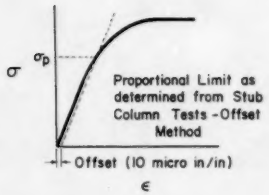

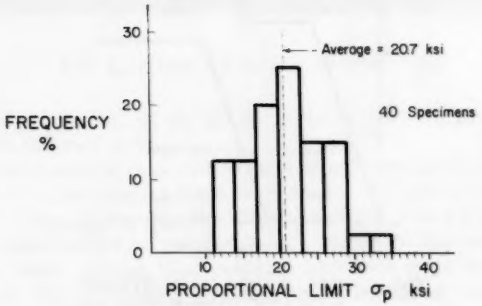

FIG. 10.—FREQUENCY DISTRIBUTION OF PROPORTIONAL LIMIT DETERMINED FROM STUB-COLUMN TESTS

column proportional limit would be lower than the value determined indirectly from Eq. 2. In the first place, the residual stresses are probably greater than the measured value by a small amount. Secondly, the flange-tip values of σ_{rc} in Table 1 are averages of measurements on the four corners and on two sides, and deviations from these averages will be reflected in a lowering of the proportional limit. Small inaccuracies of alinement also influence the observed proportional limit.

Coupon Strength, Acceptance Tests, Strain Rate, and the Yield Stress Level.— The yield stress level may be determined from the results of an ASTM acceptance test or it may be determined from a laboratory coupon test or from the results of a laboratory stub column test. Factors such as upper yield point, strain rate, and the web strength compared with flange strength cause the yield stress level of a full cross section (stub column) tested in the laboratory in compression to be markedly less than the tensile yield point determined in the routing ASTM acceptance test.[4,10]

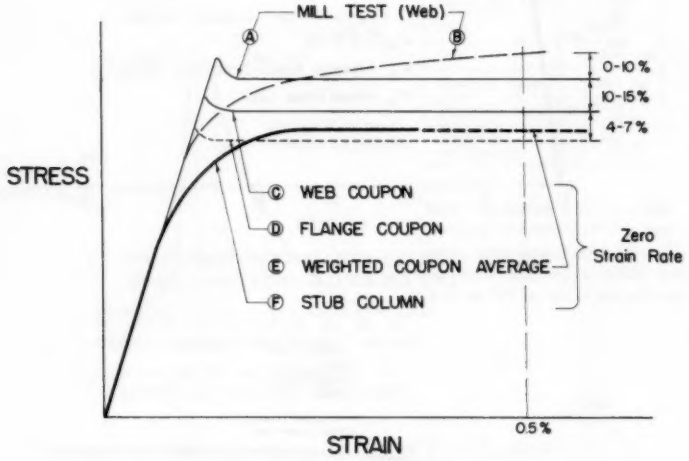

FIG. 11.—INFLUENCE OF SEVERAL VARIABLES ON YIELD STRESS LEVEL

Fig. 11 illustrates the different stress-strain curves that may be obtained depending on the type of test that is performed and shows diagrammatically the influence of the various factors as follows:

(1) Starting with curve A, the yield value reported in a mill-type acceptance test is usually (though not always) the upper yield point. Occasionally specimens will not exhibit an upper yield point (dashed line, curve B), in which case the yield stress is usually recorded at a strain of 0.5%. The upper yield point is from 0% to 10% higher than the yield stress level.

(2) Comparing curves A and C in Fig. 11, the ASTM acceptance test usually will show a higher yield stress level primarily because of the effect of strain rate. The "static" yield level (the value measured at a zero strain rate)[10,11]

10 "On the Yield Properties of Structural Steel Shapes," by L. Tall and R. L. Ketter, Lehigh Univ., Fritz Lab. Report 220A.33, November, 1958.

11 "Material Properties, Residual Stresses and Column Strength," by A. T. Gozum and A. W. Huber, Lehigh Univ., Fritz Lab. Report 220A.14, May, 1955.

of a web coupon is from 10% to 15% lower than the strength obtained in the acceptance test.[10]

(3) There is a difference in strength between the various elements of a rolled shape, the web being stronger than the flange. Thus the average yield level of a stub column is lowered still further in comparison with the mill acceptance test because the latter is made from the web (curves C and D).

(4) Finally, from Fig. 11 it is seen that a stub column (tested at "zero strain rate") reflects the effect of residual stress upon the stress-strain curve and averages out the differences between web and flange material, as shown by curve F.

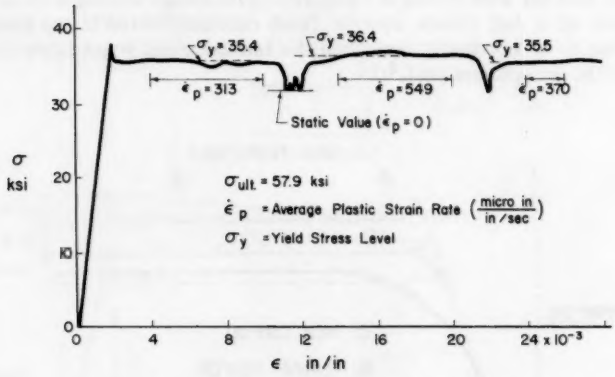

FIG. 12.—STRESS-STRAIN CURVE SHOWING INFLUENCE OF STRAIN RATE

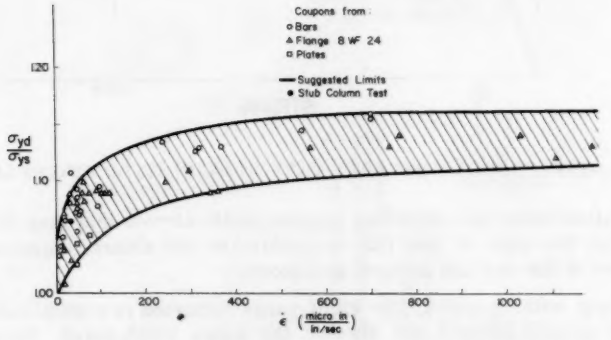

FIG. 13.—INFLUENCE OF STRAIN RATE ON YIELD STRESS LEVEL

Tests have shown that even a "very slow" laboratory strain rate used in testing coupons (an elastic strain rate of 1 micro-in. per in. per sec) can raise the apparent yield stress level by as much as 5%.[11] The effect of strain rate on the yield stress level in a typical tension coupon test is shown in Fig. 12. From the results of such tests the relationship shown in Fig. 13 may be obtained. The measured yield level compared with the static yield level is shown

as a function of the plastic strain rate. Since the plastic strain rate in a mill test is about 1,000 micro-in. per in. per sec, increases in the yield stress above the static value may be expected to be as high as 16%.

It is of interest to note that the yield stress level obtained from a stub-column test agrees well with tests of tension and compression coupons if the results of the latter are averaged according to their respective areas in the cross section, and if both the coupons and the stub column are tested at the zero strain rate.[10,11] This is shown diagrammatically in Fig. 11 (curves E and F).

A comparison of the results of acceptance tests and of stub-column tests is important in establishing a value for the yield stress to use in a basic column formula. If this relationship can be established for a fairly large sample, then it could be applied with confidence to the larger body of acceptance test data available in the mills to give a reasonable estimate of the actual strength of

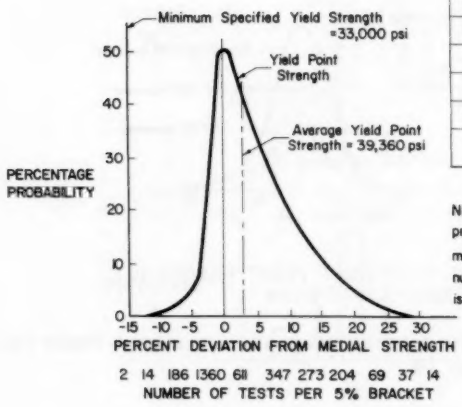
Minimum Specified Yield Strength =33,000 psi
Yield Point Strength
Average Yield Point Strength = 39,360 psi
PERCENTAGE PROBABILITY
50
40
30
20
10
0
-15 -10 -5 0 5 10 15 20 25 30
PERCENT DEVIATION FROM MEDIAL STRENGTH
2 14 186 1360 611 347 273 204 69 37 14
NUMBER OF TESTS PER 5% BRACKET

	Yield Point
No. of Mill Tests	3124
High	56,650 psi
Low	31,090 psi
Standard Deviation	3127 psi
Probability Error	2109 psi 5.5 %
Coefficient of Variation	7.8 %

Note: The ordinate is the percentage probability of indicated deviation from median being equalled or exceeded numerically according to whether curve is to the left or right of zero deviation

FIG. 14.—CUMULATIVE FREQUENCY DISTRIBUTION OF YIELD STRESS (MILL TESTS)

structural steel columns. Figs. 14, 15 and 16 show the distribution of the yield stress as determined by a number of methods as follows:[4,10,11]

1. ASTM acceptance tests in the mill: Fig. 14 (3,124 Specimens), Fig. 15 (3,010 Specimens), and Fig. 16(a) (35 Specimens).
2. Simulated ASTM tests: (Fig. 16(b) (35 Specimens).
3. Stub-column tests: (Fig. 16(c) (35 Specimens).
4. Stub-column tests: (Fig. 16(d) (47 Specimens).

Items 1, 2 and 3 (Fig. 16) are for the same control group. Comparing Fig. 16(a) with Fig. 16(b) shows that the mill test results may be approximated within about 4% by a laboratory test that simulates mill test procedures. The average value of the control group of mill tests (Fig. 16(a)) was 42.9 ksi with a standard deviation s of 4.4 ksi. Further comparisons of this type are available.[10,11]

The average value of the yield stress level determined in simulated mill tests was 41.2 ksi (Fig. 16(b)), while the average strength of the corresponding

stub columns (Fig. 16(c)) was 34.0 ksi. The average value of the yield stress level for all stub columns tested in the program was 34.5 ksi with variations from 24.6 ksi to 43.0 ksi (Fig. 16(d)).

The probable ratio of the basic compressive strength (the static yield stress level) to the "acceptance test" strength was found to be 0.80. In Fig. 17 is plotted the distribution of the individual ratios of stub column yield level to mill test "yield point." The average is 0.80 with a minimum of 0.62 and a maximum of 0.92. From this information it would be concluded that the static yield stress level of a wide-flange column averages about 20% less than the value obtained in the ASTM-type acceptance test. As pointed out, this difference is due mainly to the strain-rate effect, but also is influenced by the higher yield stress of the web and the difference between upper and lower yield points.

Applying this average ratio (0.80) to the average value of the mill tests shown in Figs. 14 and 15 (41.7 Ksi) there is obtained a probable compressive strength for this material of 33.4 ksi. The average value obtained from all stub columns tested in the program was 34.5 ksi suggesting that the sample

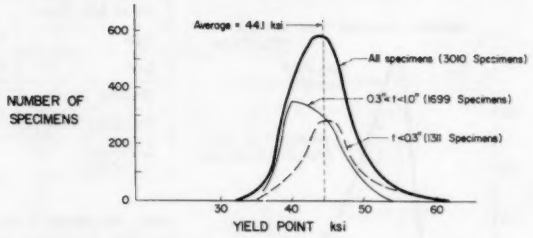

FIG. 15.—MILL TEST YIELD POINT FREQUENCY DISTRIBUTION CURVES

was fairly representative. The corresponding average stress-strain curve for a stub column is shown in Fig. 18.

CENTRALLY LOADED COLUMNS

Influence of Residual Stress on Column Strength.—For a column with material exhibiting an idealized stress-strain cruve and free from residual stresses, the buckling strength is defined by the Euler buckling curve and the yield stress of the material. The existence of residual stresses in the cross section reduces the buckling strength, since there is an early localized yielding at certain portions of the cross section. This reduction is greatest when the slenderness ratio is between 70 and 90.

This effect of residual stress may be illustrated by an example. Consider a column of rectangular cross section containing residual stresses, and bending about the weak axis. To construct the column curve, first the tangent modulus E_t is determined for various stress levels using a stress-strain diagram such as that shown in Fig. 19(a). Then a stress-E_t curve would be drawn as shown in Fig. 19(b). Applying the tangent-modulus formula, Eq. 1, the resulting column curve of stress-slenderness ratio would be obtained, Fig. 19(c). The influence of residual stresses when buckling occurs in the inelastic range is thus seen by comparing the solid line with the dashed line obtained for a member without residual stresses.

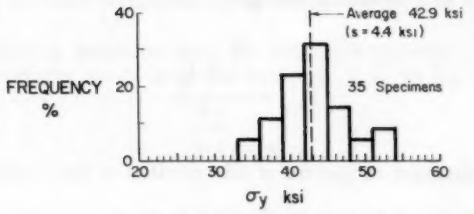

(a) Mill Test (Web Coupon)
$\dot{\epsilon}_{pl} \approx 1000$ Micro in./in./sec.

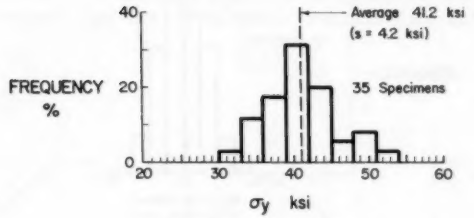

(b) Simulated Mill Test

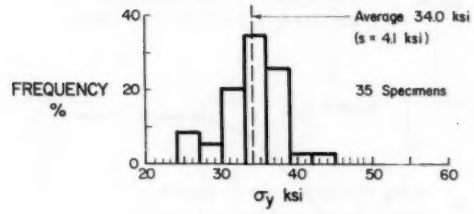

(c) Stub-Column Test
(Static Strain Rate)

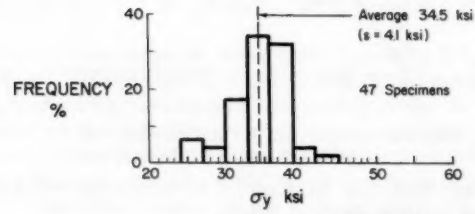

(d) Stub-Column Test

FIG. 16.—YIELD STRESS LEVEL AS DETERMINED BY VARIOUS METHODS

Eq. 1 is valid only for the special case of a rectangle bent about the weak axis. Proceeding now to a discussion of the problem of determining the strength of an actual column, the basic equation for the critical strength of a column containing residual stresses is given by[6]

$$P_{cr} = \frac{\pi^2 E I_e}{L^2} \quad \ldots\ldots\ldots\ldots\ldots\ldots (4)$$

in which I_e is the moment of inertia of that portion of the cross section which

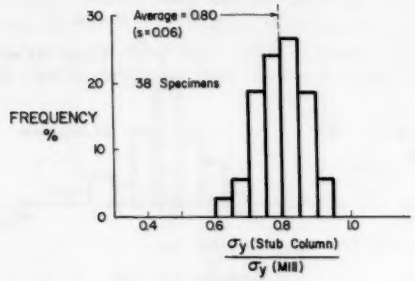

FIG. 17.—FREQUENCY DISTRIBUTION OF RATIO σ_y (STUB COL./σ_y (MILL)

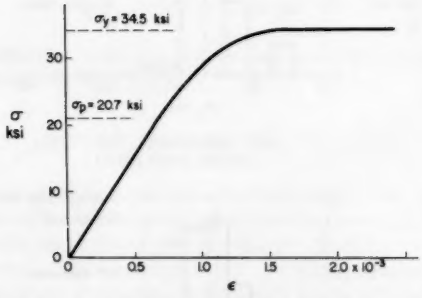

FIG. 18.—AVERAGE STRESS-STRAIN CURVE FOR STUB COLUMNS

remains elastic (Fig. 4(d), for example). In terms of the average critical stress, Eq. 4 may be written as

$$\sigma_{cr} = \frac{\pi^2 E I_e/I}{(L/r)^2} \quad \ldots\ldots\ldots\ldots\ldots\ldots (5)$$

Eq. 5 is the basic equation for a column containing axially symmetric cooling residual stresses. Since the flanges contribute significantly to the flexural resistance, E I, it is evident that residual stresses in the flanges are of more pronounced influence on column strength than are residual stresses in the web.

Effect of Flexure Axis.—There is a pronounced difference in the behavior of as-delivered columns that is dependent on the axis about which the member bends. A column will usually carry more load about one axis than about another normal to it, these directions being called the strong and weak axes, respectively.

This difference in behavior may be shown as follows: For a rectangular section bent about the weak axis the quantity $E I_e$ in Eq. 5 may be obtained from[6]

$$E I_e = E_t I \quad \ldots\ldots\ldots\ldots\ldots\ldots (6)$$

and Eq. 5 would reduce to Eq. 1. Eq. 6 is also very nearly true for a wide-flange section bent about its strong axis, since the web contributes only a small portion to the moment of inertia and thus the action is similar to that of two rectangles. However, for the rectangular section bent about its strong axis

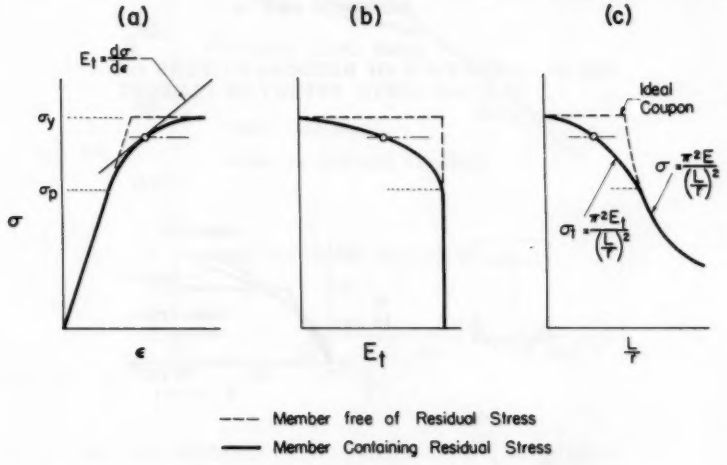

FIG. 19.—INFLUENCE OF RESIDUAL STRESS ON COLUMN CURVE

and for an H-section bent about its weak axis, the term $E I_e$ will be considerably less than $E_t I$. Thus the buckling strength will be less than the value predicted by Eq. 1, and would be computed according to Eq. 5.

Fig. 20 illustrates this difference for an idealized case (parabolic residual stress pattern, residual stress at flange edges equal to -20 ksi, residual stress at flange centers equal to +10 ksi, yield point stress equal to 40 ksi, effect of web neglected.) The lower curve is for flexure about the weak axis of an H-section, while the upper curve is for flexure about the strong axis.

Effect of Stress-Strain Relationship.—Columns of a material without definite yield level, and with a continuously curving stress-strain diagram, as with aluminum alloys, for example, show an influence of residual stress for the whole range of L/r. Although such materials can have much higher buckling strengths for a shorter column lengths (that is, $L/r < 40$), for the medium to long columns the effect of different stress-strain relationships is quite small,

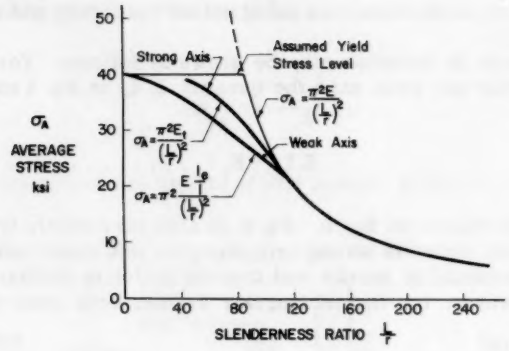

FIG. 20.—INFLUENCE OF RESIDUAL STRESS ON COLUMN CURVE: EFFECT OF FLEXURE AXIS

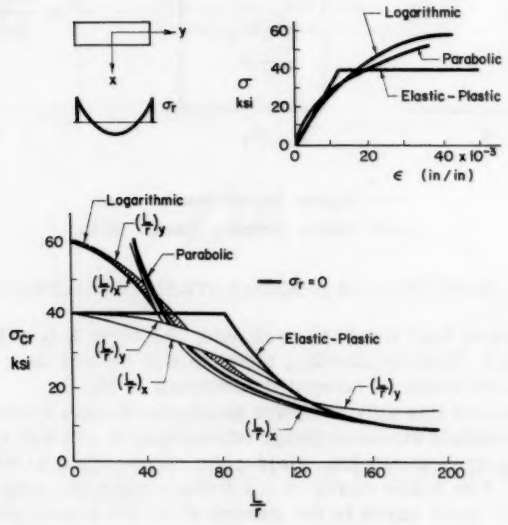

FIG. 21.—STRESS-STRAIN RELATIONSHIP AND COLUMN CURVES

particularly in comparison with other effects such as variations in yield level and in residual stress.[12,13] Fig. 21 shows column curves calculated for logarithmic, parabolic, and idealized elastic-plastic stress-strain relationships for individual fibers. The column cross section is rectangular with a parabolic residual stress distribution.

Cold-Bending Residual Stresses.—The study of the effect of cold-bending residual stresses on axial column strength indicates that for short and medium length columns, these stresses are no more critical than are cooling stresses.[5,12] This means that findings based on members with cooling residual stress patterns will be conservative when applied to straight members whose cooling patterns have been modified by cold bending (Fig. 22).

The Column Curve.—For wide-flange shapes with axially symmetric cooling residual stresses the solution to Eq. 5 (the column curve) may be obtained

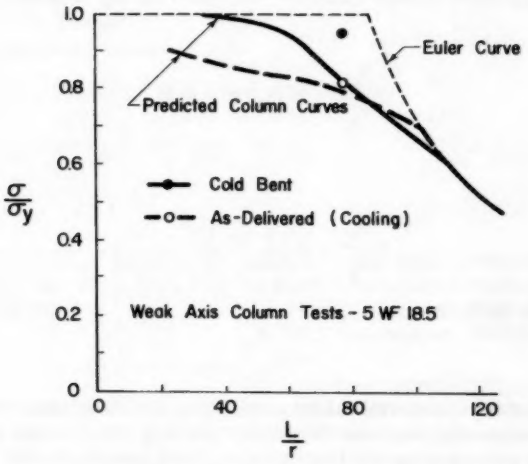

FIG. 22.—COLUMN CURVES REFLECTING INFLUENCE OF RESIDUAL STRESSES DUE TO COLD ROLLING AND TO COOLING AFTER ROLLING

either from residual stress data, or from the average stress-strain curve obtained in a stub column test.[4,9] Both methods are essentially the same, the solution to Eq. 5 requiring the function relating σ_{cr} and the geometry of the non-yielded portion of the cross section at that particular stress, which makes possible a solution for L/r. The solution will obviously depend on the distribution of residual stress. Analytical expressions for this function for certain residual stress distributions are available.[4,9,11]

The use of stub-column data to obtain the column curve is a somewhat simpler approach. If the usual situation is assumed for a loaded wide-flange column, namely, that the web does not yield (or that when it does the flanges

12 "The Influence of Residual Stress on the Instability of Columns," by A. W. Huber, Dissertation, Lehigh Univ., May, 1956.

13 Residual Stresses in High Strength Steel," by D. K. Feder and G. C. Lee, Lehigh Univ., Fritz Lab. Report 269.2, April, 1959.

have completely yielded), then the following equations will hold true:[4]

$$E\frac{I_{ex}}{I_x} = \frac{A\,E_t - \frac{2}{3}A_w E}{A_f + \frac{A_w}{3}} \quad \ldots\ldots\ldots\ldots\ldots\ldots (7a)$$

and

$$E\frac{I_{ey}}{I_y} = E\left[\frac{A\,E_t}{A_f E} - \frac{A_w}{A_f}\right]^3 \quad \ldots\ldots\ldots\ldots\ldots (7b)$$

Since for most wide-flange columns the ratio A_f/A_w is about 3, Eqs. 7 reduce to

$$E\frac{I_{ex}}{I_x} = E\,(1.2\tau - 0.2) \quad \ldots\ldots\ldots\ldots\ldots (8a)$$

and

$$E\frac{I_{ey}}{I_y} = E\left(\frac{4}{3}\tau - \frac{1}{3}\right)^3 \quad \ldots\ldots\ldots\ldots\ldots (8b)$$

where τ is given by

$$\tau = \frac{E_t}{E} \quad \ldots\ldots\ldots\ldots\ldots\ldots (9)$$

The magnitude of E_t is determined by conducting a stub-column test of a wide-flange shape containing residual stresses, plotting the average stress-strain curve, and then determining the tangent at various stress levels.

Fig. 20 was drawn using residual stress data (except that the effect of the web has been neglected). Fig. 23 has been drawn using the stub column stress-strain curve of Fig. 18. The two methods have been compared[4,11] and were found to be in very good agreement for A7 steel. Further, the results of tests also correlate well with them.

Column Curve Approximations.—A simplification to Eqs. 7 or 8 might be desirable for use as a basis for arriving at design formulas. It will be noted from Fig. 23(b) that the curve for buckling in the strong direction is approximately parabolic in shape and that for buckling in the weak direction the curve may be approximated by a straight line. Thus the two curves of Fig. 23(b) (exact solution), could be replaced by the following relationships, the first of which is of the same form as suggested by Friedrich Bleich:[14]

$$\sigma_{xx} = \sigma_y - \frac{\sigma_p}{\pi^2 E}\left(\sigma_y - \sigma_p\right)\left(\frac{L}{r}\right)^2 \quad \ldots\ldots\ldots\ldots (10a)$$

for $L/r \leq \pi\sqrt{E/\sigma_p}$,

---

14 "Buckling Strength of Metal Structures," by Friedrich Bleich, McGraw-Hill Book Co., New York, 1952.

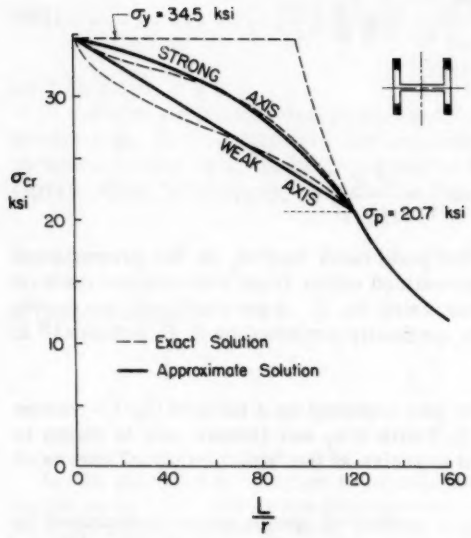

FIG. 23(a).—MOMENT OF INERTIA REDUCTION FACTOR FOR WIDE-FLANGE COLUMNS

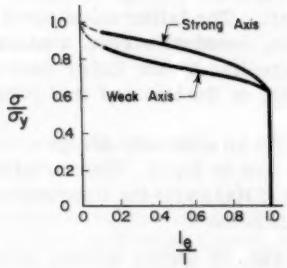

FIG. 23(b).—COLUMN CURVE FOR WIDE-FLANGE SHAPE WITH COOLING RESIDUAL STRESSES

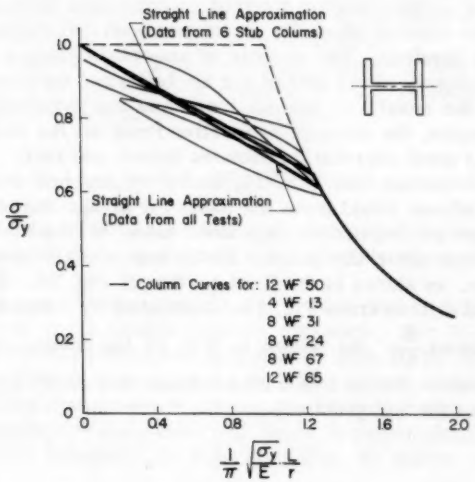

FIG. 24.—COLUMN CURVES OBTAINED FROM STUB-COLUMN TESTS

$$\sigma_{yy} = \sigma_y - \frac{(\sigma_y - \sigma_p)}{\pi}\sqrt{\frac{\sigma_p}{E}}\left(\frac{L}{r}\right) \quad \text{(10b)}$$

for $L/r \leq \pi\sqrt{E/\sigma_p}$, and

$$\sigma_{xx} = \sigma_{yy} = \frac{\pi^2 E}{(L/r)^2} \quad \text{(10c)}$$

for $L/r \leq \pi\sqrt{E/\sigma_p}$. In Eqs. 10 σ_y is the yield level and σ_p is the proportional limit. The latter value could be determined either from stub-column tests or from residual stress measurements using Eq. 2. A parabolic column curve, tangential to the Euler curve, was originally proposed by J. B. Johnson[15] in 1893, on the basis of test results.

As an alternate design procedure, one could set up a table of (I_e/I)- values for use in Eq. 5. The variation of I_e/I with σ/σ_y and flexure axis is shown in Fig. 23(a) and is the information used to arrive at the "exact solution" curves of Fig. 23(b).

Fig. 24 shows column curves for a number of specimens as determined by the "stub column" method and also the straight line approximation (Eq. 10) using average values obtained for this group. (In Fig. 24, as in many that follow, the information is presented in non-dimensional form in order to adjust for variations in σ_y and E.) The approximation of Eq. 10 is also shown in which all of the data in Table 1 has been included. While the scatter is considerable, the straight-line approximation is evidently a good one.

Fig. 25 shows the results of weak-axis column tests in comparison with the same straight-line approximation arrived at from data from all the stub columns tested. The circles show the maximum load the columns carried, not the point of first bending. The results of annealed columns are also shown; their strength is clearly above that of the as-delivered members.

Fig. 26 shows the results of column tests and the parabolic approximation of Eq. 10 using, again, the average properties from all the stub columns tested. Again there is good correlation between theory and test.

It is evident therefore that Eqs. 10, based on residual stress and tangent modulus considerations, could form the basis for design curves.

Up to this point no cognizance has been taken of the fact that structural steel strain hardens after the plastic strain has reached about ten times the elastic limit value, as shown in the first portion of Fig. 27. This results in a σ- E_t diagram that differs from Fig. 19. Instead of $E_t = 0$ at the yield stress, $E_t \approx 900$ ksi, or about $\frac{E}{40}$. As shown in Fig. 27 the column curve is affected for low (L/r)-values. Below $L/r \approx 20$ a column will carry a greater average critical stress than the full yield value.

---

[15] "Materials and Structures," by E. H. Salmon, Vol. I, Longmans, Green and Co., London, 1948.

$$\sigma_{xx} = \sigma_{yy} = \frac{2.96 \times 10^5}{(L/r)^2} \quad \ldots\ldots\ldots\ldots\ldots (14)$$

for $L/r > 122$.

In order to simplify the design procedure by eliminating the consideration of flexure axis, B. G. Johnston[17] has suggested that $\sigma_p/\sigma_y = 0.5$ be used with a parabolic curve, using the single curve for both strong and weak axis bending. The resulting "CRC curve" is shown in Fig. 28 as

$$\sigma_{cr} = 33.0 - 9.20 \times 10^{-4} (L/r)^2 \quad \ldots\ldots\ldots\ldots (15)$$

In general terms

$$\sigma_{cr} = \sigma_y - \frac{\sigma_y^2}{4\pi^2 E}\left(\frac{K L}{r}\right)^2 \quad \ldots\ldots\ldots\ldots\ldots (16)$$

In the past it was common to explain the reduction in column strength in a region up to $L/r = 100$ as due to accidental eccentricities and initial curvature. Such accidental eccentricities, in fact, were estimated and appear in certain design formulas. Although the secant type formula is derived on the basis of an idealized stress-strain curve with yield point at the elastic limit (33,000 psi), it assumes a certain value for accidental eccentricity. This latter value was arrived at analytically by correlation with a study of column tests. Since any correlating column tests must have included as-delivered specimens that contained residual stresses, the magnitude of the accidental eccentricity or initial curvature must necessarily have been arbitrary since a considerable portion of the reduction in column strength is now known to be due to the presence of residual stresses rather than eccentricities.

Thus, design curves for column strength based on the tangent modulus method modified by the presence of residual stress, reflect actual conditions rather than a reliance on assumed irregularities.

BUILT-UP MEMBERS

A pilot investigation into the influence of residual stresses on the behavior of built-up columns has been carried out.[7] Certain of the findings are summarized herewith.

Residual Stresses.—Welded columns will have high residual stresses; this is particularly true of the tensile residual stresses. For H-shaped members the compressive residual stresses may also be high. Fig. 29 shows residual stresses in a welded H-shaped member. The tensile stresses approach the yield value and the compressive stress at the flange tips averages about 21 ksi. These stresses are compared with those in rolled shapes and in Universal plates prior to welding, in Fig. 30. Fig. 30 shows that compressive

17 "Guide to Design Criteria for Metal Compression Members," Column Research Council (in preparation).

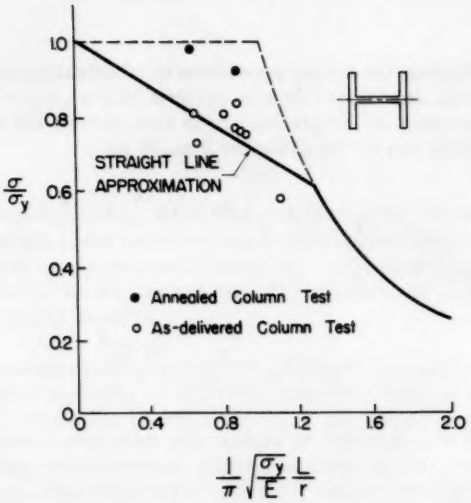

FIG. 25.—COLUMN TEST RESULTS AND STRAIGHT-LINE COLUMN CURVE—WEAK AXIS

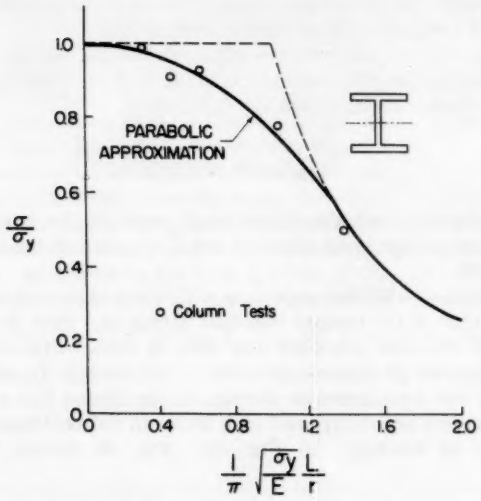

FIG. 26.—COLUMN TEST RESULTS AND PARABOLIC COLUMN CURVE —STRONG AXIS

Fig. 28 is drawn taking strain hardening into account. Assuming $L/r = 20$ as the onset of strain hardening in the column curve, Eqs. 10 become

$$\sigma_{xx} = \sigma_y - \frac{\sigma_y - \sigma_p}{\left(\pi\sqrt{\frac{E}{\sigma_p}} - 20\right)^2}\left(\frac{L}{r} - 20\right)^2 \quad \ldots\ldots\ldots \text{(11a)}$$

for $20 \leq L/r \leq \pi\sqrt{E/\sigma_p}$,

$$\sigma_{yy} = \sigma_y - \frac{\sigma_y - \sigma_p}{\pi\sqrt{\frac{E}{\sigma_p}} - 20}\left(\frac{L}{r} - 20\right) \quad \ldots\ldots\ldots\ldots \text{(11b)}$$

for $20 \leq L/r \leq \pi\sqrt{E/\sigma_p}$, and

$$\sigma_{xx} = \sigma_{yy} = \frac{\pi^2 E}{\left(\frac{L}{r}\right)^2} \quad \ldots\ldots\ldots\ldots\ldots\ldots\ldots \text{(11c)}$$

for $L/r \geq \pi\sqrt{E/\sigma_p}$.

Eqs. 11 have been replotted in Fig. 28 as Eqs. 12, 13 and 14, together with column test results. All information is presented on a dimensional basis using $\sigma_y = 33$ ksi, $\sigma_p = 20$ ksi, and $E = 30 \times 10^3$ ksi. That is the actual experimental data has been adjusted proportionately to these figures, which represent the values most appropriate as a result of this investigation. (Using the approximate values $\sigma_p = 20$ and $\sigma_y = 33$ gives a ratio $\sigma_p/\sigma_y = 0.606$. Frequently a value of $\sigma_p/\sigma_y = 0.70$ has been used for these curves. This corresponds to $\sigma_{rc} = 0.30\,\sigma_y$ which is the peak (mode) of the frequency distribution, Fig. 2.)[16] (Actually, the yield stress level, experimentally, was 33.4 ksi, but this is so close to the specification minimum of 33.0 ksi that the latter was used as the average value—particularly as the factor of safety would account for any deviation from this average.)

The test points for Fig. 28 have been plotted from the data contained in Figs. 25 and 26. For the foregoing average values, Eqs. 11 take the form

$$\sigma_{xx} = 33.0 - 12.5 \times 10^{-4}\left(\frac{L}{r} - 20\right)^2 \quad \ldots\ldots\ldots\ldots \text{(12)}$$

for $20 \leq L/r \leq 122$,

$$\sigma_{yy} = 33.0 - 0.127\left(\frac{L}{r} - 20\right) \quad \ldots\ldots\ldots\ldots\ldots \text{(13)}$$

for $20 \leq L/r \leq 122$, and

---

16 "Influence of Residual Stress on the Strength of Structural Members," by R. L. Ketter, Welding Research Council, Bulletin No. 44, November, 1958.

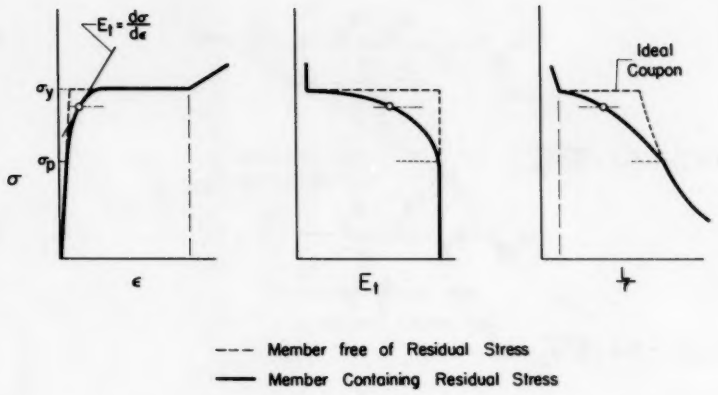

FIG. 27.—INFLUENCE OF STRAIN HARDENING ON COLUMN CURVE

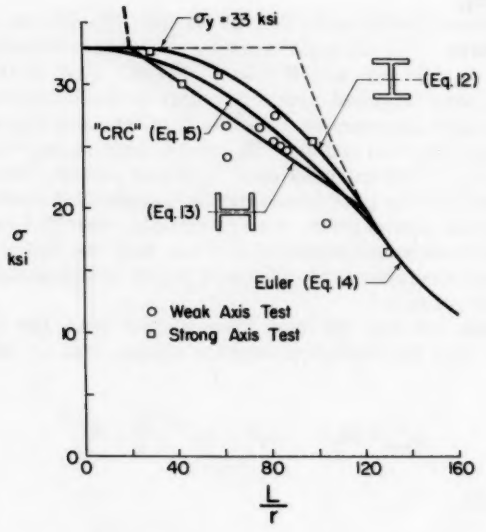

FIG. 28.—COLUMN CURVES AND TEST RESULTS

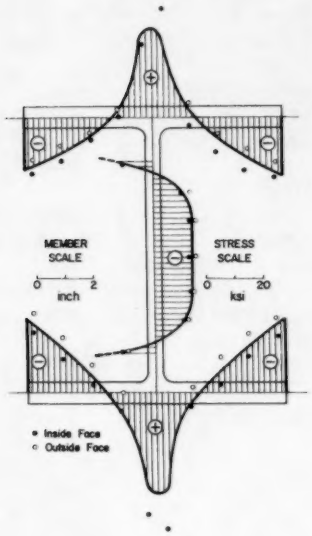

FIG. 29.—RESIDUAL STRESS PATTERN IN A WELDED SHAPE

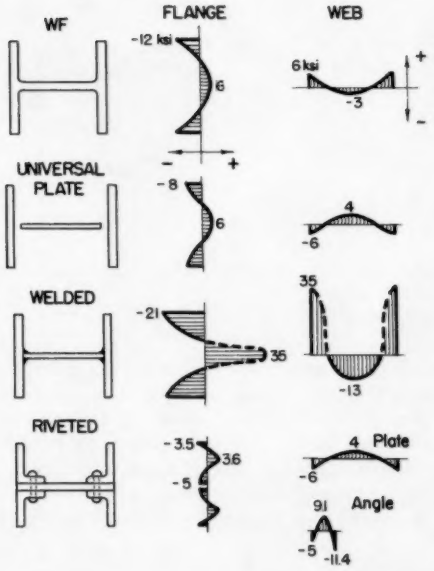

FIG. 30.—RESIDUAL STRESS PATTERNS IN ROLLED MEMBER, IN PLATES, AND IN WELDED AND RIVETED MEMBERS

stresses in welded H-shaped members may be higher than those in rolled wide-flange shapes. Compressive residual stresses in universal plates of 5 ksi to 10 ksi have been observed in flange tips (Fig. 30).[7]

Since the magnitude and distribution of welded residual stresses is markedly influenced by the geometry, further work is required on members with cross-sectional shapes other than the H-section. It would be expected that the use of welded H-shape columns would be replaced more frequently in the future by the economical "box" section.

Riveted built-up columns have a considerable variation in residual stresses that is a function of the geometry of the component parts. Figs. 30 and 31 show some measurements that have been made.

Column Strength.—The axial column strength of built-up H-shaped members can be predicted by the same techniques as were used for rolled shapes with symmetrical cooling residual stresses. The results, correlated with actual column tests, are shown in Fig. 32. The tangent-modulus concept is not realistic for the prediction of the strength of these welded columns, but an ultimate-strength analysis gives good correlation.[7]

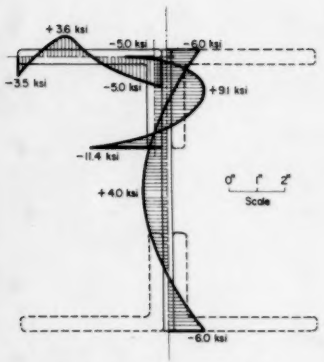

FIG. 31.—SIMPLIFIED RESIDUAL STRESS PATTERN FOR A RIVETED COLUMN

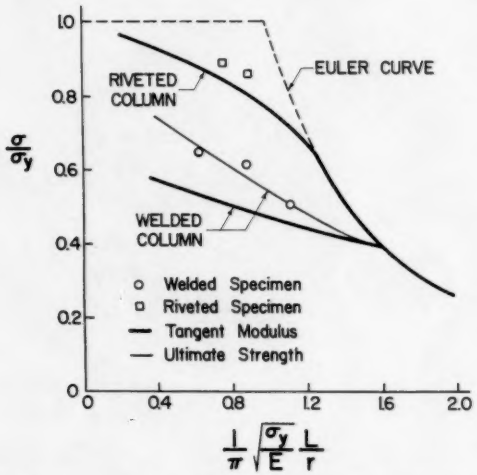

FIG. 32.—TEST RESULTS AND COLUMN CURVES FOR WELDED AND RIVETED MEMBERS—WEAK AXIS

General conclusions regarding the column strength of built-up members (particularly the welded ones) cannot be made until further studies are completed. Even though the strength of the welded H-columns was proportionately less than that of the riveted or as-rolled columns, it is very important not to draw the conclusion that welded columns usually will be "weaker" than corresponding rolled shapes. The effect would be quite different if the cross section were in box form. Studies of the effect of cross-sectional form are necessary and are underway.

LOW ALLOY HIGH STRENGTH STEELS

A program of tests on high strength low alloy steel (ASTM A242) has indicated that the column strength of such steel can be predicted in the same man-

ner as for A7 steel (Fig. 33.)[13] The residual-stress distribution in rolled shapes is the same as for A7 steel, the formation of residual stress being more dependent on shape than on variation of material properties.

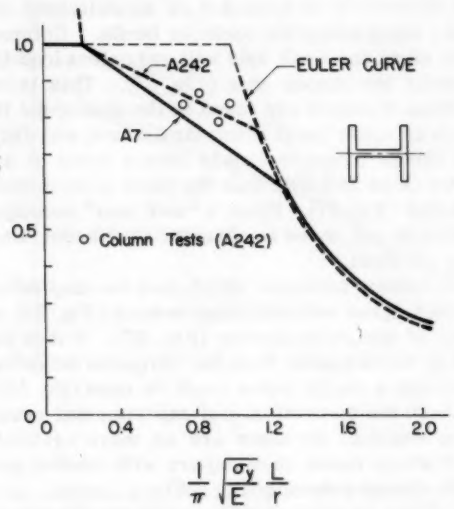

FIG. 33.—COLUMN CURVES AND TEST RESULTS FOR A242 STEEL COMPARED WITH A7 STEEL

Because of the high yield-stress level, the influence of residual stress on columns of high strength steel is not as pronounced as on A7 steel as shown in Fig. 33.

SUMMARY

1. The strength of centrally loaded steel columns may be expressed in terms of the tangent modulus E_t (Fig. 19). This modulus depends on the state of residual stress in the member.

2. Residual stresses are formed in a structural member as a result of plastic deformations that occur during cooling after rolling, after welding, or during cold-straightening operations. For rolled or welded members, the part to cool last is usually in a tensile state of residual stress (Figs. 1 and 30).

3. Insofar as H-columns are concerned, the most important of the stresses are those at the flange tips; for rolled shapes the average compressive stress there is about 13 ksi (Table 2).

4. The effect of residual stress on the stress-strain relationship is to lower the proportional limit and to cause the stress-strain diagram to be non-linear beyond that point and up to the yield stress level (Figs. 5 and 18). The proportional limit for the shapes studied was about 21 ksi (62% of yield stress level).

5. Residual stresses reduce buckling strength because of early localized yield that occurs at certain portions of the cross section. This reduction is

greatest when the slenderness ratio is between 70 and 90 and amounts to about 25% (Figs. 25 and 26). The critical stress in the inelastic range ($\sigma > \sigma_p$) is a function of the moment of inertia of the elastic portion of the cross section (Eq. 5 and Fig. 4(d)).

6. There is a difference in behavior of as-delivered columns that is dependent on the axis about which the member bends. Columns of a given slenderness ratio bent about the weak axis will carry less load than columns of the same L/r bent about the strong axis (Fig. 20). This is because the highest compressive residual stresses are found at the tips of the flanges.

7. Factors such as upper yield point, strain rate, and difference in strength between web and flange cause the yield stress level of a full cross section (stub column) to be about 20% less than the yield point determined in a routine ASTM acceptance test (Fig. 11). From a "mill test" average of all data available to date of about 42 ksi, there is obtained a probable compressive strength of about 34 ksi for A7 steel.

8. Approximate column formulas which may be adapted for design use have been developed which agree well with test results (Fig. 28) and which also reflect the influence of strain-hardening (Fig. 27). If it is desired to take into account the effect of flexure axis, then two formulas would be necessary (Eqs. 12 and 13). Otherwise a single curve could be used (Eq. 15) which provides a good approximation to the theoretical and experimental results.

9. Cold-bending residual stresses are no more critical than are cooling stresses. Thus, findings based on members with cooling patterns may be applied to rolled wide-flange columns (Fig. 22).

10. Columns built-up by welding will contain tensile residual stresses close to the yield point (Fig. 29). Compressive stresses may be higher or lower than those that form due to cooling, depending on the geometry of the cross section. Although tests of H-shaped welded members exhibit a strength that is comparatively less than that of a corresponding wide-flange shape, it might be expected that welded "box" columns would be somewhat stronger than a corresponding rolled member.

11. Low-alloy, high-strength steels contain residual stresses whose magnitude and distribution are similar to those in A7 steel. Since the formation of residual stress does not depend to the same extent on the magnitude of the yield stress level as it does on the geometry, the influence of residual stress on the strength of columns of higher strength steels is not as pronounced as on columns of A7 steel (Fig. 33).

12. Column strength is affected by the presence of residual stress, and is dependent on its magnitude and distribution. Columns of riveted and high-strength steels, for example, with proportionately smaller magnitudes of compressive residual stress, have greater strengths than columns of a welded H-shape of A7 steel (Fig. 34).

13. Residual stresses are the major factor affecting the strength of centrally loaded columns in the intermediate ranges ($40 \leq L/4 \leq 120$), and design curves for column strength based on the tangent modulus concept, modified by the presence of residual stresses, reflect actual conditions more closely than has previously been possible.

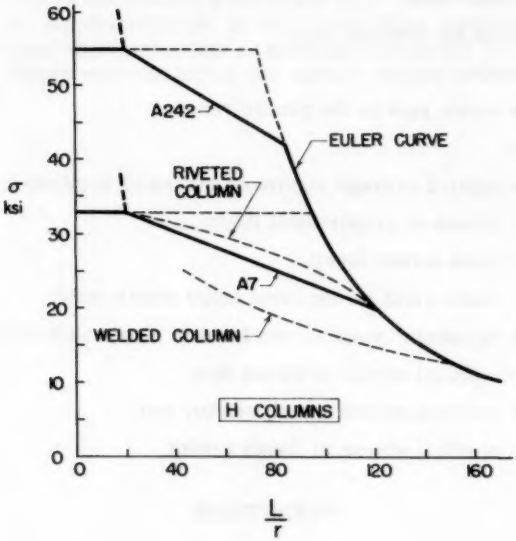

FIG. 34.—DIAGRAMMATIC COLUMN CURVES FOR A242 AND A7 ROLLED SHAPES AND FOR RIVETED AND WELDED A7 COLUMNS OF H-SHAPE—WEAK AXIS

NOMENCLATURE

A = cross-sectional area:
- A_f = area of both flanges of a wide-flange shape;
- A_w = web area;

b = width of flange of wide-flange shape;

d = depth of a wide-flange shape;

E = Young's modulus of elasticity:
- E_t = tangent modulus;

I = moment of inertia:
- I_e = moment of inertia of the unyielded (elastic) part;

L = total length of a pin-end column;

L/r = slenderness ratio;

K L/r = effective slenderness ratio;

P_{cr} = critical load on a column;

r = radius of gyration;

s = standard deviation, a statistical measure of the scattering of observations;

t = flange thickness;

x, y = directions for flexural axis;

ϵ = unit strain;

ϵ_{pl} = strain rate in the plastic range;

σ = stress:

σ_{cr} = applied average maximum stress on a column;

σ_p = stress at proportional limit;

σ_y = yield stress level;

σ_{ys} = static yield stress level (zero strain rate);

σ_{yd} = "dynamic" yield stress level (a strain rate other than zero);

σ_{rc} = residual stress at flange tips;

σ_{rw} = residual stress at web center; and

σ_{ro} = residual stress at flange center.

DEFINITIONS

Buckling.—Buckling is the process for any structure or part of a structure to pass from one deflection pattern into another without a change of load.

Critical Load.—The maximum load a column will carry. It is not coincident with the buckling load for an axially loaded column.

Plastic Strain Rate.—The strain rate in the plastic range. For a coupon test, the plastic strain rate, unlike the elastic strain rate, is independent of the elasticity of the testing machine.

Stub Column.—A short compression test specimen, sufficiently long for use in measuring the stress-strain relationship for the complete cross section, but short enough to avoid buckling in the elastic and plastic ranges.

Yield Point.—The first stress in a material, less than the maximum attainable stress, at which an increase in strain occurs without an increase in stress.

Yield Stress.—The stress at which a material exhibits a specified limiting deviation from the proportionality of stress to strain.

Yield Stress Level.—The average stress during actual yielding in the plastic range. It remains fairly constant for structural steel provided the strain rate remains constant.

ACKNOWLEDGMENTS

This report summarizes the theoretical and experimental studies made during the course of a research program on the influence of residual stress on column strength carried out at the Fritz Engineering Laboratory, Lehigh University, Bethlehem, Pa., of which William J. Eney is director.

The Pennsylvania Department of Highways and the U. S. Department of Commerce Bureau of Public Roads, the National Science Foundation, and the Engineering Foundation through the Column Research Council sponsored jointly the research program.

Since this report is essentially a summary of progress reports prepared on the investigation, acknowledgment is due those other investigators at Fritz Laboratory to whose work reference is made throughout the report, in particular, to Alfons Huber who conducted the earlier phases of this research program.

Journal of the
STRUCTURAL DIVISION
Proceedings of the American Society of Civil Engineers

LATERAL BUCKLING OF BEAMS

By J. W. Clark,[1] M. ASCE, and H. N. Hill,[2] F. ASCE

FOREWORD

The papers that form the ASCE-CRC Symposium on Metal Compression Members are representative of all phases of Column Research Council activities. Several papers represent summaries of both past and current research, prepared specifically to assist in the preparation of the "Guide to Design Criteria for Metal Compression Members." Also included are reports on recently completed research on pony truss bridges and on plate girders.

In the January 1960 Journal of the Structural Division Bruce G. Johnston documented the inception of the CRC and the many activities undertaken by the Council.

Thomas C. Kavanagh, in the February 1960 Journal of the Structural Division, reviewed the state of knowledge concerning the effective length of framed columns.

In the April 1960 Journal of the Structural Division, Robert M. Barnoff and William G. Mooney studied the effect of floor-system participation on pony truss bridges.

Bruce G. Johnston presented a digest of the "Guide" in the April 1960 Journal of the Structural Division.

In the July 1960 Journal of the Structural Division Lynn S. Beedle and Lambert Tall provided a summary of investigations of the strength of centrally loaded columns as influenced by residual stresses and variations in the yield-stress level.

Note.—Discussion open until December 1, 1960. Separate discussions should be submitted for the individual papers in this symposium. To extend the closing date one month, a written request must be filed with the Executive Secretary, ASCE. This paper is part of the copyrighted Journal of the Structural Division, Proceedings of the American Society of Civil Engineers, Vol. 86, No. ST 7, July, 1960.

[1] Asst. Chf., Engrg. Design Div., Alcoa Research Labs., New Kensington, Pa.
[2] Chf., Engrg. Design Div., Alcoa Research Lab., New Kensington, Pa.

SYNOPSIS

This paper is intended to provide a brief summary of information that may be used as background material in writing specifications for the design of beams and girders whose strength is controlled by lateral buckling.

A general formula is developed for elastic buckling strength of beams, with coefficients depending principally on the conditions of loading and support. Values of the coefficients in this formula are tabulated for a wide variety of conditions of loading and support. The relationship between theoretical buckling strength and experimental results is discussed.

Various design formulas that have been proposed for beams are compared with each other and with experimental and theoretical beam strengths.

INTRODUCTION

This paper is intended to provide a brief summary of information that may be used as background material in writing specifications for the design of beams and girders whose strength is controlled by lateral buckling. The paper is not intended to recommend specific design procedures. It is not possible to cover all the available material on this subject in a paper of reasonable length. For the sake of brevity, detailed information in the form of charts and tables is presented only in cases where the data are not readily available in published form. Much of the material in this paper is taken from a report which the authors prepared at the request of Research Committee E of Column Research Council (40).[3]

Notation.—The letter symbols adopted for use in this paper are defined where they first appear and arranged alphabetically, for convenience of reference, in Appendix III.

BUCKLING STRENGTH OF BEAMS AND GIRDERS

Elastic Buckling.—Formulas for the elastic buckling strength of beams can be used as a basis or point of departure in the preparation of design rules. The results of many of the theoretical investigations that have been made on the elastic buckling strength of beams (1 through 10) can be expressed by the following equation, which is derived in Appendix I.

$$f_{cr} = C_1 \frac{\pi^2 E I_y}{S_c (K L)^2} \left[C_2 g + C_3 k + \sqrt{\left(C_2 g + C_3 k\right)^2 + \frac{C_w}{I_y} \left(1 + \frac{G J (K L)^2}{\pi^2 E C_w}\right)} \right] \quad . . (1)$$

in which the C are coefficients, f_{cr} refers to the critical stress for lateral buckling, E is the modulus of elasticity, I_y denotes the moment of inertia of the beam cross section about the y-axis, K is a coefficient, L is the distance between points of support against lateral bending and twisting, C_w denotes the torsion warping constant, g refers to the distance from shear center to point of application of transverse load (positive when load is below shear center and

[3] Numbers in parenthesis thus, (1), refer to corresponding items in Appendix II.—Bibliography.

negative otherwise), G is the modulus of rigidity, J is the torsion constant, and S_c denotes the section modulus for stress in compression flange. The factor k - lc is defined as,

$$k = e + \frac{1}{2 I_x} \int_A^y \left(x^2 + y^2\right) dA$$

The coefficients C_1, C_2, C_3, and K depend mainly on the conditions of loading and support for the beam. Values of these coefficients for a number of different cases are listed in Table 1. These coefficient values are limited to prismatic beams bent about a principal axis. In cases where transverse loads are applied, it is assumed that the lines of action of the loads pass through the shear center and the centroid and that the loads are attached to the beam in such a way that their lines of action remain parallel to their initial directions as the beam deflects. It is also assumed that the shear center lies on a principal axis through the centroid.

Elastic buckling theory has been confirmed by tests for several types of loading and shapes of cross section. Many of these tests have been performed on aluminum alloy members. The aluminum beams tested include symmetrical I-beams under uniform bending moment (12), unequal end moments (13), and under a concentrated load at the center of the span (14); and deep rectangular beams (43), channels (15), Z's (15), and unsymmetrical I-sections (16) under uniform bending moment. Tests of structural carbon steel beams subjected to two concentrated loads on the top flange at the quarter points have also demonstrated the validity of elastic buckling theory (17).

Inelastic Buckling.—Bleich (18) has pointed out that it is possible to obtain a lower limit to the theoretical buckling stress in the inelastic range by substituting the tangent modulus E_t corresponding to the maximum stress in the beam for the elastic modulus E in the elastic buckling formula. Tests on aluminum alloy beams have shown that this method gives a close approximation to the experimental buckling stress when the bending moment is constant along the length (12)(13). Tests of aluminum alloy beams subjected to unequal end moments, with the ratio of the end moments varying from 1.0 to -1.0, resulted in experimental critical stresses varying from 8% below to 39% above the values computed by the method suggested by Bleich (18).

A study made by W. J. Austion (19) of the results of tests on steel beams reported by R. A. Hechtman, J. S. Hattrup, E. F. Styer and J. L. Tiedemann (17) showed the tangent modulus curve for structural steel suggested by Bleich (18) to be somewhat unconservative in comparison with some of these tests results. However, it is probable that a tangent modulus curve based on compressive tests of the full cross section of the members used in the beam tests would have been in better agreement with the test results. Results of Austin's study are shown in Fig. 1.

A second method of estimating the effect of plastic action on the strength of beams and girders is to assume that the relationship between the elastic and inelastic buckling strength is the same for beams as it is for columns. Inelastic buckling strength of beams may then be estimated from a column curve. This procedure is applicable to aluminum alloy members since the tangent modulus buckling curve agrees well with tests on both columns and beams (23). This method has also been recommended as a basis for design of steel beams (8)(39).

A third method of taking into account the effect of inelastic behavior is to determine the relationship between elastic and inelastic buckling strength directly from tests on beams. This procedure takes into account the effect of any

TABLE 1.—VALUES OF COEFFICIENTS IN FORMULA FOR ELASTIC BUCKLING STRENGTH OF BEAMS

Case No.	Loading	Bending Moment Diagram	Condition of Restraint Against Rotation about Vertical Axis at Ends	Values of Coefficients K	C_1	C_2	C_3	Sources of Data
Beams Restrained Against Lateral Displacement at Both Ends of Span								
1.	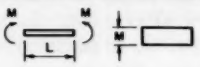		Simple Support	1.0	1.0	--	1.0	Timoshenko,[1] Goodier[2]
			Fixed	0.5	1.0	--	1.0	Nylander[3]
2.	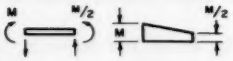		Simple Support	1.0	1.31-1.32[a]	--		Salvadori[4]
			Fixed	0.5	1.30-1.32[a]	--		
3.	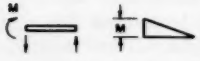		Simple Support	1.0	1.77-1.86[a]	--	6.5[b]	Pettersson[6]
			Fixed	0.5	1.78-1.85[a]	--		Salvadori[4]
4.	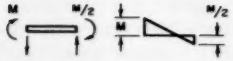		Simple Support	1.0	2.33-2.62[a]	--		Salvadori[4]
			Fixed	0.5	2.29-2.55[a]	--		
5.	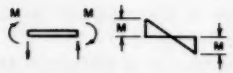		Simple Support	1.0	2.56-2.74[a]	--		Salvadori[4]
			Fixed	0.5	2.23-2.58[a]	--		
6.	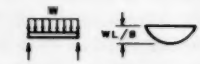		Simple Support	1.0	1.13	0.45		De Vries[30]
			Fixed	0.5	0.97	0.29		Austin, et al[5]
7.	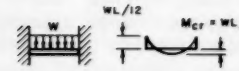		Simple Support	1.0	1.30	1.55		Austin, Yegian and Tung[5]
			Fixed	0.5	0.86	0.82		
8.	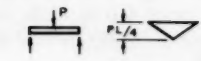		Simple Support	1.0	1.35	0.55	2.5[b]	Pettersson[6]
			Fixed	0.5	1.07	0.42		Austin, et al[5]
9.	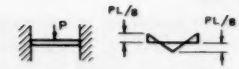		Simple Support	1.0	1.70	1.42		Austin, Yegian and Tung[5]
			Fixed	0.5	1.04	0.84		
10.	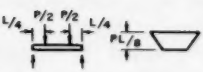		Simple Support	1.0	1.04	0.42		Winter,[9] Schrader[10]
Cantilever Beams								
11.	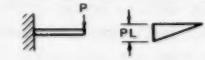		Warping Restrained at Supported End	1.0[c]	1.28-1.71[a]	0.64		Timoshenko,[1] Kerensky, Flint and Brown[8]
12.	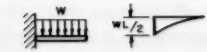		Warping Restrained at Supported End	1.0[c]	2.05-3.42[a]			Poley[7]

[a] Minimum value applies to beams with negligible resistance to warping and can be used to obtain conservative buckling stresses for all beams.

[b] Average value giving buckling stresses within about 10 per cent of values computed by Pettersson in all cases.

[c] For cantilever beams, no single combination of values of K and C_1 applies to all proportions of beams. In Case No. 11, the variation of C_1 corresponding to a single value of K is approximately a minimum for k = 1.0.

other factors such as residual stress and initial crookedness, which may have affected the test results. The curve for inelastic buckling strength of structural carbon steel beams that has been suggested by Austin on the basis of the beam tests at the University of Washington is shown in Fig. 1.

Buckling of Beams Under Various Special Conditions.

Oblique Loads.—The case of a beam subjected to a uniform bending moment that does not lie in one of the principal planes of the cross section has been discussed by J. N. Goodier (2) and by R. C. McCalley (20). The latter showed that the equation for the critical moment takes the form of Eq. 1 with $C_1 = C_3 = 1.0$, $C_2 = 0$. The quantity I_y is replaced by the expression $I_{\bar{y}}\, I_{\bar{x}} / I_x$, in which $\bar{y}$ and $\bar{x}$ denote principal axes, and the x-axis is the axis normal to the plane of bending.

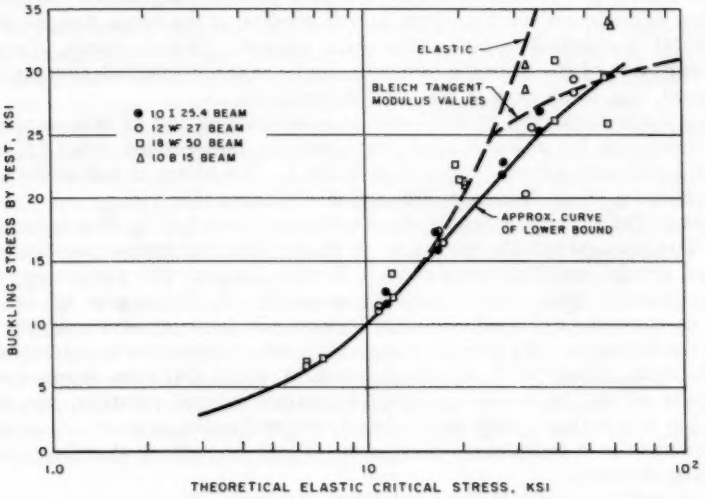

FIG. 1.—RESULTS OF BENDING TESTS ON ROLLED BEAMS OF STRUCTURAL CARBON STEEL

Nonuniform Cross Section.—The effect on the buckling strength of variations in the flange thickness along the length of an I-section girder has been investigated by O. A. Kerensky, A. R. Flint and W. C. Brown (8), who have suggested a basis of design for such members. B. Gatewood (21) has shown that for cantilever beams with negligible warping rigidity, variations in the cross section have the same effect on the buckling strength as they do for cantilever columns. A concise solution for the lateral buckling strength of a tapered narrow rectangular beam, subjected to constant bending moment and simply supported at the ends, has been presented by L. H. N. Lee (41). Tapered cantilever I-beams were investigated experimentally by W. J. Krefeld, D. J. Butler and G. B. Anderson (42).

Special End Conditions.—Austin, S. Yegian, and T. P. Tung (5) gave solutions for elastic buckling strength of I-beams under transverse load (either

uniform load or a concentrated load at the center) with various degrees of restraint against rotation of the beam about either a vertical or a transverse horizontal axis at the ends. Each type of restraint was considered to vary between zero and complete fixity. In all cases, the beams were considered to be fixed against rotation about a longitudinal axis at the ends. Tests by Hechtman, Hattrup, Styer and Tiedemann (17) demonstrated that web-angle connections at the ends of beams prevented rotation about a longitudinal axis and restrained rotation about a transverse horizontal axis, but did not provide much restraint against rotation of the flanges about a vertical axis. Top and seat angle connections resulted in higher beam buckling loads than did web angle connections since the former provided some restraint against rotation of the flanges about a vertical axis, as well as restraining rotation about the other two axis.

Frequently a cantilever beam is simply the overhanging end of a beam that extends over two or more supports. In this case, the supported end of the cantilever beam is not fixed against lateral bending of the beam flanges but some restraint is supplied by continuity at the support. In such cases, a conservative estimate of the buckling strength can be made by considering the warping constant, C_W, to be zero in the buckling formula.

If a beam supported at both ends is continuous at one or both supports, the end conditions for any one span are generally between the cases of complete fixity and simple support covered in Table 1. The effect of continuity has been discussed by M. G. Salvadori (22) and H. Nylander (3).

Large Deflections.—Beams for which the ratio I_y / I_x is relatively large may develop appreciable curvature in the plane of the applied bending moment before lateral buckling takes place. In some cases, this curvature can have an appreciable effect on the buckling strength. O. Pettersson (6) has developed an accurate expression for the increase in buckling strength that results from the deflection of a simply-supported I-beam subjected to a uniform bending moment. However, J. W. Clark and A. H. Knoll (24) have shown that, when the ends of the beam are restrained against lateral rotation, the buckling strength is not appreciably increased by the deflection prior to buckling. Initial camber in a beam may, of course, cancel any effect of deflection on the buckling strength.

Reduced Torsional Stiffness of Plate Girders.—The torsional stiffness of plate girders may be reduced because of warping of the cross sections and also as a result of slipping between the various parts of built-up sections. F. K. Chang and B. G. Johnston (25) have shown that in computing the torsional stiffness of riveted plate girders, an accurate value of J, the torsional constant, can be computed by considering the parts of the flange between the outside lines of rivets as a single solid piece, and the parts extending beyond the outside lines of rivets as individual elements. The tests of Chang and Johnston (25) showed that, if the rivets are sufficiently close together, this method of computing J causes a maximum error of about 20%, which would result in an error of not more than 10% in the computed elastic buckling stress. H. Nylander (26) has demonstrated that distortion of the cross section is not very significant for beams of conventional proportions. For very deep plate girders, the tests of Chang and Johnston (25) indicated that the shape of the cross section is maintained partly through the effect of the stiffeners. G. Winter has recommended (9) that for beams with very thin webs and for latticed trusses, the torsion constant J should be taken as zero in computing the buckling strength, since this assumtion does not cause much error in the buckling stress for these members.

Eccentric Loads and Crookedness.—The behavior of beams under eccentric loads has been investigated by Pettersson (6) and the effects of initial bow and initial twist have been studied by Kerensky, Flint and Brown (8). In general, these factors affect the buckling strength in the same way that they do for columns.

NOMOGRAPH FOR BUCKLING STRENGTH OF BEAMS

Eq. 1 appears at first glance to be too involved for use as a design tool. However, all the quantities in it except k are tabulated for many structural sections and may be computed for other sections (27)(28). The quantity k can be approximated by the quantity e, for which formulas are readily available (27). The arithmetic involved in calculating critical stresses from Eq. 1 (or values of "equivalent slenderness ratio" if the equation is put in a form so that it can be used with a column buckling curve) can be greatly reduced with the aid of a nomograph, such as that shown in Fig. 2.[4] Fig. 2 gives the equivalent slenderness ratio ($K\,L/r$) corresponding to Eq. 11 for an unsymmetrical I-beam under uniform bending moment. For symmetrical sections, the values of $K\,L/r$ from Fig. 2 can be multiplied by $1/\sqrt{C_1}$ to make them applicable to beams with other distributions of bending moment. For unsymmetrical sections under nonuniform bending moment, the quantity $e\,I_y$ should be multiplied by C_3 and the resulting value of $K\,L/r$ from Fig. 2 multiplied by $1/\sqrt{C_1}$. To take into account the effect of applying transverse loads at a point above or below the shear center, the quantity $e\,I_y$ in Fig. 2 should be replaced by $(C_2\,g + C_3\,e)\,I_y$. Again, the resulting value of KL/r must be multiplied by $1/\sqrt{C_1}$. To make Fig. 2 applicable to beams whose section properties are outside the range of values covered in the chart, the values of J, C_w, I_y, and S_c for the section can be multiplied by a constant such as 0.1 or 0.01. Use of Fig. 2 with these modified section properties (the true values of L and e must be used) will give the correct value of $K\,L/r$ for the beam. For any particular material, the answer obtained from Fig. 2 could be put in the form of an allowable stress rather than an equivalent slenderness ratio.

SIMPLIFIED FORMULAS FOR BUCKLING STRENGTH AND ALLOWABLE STRESS

There are many special cases that result in simplifications in Eq. 1 and also many approximations that can be used to reduce the complexity of the computations.

Symmetrical Sections.—For sections that are symmetrical about the horizontal axis or about a point, the quantity k in Eq. 1 is equal to zero. Further simplication results if there is no transverse load, or if the transverse loads are applied at the neutral axis, in which case $g = 0$. The expression for elastic buckling strength can then be written

$$f_{cr} = C_1 \frac{\pi \sqrt{E\,I_y\,G\,J}}{S_c\,K\,L} \sqrt{1 + \frac{\pi^2\,E\,C_w}{(K\,L)^2\,G\,J}} \quad \ldots\ldots\ldots (2)$$

[4] Large copies of this chart will be furnished upon request to J. W. Clark, Alcoa Research Laboratories, P. O. Box 772, New Kensington, Pa.

Eq. 2 can be put in the form

$$f_{cr} = C_4 \frac{\sqrt{I_y J}}{S_c L} \quad \ldots\ldots\ldots\ldots\ldots\ldots (3)$$

in which C_4 is a function of the conditions of loading and restraint, the modulus of elasticity and Poisson's ratio of the material and of the parameter $C_w/(L^2 J)$.

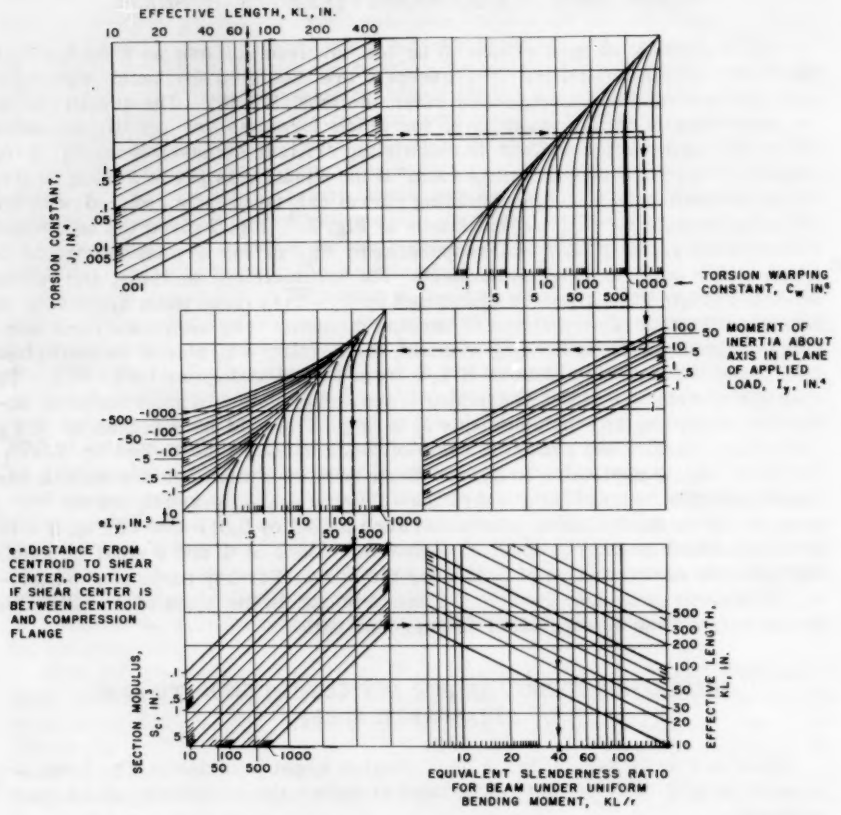
EFFECTIVE LENGTH, KL, IN.
10 20 40 60 100 200 400
TORSION CONSTANT, J, IN.⁴
.001 .005 .01 .05 .1 .5 1
TORSION WARPING CONSTANT, C_w IN.⁶
0 .1 .5 1 5 10 50 100 500 1000
MOMENT OF INERTIA ABOUT AXIS IN PLANE OF APPLIED LOAD, I_y, IN.⁴
.1 .5 1 5 10 50 100
eI_y, IN.⁵
-500 -1000 -50 -100 -5 -10 -.5 -1 -.1
.1 .5 1 5 10 50 100 500 1000
e = DISTANCE FROM CENTROID TO SHEAR CENTER, POSITIVE IF SHEAR CENTER IS BETWEEN CENTROID AND COMPRESSION FLANGE
SECTION MODULUS, S_c, IN.³
.1 .5 1 5 10 50 100 500 1000
EFFECTIVE LENGTH, KL, IN.
10 20 30 50 100 200 300 500
10 20 40 60 100
EQUIVALENT SLENDERNESS RATIO FOR BEAM UNDER UNIFORM BENDING MOMENT, KL/r

NOTE: DOTTED LINES SHOW EXAMPLE IN WHICH KL = 72 IN., J = 0.124 IN.⁴, C_w = 3047 IN.⁶, I_y = 25 IN.⁴, e = 4.1 IN., S_c = 125 IN.³

$$r^2 = \frac{I_y}{S_c}\left(e + \sqrt{e^2 + \frac{1}{I_y}\left[C_w + 0.038\, J(KL)^2\right]}\right)$$

FIG. 2.—NOMOGRAPH FOR EQUIVALENT SLENDERNESS RATIO, KL/r, OF BEAMS UNDER UNIFORM BENDING MOMENT

Eq. 3 can be used as a basis for design if a suitable factor of safety is introduced and allowance is made for inelastic action. The equation can be supplemented by a series of curves giving values of C_4 for a number of conditions of loading and restraint plotted against $C_w/(L^2 J)$. Values of the cross section

properties C_w and J are tabulated for standard aluminum I-, Z-, and channel sections (27). Values of J and $a = \sqrt{E\ C_w/G\ J}$ for rolled steel sections have also been published (28).

Symmetrical I-Sections.

General Formula.—For doubly symmetrical I-beams,

$$C_w = I_y\ d^2/4 \quad \ldots\ldots\ldots\ldots\ldots\ldots (4)$$

in which d is the distance between centroids of beam flanges (taken as depth of beam in approximate formulas). Eq. 3 can be written as

$$f_{cr} = C_5\ \frac{d\sqrt{I_y\ J}}{L\ I_x} \quad \ldots\ldots\ldots\ldots\ldots\ldots (5)$$

Values of the coefficient C_5 can be plotted against the parameter $d^2\ I_y/(L^2\ J)$, for different conditions of loading and restraint. An approach of this kind is used in German specifications (29). An additional modification in the coefficient in Eq. 5 can be introduced to take approximate account of the effects of transverse loads being applied at the top or bottom flange rather than at the neutral axis (23).

Parameters L/r_y and $L\ t/r_y\ d$.—Eq. 3 can be further simplified by introducing approximate expressions for the section properties of the beam. In this procedure, the effect of the web on the section properties is generally ignored, and the flanges are considered as rectangular sections. Expressions of this kind were derived by Winter and other discussers of K. de Vries' paper (30). One equation of this type, which has been proposed as a basis for new British specifications (8), is the following:

$$f_{cr} = \frac{C_6}{(L/r_y)^2}\ \sqrt{1 + \frac{1}{20}\ \left(\frac{L\ t}{r_y\ d}\right)^2} \quad \ldots\ldots\ldots\ldots\ldots\ldots (6)$$

in which t is the thickness at the compression flange and r_y denotes the radius of gyration of the beam cross section about the y-axis. The proposed value of the coefficient C_6 for structural carbon steel is 381,000,000 psi (8).

Parameter $L\ d/b\ t$.—An additional simplification results in cases in which the term $(L\ t/r_y\ d)^2/20$ is large in comparison to unity, so that the first term under the radical in Eq. 6 can be neglected. When r_y is expressed in terms of the flange width b, the resulting expression for the critical stress is

$$f_{cr} = C_7/(L\ d/b\ t) \quad \ldots\ldots\ldots\ldots\ldots\ldots (7)$$

Eq. 7 was developed by de Vries (30), who selected a value of 20,000,000 psi for the coefficient C_7. De Vries has shown that within the elastic range, Eq. 7 is a reasonably accurate and generally conservative expression for the buckling strength of rolled steel I-beams of usual proportions under a number of loading conditions (30). This has been further substantiated by Hechtman's tests (17). Eq. 7 was used as a basis for the present American Institute of Steel Construction (AISC) specification (31).

A rough idea of the degree of approximation involved in Eq. 7 can be obtained by comparing it with Eq. 6, which is quite accurate for symmetrical I-beams, as is demonstrated subsequently by the results in Figs. 5 to 8 for a value of $A_c/(A_c + A_t)$ of 0.5. For beam sections of a given material, the maximum difference between buckling stresses corresponding to Eqs. 6 and 7 occurs at the transition point between the elastic and plastic buckling curves.

For many materials, this transition point occurs at a stress in the vicinity of two-thirds of the compressive yield strength, f_y. Therefore, to find the approximate maximum difference between Eqs. 6 and 7 for a given material, one can set the critical stress in Eq. 6 equal to 2/3 f_y, find the proportions of a beam having this critical stress, and determine the critical stress computed for this beam from Eq. 7. This procedure results in the following equation:

$$\left(\frac{f_{cr} \text{ from Eq. 6}}{f_{cr} \text{ from Eq. 7}}\right)_{max} = 0.675 \left\{1 + \left[1 + 4.14 \left(\frac{f_y}{E}\right)^2 \left(\frac{d}{t}\right)^4\right]^{\frac{1}{2}}\right\}^{\frac{1}{2}} \quad \ldots\ldots (8)$$

The following relationships were used in obtaining Eq. 8: $C_6 = 13.1\ E$ (8); $C_7 = 0.73\ E$ (or 21,200,000 psi for steel) and $b = 4.2\ r_y$ (8).

The ratio of stresses given by Eq. 8 is plotted against d/t for various materials in Fig. 3. Fig. 3 shows that the L d/b t formula gives good accuracy for A-7 carbon steel WF and I-sections, but can be considerably in error for structural shapes in other materials. For plate girder sections in all materials, Eq. 7 can give appreciable errors.

Parameter L/r_y or L/b.—For relatively deep beams, the quantity $L\ t/r_y\ d$ may be so small that Eq. 6 can be approximated by the expression

$$f_{cr} = C_6/(L/r_y)^2 \quad \ldots\ldots\ldots\ldots\ldots\ldots (9)$$

A formula of the above form has been presented by the American Iron and Steel Institute (AISI)(35) and by H. M. Priest and J. A. Gilligen (32). For simple structural shapes, the value of r_y is approximately proportional to the flange width, b, so that Eq. 9 can be expressed in terms of the parameter L/b instead of L/r_y. Formulas involving L/b are used in the American Assn. of State Highway Officials (AASHO)(33) and American Railroad Engineers Assn. (AREA)(34) specifications for steel bridges.

In his discussion of de Vries' paper in 1947 (30), Winter mentioned that two sets of design formulas could be used, one set involving the parameter L/r_y and the other set involving the parameter L d/b t. In questionable cases, allowable stresses could be calculated from both sets of formulas and the higher allowable stress would be used. Recently, Austin has made a similar suggestion (36), incorporating the parameters L/b and L d/b t. The theoretical basis for this proposal is illustrated in Fig. 4, a graph originally presented by Austin (36). The curves labeled 1 and 2 in Fig. 4 are the theoretical buckling stress curves for beams under uniform bending moment and uniform top flange loading, respectively. The diagonal line labeled 3 in Fig. 4 can be approximated by Eq. 7, and the horizontal line labeled 4 can be approximated by Eq.

9. The specific design formulas suggested by Austin are as follows:

$$\left.\begin{aligned} &L\,d/b\,t \leq 1000, && f_b = 18{,}000 - 0.006\,(L\,d/b\,t)^2 \\ &L\,d/b\,t > 1000, && f_b = \frac{12{,}000{,}000}{L\,d/b\,t} \end{aligned}\right\} \quad \text{But not less than} \quad \left.\begin{aligned} &(L/b)^2 < 884, && f_b = 18{,}000 - 5\,(L/b)^2 \\ &(L/b)^2 \geq 884, && f_b = \frac{12{,}000{,}000}{(L/b)^2} \end{aligned}\right\} \quad \ldots\ldots (10)$$

in which f_b is the allowable stress.

In the formulas involving the parameter $L\,d/b\,t$, the quantity $b\,t$ would be replaced by $5\,I_y/b^2$ for riveted plate girders and by $6\,I_y/b^2$ for welded plate girders, as has been suggested by de Vries (30). In the formula involving L/b, Austin recommends that the quantity b^2 can be replaced by $3\,d^2\,I_y/I_x$ for plate girders. To avoid the necessity of computing allowable stresses by both sets of formulas, it could be specified that Eq. 8 would be used except when the value of $(L/b)^2$ is less than the value of $L\,d/b\,t$. This limitation can be derived approximately from Fig. 4.

Unsymmetrical I-Sections.—For I-beams symmetrical about the vertical axis but unsymmetrical about the horizontal axis, subjected to uniform bending moment, H. N. Hill (16) derived the following approximate equation for the elastic buckling stress:

$$f_{cr} = \frac{\pi^2\,E\,I_y}{S_c\,(K\,L)^2}\left[\,e + \sqrt{e^2 + \frac{C_w}{I_y}\left(1 + \frac{G\,J\,(K\,L)^2}{\pi^2\,E\,C_w}\right)}\,\right] \quad \ldots (11)$$

Eq. 11 is the same as Eq. 1 for this case, except that the quantity k is approximated by the distance from the shear center to the centroid, e.

G. Winter (9) derived the following approximate equation for the same case:

$$f_{cr} = \frac{\pi^2\,E\,d}{2\,S_c\,(K\,L)^2}\left[\,I_c - I_t + \sqrt{I_y^2 + \frac{4\,G\,I_y\,J\,(K\,L)^2}{\pi^2\,E\,d^2}}\,\right] \quad \ldots . (12)$$

Eq. 12 can be derived from Eq. 1 by replacing the quantity k by the expression $d(I_c - I_t)/(2\,I_y)$ and noting that $C_w = d^2\,I_c\,I_t/I_y$ for an unsymmetrical I-section. The foregoing equation has been further simplified in the proposal for the new British specifications (8) to the following pair of equations:

$$\left.\begin{aligned} &\text{Wide Flange in Compression:} && f_{cr} = \frac{381{,}000{,}000}{(L/r_y)^2}\left[\frac{I_c - I_t}{2\,I_y} + \sqrt{1 + \frac{1}{20}\left(\frac{L\,t}{r_y\,d}\right)^2}\,\right] \\ &\text{Wide Flange in Tension:} && f_{cr} = \frac{381{,}000{,}000}{(L/r_y)^2}\left(\frac{y_c}{y_t}\right)\left[\frac{I_c - I_t}{I_y} + \sqrt{1 + \frac{1}{20}\left(\frac{L\,t}{r_y\,d}\right)^2}\,\right] \end{aligned}\right\} \quad \ldots (13)$$

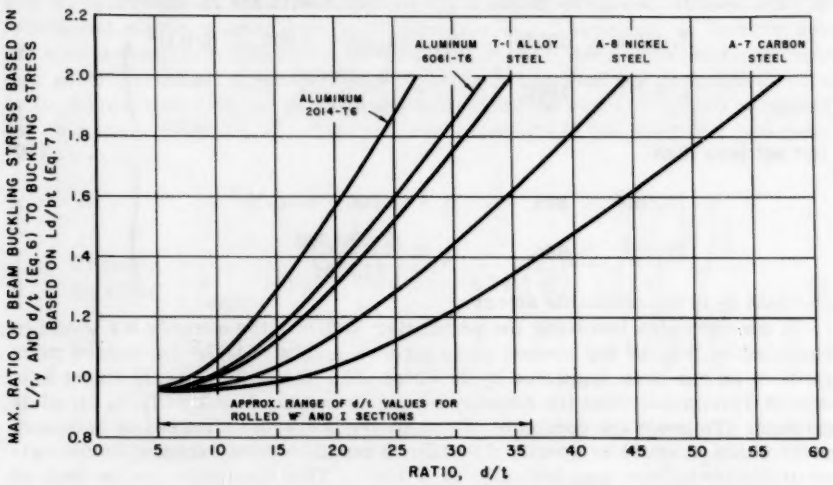
MAX. RATIO OF BEAM BUCKLING STRESS BASED ON L/r_y AND d/t (Eq.6) TO BUCKLING STRESS BASED ON Ld/bt (Eq.7)
ALUMINUM 6061-T6
T-1 ALLOY STEEL
A-8 NICKEL STEEL
A-7 CARBON STEEL
ALUMINUM 2014-T6
APPROX. RANGE OF d/t VALUES FOR ROLLED W AND I SECTIONS
RATIO, d/t

FIG. 3.—COMPARISON OF Ld/bt BEAM FORMULA WITH FORMULA BASED ON L/r_y AND d/t

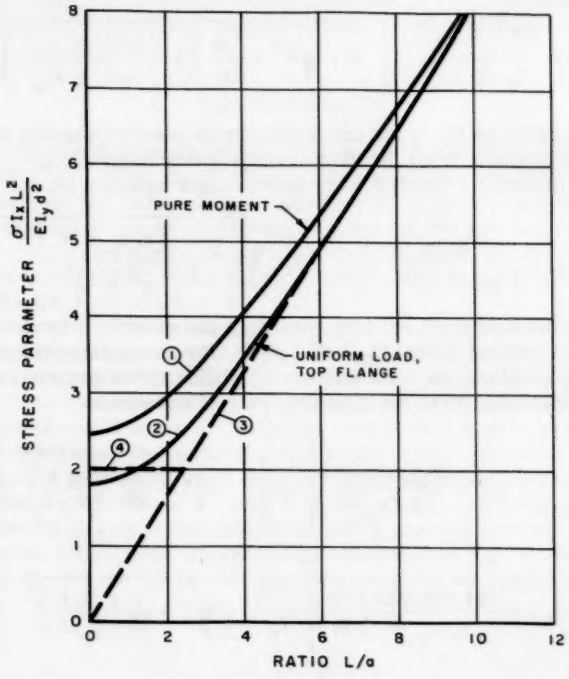

FIG. 4.—CRITICAL STRESS CURVES FOR I-BEAMS SUPPORTED AT THE ENDS

in which y_c and y_t are the distances from the centroid of the cross section to the centroid of the compression and tension flanges, respectively.

A different approach to the design of unsymmetrical sections has been suggested by de Vries (38), who recommended that the formulas involving the parameter L d/b t be used, with the quantity b t modified as follows:

$$\text{For Riveted Plate Girders:} \quad b\,t = \frac{10}{3}\left(\frac{2\,I_c}{b_c^2} + \frac{I_t}{b_t^2}\right) \qquad \text{For Welded Plate Girders:} \quad b\,t = 4\left(\frac{2\,I_c}{b_c^2} + \frac{I_t}{b_t^2}\right) \qquad \ldots\ldots\ldots (14)$$

Calculations of elastic buckling stress, using the foregoing formulas, have been made for two basic girder sections, considering several different sets of flange proportions for each girder. These basic cross sections are the same as those used in the recent study by Kerensky, Flint, and Brown (8). However, the values of length used in the present computations are somewhat different from those used in the British study. Two different length values were assumed for each girder. For one set of computations, the two flanges were assumed to be the same thickness but different widths. In another set of computations, the two flanges were assumed to be the same width but different thicknesses. The results of these calculations are shown in Figs. 5 to 8.[5]

A horizontal line is drawn on Figs. 5 to 8 at a stress of 33,000 psi. If the material is considered to be structural carbon steel, critical stresses above the level of 33,000 psi are not of practical interest. Higher values may be of interest, however, for high-strength steels or sluminum. On the charts that apply to the girders having flanges of equal widths but different thicknesses, a vertical line is drawn at a value of the ratio $A_c/(A_t + A_c)$ corresponding to a width-to-thickness ratio of 16 for the outstanding compression flange. Girders with values of $A_c/(A_t + A_c)$ less than the values corresponding to these vertical lines would not be permitted by AISC specifications (31).

Although the comparisons made in Figs. 5 to 8 are limited to specific cross sections and lengths, a fairly wide range of proportions is covered. It should be noted that all the formulas that are compared in Figs. 5 to 8 are intended to apply to a beam subjected to uniform bending moment, with the exception of Eqs. 7 and 14. The constant 20,000,000 used in Eq. 7 was recommended by de Vries for beams uniformly loaded on the top flange (30). However, several discussers of de Vries' paper showed that theoretical considerations of the uniform bending case led to a formula with a coefficient in the vicinity of 19 to 20,000,000.

A somewhat higher value of C_7 for uniform bending can be derived as follows. De Vries recommended a value of 24,000,000 for beams subjected to uniform transverse load at the centroid. The theoretical critical stress in this case is 13% greater than for the case of uniform bending, as shown by the coefficients in Table 1. Therefore, a reasonable value of the constant for uniform bending might be 24,000,000/1.13 = 21,200,000. If this value had been used, the curves in Figs. 5 to 8 for Eqs. 7 and 14 would have been about 6% higher.

Kerensky, Flint, and Brown (8) compared critical stresses computed from Eq. 6 with the "exact" solution for some built-up sections incorporating angles

[5] E was assumed to be 29,4000,000 psi and Poisson's ratio 0.25.

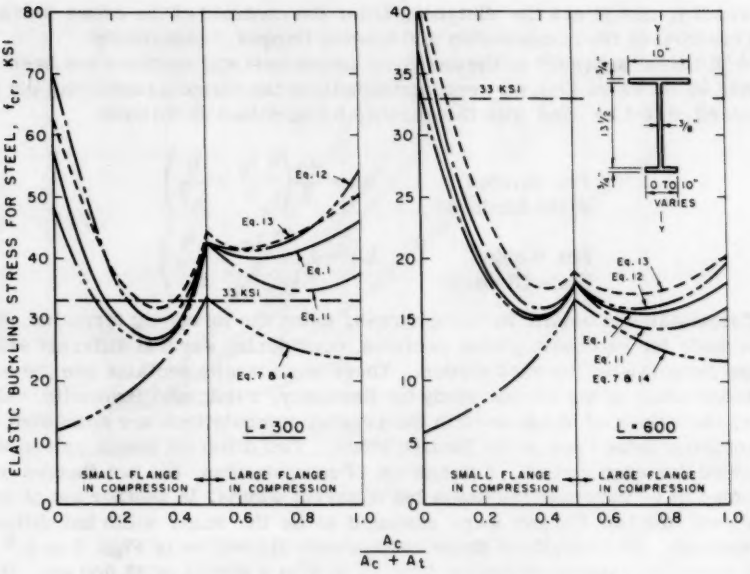

NOTES: A_c = A OF COMPRESSION FLANGE, A_t = A OF TENSION FLANGE

FIG. 5.—LATERAL BUCKLING OF UNSYMMETRICAL "I" SECTIONS

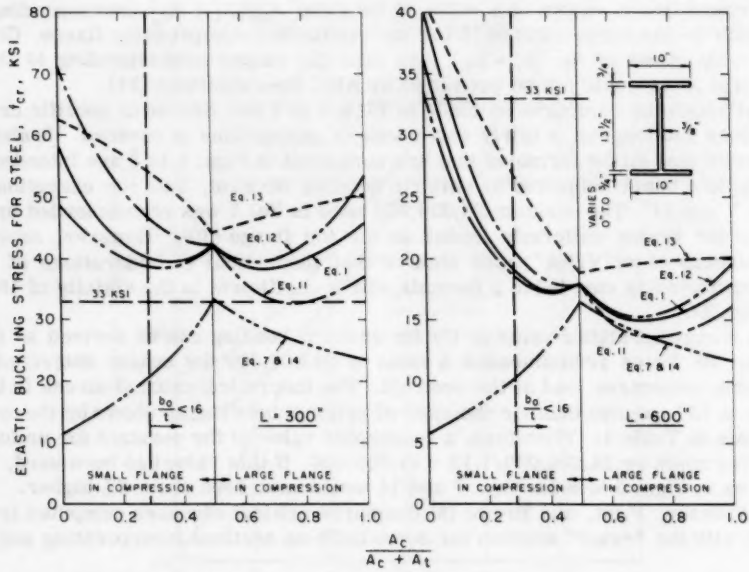

NOTES: A_c = A OF COMPRESSION FLANGE, A_t = A OF TENSION FLANGE

FIG. 6.—LATERAL BUCKLING OF UNSYMMETRICAL "I" SECTIONS

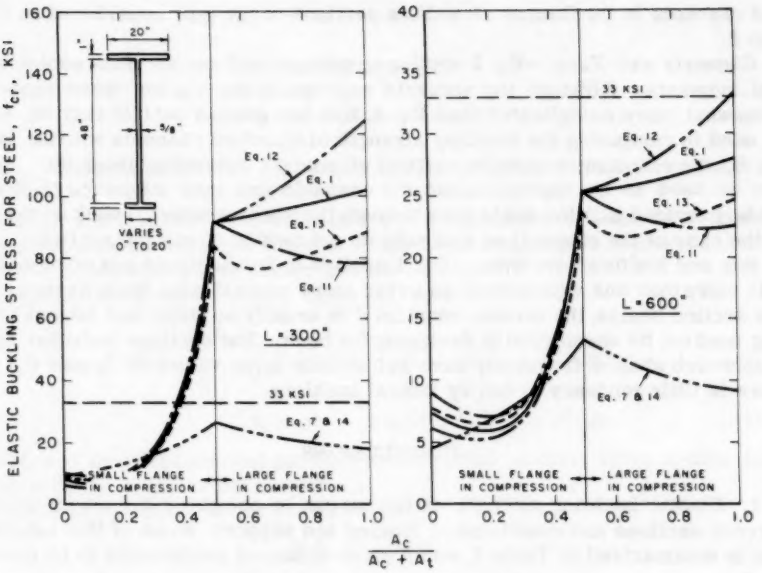

NOTES: A_c = A OF COMPRESSION FLANGE, A_t = A OF TENSION FLANGE

FIG. 7.—LATERAL BUCKLING OF UNSYMMETRICAL "I" SECTIONS

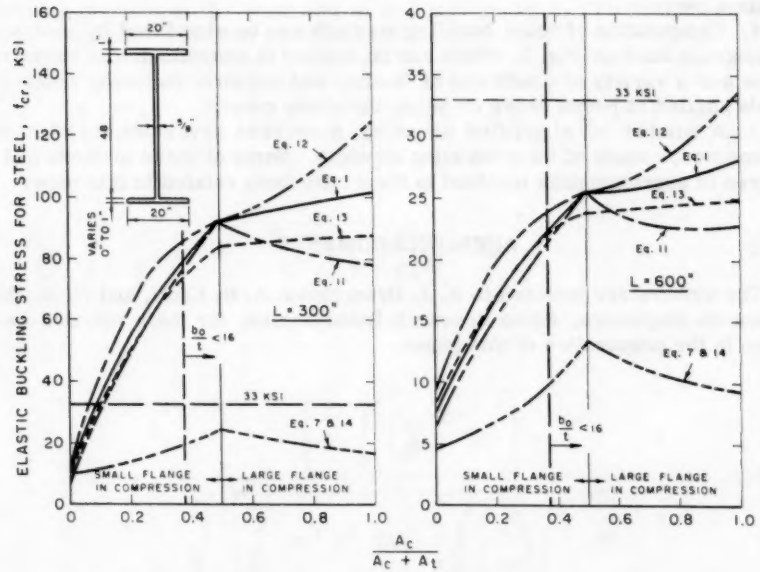

NOTES: A_c = A OF COMPRESSION FLANGE, A_t = A OF TENSION FLANGE

FIG. 8.—LATERAL BUCKLING OF UNSYMMETRICAL "I" SECTIONS

and channels in the flanges as well as sections of the type considered in Figs. 5 to 8.

Channels and Zees.—Eq. 2 applies to channel and zee sections subjected to end moments. Although the accurate expression for C_w for these shapes is somewhat more complicated than Eq. 4, Hill has pointed out (15) that Eq. 4 can be used in computing the buckling strength of standard channels with the aid of Eq. 5, the resulting errors in critical stress not exceeding about 6%. Eq. 2 can be used as an approximation for channels and zees subjected to lateral loads, provided that the loads pass through the shear center (in back of the web in the case of the channel) so that they do not tend to rotate the section.

Box and Multiweb Sections.—Eq. 1 applies to box sections and other shapes with more than one web as well as to the more conventional beam shapes. For box section beams, the torsion constant J is usually so large that lateral buckling need not be considered in designing the beam. Hat sections and other open, double-web shapes frequently have sufficiently large values of I_y and C_w that there is little tendency to fail by lateral buckling.

CONCLUSIONS

1. Elastic buckling strength of beams can be computed for a wide variety of cross sections and conditions of loading and support. Some of this information is summarized in Table 1, which gives values of coefficients to be used in Eq. 1.
2. Elastic buckling theory has been verified by a number of experimental investigations on aluminum and steel beams.
3. Inelastic buckling strength can be predicted from the elastic buckling strength with the aid of a relationship determined from beam tests or from a column curve.
4. Computation of beam buckling strength can be simplified by means of a nomograph such as Fig. 2, which can be applied to unsymmetrical cross sections and a variety of conditions of loading and support, including transverse loads applied at points above or below the shear center.
5. A number of simplified formulas have been developed for designing beams on the basis of their buckling strength. Some of these methods and the degree of approximation involved in them have been related in this paper.

ACKNOWLEDGMENTS

The writers are indebted to R. J. Brungraber, A. H. Knoll, and W. A. Dunn, Research Engineers, Alcoa Research Laboratories, for their valuable assistance in the preparation of this paper.

APPENDIX I

GENERAL EQUATION FOR LATERAL BUCKLING STRENGTH OF BEAMS

Consider a prismatic beam bent about a principal axis. If transverse loads are applied, assume that their lines of action lie in a plane that contains a principal axis through the shear center and the centroid.

The potential energy of such a beam (11) as it buckles is

$$V = \frac{1}{2}\int_0^L \left[E I_y u''^2 + E C_w \beta''^2 + G J \beta'^2 + 2 M \beta u'' + 2 k M \beta'^2 + p g \beta^2 \right] dz \quad \ldots\ldots (15)$$

in which u is the displacement parallel to the initial position of the x-axis and β is the rotation of the cross section

Equilibrium considerations require that

$$E I_y u'' = M \beta. \quad \ldots\ldots (16)$$

The load p can be expressed in terms of the moment,

$$p = -M'' \quad \ldots\ldots (17)$$

Use Eqs. 16 and 17 to eliminate u" and p in Eq. 15. Also, make the following substitutions: $Z = z/L$ and $M = \overline{M}m$, in which $\overline{M}$ is the maximum value of the bending moment in the beam and m is a function of Z. To determine the buckling load, set V = 0. Eq. 1 becomes:

$$\frac{\overline{M}^2}{E I_y}\int_0^1 m^2 \beta^2 \, dZ - \frac{\overline{M}}{L^2}\left[g\int_0^1 \frac{d^2m}{dZ^2}\beta^2 \, dZ + 2k\int_0^1 m\left(\frac{d\beta}{dZ}\right)^2 dZ \right]$$

$$- \frac{G J}{L^2}\int_0^1 \left(\frac{d\beta}{dZ}\right)^2 dZ - \frac{E C_w}{L^4}\int_0^1 \left(\frac{d^2\beta}{dZ^2}\right)^2 dZ = 0 \quad \ldots\ldots (18)$$

Letting

$$C_1 = \frac{\left[\int_0^1 \left(\frac{d\beta}{dZ}\right)^2 dZ\right]}{\sqrt{\left[\int_0^1 m^2 \beta^2 \, dZ\right]\left[\int_0^1 \left(\frac{d^2\beta}{dZ^2}\right)^2 dZ\right]}} \quad \ldots (19a)$$

$$C_2 = -\frac{1}{2} \frac{\left[\int_0^1 \frac{d^2m}{dZ^2} \beta^2 \, dZ\right]}{\sqrt{\left[\int_0^1 m^2 \beta^2 \, dZ\right]\left[\int_0^1 \left(\frac{d^2\beta}{dZ^2}\right)^2 \, dZ\right]}} \quad \ldots\ldots (19b)$$

$$C_3 = \frac{\left[\int_0^1 m\left(\frac{d\beta}{dZ}\right)^2 \, dZ\right]}{\sqrt{\left[\int_0^1 m^2 \beta^2 \, dZ\right]\left[\int_0^1 \left(\frac{d^2\beta}{dZ^2}\right)^2 \, dZ\right]}} \quad \ldots\ldots (19c)$$

and,

$$K^2 = \pi^2 \frac{\left[\int_0^1 \left(\frac{d\beta}{dZ}\right)^2 \, dZ\right]}{\left[\int_0^1 \left(\frac{d^2\beta}{dZ^2}\right)^2 \, dZ\right]} \quad \ldots\ldots\ldots\ldots (19d)$$

and solving Eq. 18 for $\overline{M}$, one obtains the equation

$$\overline{M} = C_1 \frac{\pi^2 E I_y}{(K L)^2} \left[C_2 g + C_3 k + \sqrt{\left(C_2 g + C_3 k\right)^2 + \frac{C_w}{I_y}\left(1 + \frac{G J (K L)^2}{\pi^2 E C_w}\right)}\right] \quad \ldots (20)$$

The values of C_1, C_2, C_3, and K depend on β and the moment function m. The function that describes β depends on the boundary conditions and on m, but is usually not affected greatly by the beam cross section and length. Hence, the coefficients C_1, C_2, C_3, and K depend on the boundary conditions and on the loading, but are relatively independent of the proportions of the beam. This is demonstrated by the fact that numerical solutions for the buckling strength of beams under a variety of loading conditions can be expressed in the form of Eq. 20, in which values of the coefficients depend only on the conditions of loading and support (Table 1).

APPENDIX II.--BIBLIOGRAPHY

1. Timoshenko, S., Theory of Elastic Stability, McGraw-Hill Book Company, Inc., New York (1936).
2. Goodier, J. N., Flexural-Torsional Buckling of Bars of Open Section, Bulletin No. 28, Cornell University Engineering Experiment Station (1942).
3. Nylander, H., Torsion, Bending and Lateral Buckling of I-Beams, Bulletin No. 22, Division of Building Statics and Structural Engineering, Royal Institute of Technology, Stockholm, Sweden (1956).
4. Salvadori, M. G., "Lateral Buckling of Eccentrically Loaded I-Columns," Transactions of the ASCE, Vol. 121 (1956), p. 1163.
5. Austin, W. J., Yegian, S., and Tung, T. P., "Lateral Buckling of Elastically End-Restrained I-Beams," Separate No. 673, Proceedings of the ASCE, Vol. 81 (1955).
6. Pettersson, O., Combined Bending and Torsion of I-Beams of Monosymmetrical Cross Section, Bulletin No. 10, Division of Building Statics and Structural Engineering, Royal Institute of Technology, Stockholm, Sweden, (1952).
7. Poley, S., "Lateral Buckling of Cantilevered I-Beams Under Uniform Load," Transactions of the ASCE, Vol. 121 (1956), p. 786.
8. Kerensky, O. A., Flint, A. R., and Brown, W. C., "The Basis for Design of Beams and Plate Girders in the Revised British Standard 153," Proceedings of the Institution of Civil Engineers, Part III, Vol. 5, (1956) p. 396.
9. Winter, G., "Lateral Stability of Unsymmetrical I-Beams and Trusses in Bending," Transactions of the ASCE, Vol. 108 (1943), p. 247.
10. Schrader, R. K., Discussion of paper by G. Winter, Transactions of the ASCE, Vol. 108 (1943), p. 261.
11. Masur, E. F., and Milbradt, K. P., "Collapse Strength of Redundant Beams After Lateral Buckling," Journal of Applied Mechanics, ASME, June, 1957, p. 283.
12. Dumont, C., and Hill, H. N., Lateral Stability of Equal Flanged Aluminum Alloy I-Beams Subjected to Pure Bending, Technical Note 770, NACA (1940).
13. Clark, J. W. and Jombock, J. R., "Lateral Buckling of I-Beams Subjected to Unequal End Moments," Paper No. 1291, Journal of the Engineering Mechanics Division, Proceedings of the ASCE, Vol. 83, July, 1957.
14. Flint, A. R., "The Stability and Strength of Slender Beams," Engineering, Vol. 170 (1950), p. 545.

15. Hill, H. N., "Lateral Buckling of Channels and Z-Beams," Transactions of the ASCE, Vol. 119, (1954), p. 829.

16. Hill, H. N., "Lateral Stability of Unsymmetrical I-Beams," Journal of the Aeronautical Sciences, Vol. 9 (1942), p. 175.

17. Hechtman, R. A., Hattrup, J. S., Styer, E. F., and Tiedemann, J. L., "Lateral Buckling of Rolled Steel Beams," Paper No. 797, Proceedings of the ASCE, Vol. 81 (1955).

18. Bleich, F., Buckling Strength of Metal Structures, McGraw-Hill Book Company, Inc. (1952), p. 165 and p. 55.

19. Austin, W. J., Note on Method of Estimating Stresses at Buckling in Laterally Unsupported Beams, distributed to Research Committee E, Column Research Council, March 18, 1957.

20. McCalley, R. C., Jr., Discussion of paper by H. N. Hill, E. C. Hartmann, and J. W. Clark, Transactions of the ASCE, Vol. 121 (1956), p. 15.

21. Gatewood, B., "Buckling Loads for Beams of Variable Cross Section Under Combined Loads," Journal of the Aeronautical Sciences, Vol. 22 (1955), p. 281.

22. Salvadori, M. G., "Lateral Buckling of I-Beams," Transactions of the ASCE, Vol. 120 (1955), p. 1165.

23. Hill, H. N., Hartmann, E. C., and Clark, J. W., "Design of Aluminum Alloy Beam-Columns," Transactions of the ASCE, Vol. 121, (1956), p. 1.

24. Clark, J. W., and Knoll, A. H., "Effect of Deflection on Lateral Buckling Strength," paper to be presented at Chicago meeting of ASCE, February, 1958.

25. Chang, F. K., and Johnston, B. G., "Torsion of Plate Girders," Transactions of the ASCE, Vol. 118 (1953), p. 337.

26. Nylander, H., "Drehungsvorgänge und gebundene Kippung bei geraden, doppeltsymmetrischen I-Trägern," Proceedings of the Royal Institute for Engineering Research, Stockholm, Sweden, No. 174 (1943).

27. Alcoa Structural Handbook, Aluminum Company of America, Pittsburgh, Pennsylvania (1958).

28. Torsional Stresses in Structural Beams, Booklet S-57, Bethlehem Steel Company, Bethlehem, Pennsylvania, (1950).

29. German Specifications DIN 4114 (1952).

30. de Vries, K., "Strength of Beams as Determined by Lateral Buckling," Transactions of the ASCE, Vol. 112 (1947), p. 1245.

31. Specification for the Design, Fabrication, and Erection of Structural Steel for Buildings, AISC, June, 1949.

32. Priest, H. M., and Gilligan, J. A., Design Manual for High-Strength Steels, U. S. Steel Corporation, (1954).

33. Standard Specifications for Highway Bridges, AASHO, (1953).

34. Specifications for Steel Railway Bridges, AREA, (1953).

35. Specification for the Design of Light-Gage Cold-Formed Steel Structural Members, AISI, (1956).

36. Austin, W. J., Comments on Lateral Buckling Formulas, Notes distributed to Research Committee E, Column Research Council, May 24, 1956.

37. de Vries, K., Letter to W. J. Austin, Chairman, Research Committee E, November 9, 1956.

38. de Vries, K., "Discussion of Lateral Torsional Strength," The Philosophy of Column Design, Column Research Council, (1954), p. 37.

39. Johnston, B. G., Letter to Research Committees A and E, Column Research Council, October 14, 1957.

40. Clark, J. W., and Hill, H. N., Lateral Buckling of Beams and Girders, Commentary for Research Committee E, Column Research Council, November 17, 1957.

41. Lee, L. H. N., "On the Lateral Buckling of a Tapered Narrow Rectangular Beam," ASME Journal of Applied Mechanics, September, 1959, p. 457.

42. Krefeld, W. J., Butler, D. J., and Anderson, G. B., "Welding Cantilever Wedge Beams," The Welding Journal Research Supplement, March, 1959, p. 97-s.

43. Dumont, C., and Hill, H. N., The Lateral Stability of Deep Rectangular Beams, Technical Note 601, NACA, (1937).

APPENDIX III.--NOTATION

The symbols used in this paper are defined as follows:

a = $\sqrt{E\,C_w/G\,J}$

b = flange width of symmetrical I-section or channel

b_c = width of compression flange

b_o = width of outstanding portion of compression flange

b_t = width of tension flange

$C_1, \ldots . C_7$ = coefficients

C_w = torsion warping constant

d = distance between centroids of beam flanges (taken as depth of beam in approximate formulas)

e = distance from shear center to centroid (positive if shear center lies between centroid and compression flange, negative otherwise)

E = modulus of elasticity

E_t = tangent modulus

f_{cr} = critical stress for lateral buckling

f_b = allowable stress

f_y = compressive yield strength

g = distance from shear center to point of application of transverse load (positive when load is below shear center; otherwise negative)

G = modulus of rigidity

I_c = moment of inertia of compression flange about axis parallel to web

I_t = moment of inertia of tension flange about axis parallel to web

I_x = moment of inertia of beam cross section about x-axis

I_y = moment of inertia of beam cross section about y-axis

$I_{\bar{x}}$ = major moment of inertia (when different from I_x)

$I_{\bar{y}}$ = minor moment of inertia (when different from I_y)

J = torsion constant

$k = e + \frac{1}{2 I_x} \int_A y (x^2 + y^2)\, dA$

K = coefficient

L = distance between points of support against lateral bending and twisting

$m = M/\overline{M}$

M = bending moment at any point in a beam

$\overline{M}$ = maximum value of M for a given beam

p = transverse load on a unit length of beam

r_y = radius of gyration of beam cross section about y-axis

S_c = section modulus for stress in compression flange

t = thickness of compression flange

u = displacement parallel to initial position of x-axis

V = potential energy (increase in strain energy during buckling minus work done by external forces)

x = coordinate through centroid normal to axis of beam and normal to plane of bending

y = coordinate through centroid normal to axis of beam and parallel to plane of bending, positive downward

y_c = distance from centroid of cross section to centroid of compression flange

y_t = distance from centroid of cross section to centroid of tension flange

z = coordinate along centroidal axis of beam

$Z = z/L$

β = rotation of cross section

Journal of the
STRUCTURAL DIVISION
Proceedings of the American Society of Civil Engineers

DISCUSSION

WIND FORCES ON STRUCTURES: NATURE OF THE WIND[a]

Closure by Robert H. Sherlock

ROBERT H. SHERLOCK,[1] F. ASCE.—Appreciation is expressed to those who have presented discussions of this paper. Several of the discussions have dealt with the variation of wind velocity with height in coastal areas during hurricanes, a subject on which adequately controlled observations are indeed meagre and where code recommendations must, therefore, be based on inferences drawn from what little is available. As a result of these discussions, it has become clear that separate tables must be presented for design velocities in coastal and inland areas. The one-seventh-power approximation to the variation of wind velocity with height at inland stations has been retained, as was done in Table 1 for basic velocities (fastest mile of wind at 30 ft level) up to 75 mph, but the assumption, based on a paper by Mr. Bunting (6), that the variation of wind velocity with height could be neglected in mature hurricanes, has been discarded. Curves J, K, L, and Q in Fig. 2A (which was entitled Fig. 3) must, therefore, be discarded, as must the design velocities in Table 1 for basic winds above 75 mph. The reasons for this drastic change will appear subsequently.

Another drastic change is that Fig. 1 has been superseded by two maps, Figs. 5 and 6, which first appeared in July, 1959 in a manuscript of the United States Weather Bureau (USWB), and have since been published in Proceedings, ASCE, in April 1960 (9).[2] They were prepared in the Office of Climatology of the USWB under the direction of H. C. S. Thom. The maps show contour lines, each of which gives the fastest mile of wind at 30 ft above the ground at the points through which the contour line passes. The contour lines were based upon an average of about 15 yr of USWB records at each of 141 airport stations throughout the United States. By means of statistical analysis the records were extrapolated to velocities having a 50-yr probable period of recurrence in Fig. 5 and a 100-yr probable period in Fig. 6. It should be noted that

Note.—This paper is a part of the copyrighted Journal of the Structural Division, Proceedings of the American Society of Civil Engineers, Vol. 86, No. ST 7, March, 1960.

[a] July, 1958, by Robert H. Sherlock.

[1] Prof. of Civ. Engrg., Univ. of Mich., Ann Arbor, Mich.

[2] Numerals in parentheses, thus (1), refer to corresponding items in the Bibliography.

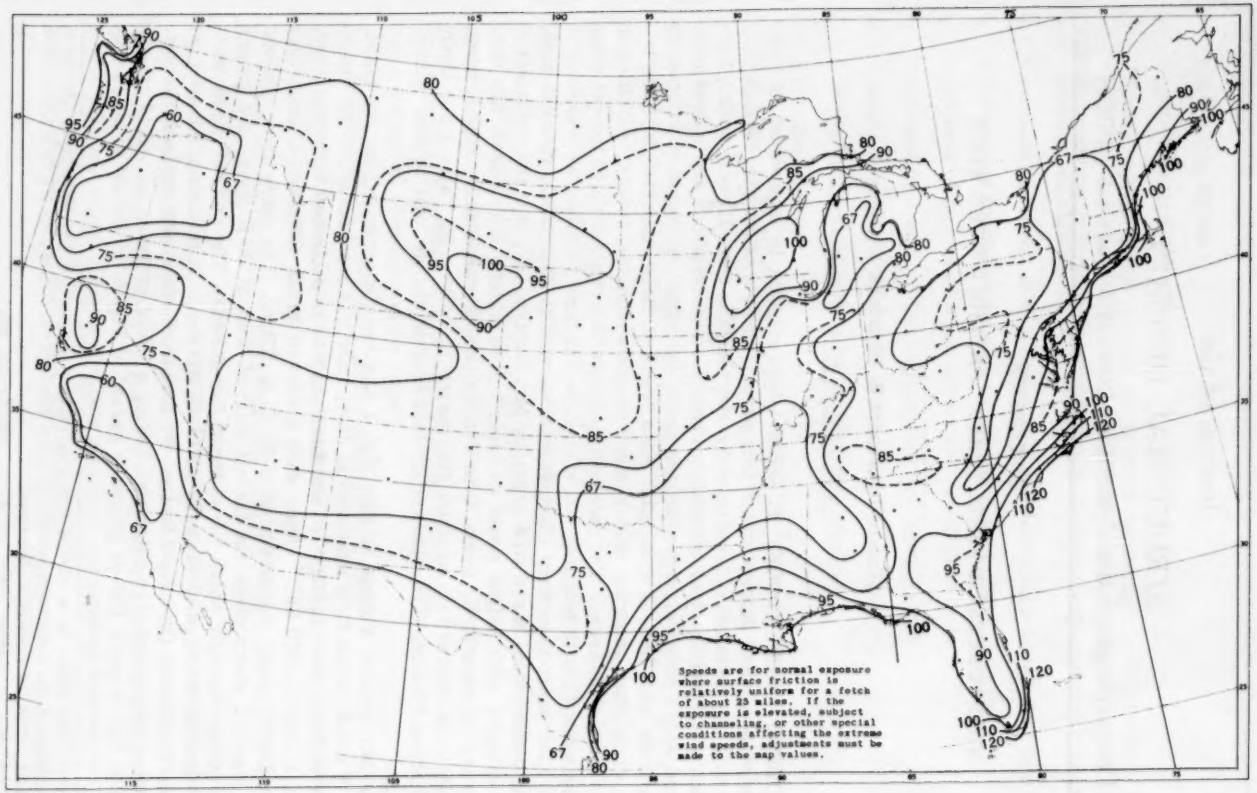
Speeds are for normal exposure where surface friction is relatively uniform for a fetch of about 25 miles. If the exposure is elevated, subject to channeling, or other special conditions affecting the extreme wind speeds, adjustments must be made to the map values.

FIG. 5.—MAP OF U. S. A. SHOWING EXTREME BASIC WINDS WITH 50-YR PERIOD OF RECURRENCE.

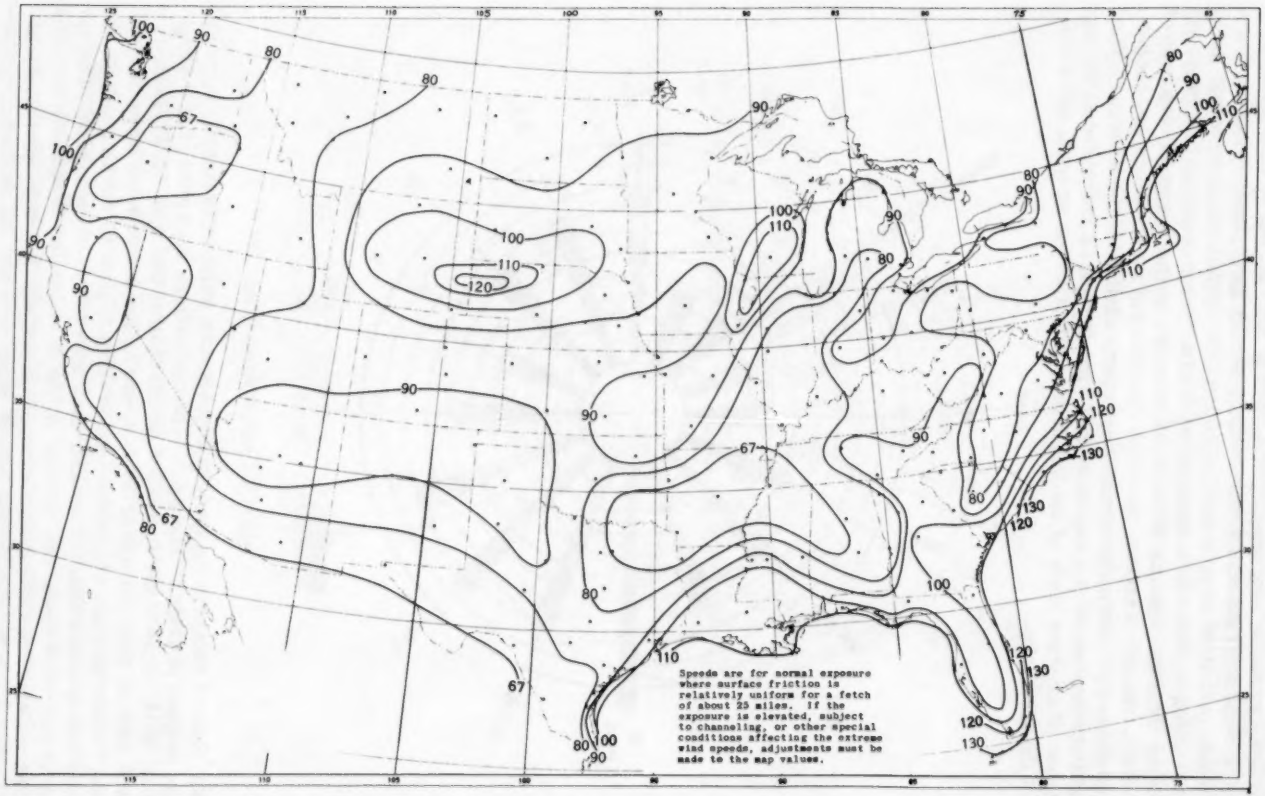
Speeds are for normal exposure where surface friction is relatively uniform for a fetch of about 25 miles. If the exposure is elevated, subject to channeling, or other special conditions affecting the extreme wind speeds, adjustments must be made to the map values.

FIG. 6.—MAP OF U. S. A. SHOWING EXTREME BASIC WINDS WITH 100-YR PERIOD OF RECURRENCE.

these are "probable" values and that, over a long period of time there may occur a 50 yr interval which may include two or more basic winds having a "probable period of recurrence" of 100 yr. Nevertheless, this method gives the designing engineer a "conservative" and a "more conservative" basis for choosing the wind velocity which is appropriate in the design of each type of structure, taking into account the wind-sensitivity of the structure, and the hazard to life and property which would accompany a failure of the structure. Wind sensitivity depends on the importance of wind loading as compared to the importance of all other kinds of loading in their effect on the strength and stability of the structure.

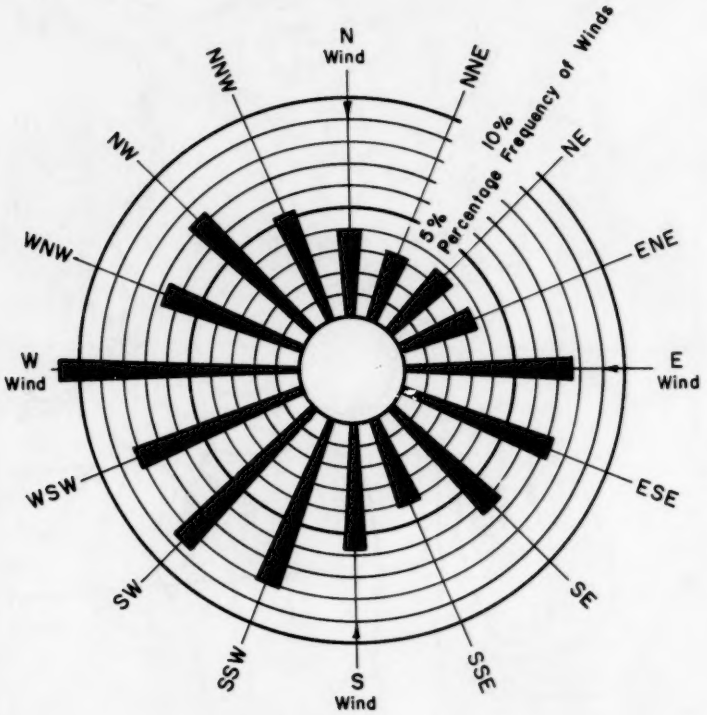

FIG. 7.—SIMPLE WIND ROSE

Mr. Gilbert refers to the typographical errors which unfortunately occurred in the original printing of this paper. The corrections were printed in the September, 1958, issue of the Journal of the Structural Division, pp. 1787-71.

Mr. Gilbert asks the writer to comment on the design usefulness of "wind roses," since they are sometimes available to engineers working outside the United States where detailed weather data are not readily available. The answer is that wind roses may or may not be useful to the design engineer who wishes to select the fastest-mile of wind, or the fastest-1-min velocity, for use in his design. It depends on the type of wind rose and the amount of supplementary information available to him.

Fig. 7 is a very simple wind rose given in the form of a bar diagram and indicating the percentage of time when the wind has blown from the different points of the compass in some previous sample of wind history. For example, this diagram indicates that, for the 5-yr sample shown, the winds at Grand Rapids blew from the southwest for about 8.6% of all the hours. Wind velocities are not given.

Fig. 8 is a type of wind rose in which each of the bars has been sub-divided into the percentage of time when the wind velocity lay between certain limits.

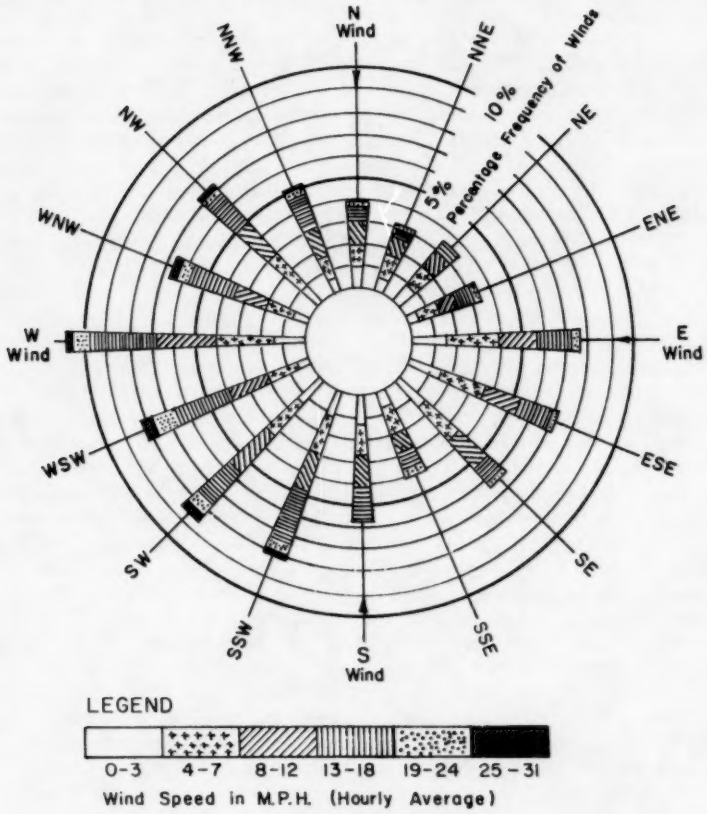

FIG. 8.—MODIFIED WIND ROSE

Usually, the diagram is based on the hourly average as obtained from the USWB or some local installation of instruments. This wind rose shows that about 0.3% of all winds blew from the southwest with an hourly average velocity between 25 mph and 31 mph. This is of little use to the designer unless he is able to convert the maximum hourly average wind velocity into a distribution from which he can obtain the fastest-mile of wind or some other subdivision which he needs. For this purpose he may approximate the answer by using published information from other locations which gives the distribution of the average wind velocity for shorter periods of time within the recorded longer period (10).

The writer has assumed that Mr. Gilbert's question referred to the simpler forms of the many types of wind roses which are available. A type which involves more complicated statistical concepts and which was developed for use in planning aircraft flights is described by H. L. Crutcher (11).

Mr. Scruton would like to see the subject of the maximum gust period, which is significant in various design problems, developed in more detail. Mr. Davenport raises the same question in regard to bluff or sharp edged structures. Unfortunately, the writer knows of no progress which has been made in this subject beyond that quoted in a previous paper (12) under the heading "Minimum Effective Gusts."

Mr. Perrin points out several problems, in connection with the choice of wind velocities and gust factors for the design of a guyed tower, in which the judgement of the engineer may supplement or modify the specified Code or Manual. The writer has limited his presentation to material of widespread usefulness in structural design on the assumption that the more highly specialized structural problems will receive the attention of engineers with specialized competence to make or direct such modifications. He has had to face the problem of limitation, since the number of special problems is very great. An example of such a special problem is the selection of appropriate wind velocities to be used for the design of the bowl, supporting structures, and machinery of a large radio telescope.

Mr. Feld presents a list of eighteen severe storms which have previously been reported in the appropriate literature and for which he has reduced the recorded wind velocities so as to allow for instrumental errors. This is important since the long-time records of wind velocity reported by the USWB are not all based on the use of the same design of instruments, or the same methods of reporting. He has so indicated in a later paragraph of his discussion. This list may prove valuable to those who feel that a particular structure deserves a closer study of probable basic wind velocities than can be obtained from Figs. 5 or 6. He also cites the failure of radio towers in which subsequent stress analysis failed to check recorded wind velocities. He mentions the possibility that the higher kinetic energy of a driving rain may have been responsible. This question has been under study in recent years but the writer feels that the results are not yet ready for inclusion in recommendations by the Committee on Wind Forces. The writer knows of a case where subsequent stress analysis has shown that the failure to include the "moving load" effect in the design, as in Fig. 4, was sufficient to account for the failure of a guyed tower.

The writer is indeed grateful to Mr. Davenport for his extended discussion, especially in regard to the effect of surface roughness on the variation of wind velocity with height. His remarks contrasting surface roughness with the stability of the atmosphere as the controlling factor in the variation of wind velocity with height are pertinent to the later discussion of the Brookhaven records in this closure. This is not because the degree of surface roughness on Long Island stands alone in determining the variation of wind velocity with height, because these records illustrate the stage where the transition from conditions of roughness over water to those over land is a major influence.

It is not practicable to separate the influences of surface roughness and atmospheric stability in the usual cases, since both influences are so variable. For example, even in a uniformly wooded area the coefficient of roughness will decrease with increasing wind velocity, due to the streamlining of the leaves in summer and the twigs in winter as they bend in the wind. Nevertheless, it may be useful to discuss, briefly, the question of atmospheric stability and surface roughness as influences in the variation of wind velocity with height.

The widely accepted exponential relation is given by

$$\bar{u}(Z) = \bar{u}_1 \left[\frac{Z}{Z_1}\right]^x \quad \ldots\ldots\ldots\ldots\ldots\ldots (1)$$

where $\bar{u}(Z)$ is the average velocity at height Z and $\bar{u}_1$ denotes the average velocity at height Z_1. Sutton (13) gives the equation in the form

$$\bar{u}(Z) = \bar{u}_1 \left[\frac{Z}{Z_1}\right]^{n/2-n} \quad \ldots\ldots\ldots\ldots\ldots\ldots (2)$$

where n is a parameter which varies with the conditions of stability. Sutton states that, "No reliable values are yet available for large lapse rates and large

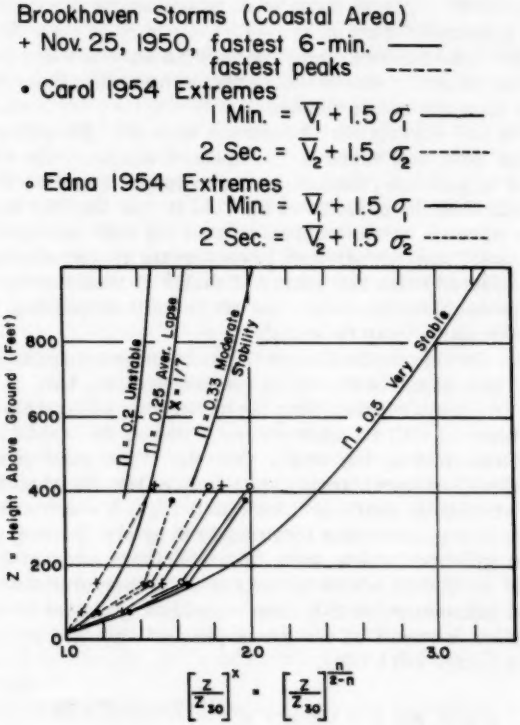

FIG. 9.—VERTICAL WIND PROFILE VS. STABILITY

inversions." Hewson (14) states that n "has the value of 1/4 under average conditions of lapse rate, with a range from 1/2 for a large inversion to 1/5 for a large lapse."

The curves showing the variation of wind velocity with height for each of these three values of n are shown in Fig. 9. The data for the three Brookhaven storms (15) are also shown and it will be seen that they lie to the right of the line which indicates average lapse rate (n = 0.25), that is, they lie in the area

of moderate stability, where a relatively rapid increase of velocity with height may be expected because of the small amount of vertical interchange present under conditions of moderate stability.

The vertical temperature gradients are available (15) for the two hurricanes Carol and Edna (1954), but not for the violent extra-tropical storm of November 25, 1950. The temperature gradients which are reported for Carol and Edna are not inconsistent with the rapid variation of wind velocity with height shown in Fig. 9.

It will be shown subsequently that as the wind passes from the water area to the land area it must undergo a transition from a vertical profile that is compatible with the surface drag over the water to one that is compatible with the surface drag over land. This is quite different however, from a situation where a rapid variation of velocity with height might be attributed solely to a constant condition of surface roughness. Consequently, the explanations of the rapid increase of velocity with height must be sought in some combination of surface roughness and atmospheric stability.

It may be that some future Committee on Wind Forces will see fit to include additional tables based on several different conditions of surface roughness, but at this time it is not recommended.

The writer is not certain that he agrees with Mr. Davenport's statement, given in his item (2), that there is "no marked tendency for violent thermal interchange" in large scale, mature, extra-tropical storms. It is in the zone of transition, following the passage of the cold fronts, that the most violent and prolonged gusts occur in extra-tropical storms and these are caused by thermal interchange between the higher and lower strata of the storms (16). If the statement is restricted to the last stages of maturity where decay is impending; that is, where an occluded situation has set in or is impending, then it is true that thermal interchange may be small.

There is considerable duplication in the discussion concerning the variation of wind velocity with height in hurricanes, and therefore, this closure will deal with the subject in general rather than the discussion separately. Some exceptions to this procedure will be made where it seems desirable for clarity.

It has been assumed by the writer that the "first gust" of thunderstorms and the "plow winds" of hurricanes, mentioned by Mr. Bunting, have both been included in the statistical analysis upon which Figs. 5 and 6 are based.

The writer does not understand the statement by Mr. Bunting that "the computed maximum gradient winds were obtained from averaging over 10 to 15 minute intervals so that it would be improper to compare observed 1 minute maximum winds with computed 15 minute maximum gradient winds." The gradient wind equation is based on the assumption of steady-state conditions and contains no time factor (27) (28):

$$2\,\omega\,V\,\sin\phi + V^2\,r^{-1} = \frac{\text{Pressure gradient}}{\rho} \quad \ldots\ldots\ldots (3)$$

in which ω is the angular velocity of the earth's rotation, ϕ denotes the latitude, r is the radius of curvature of the wind path, ρ represents air density, and V is the gradient wind.

The Ekman spiral fitted to the storm data taken at Ann Arbor (17) shows that the time required to establish steady state conditions appropriate for the spiral and gradient wind theories lay somewhere between 1 min and 5 min, while the Ekman spiral Curve I of Fig. 2A, fitted to the peaks of the storm of November 25, 1950 at Brookhaven, shows that the required time lay somewhere

between 6 min and the period of the peaks. Of course, these two storms were extra-tropical in character while those quoted by Mr. Bunting were definitely tropical storms.

Mr. Gentry states that in the work quoted by Mr. Bunting the "gradient winds" were really estimated cyclostrophic winds ($v^2 r^{-1}$). It is obvious, from the discussions, that these "gradient winds" cannot be used in the conventional meaning of the term, as was done in Fig. 2A and in Table 1, and, consequently, curves J, K, L, and Q of Fig. 2A must be discarded together with the design velocities above 75 mph in Table 1.

Mr. Feld has also included abstracts from material reported by Smith and Singer (15). It is based on observations made on the 410 ft tower at Brookhaven, L. I., during the severe storm of November 25, 1950, and the two hurricanes of 1954, Carol and Edna. The following comments will draw on the report of Smith and Singer, rather than on the abstracts quoted by Mr. Feld:

The records from the storm of November 25, 1950, were discussed under the heading "Extra-Tropical Cyclones." The velocities were reported as the fastest 6-min means and the fastest peaks at each of the tower stations. The data were plotted as Curves H and I in Fig. 2A and an Ekman spiral was fitted to the peak values and extrapolated to the gradient level. Since these are extreme values they may be used directly by the Committee on Wind Forces. However, the records from the two hurricanes were reported as "Means and Standard Deviations of 1-Min Mean Speeds, 2-Sec Lulls, 2-Sec Peaks," and for the purposes of the Committee on Wind Forces some approximation to extreme values must be made by statistical extrapolation.

Since only the averages and standard deviations are given, it will be assumed that the distribution curves for the data are not skewed and that the symmetrical normal law may be used as an acceptable approximation in choosing extreme values. This assumption is supported by many observations made during storms at Ann Arbor, an example of which is shown in Fig. 10 from the storm of January 19, 1933. Fig. 10(a) shows the variation of skewness with height for the distribution of 1/2 sec average velocities within 5 min intervals, for a total time on 1 hr. The positive skewness at the bottom stations of the tower indicates a preponderance of low velocities with less frequent high velocities, while the negative skewness at the upper stations indicates a preponderance of high velocities with less frequent low velocities. At a height of about 125 ft, the high and low velocities have an equal chance of occurrence, that is, the distribution curve has zero skewness. If it is assumed that an acceptable approximation to extreme values may be obtained by adding 1.5 times the standard deviation to the average ($\bar{u} + 1.5\,\sigma$), Fig. 10(b) shows that at least 93% of all cases will be included regardless of which skewness is used. The data for curves O and P in Fig. 2A, for Carol, 1954, were derived in this way, as were the data in Table 2.

The storm winds observed at Brookhaven are typical of the transition zone which is present where the wind crosses a coast line and blows over a land surface after having blown over an extensive water surface such as the ocean, Long Island Sound or the Great Lakes. The coast lines in this case are irregular and impossible to define exactly. The winds blew from the two quadrants of the compass from the east through the north to the west, and the coast line varied between approximately 6 miles and 20 miles.

Storm winds approaching a coast line have a velocity profile which is compatible with the pressure gradient, the curvature of the wind path, the roughness of the water surface, and other things which affect the air movements.

u = wind velocity, a particular value β = coefficient of skewness

$\bar{u}$ = average wind velocity σ = standard deviation = $\sqrt{\frac{(u-\bar{u})^2}{N}}$

N = number of cases

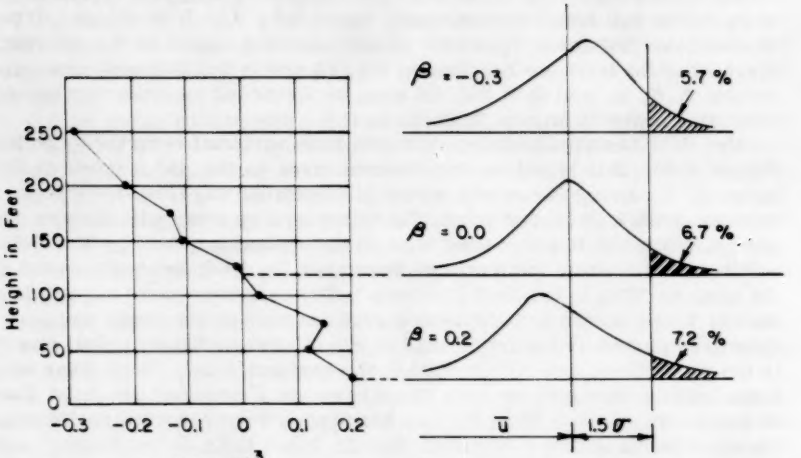

(a) $\beta = \frac{1}{\sigma^3} \frac{\sum(u-\bar{u})^3}{N}$

(b) Distribution of 1/2 sec. average velocities within a 5 minute intervals (average of 12 intervals)

FIG. 10.—STATISTICAL SKEWNESS OF WIND DATA VS. HEIGHT ABOVE GROUND.

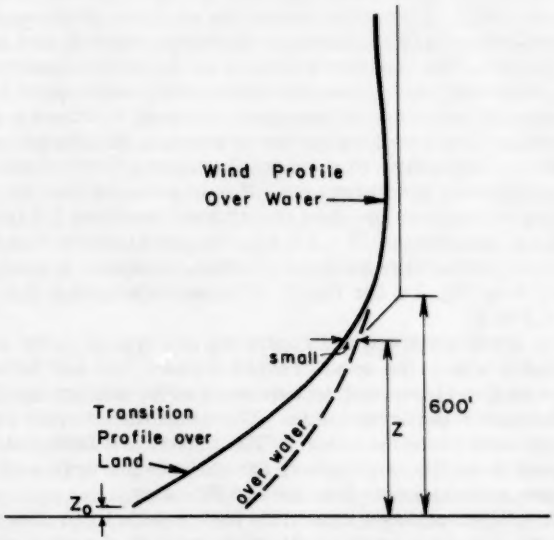

FIG. 11.—RAPID INCREASE OF WIND VELOCITY WITH HEIGHT IN TRANSITION ZONE.

As the wind passes the coast line there are two main influences which are responsible for slowing down its velocity. First, it encounters an increased frictional drag which generates an increase of turbulence and this, in turn, diffuses the drag upwards. Second, the supply of water vapor is no longer available from the ocean and consequently can no longer provide a source of energy wherein water vapor is condensed into cloud droplets with the accompanying release of latent heat. The greater the distance which the wind moves inland from the coast line, the greater will be the height to which the increased turbulence will be effective in modifying the wind profile.

Fig. 11 is a diagrammatic representation of the foregoing idea regarding the role of frictional drag. Brunt (18) gives an approximate equation based on

TABLE 2.—EXTREME VALUES OF WIND VELOCITY (MPH) BASED ON BROOKHAVEN DATA

Height, in Feet (1)	Carol		Edna	
	$\bar{u}_1 + 1.5\ \sigma_1$ (2)[a]	$\bar{u}_2 + 1.5\ \sigma_2$ (3)[b]	$\bar{u}_1 + 1.5\ \sigma_1$ (4)[a]	$\bar{u}_2 + 1.5\ \sigma_2$ (5)[b]
37	43.8	65.8	32.8	47.9
75	57.7	79.3		
150	73.4	92.8	53.8	69.2
355	86.7	104.6		
410			65.7	75.9

[a] Minimum mean speeds. [b] Second peaks.

previous work by G. I. Taylor, for the "height to which turbulence is effective in a time interval t" in the eddy diffusion of heat. It may be used also for the eddy transfer of velocity.

$$Z^2 = 4\,k\,t \quad \ldots\ldots\ldots\ldots\ldots\ldots (4)$$

in which Z is the height (in centimeters) to which turbulence is significantly effective in time interval t (in seconds), K is the eddy diffusivity = 10^5 cm^2 sec^{-1}. If L is the distance inland from the coast line (in centimeters) and $\bar{u}$ is the average wind velocity (cm sec^{-1}) at height Z_o in time t, then

$$Z^2 = 4\,K\left[\frac{L}{\bar{u}}\right] \quad \ldots\ldots\ldots\ldots\ldots\ldots (5)$$

Because of the approximations used in the derivation of Eq. 5, it should be considered as giving only the order of magnitude of Z. The degree of approximation is also affected by the loss of water vapor as a source of energy when the wind moves away from the coast causing the upper winds to decrease more than the amount caused by surface drag. The moderate thermal stability, previously discussed, is also ignored by Eq. 5. The value of K = 10^5, recommended by Brunt, has been successfully used by Hewson (19) for an investigation in which $\bar{u}$ was approximately 30 mph for a period of about 9 hr.

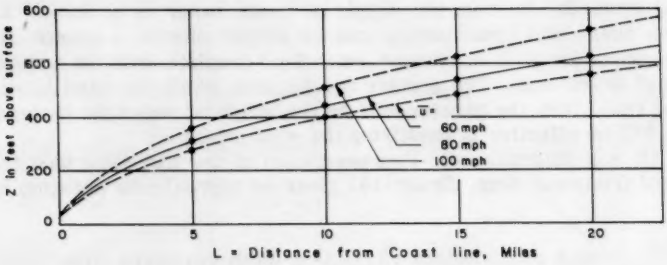

FIG. 12.—HEIGHT TO WHICH TURBULENCE IS EFFECTIVE IN TRANSITION ZONE.

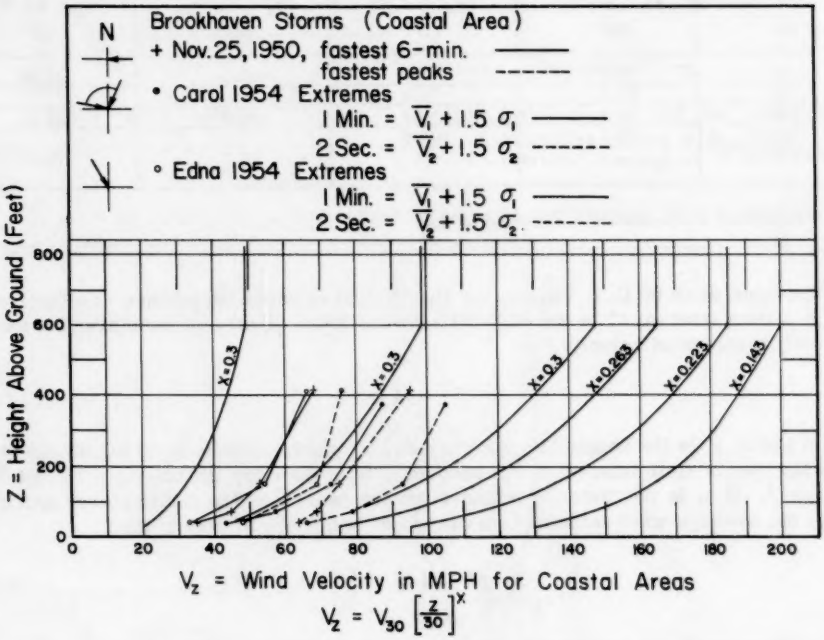

FIG. 13.—WIND VELOCITY VS. HEIGHT IN COASTAL AREAS.

Fig. 12 shows curves fitted to some computed values of Z for different values of L and $\bar{u}$. From a consideration of these curves and the foregoing discussion, it is concluded that in coastal areas, such as Brookhaven, Long Island, the rapid increase of wind velocities with height need not be continued beyond 600 ft, above which a constant velocity may be used.

The Brookhaven data for Carol and Edna, as given in Table 2, are plotted in Fig. 13 together with the curves for the 6-min winds and the peaks of the storm of November 25, 1950. Three 0.3-power curves are shown for comparison. They seem to indicate that the exponent 0.3 gives a conservative estimate of the variation of wind velocity with height during these three Brookhaven storms.

Fig. 5 assigns a basic wind velocity of 75 mph to 90 mph to the Long Island area (fastest mile at 30 ft level, with a 50-yr period of return). This is far greater than the extreme 1-min winds shown in Table 2 for Carol and Edna at the 37 ft level and even exceeds the extreme 2-sec peaks for this level. This indicates that, in this coastal area, even stronger winds must be expected by the structural designer than those observed during Carol and Edna. Two questions arise:

(1) Should the very rapid increase of wind velocity with height ($x = 0.3$), shown by these two hurricanes in their decaying stages and by the one intense extra-tropical storm, be used for future guidance in this coastal area when the specified basic wind (75 mph to 90 mph) is twice as great as the basic velocities accompanying the observation (Carol 43.8 mph)?

(2) Should it be used in those coastal areas which may be visited by hurricanes during their mature stages?

Mr. Gentry quotes the fastest mile of wind recorded by the USWB at Miami for each of five hurricanes. He compares the velocities at the Airport Station (50 ft) and the City Office (229 ft). The ratios of V_Z to V_{50} are, respectively, 1.01, 1.14, 1.26, 1.30, and 1.53, and the corresponding values of x (the exponent) are 0.0, 0.082, 0.083, 0.085 and 0.28. Only the largest of the exponents compares at all closely with those obtained at Brookhaven, as shown by the appropriate curve for the corresponding basic wind (V_{30}) in Fig. 13. Mr. Gentry points out that "these data unfortunately cannot be used satisfactorily for determining the variation of the wind with height because of the different exposure of the two stations and the distance between them (approximately 5 miles)." It might also be added that in each pair the readings are not coincidental, that the two stations are in different parts of the transition zone for winds blowing from the ocean, and that the anemometer at the City Office is mounted on a tall office building which affects the wind differently for different wind directions. All of this emphasizes the difficulty of obtaining reliable quantative information regarding the variation of wind velocity with height at any situation except where anemometers are mounted on an exposed tower. In these five hurricanes, the increase of maximum wind speed with 179 ft increase of height varied from 1% to 53%, and only one storm in five gave results comparable to the storms at Brookhaven. Although both Miami and Brookhaven are in transition zones of coastal areas one is likely to experience mature hurricanes, while at the other, the two recorded hurricanes were in the decaying stage.

Riehl (20) states that "no one knows how high wind speeds can rise in tropical storms." Also, that a wind speed of 200 mph may be attained "over the sea and at a few hundred feet above the ground" in a very small area. He also

quotes L. A. Hughes (21) to the effect that an average of 90 knots (103 mph) was observed near the center of 28 storms during 84 reconnaissance flights of the United States Navy near the 1,000 ft level. This average value should be increased by two factors of at least 1.3 each, one to obtain the extreme storm and the other to obtain the fastest mile of wind within that storm. This would give a "fastest mile of wind" of at least 175 mph at the 1,000 ft level.

Fig. 5 does not specify basic velocities in excess of 120 mph but even this value would require the fastest mile of wind at 600 ft to be taken at 295 mph if the 0.3 exponent were used. Also, for the benefit of engineers who may feel the need of still higher basic winds in unusual situations, basic winds as high as 130 mph are included in Table 3(b). The accompanying wind speed at 600 ft would need to be 320 mph if 0.3 were used as an exponent.

The velocities of 295 and 320 mph at the 600-ft level are believed to be excessive, but the writer knows of no well-controlled observations in mature

TABLE 3.—FASTEST MILE OF WIND (MPH) FOR VARIOUS HEIGHT ZONES ABOVE GROUND (SEE FIGS. 5 AND 6)

Height Zone, in Feet	Basic Wind-Velocity									
	60	67	75	80	85	90	95	100		
(a) For Inland Areas										
0 to 50	60	70	75	80	85	90	95	100		
50 to 150	70	80	90	95	100	105	110	120		
150 to 400	80	90	100	110	115	125	130	140		
400 to 700	90	100	115	120	130	135	145	150		
700 to 1,000	100	110	125	130	140	145	155	160		
1,000 to 1,500	105	115	130	135	145	150	160	165		
(b) For Coastal Areas										
0 to 50	60	70	75	80	85	90	95	100	115	130
50 to 150	85	95	100	105	110	115	120	125	140	150
150 to 400	115	125	130	135	140	145	150	155	170	180
400 to 600	140	150	160	165	170	175	180	185	190	195
600 to 1,500	150	160	165	170	175	180	185	190	195	200

hurricanes, such as those which were made on the tower at Brookhaven for the two decaying hurricanes. Consequently, a prudent compromise between recklessness and extravagant conservatism requires a careful consideration of any relevant material from which reasonable inferences may be drawn. It is believed that it is the duty of the Committee on Wind Forces to make recommendations for the guidance of structural engineers even in this area to which field research has not yet penetrated.

The answers to the two questions posed in a previous paragraph will be adopted as follows:

(1) In coastal areas where the basic wind $V_{30} \gtrless 60$ mph, the variation of wind velocity with height $V_Z = V_{30} \left[\frac{Z}{30}\right]^{0.3}$, will be adpoted for heights up to the 600-ft level, above which a constant velocity will be used.

(2) In coastal areas where the basic wind $V_{30} \geqq 60$ mph, variable exponents will be adopted such that V_z is never greater than 200 mph at 600 ft in Table 3(b):

$$V_z = V_{30} \left[\frac{/z}{30}\right]^x$$

x varies from 0.3 when $V_{30} = 60$ mph to 0.143 when $V_{30} = 130$ mph. Curves are shown in Fig. 13 for some of the intermediate values of x.

In the present state of information it seems undesirable for the Committee on Wind Forces to try to distinguish between the wind velocities which, in coastal areas, are appropriate for structures located at the coast-line and those located farther inland. It is recommended that coastal areas be considered to extend at least 30 miles inland (22) from a well-defined coast line.

For all situations which, in the judgement of the engineer, deserve the classification of "coastal area," the wind velocities shown in Table 3(b) should be used together with the "Basic velocities" shown in Figs. 5 or 6. Special analysis should be made for promontories and in areas where the coast line is precipitous.

For all inland areas Table 3(a) should be used together with Figs. 5 or 6. These values are minimum and should be increased where higher basic velocities have been recorded locally, or are likely to occur, due to mountains, gorges, or for other unusual reasons.

There is a considerable decrease in the density of the air at locations high above sea level and consequently there is a reduction in the dynamic pressure (velocity pressure) as compared to the same wind speed and temperature at sea level. If, however, the fastest mile of wind, for which the contours of Figs. 5 and 6 are drawn, should occur at a temperature greatly below that of the standard atmosphere (59° F), the loss in density due to elevation may be completely compensated by the increase in density due to lower temperature. For example, Brekke (23) gives a table which shows that, at 4,000 ft elevation and standard temperature, there is a decrease of 14% in the density compared to sea-level elevation, but if the temperature were reduced to -10° F there would be no overall reduction in density of the atmosphere. Consequently, it is recommended that the engineer make no reduction in wind pressure based on reduced density at high elevations unless he has investigated the probability that the fastest mile of wind used in the design may be coincident with a significant reduction of temperature.

ACKNOWLEDGEMENT

This paper was written as part of the work of the Committee on Wind Forces of the Structural Division, ASCE. The writer is indebted to the other members of the Committee for their suggestions and criticisms as the work progressed. The discussions which followed the publication of the paper have been a rich source of additional information and of criticisms which have indicated the need for important revisions in the original paper. The writer wishes especially to acknowledge his indebtedness to E. Wendell Hewson, Professor of Meteorology, Department of Civil Engineering, The University of Michigan, for valuable suggestions, and to R. J. Deland, of Systems Division, Bendix Aviation Corporation,

Ann Arbor, Michigan, who not only read and criticised the paper and its closure but also read the discussions and commented on the inferences from the various references.

SUMMARY OF RECOMMENDATIONS

The scope of these recommendations has been limited to those general considerations which are common to most problems in the selection of appropriate wind velocities for the design of bridges, buildings, towers, and similar structures. It has been assumed that highly specialized problems will receive the attention of engineers with competence to make or direct the necessary modifications or additions to the recommendations.

Several important changes have been made in the original recommendations of this paper. These have resulted chiefly from additional information furnished by the writers of the discussions. Consequently, a complete summary of revised recommendations is given here:

1. All recommendations herein are based on conditions in open, level country as a standard of reference, and the influence of shielding, or of deflections and channeling due to unusual topography or to large obstructions shall be evaluated by the engineer in each individual case.
2. The effective ground (that is, the height in open, level country or its equivalent) at which minor obstructions are unimportant, and which approximates the height of anemometers now in use by the USWB in the first-order stations at airports, shall be taken at 30 ft.
3. Basic wind velocity shall be defined as the fastest-mile-of wind, reduced to a height of 30 ft, as shown in Figs. 5 and 6 for the various geographical areas of the United States. Fig. 5 shows the basic winds which have a statistically derived probable period of recurrence of 50 yr and Fig. 6 a probable period of recurrence of 100 yr.
4. A basic wind velocity with a 50-yr period of recurrence (Fig. 5) may be used for all permanent structures except those which, in the judgment of the engineer, have a high degree of wind sensitivity and an unusually high degree of hazard to life and property in case of failure. In the latter case, a 100-yr period of recurrence should be used (Fig. 6). In the case of temporary structures, such as those used during construction only, basic winds having velocities equal to three-quarters of the velocities shown in Fig. 5 may be used at the discretion of the engineer.
5. In special locations, such as on promontories, on mountains, in gorges, or for other unusual reasons, where records or experience indicate that the basic velocities given in Table 1A or 1B are inadequate, higher basic velocities shall be used at the discretion of the engineer.
6. Table 3 (a) shall be used in inland areas to obtain the variation of wind velocity with height after Figs. 5 or 6 has been used to obtain the minimum basic wind velocity for that area. For each basic wind velocity a stepped approximation to the one-seventh-power law has been used in Table 3 (a) to a height of 1,000 ft above which a constant velocity has been used.
7. Table 3 (b) shall be used in coastal areas to obtain the variation of wind velocity with height after Figs. 5 or 6 has been used to obtain the minimum basic wind velocity for that area. For each basic wind velocity a stepped approximation to a power law has been used up to a height of 600 ft, as follows: (a) where the basic wind velocity is equal to or less than 60 mph, an exponent

of 0.3; (b) where the basic wind velocity is greater than 60 mph, an exponent varying from 0.3 to 0.143 at 130 mph. Above 600 feet a constant velocity is used in each case. Coastal areas shall be considered to extend at least 30 miles inland from a well-defined coast line along the oceans, great lakes, or other large bodies of water.

8. Appropriate gust factors shall be used for structures which are small enough to be responsive to gusts involving less than one mile of passing wind. The gust-factor (gust velocity ÷ velocity of the fastest mile of wind) should bear some relation to the minimum size of gust necessary to envelope the structure and its accompanying pattern of flow (24). A gust-factor of 1.3 will allow for gusts of approximately one-second duration (25) which, in a 90 mph basic wind, would have a length downwind of about 130 ft. This will be adequate for sign boards and small residences. A gust-factor of 1.1 will allow for gusts of approximately 10-sec duration which, in a 90 mph basic wind, would have a length downwind of about 1,300 ft, and which is adequate for structures having a horizontal dimension transverse to the wind of about 125 ft.

9. Guyed towers shall be designed for the moving load effects of aerial jets (26) and descending gust fronts, as indicated in Fig. 4.

10. In those geographical areas where ice storms may be followed by strong winds, at least a 1/2 in. thickness of ice shall be assumed on all structural members.

REFERENCES

9. "Distributions of Extreme Winds in the United States," by H. C. S. Thom, Proceedings, ASCE, Vol. 86, No. ST4, April, 1960, Figs. 3 and 4.

10. "Gust Factors for the Design of Buildings," by R. H. Sherlock, Publications, Vol. 8, Fig. 4 to 10, Internatl. Assn. for Bridge and Structural Eng. Zurich, 1947.

11. "Wind Aid from Wind Roses," by H. L. Crutcher, Bulletin, Amer. Meteorological Soc., Vol. 37, No. 8 October, 1956, pp. 391-402.

12. "Variation of Wind Velocity and Gusts with Height," by R. H. Sherlock, Transactions, ASCE, Vol. 118A, 1953, pp. 479-481.

13. "Micrometeorology," by O. G. Sutton, McGraw-Hill Book Co., Inc., 1953, pp. 291-292.

14. "Compendium of Meteorology," by E. W. Hewson, Amer. Meteorological Soc., Boston, 1951, p. 1141.

15. "Hurricane Winds at Brookhaven National Laboratory," by Maynard E. Smith, and Irving A. Singer, January 24, 1956, (unpublished report in typewritten form).

16. "Variation of Wind Velocity and Gusts with Height," by R. H. Sherlock, Transactions, ASCE, Vol. 118A, 1953, p. 472.

17. "Variation of Wind Velocity and Gusts with Height," by R. H. Sherlock, Transactions, ASCE, Vol. 118A, 1953, p. 470.

18. "Physical and Dynamical Meteorology," by David Brunt, Cambridge University Press, London, 1941, p. 228.

19. "The Application of Wet-Bulb Potential Temperature to Air Mass Analysis, IV.," by E. W. Hewson, Q. J. Royal Meteorological Soc., Vol. LXIV, No. 276, July, 1938, p. 419.

20. "Tropical Meteorology," by Herbert Riehl, McGraw-Hill Book Co., Inc., 1954, p. 288.

21. "On the Low-Level Wind Structure of Tropical Storms," by L. A. Hughes, Journal of Meteorology, Vol. 9, 1952, p. 422.

22. "Wind Pressures in Various Areas of the United States," by G. N. Brekke, Building Materials and Structures Report 152, p. 4, Natl. Bur. of Stds., April, 1959.

23. "Wind Pressures in Various Areas of the United States," by G. N. Brekke, Building Materials and Structures Report 152, p. 7, Natl. Bur. of Stds., April, 1959.

24. "Gust Factors for the Design of Buildings," by R. H. Sherlock, Publications, Vol. 8, Fig. 11, Internatl. Assn. for Bridge and Structural Eng., Zurich, 1947.

25. Ibid., Figure 19.

26. "Variation of Wind Velocity and Gusts with Height," by R. H. Sherlock, Transactions, ASCE, Vol. 118A, pp. 464, 470, 478-479, 488, 1953.

27. "Physical and Dynamical Meteorology," by David Brunt, Cambridge University Press, London, 1941, p. 189.

28. "Weather Analysis and Forecasting," by S. Petterssen, McGraw-Hill Book Co., Inc., 1940, p. 208.

CONTINUOUS GIRDER BRIDGE WITH VARIABLE MOMENT OF INERTIA[a]

Discussion by A. A. Eremin

A. A. EREMIN,[7] F. ASCE.—An interesting method of computing redundant forces in continuous beams with variable sections has been developed by Mr. Sami in this paper. To simplify this method, Mr. Sami took advantage of the symmetry of the spans. In recent years, many simplified analytical and graphical methods have been developed.

By solving the same problem with various computation methods, the advantages of the methods may be revieved. With this purpose the illustrative problem shown by Mr. Sami is solved by the graphical method of moment distribution (Fig. 18). The distance to the central point is determined from

$$C = 0.45 \times 60 = 27.0$$

The central-point location was explained elsewhere.[8] Line DE is the closing line of the fixed end bending moments which may be determined by any method.

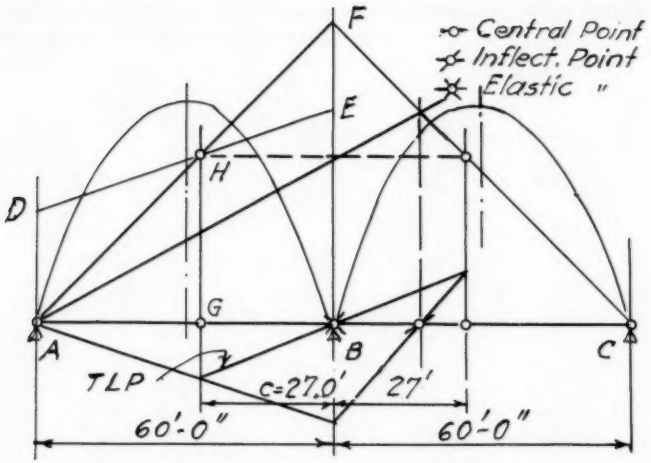

FIG. 18.—BENDING MOMENT DIAGRAM

[a] January, 1960, by Sabri Sami.
[7] Assoc. Bridge Engr., Calif. State Highways, Sacramento, Calif.
[8] Discussion of "Arches and Bents," Transactions, ASCE, 1950, p. 630.

With graphical construction of a three line polygon and cross lines, the bending moment diagram is drawn.

All graphical constructions may be performed in less than 15 min. The additional graphical constructions for the varied properties of beams may be completed in a fraction of this time.

It is interesting to note that the redundant forces computed in Fig. 18, differ from those computed by the author by an amount which is less than 3%. The graphical construction of the bending moments may be further simplified by drawing the bending moment closing line directly through the central point (vertical GH).

In conclusion, it may be stated that, in selecting the computation method of solving continuous beams, important consideration should be given to the designer's personal conception of expressing the redundant forces either by numerical factors, or graphical ordinates.

Mr. Sami performed tremendous algebraic work to simplify the expressions for the redundant forces. In practical application of the method only the final equations or diagrams are needed. Yet, the designer always has to be prepared to trace the effect of various features of continuous beams. This fact may be found quite involved. It is gratifying that the author performed such tremendous work in illustrating a quite unique approach in solving continuous beam with redundant forces.

STABILITY CONSIDERATIONS IN THE DESIGN OF STEEL PLATE GIRDERS[a]

Discussion by A. A. Eremin

A. A. EREMIN,[2] F. ASCE.—In this paper Mr. Massonnet has presented some interesting tests of steel plate girder stability. The tests have proved that the stresses in the stiffeners, web plate, and girder flanges are interrelated. From the tests it may be concluded that tight fitting at the ends of intermediate vertical stiffeners does not contribute to a uniform distribution of stresses in the web plate. Likewise, the stresses in the horizontal stiffeners (when they are placed a short distance from the flanges) may be affected by the stresses in the flanges.

At present, there is a tendency for continuous steel plate girders to be designed with haunched web plates at the intermediate support. It would be interesting to extend the tests to the steel plate girders with variable width of web plate. Furthermore, the stiffners are often combined with intermediate diaphragms or wind cross frames. Obviously, the stresses in the cross frames will affect the distribution of stresses in the stiffeners. This may be especially true in relation to the horizontal stiffeners.

[a] January, 1960, by Charles E. L. Massonnet.
[2] Assoc. Bridge Engr., Calif. State Highways, Sacramento, Calif.

PROPERTIES OF STEEL AND CONCRETE AND THE BEHAVIOR OF STRUCTURES[a]

Discussion by Lester H. Gabriel

LESTER H. GABRIEL,[6] M. ASCE.—The author quite rightly points to the fact that the material testing procedures in common use and the interpretations placed thereon are an attempt to make explicit some of the more significant variables of a design model thought to apply.

In a design model (method), the consequences of the design are, of necessity, a function of not only the explicit factors of material composition, stress, strain, modulus of elasticity, yield point, etc., but also of many (perhaps hundreds or even thousands) of neglected factors. A good design method will satisfy the following:

(1) The variables of the properties of the material that have a significant effect will be well understood and properly evaluated so that the explicit factors will properly influence the design procedures.

(2) All the major factors of influence will have been made explicit and properly evaluated so that those many factors which are considered negligible and omitted are in fact negligible and act as a chance variable. If negligible factors of influence act as something other than a chance variable then the total effect of the negligible factors may be quite significant.

(3) The design method itself will be subject to test and the consequences thereof will reflect on the value of the method. If the results of the tests fail to satisfy the constraints of the design method, then the entire method itself must be scrutinized for erroneous assumptions; that is the explicit factors, the negligible factors that are assumed to act as a chance variable, and the test instruments themselves (the maintained hypotheses).

To those initiated in the area of reinforced concrete design by the elastic analysis method, it is immediately apparent just how important is the modulus of elasticity of concrete (E_c). In fact E_c and n, the ratio of the modulii of steel to concrete, underly the very substance of the method of the transformed section for elastic design. The ACI Building Code[7] calls for $n = 30{,}000/f'_c$ which in turn, gives E_c a value of $1{,}000\ f'_c$. This is the well known secant modulus and the design methods of present and past accept this estimate of one very significant factor of the many explicit factors of the design method.

---

[a] February, 1960, by George Winter.

[6] Asst. Prof. of Civ. Engrg., Sacramento State College, Sacramento, Calf.

[7] "Building Code Requirements for Reinforced Concrete," American Concrete Institute, ACI, 318-56.

The fact that it is known that the secant modulus estimate of $E_c = 1{,}000\ f'_c$ is low for moderate strength concrete and high for high strength concrete,[8] coupled with the fact that any kind of variability in E_c is ignored in the classical design methods, puts this variability in E_c in the group of neglected factors. The fact that the variability in E_c does not present itself as a chance variable but rather a function of f'_c itself, leads to a bias in the design method. How then does this one type of variation (which is not subject to chance alone) effect the strength of the structure? How does it effect the apparent factor of safety? How do variations of other factors in the design model, both explicit and neglected, effect the strength of the structure or the apparent factor of safety?

The writer wishes to lend support to the author's statements

> "The attempt is to reduce the amount of judgment and increase the factual and quantitative basis on which safety and load factors are determined. While it is unlikely that it will ever be possible to deal with safety entirely on a statistical-probabilistic basis, -------, it (information) can be incorporated in the safety factor explicitly and numerically."

This writer feels very strongly that now—when new methods of design and analysis are bursting forth, when older methods are being re-examined, and when the philosophy of the action of structures under load (s) and all the design methods related thereto are being explored anew—is the time to attempt to include probabilistic estimates of variability as a parameter of the methods themselves. This would lead to (1) more significant testing and test procedures, (2) a realization on the part of the designer that variability does exist and must be considered in the design, and (3) a more sophisticated concept of safety factor or load factor in terms of probability of failure and the related consequences.

Once a design method is developed and accepted as a "modus operendii" of the design profession, it becomes exceedingly difficult to effect changes. It is with anxiety that this writer has followed the development of plastic design so that the margin of safety of design "is not less than that provided against failure of a simply supported beam according to usual past practice."[9]

This writer believes that the structural engineering profession has arrived at that degree of sophistication whereby notions of factor of safety or margin of safety that describe a vague condition of expected strength without describing some estimate of likelihood of failure are grievously wrong. Variations of all kinds must be considered and be part of the thinking of the developers of design methods. To develop new methods so they are as safe as old methods is a step backwards because of the time lag it generates in the eventual definition of factor of safety as an estimate of the probabilities of failure or success.

---

[8] "Reinforced Concrete Fundamentals," by Phil M. Ferguson, John Wiley and Sons, Inc., New York, 1958, p. 10.

[9] "Plastic Design of Steel Frames," by L. S. Beedle, John Wiley and Sons, Inc., New York, 1958, p. 3.

DIGEST OF THE GUIDE TO DESIGN CRITERIA FOR METAL COMPRESSION MEMBERS[a]

Discussion by Richard H. J. Pian

RICHARD H. J. PIAN,[3] M. ASCE.—One of the objections to the initial-yield-criterion approach to beam-column design, as outlined by the author, is as follows: "The effect of end restraint cannot be rationally introduced into the secant formula analysis since the procedure is based on the analysis of an unrestrained member."

The writer has developed a general approach for the analysis of metal columns[4] on a rational basis similar to the secant formula. A non-dimensional formula for column design with different degrees of imperfections, different end conditions, and with materials having different yielding stresses can be written in the following form.

(1) For columns with initial deflection a:

$$\frac{\sigma_1}{\sigma_y} = \frac{1}{2}\left[1 + (1+k)\frac{\sigma_{cr}}{\sigma_y} - \sqrt{\left\{1+(1+k)\frac{\sigma_{cr}}{\sigma_y}\right\}^2 - 4\frac{\sigma_{cr}}{\sigma_y}}\right] \quad \ldots (35)$$

(2) For columns with initial eccentricity e:

$$\frac{\sigma_1}{\sigma_y} = \frac{1}{2(1-0.26\,k)}\left[1+(1+k)\frac{\sigma_{cr}}{\sigma_y} - \sqrt{\left\{1+(1+k)\frac{\sigma_{cr}}{\sigma_y}\right\}^2 - 4(1-0.26\,k)\frac{\sigma_{cr}}{\sigma_y}}\right] \quad \ldots (36)$$

in which σ_1 is the axial stress, σ_y denotes the yielding stress, $\sigma_{cr} = P_{cr}/A$, the critical axial stress, and $k = a\,c/r^2$ or $e\,c/r^2$.

A set of curves may be plotted from Eqs. 35 or 36 for various values of k and these curves can be used for any σ_y. A number of other curves are included in the four-quadrant chart (Fig. 8). The third quadrant curves, which are first to be used for computation, give the relation between L/r and $1/\sigma_{cr}$. Here the effect of end conditions of compression members can be taken into account by using different values of K in the expression of $P_{cr} = \pi^2 E I/(K L)^2$.

---

[a] April, 1960, by Bruce G. Johnston.

[3] Prof. of Engrg., Arizona State University, Tempe, Ariz.

[4] "Column Design Simplified," by Richard H. J. Pian, Proceedings, ASCE, ST 3, May, 1957.

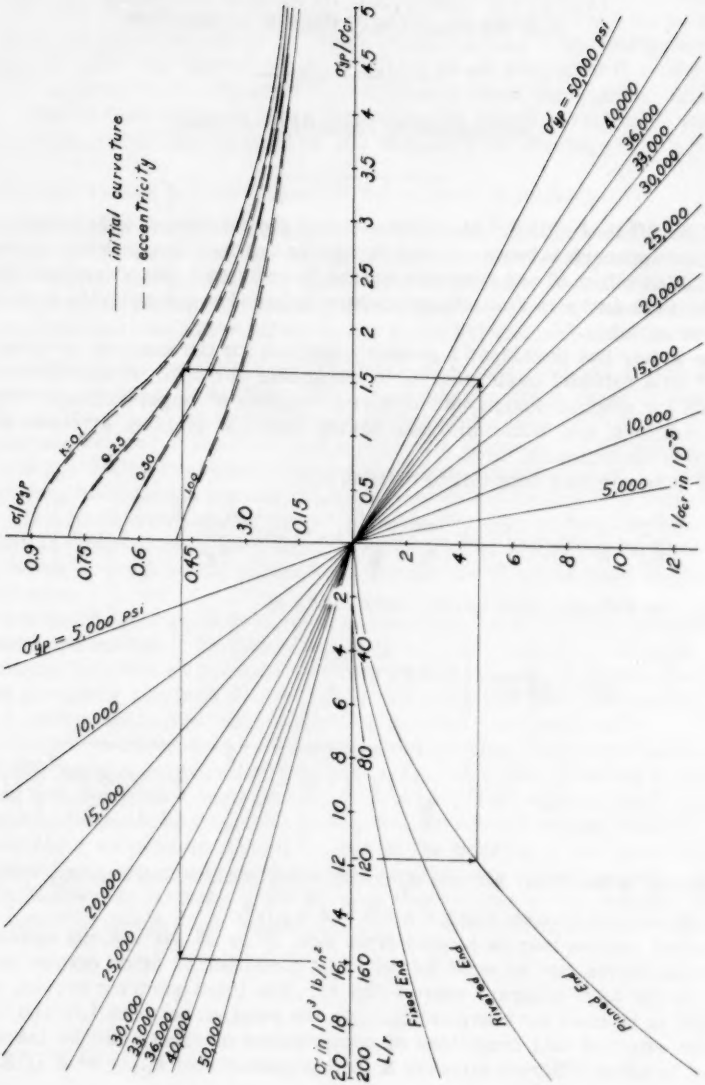

FIG. 8.—COLUMN DESIGN CHART

The term K L is defined as the effective length of the column. Next, the straight lines in the fourth and second quadrants are drawn for different values of σ_y. The curves in the first quadrant are those plotted from values obtained by evaluating Eq. 35 or Eq. 36.

PROCEEDINGS PAPERS

The technical papers published in the past year are identified by number below. Technical-division sponsorship is indicated by an abbreviation at the end of each Paper Number, the symbols referring to: Air Transport (AT), City Planning (CP), Construction (CO), Engineering Mechanics (EM), Highway (HW), Hydraulics (HY), Irrigation and Drainage (IR), Pipeline (PL), Power (PO), Sanitary Engineering (SA), Soil Mechanics and Foundations (SM), Structural (ST), Surveying and Mapping (SU), and Waterways and Harbors (WW), divisions. Papers sponsored by the Department of Conditions of Practice are identified by the symbols (PP). For titles and order coupons, refer to the appropriate issue of "Civil Engineering." Beginning with Volume 82 (January 1956) papers were published in Journals of the various Technical Divisions. To locate papers in the Journals, the symbols after the paper number are followed by a numeral designating the issue of a particular Journal in which the paper appeared. For example, Paper 2270 is identified as 2270(ST9) which indicates that the paper is contained in the ninth issue of the Journal of the Structural Division during 1959.

VOLUME 85 (1959)

JULY: 2079(HY7), 2080(HY7), 2081(HY7), 2082(HY7), 2083(HY7), 2084(HY7), 2085(HY7), 2086(SA4), 2087(SA4), 2088(SA4), 2089(SA4), 2090(SA4), 2091(EM3), 2092(EM3), 2093(EM3), 2094(EM3), 2095(EM3), 2096(EM3), 2097(HY7)[c], 2098(SA4)[c], 2099(EM3)[c], 2100(AT3), 2101(AT3), 2102(AT3), 2103(AT3), 2104(AT3), 2105(AT3), 2106(AT3), 2107(AT3), 2108(AT3), 2109(AT3), 2110(AT3), 2111(AT3), 2112(AT3), 2113(AT3), 2114(AT3), 2115(AT3), 2116(AT3), 2117(AT3), 2118(AT3), 2119(AT3), 2120(AT3), 2121(AT3), 2122(AT3), 2123(AT3), 2124(AT3), 2125(AT3).

AUGUST: 2126(HY8), 2127(HY8), 2128(HY8), 2129(HY8), 2130(PO4), 2131(PO4), 2132(PO4), 2133(PO4), 2134(SM4), 2135(SM4), 2136(SM4), 2137(SM4), 2138(HY8)[c], 2139(PO4)[c] 2140(SM4)[c].

SEPTEMBER: 2141(CO2), 2142(CO2), 2143(CO2), 2144(HW3), 2145(HW3), 2146(HW3), 2147(HY9), 2148(HY9), 2149(HY9), 2150(HY9), 2151(IR3), 2152(ST7)[c], 2153(IR3), 2154(IR3), 2155(IR3), 2156(IR3), 2157(IR3), 2158(IR3), 2159(IR3), 2160(IR3), 2161(SA5), 2162(SA5), 2163(ST7), 2164(ST7), 2165(SU1), 2166(SU1), 2167(WW3), 2168(WW3), 2169(WW3), 2170(WW3), 2171(WW3), 2172(WW3), 2173(WW3), 2174(WW3), 2175(WW3), 2176(WW3), 2177(WW3), 2178(CO2)[c], 2179(IR3)[c], 2180(HW3)[c], 2181(SA5)[c], 2182(HY9)[c], 2183(SU1)[c], 2184(WW3)[c], 2185(PP2)[c], 2186(ST7)[c], 2187(PP2), 2188(PP2).

OCTOBER: 2189(AT4), 2190(AT4), 2191(AT4), 2192(AT4), 2193(AT4), 2194(EM4), 2195(EM4), 2196(EM4), 2197(EM4), 2198(EM4), 2199(EM4), 2200(HY10), 2201(HY10), 2202(HY10), 2203(PL3), 2204(PL3), 2205(PL3), 2206(PO5), 2207(PO5), 2208(PO5), 2209(PO5), 2210(SM5), 2211(SM5), 2212(SM5), 2213(SM5), 2214(SM5), 2215(SM5), 2216(SM5), 2217(SM5), 2218(ST8), 2219(ST8), 2220(EM4), 2221(ST8), 2222(ST8), 2223(ST8), 2224(HY10), 2225(HY10), 2226(PO5), 2227(PO5), 2228(PO5), 2229(ST8), 2230(EM4), 2231(EM4), 2232(AT4)[c], 2233(PL3)[c], 2234(EM4)[c], 2235(HY10)[c], 2236(SM5)[c], 2237(ST8)[c], 2238(PO5)[c], 2239(ST8), 2240(PL3).

NOVEMBER: 2241(HY11), 2242(HY11), 2243(HY11), 2244(HY11), 2245(HY11), 2246(SA6), 2247(SA6), 2248(SA6), 2249(SA6), 2250(SA6), 2251(SA6), 2252(SA6), 2253(SA6), 2254(SA6), 2255(SA6), 2256(ST9), 2257(ST9), 2258(ST9), 2259(ST9), 2260(HY11), 2261(ST9)[c], 2262(ST9), 2263(HY11), 2264(ST9), 2265(HY11), 2266(SA6), 2267(SA6), 2268(SA6), 2269(HY11)[c], 2270(ST9).

DECEMBER: 2271(HY12)[c], 2272(CP2), 2273(HW4), 2274(HW4), 2275(HW4), 2276(HW4), 2277(HW4), 2278(HW4), 2279(HW4), 2280(HW4), 2281(IR4), 2282(IR4), 2283(IR4), 2284(IR4), 2285(PO6), 2286(PO6), 2287(PO6), 2288(PO6), 2289(PO6), 2290(PO6), 2291(PO6), 2292(SM6), 2293(SM6), 2294(SM6), 2295(SM6), 2296(SM6), 2297(WW4), 2298(WW4), 2299(WW4), 2300(WW4), 2301(WW4), 2302(WW4), 2303(WW4), 2304(HW4), 2305(ST10), 2306(CP2), 2307(CP2), 2308(ST10), 2309(CP2), 2310(HY12), 2311(HY12), 2312(PO6), 2313(PO6), 2314(ST10), 2315(HY12), 2316(HY12), 2317(HY12), 2318(WW4), 2319(SM6), 2320(SM6), 2321(ST10), 2322(ST10), 2323(HW4)[c], 2324(CP2)[c], 2325(SM6)[c], 2326(WW4)[c], 2327(IR4)[c], 2328(PO6)[c], 2329(ST10)[c], 2330(CP2).

VOLUME 86 (1960)

JANUARY: 2331(EM1), 2332(EM1), 2333(EM1), 2334(EM1), 2335(HY1), 2336(HY1), 2337(EM1), 2338(EM1), 2339(HY1), 2340(HY1), 2341(SA1), 2342(EM1), 2343(SA1), 2344(ST1), 2345(ST1), 2346(ST1), 2347(ST1), 2348(EM1)[c], 2349(HY1)[c], 2350(ST1), 2351(ST1), 2352(SA1)[c], 2353(ST1)[c], 2354(ST1).

FEBRUARY: 2355(CO1), 2356(CO1), 2357(CO1), 2358(CO1), 2359(CO1), 2360(CO1), 2361(PO1), 2362(HY2), 2363(ST2), 2364(HY2), 2365(SU1), 2366(HY2), 2367(SU1), 2368(SM1), 2369(HY2), 2370(SU1), 2371(HY2), 2372(PO1), 2373(SM1), 2374(HY2), 2375(PO1), 2376(HY2), 2377(CO1)[c], 2378(SU1), 2379(SU1), 2380(SU1), 2381(HY2)[c], 2382(ST2), 2383(SU1), 2384(ST2), 2385(SU1)[c], 2386(SU1), 2387(SU1), 2388(SU1), 2389(SM1), 2390(ST2)[c], 2391(SM1)[c], 2392(PO1)[c].

MARCH: 2393(IR1), 2394(IR1), 2395(IR1), 2396(IR1), 2397(IR1), 2398(IR1), 2399(IR1), 2400(IR1), 2401(IR1), 2402(IR1), 2403(IR1), 2404(IR1), 2405(IR1), 2406(IR1), 2407(SA2), 2408(SA2), 2409(HY3), 2410(ST3), 2411(SA2), 2412(HW1), 2413(WW1), 2414(WW1), 2415(HY3), 2416(HW1), 2417(HW3), 2418(HW1)[c], 2419(WW1)[c], 2420(WW1), 2421(WW1), 2422(WW1), 2423(WW1), 2424(SA2), 2425(SA2)[c], 2426(HY3)[c], 2427(ST3)[c].

APRIL: 2428(ST4), 2429(HY4), 2430(PO2), 2431(SM2), 2432(PO2), 2433(ST4), 2434(EM2), 2435(PO2), 2436(ST4), 2437(ST4), 2438(HY4), 2439(EM2), 2440(EM2), 2441(ST4), 2442(SM2), 2443(HY4), 2444(ST4), 2445(EM2), 2446(ST4), 2447(EM2), 2448(SM2), 2449(HY4), 2450(ST4), 2451(HY4), 2452(HY4), 2453(EM2), 2454(EM2), 2455(EM2)[c], 2456(HY4)[c], 2457(PO2)[c], 2458(ST4)[c], 2459(SM2)[c].

MAY: 2460(AT1), 2461(ST5), 2462(AT1), 2463(AT1), 2464(CP1), 2465(CP1), 2466(AT1), 2467(AT1), 2468(SA3), 2469(HY5), 2470(ST5), 2471(SA3), 2472(SA3), 2473(ST5), 2474(SA3), 2475(ST5), 2476(SA3), 2477(ST5), 2478(HY5), 2479(SA3), 2480(ST5), 2481(SA3), 2482(CO2), 2483(CO2), 2484(HY5), 2485(HY5), 2486(AT1)[c], 2487(CP1)[c], 2488(CO2)[c], 2489(HY5)[c], 2490(SA3)[c], 2491(ST5)[c], 2492(CP1), 2493(CO2).

JUNE: 2494(IR2), 2495(IR2), 2496(ST6), 2497(EM3), 2498(EM3), 2499(EM3), 2500(EM3), 2501(SM3), 2502(EM3), 2503(PO3), 2504(WW2), 2505(EM3), 2506(HY6), 2507(WW2), 2508(PO3), 2509(ST6), 2510(EM3), 2511(EM3), 2512(ST6), 2513(HW2), 2514(HY6), 2515(PO3), 2516(EM3), 2517(WW2), 2518(WW2), 2519(EM3), 2520(PO3), 2521(HY6), 2522(SM3), 2523(ST6), 2524(HY6), 2525(HY6), 2526(HY6), 2527(IR2), 2528(ST6), 2529(HW2), 2530(IR2), 2531(HY6), 2532(EM3)[c], 2533(HW2)[c], 2534(WW2), 2535(HY6)[c], 2536(IR2)[c], 2537(PO3)[c], 2538(SM3)[c], 2539(ST6)[c], 2540(WW2)[c].

JULY: 2541(ST7), 2542(ST7), 2543(SA4), 2544(ST7), 2545(ST7), 2546(HY7), 2547(ST7), 2548(SU2), 2549(SA4), 2550(SU2), 2551(HY7), 2552(ST7), 2553(SU2), 2554(SA4), 2555(ST7), 2556(SA4), 2557(SA4), 2558(SA4), 2559(ST7), 2560(SU2)[c], 2561(SA4)[c], 2562(HY7)[c], 2563(ST7)[c].

c. Discussion of several papers, grouped by divisions.

AMERICAN SOCIETY OF CIVIL ENGINEERS

OFFICERS FOR 1960

PRESIDENT

FRANK A. MARSTON

VICE-PRESIDENTS

Term expires October, 1960:
PAUL L. HOLLAND
LLOYD D. KNAPP

Term expires October, 1961:
CHARLES B. MOLINEAUX
LAWRENCE A. ELSENER

DIRECTORS

Term expires October, 1960:
PHILIP C. RUTLEDGE
WESTON S. EVANS
TILTON E. SHELBURNE
CRAIG P. HAZELET
DONALD H. MATTERN
JOHN E. RINNE

Term expires October, 1961:
THOMAS J. FRATAR
EARL F. O'BRIEN
DANIEL B. VENTRES
CHARLES W. BRITZIUS
WAYNE G. O'HARRA
FRED H. RHODES, JR.
N. T. VEATCH

Term expires October, 1962:
ELMER K. TIMBY
SAMUEL S. BAXTER
THOMAS M. NILES
TRENT R. DAMES
WOODROW W. BAKER
BERNHARD DORNBLATT

PAST PRESIDENTS

Members of the Board

LOUIS R. HOWSON
FRANCIS S. FRIEL

EXECUTIVE SECRETARY

WILLIAM H. WISELY

TREASURER

E. LAWRENCE CHANDLER

ASSISTANT TREASURER

ENOCH R. NEEDLES

PROCEEDINGS OF THE SOCIETY

HAROLD T. LARSEN
Manager of Technical Publications

PAUL A. PARISI
Editor of Technical Publications

MARVIN L. SCHECHTER
Associate Editor of Technical Publications

IRVIN J. SCHWARTZ
Assistant Editor of Technical Publications

COMMITTEE ON PUBLICATIONS

PHILIP C. RUTLEDGE, *Chairman*

THOMAS M. NILES, *Vice-Chairman*

TILTON E. SHELBURNE
WESTON S. EVANS
WAYNE G. O'HARRA
BERNHARD DORNBLATT